SEARS FOUNDATION FOR MARINE RESEARCH
BINGHAM OCEANOGRAPHIC LABORATORY, YALE UNIVERSITY

JOURNAL OF
MARINE RESEARCH

VOLUME 14 1955 NUMBER 1

THE TRANSIENT DEVELOPMENT OF A LEE WAVE[1]

By

M. G. WURTELE

Massachusetts Institute of Technology

ABSTRACT

A stream with an initially undisturbed free surface is set impulsively in motion and a (small) pressure perturbation is applied to the surface. The form of the free surface as a function of time is examined in detail up to the point where the disturbance is sensibly that of a steady-state lee wave.

INTRODUCTION

The theoretical problem of waves in the lee of a surface disturbance was first attacked by Lord Rayleigh (1883). He pointed out that, if a steady state is assumed, the problem is indeterminate in that an infinite number of solutions exist. Stationary free waves of any amplitude are solutions; and in a fluid of infinite depth it is always possible to assign a wave length such that the free wave will move with velocity equal and opposite to that of the current and so remain stationary relative to the point of disturbance.

To specify a unique solution, Rayleigh employed the much used device of a small fictitious dissipative force proportional to the relative velocity. This has the effect of prohibiting any upstream wave (except one with infinite amplitude at infinity), hence the only physically acceptable solution is the lee wave.

Lord Kelvin (1886), in his investigation of the slightly different problem of irregularities in the bed of a stream, used a different method.

[1] This paper was presented at the Johns Hopkins Symposium on the Application of Experimental Models to Geophysical Research, September 1–4, 1953.

After obtaining a solution which satisfied the boundary conditions, he added free waves with just such amplitudes as would render the upstream disturbance monotonically decreasing at large distances. The result is exactly that obtained by the method of Rayleigh when Kelvin's method is applied to this problem, as shown by Höiland (1951).

The indeterminateness of the problem persisted *a fortiori* in the more complex models, as in that of Lyra (1943), with continuously distributed stability. However, recently Höiland (1951) has shown that if the stream is allowed to begin from a state of rest with an undisturbed surface, the disturbance, after sufficient time has elapsed, will be sensibly the same as the steady-state lee wave of Rayleigh and Kelvin. Höiland's explanation of the lee wave has considerable intuitive appeal, and it is the purpose of this paper to show in some detail the transient development of such a wave by using Rayleigh's original model.

THE PROBLEM AND ITS FORMAL SOLUTION

Consider a homogeneous incompressible fluid stream which is bounded on top by a free surface but which is infinite in depth and breadth. We fix a co-ordinate system in the stream so that the fluid is moving with constant speed U in the direction of the x-axis. The z-axis will be taken increasing upward, with origin in the free surface. If a disturbing pressure of sinusoidal form, $p = p_0 e^{ikx}$, is applied to the surface of the stream, the resulting motion may be determined. The disturbance, assumed to be of small amplitude, may be represented by a velocity potential ϕ and a stream function ψ, both of which satisfy Laplace's equation. Since the current is uniform, the vertical displacement ζ satisfies the same equation. We may thus discuss these quantities in terms of their amplitudes ϕ_0, ψ_0, ζ_0 at the surface:

$$\phi = \phi_0 e^{kz + ikx}, \qquad \psi = \psi_0 e^{kz + ikx}, \qquad \zeta = \zeta_0 e^{kz + ikx}. \quad (2.1)$$

For steady conditions, therefore, the dynamic condition at the surface reduces to $\rho(kU^2 - g)\zeta_0 = p_0$.

If we employ Rayleigh's notation, $\kappa = g/U^2$, we have the result in his form,

$$\zeta_0 = \frac{p_0}{\rho k} \cdot \frac{e^{ikx}}{U^2 - C^2} = \frac{p_0}{\rho U^2} \frac{e^{ikx}}{k - \kappa}, \quad (2.2)$$

where $C^2 = g/k$.

We may now consider the time-dependent problem. The initial state of the system is specified and the assumption of steady state is relinquished; the problem, then, is to determine the motion of

the system at any future time. A simple rule may be given (Wurtele, 1953) for the construction of the required solution. There are two possible free waves of the system, that is, waves which move so that their corresponding perturbation pressures at the free surface are zero. These waves have the Stokesian velocities $\pm C$, and they may be added with arbitrary amplitudes to the stationary solution (2.2), which is needed to satisfy the boundary conditions. The time-dependent solution may be written

$$\zeta_0 \frac{p_0}{k(U^2 - C^2)} \{ \exp ikx - \alpha \exp ik[x - (U - C)t] - \beta \exp ik[x - (U + C)t] \} . \tag{2.4}$$

This solution may be verified mathematically by elimination of the velocity potential between the dynamic surface condition for non-steady flow,

$$\frac{\partial \phi}{\partial t} + U \frac{\partial \phi}{\partial x} = g\zeta + \frac{1}{\rho} p ,$$

and the identity,

$$- \frac{\partial \phi}{\partial z} = \frac{\partial \zeta}{\partial t} + U \frac{\partial \zeta}{\partial x}$$

with the use of (2.1). The resulting equation is

$$\frac{\partial^2 \zeta_0}{\partial t^2} + 2iUk \frac{\partial \zeta_0}{\partial t} - k^2(U^2 - C^2)\zeta_0 = \frac{kp_0}{\rho} , \tag{2.5}$$

of which (2.4) is the general solution. Of course the constants α and β are to be determined by the given initial state of the system, more specifically by the vertical displacement and vertical velocity of the free surface at $t = 0$. For present purposes, we shall select these values so as to exhibit the simplest possible pattern of development of the disturbance. At the initial moment we specify that the free surface shall be undisturbed

$$\zeta_0 = 0 \text{ at } t = 0 \tag{2.6}$$

but that the motion of the free surface is a simple sinusoidal pattern

$$\frac{\partial \zeta_0}{\partial t} = \frac{ip_0 e^{ikx}}{\rho(U + C)} \text{ at } t = 0 . \tag{2.7}$$

If these two conditions are imposed upon the general solution (2.4), we find that $\alpha = 1, \beta = 0$; there the solution of the particular physical problem proposed is

$$\zeta_0 = \frac{p_0}{k(U^2 - C^2)} \{ \exp ikx - \exp ik[x - (U - C)t] \} . \tag{2.8}$$

The wave moving forwards (relative to the fluid) is not excited in this system owing to the particular initial state specified. But the physical mechanism of the development is made more evident thereby, since, as we shall see, this advancing wave does not contribute to the establishment of the lee wave.

Following Rayleigh, we may consider the applied pressure as concentrated in a narrow band at the origin so that it may be represented mathematically as a delta function. The Fourier-component amplitudes are therefore equal for all waves, and p_0 may be treated as constant. The solution may be written as

$$\zeta_0 = \frac{p_0}{\rho} \int_0^\infty \{ \exp ikx - \exp ik[x - (U - C)t] \} \frac{dk}{k(U^2 - C^2)} . \quad (2.9)$$

It can easily be shown by methods developed for a similar model (Wurtele, 1953) that (2.9) approaches the classical steady-state solution as $t \to \infty$. In the next sections the transient state will be examined and interpreted.

EVALUATION OF THE INTEGRAL

For the purpose of evaluation, the integral (2.9) should be written in terms of the fundamental wave number κ. If we take κ^{-1} as the unit of length, the integral is made nondimensional; and if we absorb the constant factor $p_0/\rho U^2$ into ζ_0 and take the real part of (2.9), we have

$$\zeta_0 = \int_0^\infty \{ \cos kx - \cos [kx - Ut(k - k^{\frac{1}{2}})] \} \frac{dk}{k - 1} \quad (3.1a)$$

$$= P \int_0^\infty \cos kx \frac{dk}{k - 1} - P \int_0^\infty \cos [kx - Ut(k - k^{\frac{1}{2}})] \frac{dk}{k - 1}$$

$$= I_1 - I_2 \quad (3.1b)$$

where the integrals in (3.1b) take Cauchy principle values at the point $k = 1$. The integral I_1 is a solution of the corresponding stationary problem. It may be expressed in terms of tabulated functions as follows:

$$P \int_0^\infty \cos kx \frac{dk}{k - 1} = \cos x \, P \int_{-1}^\infty \cos xy \frac{dy}{y} - \sin x \, P \int_{-1}^\infty \sin xy \frac{dy}{y}$$

$$= - \cos x \, Ci(x) - \sin |x| \, [\tfrac{1}{2}\pi + Si(|x|)] , \quad (3.2)$$

where the sine and cosine integrals have their usual notations,

$$Ci(x) = -\int_x^\infty \cos y \frac{dy}{y}, \qquad Si(x) = \int_0^x \sin y \frac{dy}{y}.$$

Using the asymptotic expansions of Ci and Si, we may write

$$I_1 = -\pi \sin |x| + 0(1/x). \tag{3.2a}$$

The second integral I_2 in (3.1b) is time-dependent and less easily evaluated. We may write it as

$$I_2 = Re\, P \int_0^\infty \exp i(kx' - n't) \frac{dk}{k-1}, \tag{3.3}$$

where we have introduced the co-ordinate moving with the current, $x' = x - Ut$, and the corresponding frequency,

$$n' = -Uk^{\frac{1}{2}}. \tag{3.4}$$

We may eliminate the radical in the exponent by writing

$$I_2 = 2\, Re\, P \int_0^\infty \exp if(y) \frac{ydy}{y^2 - 1}, \tag{3.5}$$

where $f(y) = x'y^2 + Uty$.
There may be two neighborhoods on the path of integration which contribute significantly to the integral. The first is the pole,

$$y = 1, \tag{3.6}$$

which is on the path for all values of the parameters. The second is the saddle-point, given by $df/dy = 0$,

$$y_0 = \tfrac{1}{2}(1 - x/Ut)^{-1}, \tag{3.7}$$

which can lie on the path of integration only if $x < Ut$. So long as these two points are separated by an appropriate distance, the integral can be evaluated by indenting the contour at the pole and by deforming the path of integration so it will traverse the saddle-point in a path of steepest descent. When the parameters assume certain values, specifically when $Ut \doteq 2x$, the saddle-point approaches and then passes over the pole. In this region special methods must be used. So that the essential features of the wave development do not become obscured, we assume that the system has been in motion long enough for the dispersion to be significant, that is, $Ut \gg 1$.

The stages of the wave development are then as follows.

(*i*) $Ut < x$. As in all models involving an incompressible fluid, a disturbance appears instantaneously throughout the fluid. In general also, since the fluid is infinite in depth, the forward-moving waves will always show dispersive effects in advance of the point Ut. However, under the assumed initial conditions, only the backward-moving waves are excited, and the group velocity corresponding to the frequency (3.4) will be negative: $C_g' = dn'/dk = -\frac{1}{2}Uk^{-\frac{1}{2}}$. The component waves cannot reinforce each other except in the region $x' = C_g't$, that is, $x = Ut(1 - \frac{1}{2}k^{-\frac{1}{2}})$; therefore, in the region $Ut < x$ we may expect completely negligible contributions from (3.1). To show this formally, we note that I_2 may be evaluated

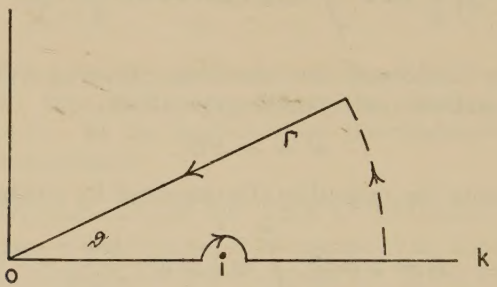

Figure 1. Path for evaluation of integral I_2 when $Ut < x$.

along the path Γ (Fig. 1) and that the angle ϑ is determined by the relative magnitudes of x' and Ut. The integral is thus expressed as a residue term and an asymptotic term:

$$I_2 = -\pi \sin x + 2\,Re \int_0^\infty \exp\{ -x' \sin 2\vartheta\, y^2 - Ut \sin\vartheta\, y \; i\,[x' \cos 2\vartheta\, y^2 + Ut \cos\vartheta\, y]\} \frac{y\,dy}{y^2 - e^{-2i\vartheta}}.$$

The asymptotic term is $0(1/x')$ or $0(1/Ut)$, whichever is smaller; since both of these are negligible compared to the amplitude of the lee wave, using (3.2a) we may write for this region

$$\zeta_0 = 0(1/x') \text{ or } 0(1/Ut)\,. \tag{3.8}$$

(*ii*)[2] When $Ut > x$, the dispersive effects of the backward-moving waves first appear. When $\frac{1}{2}Ut \ll x < Ut$, the classical method of

[2] Readers concerned with the result rather than with its derivation may omit this discussion without loss and skip to Section (iii).

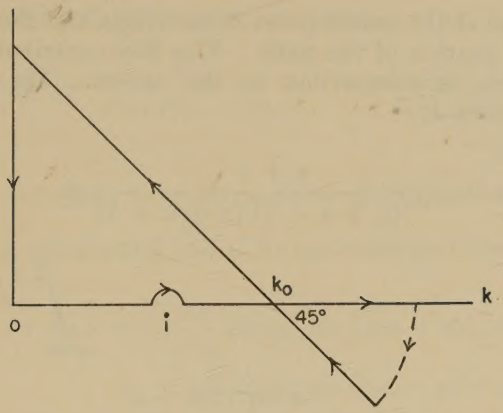

Figure 2. Path for evaluation of integral I_2 when $\frac{1}{2}Ut < x < Ut$.

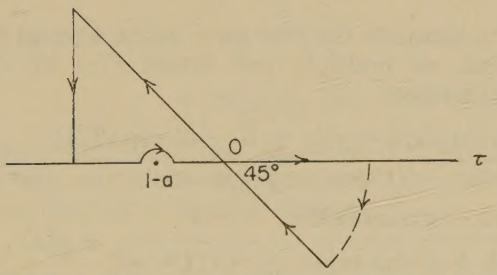

Figure 3. Path for evaluation of integral J when $\frac{1}{2}Ut < x < Ut$.

steepest descent is applicable, but if we are to obtain a formula which has validity also as the time increases and as the saddle-point (3.7) approaches the pole (3.6), we must employ the more general method of Pauli (1938) and Ott (1943). The path is now that in Fig. 2. By the substitution $u^2 = y^2 + Uty/(Ut - x)$, we may write (3.5) as

$$I_2 = 2\,Re\, e^{i(k_0 x - n_0 t)}\, P\, J\,,$$

where

$$J = \int_{-a}^{\infty} e^{-i(Ut-x)u^2} \frac{a + u}{(u + a - 1)\,(u + a + 1)}\, du$$

and

$$k_0 = \tfrac{1}{4}(1 - x/Ut)^{-2}\,,\ n_0 = \tfrac{1}{4}U(2x/Ut - 1)\,(1 - x/Ut)^{-2}\,,$$

$$a = k_0^{\frac{1}{2}}\,. \qquad (3.9)$$

The path is thereby transformed into that shown in Fig. 3. The integral is thus expressible as the sum of the residue term at $u = 1 - a$,

the contribution of the saddle-point at the origin and the contribution of the vertical portion of the path. This last contribution is shown to be negligible in comparison to the others. The contribution of the saddle-point J_s is

$$J_s = \int_{-\sqrt{2}a \exp -i\pi/4}^{\infty \exp -i\pi/4} e^{-i(Ut-x)u^2} \frac{u + a}{(u + a - 1)(u + a + 1)} du$$

$$= \int_{-\sqrt{2}a}^{\infty} e^{-(Ut-x)\tau^2} F(\tau) d\tau ,$$

where

$$F(\tau) = \frac{a \exp i\pi/4 + \tau}{[(1 - a) \exp i\pi/4 + \tau][(1 + a) \exp i\pi/4 + \tau]} ,$$

It is sufficient to compute the first term in the asymptotic expansion. Toward this end, we multiply and divide $F(\tau)$ by $\tau^2 - i(1 - a)^2$, obtaining the expansion

$$F(\tau) = \frac{(a \exp i\pi/4 + \tau)[\tau + U - a) \exp iT/4]}{(1 + a) \exp i\pi/4 + \tau} \cdot \frac{1}{\tau^2 - i(1 - a)^2}$$

$$= \frac{a(1 - a) \exp i\pi/2}{(1 + a) \exp i\pi/4} \cdot \frac{1}{\tau^2 - i(1 - a)^2} + 0(\tau) .$$

Thus the first term in the asymptotic expansion is

$$J_s \sim e^{i\pi/4} \frac{a(1 - a)}{1 + a} \int_{-\sqrt{2}a}^{\infty} e^{-(Ut-x)\tau^2} \frac{d\tau}{\tau^2 - i(1 - a)^2} .$$

Since $a[2(Ut - x)]^{\frac{1}{2}}$ is large, we may treat the lower limit of this integral as infinite. This integral can be transformed into an expression containing the Fresnel integrals. However, it is strange but true that these functions which appear so frequently in mathematical physics have never been tabulated in sufficient detail for even such a simple study as the present one. The only applicable tabulation known to the author is that by Rosser (1948) of a related pair of functions, $Rr(y)$ and $Ri(y)$, defined by the integrals

$$Rr(y) = \frac{\sqrt{2}}{\pi} \int_0^{\infty} e^{-\frac{\pi}{2}y^2\tau^2} \frac{d\tau}{1 + \tau^4} , \qquad Ri(y) = \frac{\sqrt{2}}{\pi} \int_0^{\infty} \tau^2 e^{-\frac{\pi}{2}y^2\tau^2} \frac{d\tau}{1 + \tau^4} .$$

By simple transformations we may show that

$$(1 - a) \int_{-\infty}^{\infty} e^{-(Ut-x)\tau^2} \frac{d\tau}{\tau^2 - i(a-1)^2} = \pi\sqrt{2}e^{-\frac{i\pi}{2}} \{Rr(\alpha) - i\, Ri(\alpha)\} ,$$

where

$$\alpha = (a - 1)[2(Ut - x)/\pi]^{\frac{1}{2}} = (2x - Ut)/[2\pi(Ut - x)]^{\frac{1}{2}} .$$

If this result is substituted into (3.8) and added to the contribution of the pole, we have

$$I_2 = -\pi \sin x + \frac{2^{3/2}\pi a}{1 + a} \{Rr(\alpha) \cos (k_0x - n_0t - \tfrac{1}{4}\pi) + Ri(\alpha) \sin (k_0x - n_0t - \tfrac{1}{4}\pi) \} .$$

The displacement is therefore

$$\zeta_0 = -\frac{2^{3/2}\pi a}{1 + a} \{ Rr(\alpha) \cos (k_0x - n_0t - \tfrac{1}{4}\pi) + Ri(\alpha) \sin (k_0x - n_0t - \tfrac{1}{4}\pi)\} . \quad (3.10)$$

(*iii*) When $\frac{1}{2}Ut \ll x < Ut$, that is, when $a \gg 1$, $\alpha \gg 1$, the sine wave of (3.10) has negligible amplitude and the result[3] is exactly that given by the method of steepest descent,

$$\zeta_0 \doteq \frac{2a}{a^2 - 1}\left[\frac{\pi}{Ut - x}\right]^{\frac{1}{2}} \cos (k_0x - n_0t - \pi/4) . \quad (3.11)$$

These waves begin at x when $Ut = x$ with small wave lengths, small amplitudes, and with phase speed almost equal to the current speed. As time increases at a point they grow in amplitude and wave length, but diminish in phase speed.

(*iv*) As $Ut \to 2x$ and $\alpha \to 0$, the quasi resonance effect discovered by Höiland (1951) augments the amplitude of the sine wave. The result[3] is $\zeta_0 \doteq -\pi \sin (k_0x - n_0t)$.

At the moment $Ut = 2x$, that is, when $a = 1$, $k_0 = 1$, $n_0 = 0$, $\alpha = 0$, we have

$$\zeta_0 = -\pi \sin x . \quad (3.12)$$

[3] The results of (iii) and (iv) may be verified mathematically by substitution into (3.10) of the values of the Rosser functions for large and small arguments, respectively.

$Rr(y) = 1/\pi y - 0(y^{-5})$ $\qquad$ $Rr(y) = \frac{1}{2}\cos \frac{1}{2}\pi y^2 - \frac{1}{2}\sin \frac{1}{2}\pi y^2 + 0(y^3)$

$Ri(y) = 0(y^{-3})$ $\qquad$ $Ri(y) = \frac{1}{2}\cos \frac{1}{2}\pi y^2 + \frac{1}{2}\sin \frac{1}{2}\pi y^2 + 0(y)$

There are no propagating waves at x at this moment, and through this window we can see the stationary lee wave, now developed to one-half its final amplitude. Interpreted differently, the situation at this moment is a result of the fact that the group velocity of the stationary wave ($k_0 = 1$) is exactly $\frac{1}{2}U$.

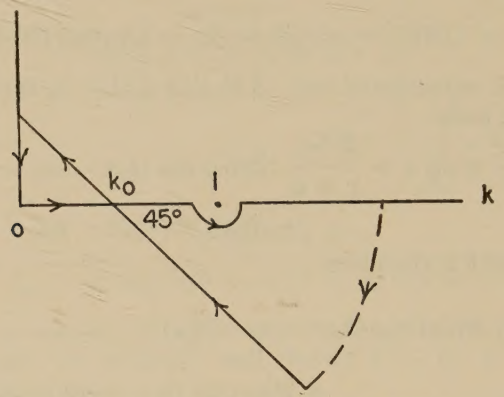

Figure 4. Path for evaluation of integral I_2 when $x < \frac{1}{2}Ut$.

(*v*) When $0 < x \ll \frac{1}{2}Ut$, we may apply the analysis of section (*ii*) to the path shown in Fig. 4. The residue term is now of the opposite sign, and since $a < 1$, we have $[(a-1)^2]^{\frac{1}{2}} = 1 - a$. The equation for the displacement corresponding to (3.10) is therefore

$$\zeta_0 = -2\pi \sin x + \frac{2^{3/2}\pi a}{1+a}\{Rr(\alpha)\cos(k_0x - n_0t - \tfrac{1}{2}\pi) + Ri(\alpha)\sin(k_0x - n_0t - \tfrac{1}{2}\pi)\}, \quad (3.13)$$

where now

$$\alpha = (Ut - 2x)/[2n(Ut - x)]^{\frac{1}{2}}.$$

As the stationary lee wave grows in amplitude, the propagating waves die out. The sine wave rapidly becomes negligible in amplitude, leaving the solution

$$\zeta_0 = -2\pi \sin x - \frac{2a}{1-a^2}\left[\frac{\pi}{Ut - x}\right]^{\frac{1}{2}} \cos(k_0x - n_0t - \tfrac{1}{4}\pi). \quad (3.14)$$

This solution remains valid for all subsequent times, but it is seen that the stationary wave becomes rapidly established as the only sensible disturbance. For example, by the time $Ut = 4x$, $a = \frac{2}{3}$, the ratio of the amplitude of the propagating wave to that of the stationary wave is less than $0.4x^{-\frac{1}{2}}$. Thus if x is one stationary wave length from the origin (2π non-dimensional units), this ratio is about 0.16, and the lee wave is sensibly established.

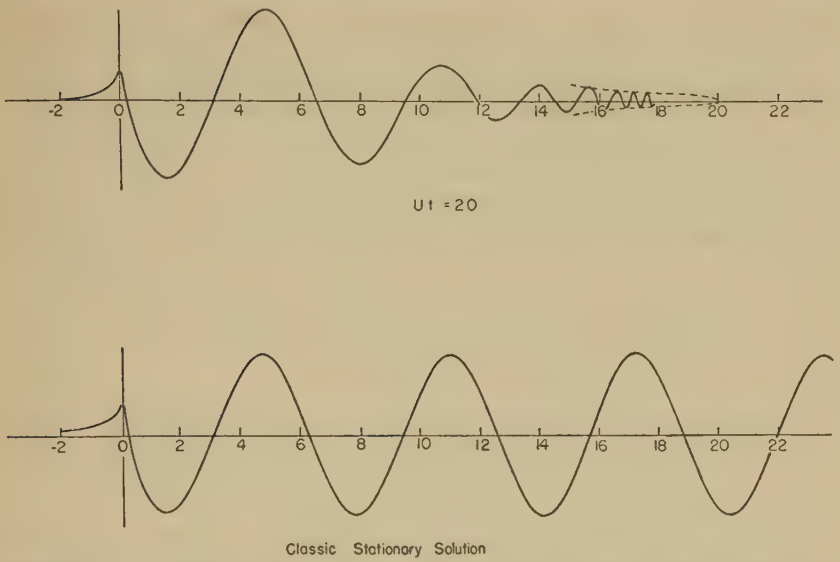

Figure 5. Form of the free surface when $Ut = 20$, with Rayleigh's classical stationary solution for comparison.

(*vi*) When $x < 0$, the analysis of section (v) remains valid. However, in this region the residue term of (3.14) has a different sign whereas that of the stationary integral I_1 in (3.2*a*) does not. These terms cancel, leaving only the transient term

$$\zeta_0 = -\frac{2a}{1-a^2}\left[\frac{\pi}{Ut-x}\right]^{\frac{1}{2}} \cos\left(k_0 x - n_0 t - \tfrac{1}{4}\pi\right). \qquad (3.15)$$

The very long waves have sufficiently high negative group velocities to show dispersive effects in this region, but the group velocity of the stationary wave is always positive. Thus, in this initial-value model, the upstream stationary wave occasions no difficulties because there is no mechanism for its generation. Further, since $a < \frac{1}{2}$ and $Ut - x > Ut$, the amplitudes of the propagating waves are negligible in comparison with the amplitude of the lee wave.

4. *An example computed.* By use of formulas (3.10) and (3.13) a straightforward computation of the elevation of the free surface at any time is possible. Fig. 5 (still in non-dimensional units) shows the system at the moment $Ut = 20$, with the stationary (Rayleigh) solution for comparison. The particle with co-ordinate 20 is therefore the one which was at the origin when the system began from rest. Ahead of it the disturbance exists though it is negligible on

the scale of the diagram. Just behind it the free surface is oscillating rapidly with short wave length, and these oscillations give way further back to a pattern which resembles more and more the stationary wave. At $x = 10$ the amplitude is just half that of the stationary wave, and by $x = 5$, the disturbance is seen to be almost indistinguishable from the classical stationary solution.

The oscillations of the free surface at an isolated point as a function of time are pictured in Fig. 6. The point chosen is $x = 5$, which has an amplitude of 6.03 as $t \to \infty$. The small rapid oscillations

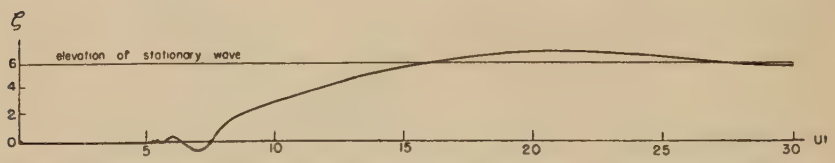

Figure 6. Elevation ζ (5, t) of the free surface at the point $x = 5$, as a function of time.

begin at $Ut = 5$ and end at about $Ut = 7.6$, after which the displacement of the free surface is never negative. This displacement increases steadily until it reaches the stationary value, which occurs at $Ut = 16$. Thereafter, it oscillates about this stationary value with period approaching 8π, but after about $Ut = 20$ it is always within 10% of this value.

NOTE: Since the above paper was presented, two articles, Palm (1953) and Stoker (1953), have appeared on the problem of flow over a corrugated bed. Their models have the advantage of resembling more closely actual flow over an obstacle, but their greater complexity makes it difficult or impossible to examine the transient state of the lee wave in the detail afforded by the model of this paper with a surface pressure disturbance.

REFERENCES

Höiland, E.

1951. Fluid flow over a corrugated bed. Fifth Progress Report, Sierra Wave Project, Contract No. AF 19(122)–263, Appendix A, 33 pp.

Kelvin, Lord

1886. On stationary waves in flowing water. Phil. Mag., Ser. 5, *22:* 353–57, 445–52, 517–70.

Lyra, G.

1943. Theorie der stationären Leewellenströmung in freier Atmosphäre. Z. angew. Math. Mech., *23:* 1–28.

Ott, H.

1943. Die Sattelpunktsmethode in der Umgebung eines Pols. Ann. Phys., Ser. 5, *43:* 393–403.

Palm, E.
1953. On the formation of surface waves in a fluid flowing over a corrugated bed and on the development of mountain waves. Astrophys. Norveg., *5* (3), 129 pp.
Pauli, W.
1938. On asymptotic series for functions in the theory of diffraction of light. Phys. Rev., *54:* 924–31.
Rayleigh, Lord
1883. The form of standing waves on the surface of running water. Proc. Lond. Math. Soc., *15:* 69–78.
Rosser, J. B.
1948. Theory and application of $\int_0^p e^{-x^2}\,dx$. Mapleton House, Brooklyn. 192 pp.
Stoker, J. J.
1953. Unsteady waves on a running stream. Commun. Pure App. Math., *6:* 471–81.
Wurtele, M. G.
1953. On lee waves in the interface separating two barotropic layers. Scientific Report No. 2, Contract No. AF 19(122)–263. 32 pp.

ON CONVECTIVE INSTABILITY OF A ROTATING FLUID WITH A HORIZONTAL TEMPERATURE CONTRAST

By

H. L. KUO

Massachusetts Institute of Technology[1]

ABSTRACT

A simple expression of the criterion for the onset of symmetrical thermal convection of a rotating fluid subject to a horizontal temperature contrast is obtained. It is shown that both the rotation and a positive static stability act to inhibit convection. The extent of these inhibitions depends upon the nondimensional parameters $T = 4\Omega^2 d^4 \nu^{-2}$ and $R = gd^4\kappa^{-1}\nu^{-1}\alpha d\theta_o/dz$, where d denotes the depth of the layer, Ω the rotation rate, α the thermal expansion coefficient, κ the thermometric conductivity, ν the kinematic viscosity, and $d\theta_o/dz$ the vertical temperature gradient. For given values of T and R, the onset of convection requires the nondimensional parameter $Q = gd^4\kappa^{-1}\nu^{-1}\alpha d\theta_o/dr$ to be higher than a critical value Q_c, and furthermore there is a most favorable cell size l_c for which the required value of Q is lowest. Q_c generally increases with T and also increases with l for l larger than l_c. When T is very large, the parameter $K_c = 4dQ_c(lT)^{-1}$, which is the product of a Rossby number and the Prandtl number ν/κ, approaches a constant, suggesting that the onset of such convection in the atmosphere and in the ocean may be determined by this product. In order to examine the possible difference of conditions in systems such as the atmosphere and ocean on the one hand and that in model experiments on the other, two cases are discussed: (a) when the horizontal extent a of the fluid is infinitely large compared with its depth d, and (b) when $a = d$.

INTRODUCTION

The most important factor that keeps the atmosphere in motion is differential heating, particularly that in horizontal directions, since the vertical stratification of the atmosphere is normally stable. Another factor that controls the nature of large scale motions in both atmosphere and ocean is the earth's rotation. In this paper we shall discuss the effects of these two factors. However, because of the complex nature of the motions of these fluid systems, we shall limit ourselves here to a discussion of symmetric thermal convection and leave other types of motion for discussion at a later date.

Some problems concerning symmetric thermal convection in a thin layer of fluid have been discussed in another paper (Kuo, 1954),

[1] The research reported in this paper has been sponsored by the Geophysics Research Directorate, Air Research and Development Command, under Contract No. AF 19(122)–153.

where the relevant equations have been solved in an exact manner. However, the frequency equation derived there is so complicated that the desired information can be obtained only through tedious computations. In this paper we shall discuss symmetric convection by expanding the solution in a double Fourier series with a view to finding a simple approximate expression of the stability criterion for the onset of such motion. Such an approximate method is also useful in dealing with the more complicated asymmetric motions.

Since this type of thermal convection is of particular interest to meteorologists, who commonly believe that the general circulation of the atmosphere is maintained by such a large thermal convection, many attempts have been made to derive such motion from the hydrodynamic equations [for example by Oberbeck (1888), Prandtl (1939), Arakawa (1940) and Davies (1953)]. In most of these efforts the authors assumed fundamentally that the temperature distribution in the fluid is not affected by motion and that this unchanging mean temperature distribution results in an unchanging buoyancy force which drives the symmetric convection continuously. Thus, the motion becomes a forced motion which must therefore be present at all times.

However, a closer scrutiny of these assumptions shows that neither of them are adequate when applied to a fluid system such as the atmosphere. First, in such a shallow layer of fluid with so large a horizontal extent, it is difficult to conceive that the motion of a particle is determined by the mean temperature at points very far away. It must depend primarily upon the temperature or density distribution in its immediate surroundings, i.e., upon the local temperature anomaly. Second, more heat is transported by the motion than by heat conduction, therefore the local temperature anomaly depends directly on the motion. Thus the motion must be treated as a natural motion, in which the velocity field and temperature field are mutually dependent and must be determined simultaneously.

Since the basic concept of the present treatment is quite different from that used by others, it seems worthwhile to dwell again on some of the physical considerations before attacking the problem mathematically. As noted before, we consider the rotation and the differential heating as the two most important factors that determine the motion, the main function of the latter being to produce and to maintain a temperature and thereby a density contrast. It is well known that both rotation and stable stratification tend to suppress the motion whereas the horizontal temperature contrast has the direct effect of increasing the motion by way of the buoyancy force it introduces. Therefore the occurrence of different types of motion under different conditions must have its explanation in the adjustment

of the motion to two different effects, the inhibiting effect of rotation and stable stratification and the motion-producing effect of horizontal temperature contrast. Only when the temperature contrast is large and the rotation rate small can a symmetrical direct thermal convection take place. When the rotation rate is high and the temperature contrast relatively small, the fluid particles are not capable of following such a direct circulation; the motion must then be asymmetrical and more horizontal, hence it must appear as waves in the zonal direction, as shown by Fultz (1951) and Hide (1953).

The problem may also be elucidated by another consideration. Since heat is supplied by a heat source and is removed by a cold source, the motion may be considered a necessity in order to transport heat in addition to heat conduction. Since the total kinetic energy that can be developed in such a fluid system from an initial state of relative rest is determined roughly by the total available potential energy or by the temperature contrast, it may be considered as given by the heating. However, the efficiency of different types of motion in transporting heat is quite different, even when the amount of total kinetic energy is the same, because only the cross-isothermal velocity component can produce a net transfer of heat. Therefore the efficiency of the motion in transporting heat depends upon the nature of the motion which is much affected by rotation. If the rotation rate is not too small and if the motion appears in the form of symmetric convection, then the ratio between the zonal velocity and the meridional velocity is roughly of the order $T^{\frac{1}{2}}$ (Kuo, 1954) while the vertical velocity is comparable with the meridional velocity. Therefore most of the total kinetic energy is in the zonal kinetic energy. On the other hand, the meridional velocity becomes comparable with the zonal velocity in the asymmetric motions, particularly when the wave number is large. Thus, large symmetric convection is far less efficient in transporting heat than the asymmetric motions with larger wave numbers, when the rotation rate is high. Since the net amount of heat transported is proportional to the temperature gradient, symmetric motion must occur together with a larger temperature gradient.

In this paper we shall discuss the stability criterion for the onset of symmetric convection in two different cases. In case (a) we consider the depth of fluid much smaller than the horizontal dimension so that the lateral boundary conditions can be replaced by a harmonic requirement. In case (b) we assume the depth of the layer equal to its horizontal extent. As in the other paper (Kuo, 1954), we consider that a temperature contrast in the radial direction is introduced and is later maintained to a degree within the fluid by heat

conduction. At the initial moment we may assume that the fluid is in purely zonal motion which balances the radial pressure gradient due to the mean temperature contrast, or, more simply, we may assume that the fluid is initially at relative rest. The latter case can be realized by imagining that the finite horizontal temperature contrast is produced suddenly or that the fluid is in a highly viscous state before the initial moment. Our problem is to determine the minimum horizontal temperature contrasts that are required for the onset of symmetric motion at different rates of rotation. The criterion thus obtained may also be the one that marks the transition from the low to the high-rotation regime with the lowest wave number, if the state of solid rotation is to be disturbed at all.

EQUATIONS OF THE PROBLEM

At the initial moment the fluid is at relative rest or in a purely zonal motion with velocity v_0, and a variable mean temperature θ_0 has been produced and maintained in the fluid by external heating so that θ_0 satisfies the steady state heat conduction equation

$$\nabla^2\theta_0 = 0\,, \tag{1}$$

where ∇^2 stands for the standard Laplacian operator.

As is permissible in this problem, we allow for the variation of density due to thermal expansion only in so far as it modifies gravity and introduces a buoyancy force. Thus ρ, which occurs as a factor of g, is replaced by

$$\rho = \bar{\rho}\,(1 - \alpha\Delta\theta)\,, \tag{2}$$

where α denotes the coefficient of thermal expansion, $\bar{\rho}$ the density corresponding to a mean temperature $\bar{\theta}_0$, and $\Delta\theta$ the deviation of the local temperature from θ_0. Where ρ occurs elsewhere in the equations of motion we regard it as a constant equal to $\bar{\rho}$ and we consider the fluid as incompressible during the motion.

We denote the velocity components in the radial, zonal and vertical directions by u, v and w, the departures of local pressure and temperature from the initial mean values p_0 and θ_0 by p and θ, and we assume that all these quantities are independent of the longitude and are small; then the linearized equations of motion, continuity and heat transfer in cylindrical co-ordinates r, ϕ, and z are

$$\frac{\partial u}{\partial t} - 2\Omega v = -\frac{1}{\bar{\rho}}\frac{\partial p}{\partial r} + \nu\left(\nabla^2 u - \frac{u}{r^2}\right) \tag{3}$$

$$\frac{\partial v}{\partial t} + 2\Omega u + w\frac{\partial v_0}{\partial z} = \nu\left(\nabla^2 v - \frac{v}{r^2}\right) \tag{4}$$

$$\frac{\partial w}{\partial t} = g\alpha\theta - \frac{1}{\bar{\rho}}\frac{\partial p}{\partial z} + \nu\nabla^2 w \tag{5}$$

$$\frac{1}{r}\frac{\partial ru}{\partial r} + \frac{\partial w}{\partial z} = 0 \tag{6}$$

and

$$\frac{\partial \theta}{\partial t} + u\frac{\partial \theta_0}{\partial r} + w\frac{\partial \theta_0}{\partial z} = k\nabla^2\theta\,. \tag{7}$$

Here ∇^2 stands for the operator $\frac{1}{r}\frac{\partial}{\partial r}r\frac{\partial}{\partial r} + \frac{\partial^2}{\partial z^2}$ and ν and κ are kinematic viscosity and thermometric conductivity. In equations (3) and (4) we have neglected $\partial v_0/\partial r$ and v_0/r against 2Ω so that the possibility of having inertial instability is eliminated. Since v_0 satisfies the steady state hydrodynamic equations, its vertical variation is determined approximately by the thermal-geostrophic-wind relation

$$\frac{\partial v_0}{\partial z} = \frac{g\alpha}{2\Omega}\frac{\partial \theta_0}{\partial r}\,. \tag{8}$$

Eliminating u from (4) and (6) and neglecting w/r against $\partial w/\partial r$ we obtain

$$\left(\frac{\partial}{\partial t} - \nu\nabla^2\right)\zeta = 2\Omega\frac{\partial w}{\partial z} - \frac{\partial v_0}{\partial z}\frac{\partial w}{\partial r}\,, \tag{9}$$

where $\zeta = r^{-1}\partial(rv)/\partial r$ is the vertical component of the relative vorticity. Multiplying (3) by r, then differentiating with respect to r and z, and making use of the continuity equation we get

$$\left(\frac{\partial}{\partial t} - \nu\nabla^2\right)\frac{\partial^2 w}{\partial z^2} = -2\Omega\frac{\partial \zeta}{\partial z} + \frac{1}{\bar{\rho}r}\frac{\partial}{\partial r}\left(r\frac{\partial^2 p}{\partial r\partial z}\right). \tag{10}$$

Applying the operator $\partial^2/\partial r^2 + r^{-1}\partial/\partial r$ to (5) and combining with (10) we obtain

$$\left(\frac{\partial}{\partial t} - \nu\nabla^2\right)\nabla^2 w = -2\Omega\frac{\partial \zeta}{\partial z} + \frac{g\alpha}{r}\frac{\partial}{\partial r}\left(r\frac{\partial \theta}{\partial r}\right). \tag{11}$$

Eliminating ζ from (9) and (11) and making use of (8) we arrive at the following equation:

$$\left(\frac{\partial}{\partial t} - \nu\nabla^2\right)^2\nabla^2 w + 4\Omega^2\frac{\partial^2 w}{\partial z^2} - g\alpha\frac{\partial \theta_0}{\partial r}\frac{\partial^2 w}{\partial r\partial z} - g\alpha\left(\frac{\partial}{\partial t} - \nu\nabla^2\right)\left(\frac{1}{r}\frac{\partial}{\partial r}r\frac{\partial \theta}{\partial r}\right) = 0\,. \tag{12}$$

In this study we shall find only the lowest mean temperature contrast required for the onset of the symmetric motion. This contrast must correspond to the slowest rate of development, and therefore it can be found by letting $\partial/\partial t$ approach zero, since the developing disturbances are not oscillatory (see Kuo, 1954). We shall therefore put $\partial/\partial t = 0$ in the preceding equations. The elimination of θ between (12) and (7) and use of the continuity equation then give

$$\nabla^6 w + \frac{4\Omega^2}{\nu^2}\frac{\partial^2 w}{\partial z^2} - \frac{g\alpha}{\kappa\nu}\left(1 + \frac{\kappa}{\nu}\right)\frac{\partial\theta_0}{\partial r}\frac{\partial^2 w}{\partial r\partial z} + \frac{g\alpha}{\kappa\nu}\frac{\partial\theta_0}{\partial z}\frac{1}{r}\frac{\partial}{\partial r}\left(r\frac{\partial w}{\partial r}\right) = 0. \quad (13)$$

The second term represents the effect of rotation while the last two terms represent the effects of the horizontal and vertical temperature contrasts respectively. Note that if there is no mean temperature contrast in the horizontal directions, this equation then reduces to the equation discussed by Chandrasekhar (1953) if we replace $\partial^2/\partial r^2 + r^{-1}\partial/\partial r$ by the ordinary two-dimensional Laplacian operator. The presence of the term with the factor $\partial\theta_0/\partial r$ makes this equation more difficult to solve, because the method of separation of variables is not applicable. Since we are more concerned with the effects of different physical factors, we shall introduce some approximations by neglecting certain effects which are due to the particular geometry of the cylindrical vessel. Thus we shall replace $\partial^2/\partial r^2 + r^{-1}\partial/\partial r$ by $\partial^2/\partial r^2$ in the Laplacian operator. Since the side boundary conditions have to be considered, it is more convenient to use the stream function ψ as the dependent variable, which, according to the approximation discussed above, may be defined by

$$u = -\frac{\partial\psi}{\partial z}, \quad w = \frac{\partial\psi}{\partial r}. \quad (14)$$

The differential equation for ψ is then the same as (13), namely

$$\left(\frac{\partial^2}{\partial r^2} + \frac{\partial^2}{\partial z^2}\right)^3\psi + \frac{4\Omega^2}{\nu^2}\frac{\partial^2\psi}{\partial z^2} - \frac{g\alpha}{\kappa\nu}\left(1 + \frac{\kappa}{\nu}\right)\frac{\partial\theta_0}{\partial r}\frac{\partial^2\psi}{\partial r\partial z} + \frac{g\alpha}{\kappa\nu}\frac{\partial\theta_0}{\partial z}\frac{\partial^2\psi}{\partial r^2} = 0. \quad (15)$$

In seeking solutions of this equation we must satisfy certain boundary conditions. Certainly the normal velocity components along the boundaries must vanish, which requires that ψ be constant along

the surfaces $z = 0, z = d, r = 0$ and $r = a$. We denote this stream line by $\psi = 0$. If these boundaries are rigid, then the tangential velocity components must also vanish, which requires that the normal derivative $\partial\psi/\partial n$ and also $\partial^2\psi/\partial r\partial z$ vanish because of the continuity equation. On the other hand, tangential stresses vanish on a free surface, which requires that the second normal derivative $\partial^2\psi/\partial n^2$ be zero. Since the normal velocity vanishes at all points on the boundaries, this latter condition is equivalent to $\nabla^2\psi = 0$. Additional boundary conditions follow from the basic equations. For example, the elimination of p from (3) and (5) gives

$$\nu\nabla^4\psi - 2\Omega\frac{\partial v}{\partial z} = -g\alpha\frac{\partial\theta}{\partial r}. \tag{16}$$

On a horizontal free surface $\partial v/\partial z$ vanishes. If the radial temperature contrast is kept constant on such a surface so that $\partial\theta/\partial r$ is to vanish, then $\Delta^4\psi$ must vanish. For simplicity, we shall treat all boundaries as free surfaces and shall require that $\Delta^4\psi$ vanish on each of them.[2] Therefore our boundary conditions are

$$\psi = 0, \nabla^2\psi = 0 \text{ and } \nabla^4\psi = 0 \tag{17}$$

on the boundaries $z = 0, z = d, r = 0, r = a$.

We now express the solution of (15) in double Fourier series[3]:

$$\psi = \sum_{m=1}^{\infty}\sum_{n=1}^{\infty} A_{mn}\sin\frac{m\pi r}{a}\sin\frac{n\pi z}{d}, \tag{18}$$

which satisfies the boundary conditions (17). Then the problem is to determine the coefficients A_{mn} so as to make (18) a solution of (15). If we substitute (18) in (15) and change m to t and n to s, we obtain

$$\sum_{t=1}^{\infty}\sum_{s=1}^{\infty} A_{ts}\sin\frac{t\pi r}{a}\sin\frac{s\pi z}{d}\left\{\left[\left(\frac{t\pi}{a}\right)^2+\left(\frac{s\pi}{d}\right)^2\right]^3+\frac{4\Omega^2}{\nu^2}\left(\frac{s\pi}{d}\right)^2 + \frac{g\alpha}{\kappa\nu}\frac{\partial\theta_0}{\partial z}\left(\frac{t\pi}{a}\right)^2\right\}+\frac{g\alpha}{\kappa\nu}\left(1+\frac{\kappa}{\nu}\right)\frac{\partial\theta_0}{\partial r} \cdot \sum_{t=1}^{\infty}\sum_{s=1}^{\infty} A_{ts}\cdot\frac{ts\pi^2}{ad}\cdot\cos\frac{t\pi r}{a}\cos\frac{s\pi z}{d} = 0. \tag{19}$$

[2] More realistic boundary conditions can be obtained from (16). However, it is generally impossible to express these conditions in terms of ψ alone.

[3] This method is widely used in the field of elasticity, where the equations dealt with are generally of a lower order. For example; see Seynel, 1933; Trefftz and Willers, 1936.

If we multiply this equation by $\sin(m\pi r a^{-1}) \cdot \sin(n\pi z d^{-1})$ and then integrate over the entire meridional cross-section, and if we make use of the relations

$$\begin{aligned} &\int_0^a \sin^2 \frac{m\pi r}{a}\, dr = \frac{a}{2}, \\ &\int_0^a \sin \frac{m\pi r}{a} \cos \frac{t\pi r}{a}\, dr = \frac{2a}{\pi} \frac{m}{m^2 - t^2} \text{ when } m \pm t \text{ is odd} \\ &\qquad = 0 \text{ when } m \pm t \text{ is even} \end{aligned} \tag{20}$$

and of two similar relations for the z integrations, we obtain

$$\left\{\frac{n^2}{\pi^4} T + \frac{m^2}{\pi^4} \cdot \frac{d^2}{a^2} R + d^6 \left[\left(\frac{m}{a}\right)^2 + \left(\frac{n}{d}\right)^2\right]^3\right\} A_{mn} + mn \frac{d}{a} \cdot C \sum_{t=1}^{\infty} \sum_{s=1}^{\infty} A_{ts} \cdot \frac{t}{m^2 - t^2} \cdot \frac{s}{n^2 - s^2} = 0, \tag{21}$$

where the summations over t and s are for odd $m \pm t$ and $n \pm s$; the even terms vanish. In this equation we have

$$T = \frac{4\Omega^2}{\nu^2} d^4, \quad R = \frac{g\alpha}{\kappa\nu} d^4 \frac{\partial\theta_0}{\partial z}, \quad C = \frac{16}{\pi^6} \frac{g\alpha}{\kappa\nu} \left(1 + \frac{\kappa}{\nu}\right) d^4 \frac{\partial\theta_0}{\partial r}. \tag{22}$$

Thus T is the square of a Reynolds number in terms of which the effect of rotation is measured, sometimes called the Taylor number; $-R$ is the Rayleigh number which plays an important part in the problem of thermal convection produced by a vertical temperature contrast; and C is a parameter representing the effect of the horizontal temperature contrast. We now put eq. (21) in the following simple form:

$$A_{mn} \cdot \frac{\varphi(m,n)}{\beta mn} + C \sum_{t=1}^{\infty} \sum_{s=1}^{\infty} A_{ts} \cdot \frac{t}{m^2 - t^2} \cdot \frac{s}{n^2 - s^2} = 0, \tag{23}$$

where $\varphi(m,n) = n^2 T' + m^2\beta^2 R' + (n^2 + m^2\beta^2)^3$, with $T' = \pi^{-4} T$, $R' = \pi^{-4} R$ and $\beta = da^{-1}$.

An examination of eq. (21) shows that there are two mutually independent systems of equation; one system is for the unknowns A_{mn} with $m + n$ even, the other is for the unknowns with odd $m + n$. Thus, if $m + n$ is even, we must have both m and n even or both must be odd. Both t and s are then odd or even, since only terms with odd $m \pm t$ and $n \pm s$ occur. On the other hand, if the sum of m and n is odd, then one must be even while the other must be odd,

hence the sum of t and s is also odd. In each of these two systems the number of the unknowns and the number of equations is infinite. Since these are homogeneous equations, the determinant Δ formed by the coefficients of these unknowns must be zero. The equation $\Delta = 0$ gives the required critical values of C for given values of T and R.

However, this procedure of computing the critical values can be carried out only when Δ converges rapidly, which requires that there be only a finite number of A_{mn} so that these unknowns can be computed to a sufficient degree of accuracy by neglecting all the other unknowns in the system. This is equivalent to saying that solution (18) can be approximated by a finite number of terms. The mathematical problem is to make this series representation converge rapidly, which requires different arrangements for different cases.

CASE A. A THIN LAYER OF FLUID WITH LARGE HORIZONTAL EXTENT

In this case we assume that the horizontal dimension a is infinitely large compared with the depth d, so that the length ratio $\beta = d/a \to 0$. This case has been discussed by an exact method (Kuo, 1954). In order to express the results more clearly, we shall derive an approximate formula for the critical temperature contrast by the present method. For this case a finite m represents an infinitely large horizontal wave length; the critical C thus obtained is evidently infinity. To have a finite horizontal wave length, m and t must be of the same order of magnitude as the length ratio $\beta^{-1} = a/d$. When β^{-1} approaches infinity, m and t must also approach infinity, so that βm approaches a finite value λ. Thus we put

$$m = \frac{\lambda}{\beta} + m_1 = p + m_1 \qquad t = p + t_1 \tag{24}$$

where m_1 and t_1 are finite integers with zero included and λ is a finite number so that $\lambda\beta^{-1} = p$ is an integer. When $\beta \to 0$, we have $p >> m_1$ and $p >> t_1$ and therefore

$$\frac{t}{m^2 - t^2} \doteq \tfrac{1}{2}\frac{1}{m_1 - t_1}, \qquad l = \frac{a}{m} = \frac{d}{\lambda + \beta m_1} \doteq \frac{d}{\lambda},$$

where l is the horizontal half wave length. The function $\varphi(m,n)$ is then given by

$$\varphi(m,n) \doteq n^2T' + \lambda^2R' + (n^2 + \lambda^2)^3 = \varphi(\lambda,n).$$

Thus equation (23) becomes

$$A_{p+m_1,n}\frac{\varphi(\lambda,n)}{\lambda n} + \tfrac{1}{2}C\sum_{t_1=-\infty}^{\infty}\sum_{s=1}^{\infty}A_{p+t_1,s}\cdot\frac{1}{m_1-t_1}\cdot\frac{s}{n^2-s^2} = 0\,. \quad (25)$$

Here we must determine the characteristic value of C by solving the determinant of this system of equations, which contains two mutually independent systems, one with even m_1+n and even t_1+s, another with odd m_1+n and odd t_1+s. For the present case these two systems give the same characteristic value of C. We shall use the second system, with odd m_1+n and odd t_1+s. We then have the following relations

$$A_{p+m_1,n} = +A_{p-m_1,n} \text{ when } n \text{ is odd},$$

$$A_{p+m_1,n} = -A_{p-m_1,n} \text{ when } n \text{ is even}. \quad (26)$$

We may divide the unknowns $A_{p+m_1,n}$ and $A_{p+t_1,s}$ into two different classes, one class with even n or s and one class with odd n or s. Thus, if $A_{p+m_1,n}$ belongs to one class, then all the other unknowns $A_{p+t_1,s}$ belong to the other class, because if s is odd then n must be even, and vice versa. Since the $A_{p+t_1,s}$ always occur with C, we may take $CA_{p+t_1,s}$ as the unknowns and write equation (25) in the following form

$$\frac{2\varphi(\lambda,n)}{\lambda\cdot n}A_{p+m_1,n} + \sum_{t_1=-\infty}^{\infty}\sum_{s=1}^{\infty}CA_{p+t_1,s}\frac{1}{m_1-t_1}\frac{s}{n^2-s^2} = 0\,. \quad (27)$$

In this way C occurs in the form of C^{-2} in some coefficients and does not occur in the others. We shall compute the determinant of this system of equations by using only the first fourteen, letting m_1 and t_1 take the values of the nine integers from -4 to $+4$ and letting n and s take the values from 0 to 3. However, because of the relations (26), we actually have eight equations, of which the coefficients of the eight unknowns, written in the form of (27), are given in Table I. It is seen that C^{-2} occurs only in two of the diagonal coefficients, hence the determinant is a quadratic equation in C^2.

We note that the sixth order determinant Δ_6, formed by the first six coefficients, is a diagonal determinant; therefore the eighth order determinant formed by the coefficients given in Table I can be reduced to the product of Δ_6 and a second order determinant Δ_2. Thus, multiplying the first row by $-\lambda/3\varphi(\lambda,1)$, the second row by $9\lambda/5\varphi(\lambda,3)$, the third row by $2\lambda/9\varphi(\lambda,1)$, the fourth row by $-6\lambda/5\varphi(\lambda,3)$, the fifth row by $2\lambda/45\varphi(\lambda,1)$ and the sixth row by $-6\lambda/25\varphi(\lambda,3)$, and by adding to the seventh row, all of the first six elements of the seventh row are reduced to zero while the last two elements of this row become

Table I The coefficients of the unknowns of equation (27).

$(p+m,1)\cdot n$ / $A_{p+t,s}$	$A_{p,1}$	$A_{p,3}$	$A_{p+2,1}$	$A_{p+2,3}$	$A_{p+4,1}$	$A_{p+4,3}$	$CA_{p+1,2}$	$CA_{p+3,2}$
$p\cdot 1$	$\frac{\varphi(\lambda,1)}{\lambda\cdot 1}$	0	0	0	0	0	$\frac{2}{3}$	$\frac{2}{9}$
$p\cdot 3$	0	$\frac{\varphi(\lambda,3)}{\lambda\cdot 3}$	0	0	0	0	$-\frac{2}{5}$	$-\frac{2}{15}$
$(p+2)\cdot 1$	0	0	$\frac{\varphi(\lambda,1)}{\lambda\cdot 1}$	0	0	0	$-\frac{2}{9}$	$\frac{2}{5}$
$(p+2)\cdot 3$	0	0	0	$\frac{\varphi(\lambda,3)}{\lambda\cdot 3}$	0	0	$\frac{2}{15}$	$-\frac{6}{25}$
$(p+4)\cdot 1$	0	0	0	0	$\frac{\varphi(\lambda,1)}{\lambda\cdot 1}$	0	$-\frac{2}{45}$	$-\frac{2}{7}$
$(p+4)\cdot 3$	0	0	0	0	0	$\frac{\varphi(\lambda,3)}{\lambda\cdot 3}$	$\frac{2}{75}$	$\frac{6}{35}$
$(p+1)\cdot 2$	$\frac{1}{3}$	$-\frac{3}{5}$	$-\frac{2}{9}$	$\frac{2}{5}$	$-\frac{2}{45}$	$\frac{2}{25}$	$\frac{\varphi(\lambda,2)}{\lambda}C^{-2}$	0
$(p+3)\cdot 2$	$\frac{1}{9}$	$-\frac{1}{5}$	$\frac{2}{5}$	$-\frac{18}{25}$	$-\frac{2}{7}$	$\frac{18}{35}$	0	$\frac{\varphi(\lambda,2)}{\lambda}C^{-2}$

$$a_{77} = \frac{\varphi_2}{\lambda C^2} - \frac{554\lambda}{2025\varphi_1} - \frac{554\lambda}{625\varphi_3}, \qquad a_{78} = \frac{2\lambda}{945\varphi_1} + \frac{6\lambda}{875\varphi_3},$$

where φ_n is written for $\varphi(\lambda,n)$. In a similar manner, we multiply the first six rows by $-\lambda/9\varphi_1$, $3\lambda/5\varphi_3$, $-2\lambda/5\varphi_1$, $54\lambda/25\varphi_3$, $2\lambda/7\varphi_1$ and $-54\lambda/35\varphi_3$, respectively, and by adding to the eighth row, the first six elements of this row are then reduced to zero while the last two elements become

$$a_{87} = \frac{2\lambda}{35}\left(\frac{1}{27\varphi_1} + \frac{3}{25\varphi_3}\right), \quad a_{88} = \frac{\varphi_2}{\lambda C^2} - \frac{26426\lambda}{1225}\left(\frac{1}{27\varphi_1} + \frac{3}{25\varphi_3}\right).$$

In this way we find $\Delta = \Delta_6 \cdot \Delta_2$, where Δ_2 is the second order determinant formed by a_{77}, a_{78}, a_{87} and a_{88}. Since Δ_6 is always positive, we must have Δ_2 equal to zero, i.e.,

$$\Delta_2 = \begin{vmatrix} a_{77} & a_{78} \\ a_{87} & a_{88} \end{vmatrix} = 0. \tag{28}$$

This gives a quadratic equation in $\chi = \varphi_2 C^{-2}/2\lambda$,

$$x^2 - \frac{26786}{3675} bx + \frac{3659776}{275625} b^2 = 0, \tag{29}$$

where $b = \dfrac{\lambda}{27\varphi_1} + \dfrac{3\lambda}{25\varphi_3}$. The two roots are $\chi_1 = 3.701b$ and $\chi_2 = 3.585b$ respectivcly.[4] The former gives the lower value of C^2 and

[4] If only the first seven equations in table I are used, the determinant reduces to $a_{77} = 0$ which gives $x = 3.6933b$. The value of C so obtained is only slightly higher than that given by $\Delta_2 = 0$.

is therefore the one we want. From χ_1 we find that the critical values of C^2 are given by

$$C^2 = \frac{675}{7.402} \cdot \frac{1}{\lambda^2} \cdot \frac{\varphi_1 \cdot \varphi_2 \cdot \varphi_3}{81\varphi_1 + 25\varphi_3}, \tag{30}$$

where $\varphi_n = n^2T' + \lambda^2R' + (n^2 + \lambda^2)^3$. From this formula we see that, as $T' \to \infty$, C becomes proportional to T' and inversely proportional to λ. The asymptotic value of C is

$$\lim_{T' \to \infty} C = 3.28 \frac{T'}{\lambda} = 3.28 \frac{l}{d} T'. \tag{31}$$

This asymptotic value is approached rapidly as $T(= \pi^4 T')$ becomes larger than 5×10^3. Thus, for fairly large Taylor numbers, the critical temperature contrast required to produce a symmetric convection is proportional to the square of the rotation rate as well as to the horizontal dimension of the convection.

Formula (30) shows that, for any given values of T and R, there is a particular value of $\lambda = \lambda_c$ for which C^2 is a minimum. This λ_c is the root of the equation

$$\frac{dC^2}{d\lambda} = 0. \tag{32}$$

The value of C corresponding to this value of λ is an absolute minimum below which no symmetric motion is possible. We denote this C by C_m. When the value of C reaches the value C_m, symmetric convection with the horizontal dimension $l_c = d \cdot \lambda_c^{-1}$ will appear. When C is above C_m, larger and smaller convective cells may also be produced. The values of λ_c for different Taylor numbers and zero R are given in Table II, together with the minimum horizontal temperature contrast, represented by the minimum value of the parameter Q, given by

$$Q_c = \frac{\pi^6}{16} C = \left(1 + \frac{k}{\nu}\right) \frac{gd^4}{k\nu} \alpha \frac{\partial \theta_0}{\partial r} = 0.5968\, \pi^6 \frac{l}{d} \left(\frac{\varphi_1 \cdot \varphi_2 \cdot \varphi_3}{81\varphi_1 + 25\varphi_3}\right)^{\frac{1}{2}}. \tag{33}$$

The variations of Q_{cm} as a function of T are illustrated in curve a of Fig. 1.

The minimum values of Q_c in Table II, given by formula (33), correspond to $\lambda = \lambda_c$ and are to be compared with values obtained from the exact solutions (Kuo, 1954). As expected, these values are slightly higher than those obtained from the exact solutions. However, the difference is small for small values of T and is less than 1% for T smaller than 10^3; the difference is only 6.7% for $T = 10^6$. In view of the simplicity of this formula and the ease with which the

Table II. Minimum critical values of Q, P and K corresponding to $\lambda = \lambda_c = d/l_c$, for the case when the vertical stability is zero.

T	λ_c	Q_c	P_c	K_c
0	0.5868	2,747	6,448	∞
10	0.5990	2,810	6,733	673.30
50	0.6395	3,039	7,774	155.50
10^2	0.6791	3,291	8,940	89.40
5×10^2	0.8507	4,766	16,218	32.40
1.0×10^3	0.9644	6,146	23,709	23.70
2.5×10^3	1.1576	9,391	43,484	17.40
5.0×10^3	1.3390	13,736	73,570	14.71
1.0×10^4	1.5530	20,975	130,297	13.03
2.5×10^4	1.8870	38,714	292,213	11.69
5.0×10^4	2.1860	63,500	556,000	11.12
1.0×10^5	2.5094	106,449	1,069,000	10.69
5.0×10^5	3.4360	371,000	5,090,000	10.18
1.0×10^6	3.8990	646,500	10,070,000	10.07
∞		∞	∞	8.10

different physical factors can be discussed, including those involving the vertical stability, and in view of the enormous computation required to obtain information from the exact solutions, we may consider this approximate result quite satisfactory.

Since the critical temperature contrast becomes proportional to the horizontal dimension l for large values of T and $l > l_c$, it is more convenient to use the parameter $p = 4dl^{-1}Q$ instead of Q, especially for large values of T since p_c is nearly independent of l. The values of p_c corresponding to $\lambda \leqslant \lambda_c$ are also given in Table II and are plotted against T in Fig. 2. These values and the graphs show that Q_{cm}, p_c and λ_c increase as T increases, and that, as $T \to \infty$, $Q_{cm} \alpha T^{0.79}$ and $\lambda_c \alpha T^{0.21}$, so that p_c becomes directly proportional to T. Thus, when the rotation rate is high, not only is a larger horizontal temperature contrast required to produce symmetric convection but the motion also tends to break up into cells of smaller horizontal dimensions.

In Fig. 2, the parameters p and T obtained from experimental data on symmetric convection, supplied by Dr. Fultz (as yet unpublished) and Miss Sabin (1954), have also been entered. The theoretical curve for $a = d$, which will be derived in the following, is also plotted in Fig. 2.

Since p_c becomes proportional to T and varies but little with l for large values of T and $l > l_c$, its ratio to T approaches a constant as T increases. We denote this ratio by K_c, which is given by

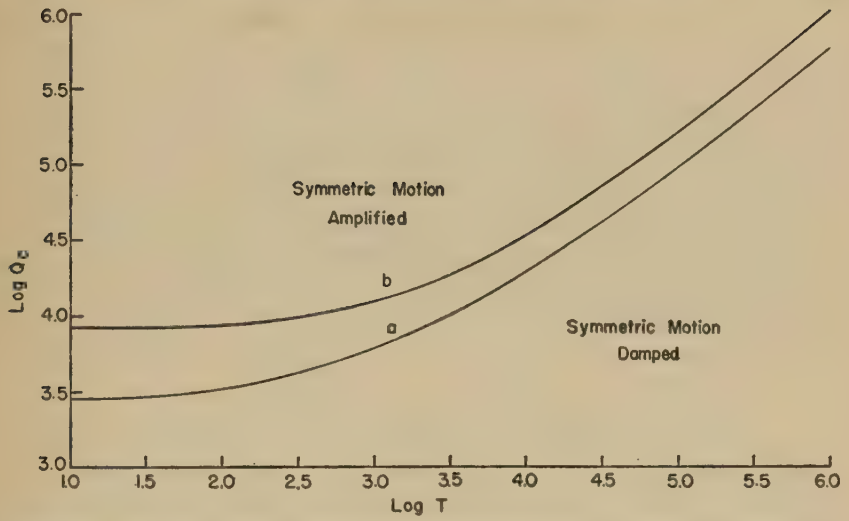

Figure 1. Variation of the critical value of Q for the onset of symmetric convection as a function of T for two cases: (a) when the horizontal extent of the fluid is infinitely large as compared with depth; (b) when the horizontal extent is equal to depth.

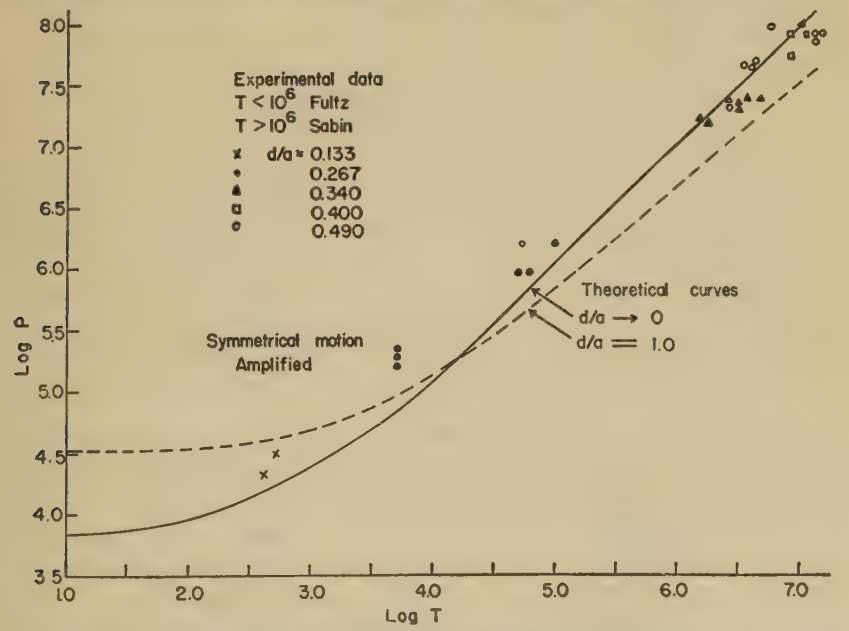

Figure 2. The variation of the parameter p as a function of T. The experimental data are obtained from Dr. Fultz' and Miss Sabin's (1954) observations on the fully developed symmetric motions.

$$K_c = \frac{4d}{l}\frac{Q_c}{T} = \left(\frac{\nu}{k} + 1\right)\frac{gd}{\Omega^2 l}\alpha\left(\frac{\partial\theta_0}{\partial r}\right)_c . \tag{34}$$

The asymptotic value of K_c corresponding to an infinite T is 8.10. This asymptotic value is approached rapidly when T becomes larger than 5×10^3 and even more so when l is larger than l_c.

It may be noted that the factor $gdl^{-1}\Omega^{-2}\alpha\partial\theta_0/\partial r$ depends primarily on the heating and the rotation. We shall call this factor the Rossby number. Thus, when the Taylor number is large ($T > 5 \times 10^3$) and R is positive, the criterion for the motion can also be represented by the product of a properly defined Rossby number and the Prandtl number ν/k.

CASE B. A LAYER OF FLUID WITH A DEPTH EQUAL TO ITS HORIZONTAL EXTENT

Although the ratio of depth to horizontal extent in Case A is similar to that of the earth's atmosphere and oceans, such a ratio can hardly be reproduced in a model experiment. In order to examine the effect of this ratio on the motion, we shall discuss in this section another case with depth d equal to horizontal extent a. For this case, equation system (21) may be written

$$\frac{1}{mn}\varphi_{mn} A_{mn} + \sum_{t=1}^{\infty}\sum_{s=1}^{\infty} CA_{ts}\frac{t}{m^2 - t^2}\cdot\frac{s}{n^2 - s^2} = 0 , \tag{35}$$

where $\varphi_{mn} = n^2T' + m^2R' + (m^2 + n^2)^3$.

As noted before, the system of equations (35) contains two mutually independent systems, the first with $m + n$ and $t + s$ even, the second with odd $m + n$ and odd $t + s$. For this case, the first system gives the lowest Eigen-value C; therefore we shall compute C from this system by using only the first eight equations with both m and n and also t and s, taking the values of the five integers from 1 to 4.

The coefficients of the unknowns in these equations are given in Table III, where we have used CA_{mn} as the unknown for even m and even n.

We note that C^{-2} occurs in only four of the diagonal coefficients; therefore the determinant is a quartic equation in C^2 which has four roots, which we can show are real. By clearing the fractions of the diagonal elements, we obtain a symmetric determinant. A quartic equation of C^2 is also obtained if we use the first 13 equations of (35) and take integers for m and n as well as t and s from 1 to 5. On the other hand, if we use only the first five equations by taking m and n and t and s from 1 to 3, then the determinant reduces to a linear equation in C^2 which is given by

$$C^2 = \frac{\varphi_{22}}{16} \cdot \frac{1}{\frac{1}{81\varphi_{11}} + \frac{1}{25\varphi_{13}} + \frac{1}{25\varphi_{31}} + \frac{81}{625\varphi_{33}}}. \tag{36}$$

This solution represents a fairly accurate approximation to the lowest root of the quartic equation obtained from the eighth order determinant of the system in Table III. Since we are concerned with only the rough values of C, it suffices to use this simple expression. The critical values of Q computed from this approximate solution for different values of T and $R = 0$ are given in Table IV and are ploted in curve b of Fig. 1. The corresponding values of K are also given in Table IV.

Table III. The coefficients of the unknowns of equation (35).

$A_{r,s}$ / m,n	A_{11}	A_{13}	A_{31}	A_{33}	CA_{22}	CA_{24}	CA_{42}	CA_{44}
1·1	$\frac{1}{1\cdot1}\varphi_{11}$	0	0	0	$\frac{4}{9}$	$\frac{8}{45}$	$\frac{8}{45}$	$\frac{16}{225}$
1·3	0	$\frac{1}{1\cdot3}\varphi_{13}$	0	0	$-\frac{4}{15}$	$\frac{8}{21}$	$-\frac{8}{75}$	$\frac{16}{105}$
3·1	0	0	$\frac{1}{3\cdot1}\varphi_{31}$	0	$-\frac{4}{15}$	$-\frac{8}{75}$	$\frac{8}{21}$	$\frac{16}{105}$
3·3	0	0	0	$\frac{1}{3\cdot3}\varphi_{33}$	$\frac{4}{25}$	$-\frac{8}{35}$	$-\frac{8}{35}$	$\frac{16}{49}$
2·2	$\frac{1}{9}$	$-\frac{1}{5}$	$-\frac{1}{5}$	$\frac{9}{25}$	$\frac{1}{2\cdot2}\varphi_{22}C^{-2}$	0	0	0
2·4	$\frac{1}{45}$	$\frac{1}{7}$	$-\frac{1}{25}$	$-\frac{9}{35}$	0	$\frac{1}{2\cdot4}\varphi_{24}C^{-2}$	0	0
4·2	$\frac{1}{45}$	$-\frac{1}{25}$	$\frac{1}{7}$	$-\frac{9}{35}$	0	0	$\frac{1}{4\cdot2}\varphi_{42}C^{-2}$	0
4·4	$\frac{1}{225}$	$\frac{1}{35}$	$\frac{1}{35}$	$\frac{9}{49}$	0	0	0	$\frac{1}{4\cdot4}\varphi_{44}C^{-2}$

Table IV. Critical values of Q and K for the two cases. Both are for $R = 0$ and $l = d$.

T	Q_{cb}	K_{cb}	Q_{ca}	K_{ca}
0	8320	∞	3580	∞
10	8350	3350	3620	1450
50	8590	688	3710	297
10^2	8850	355	3850	154
5×10^2	10700	85.6	4900	39.2
10^3	12650	50.7	6150	24.6
2.5×10^3	17350	27.8	9620	15.4
5.0×10^3	24100	19.3	15100	12.1
10^4	33500	13.5	26600	10.6
2.5×10^4	59000	9.5	56500	9.1
5.0×10^4	95000	7.6	107000	8.6
10^5	165000	6.6	208000	8.3
5×10^5	660000	5.3	1015000	8.1
10^6	1270000	5.1	2024000	8.1
∞	∞	4.8	∞	8.1

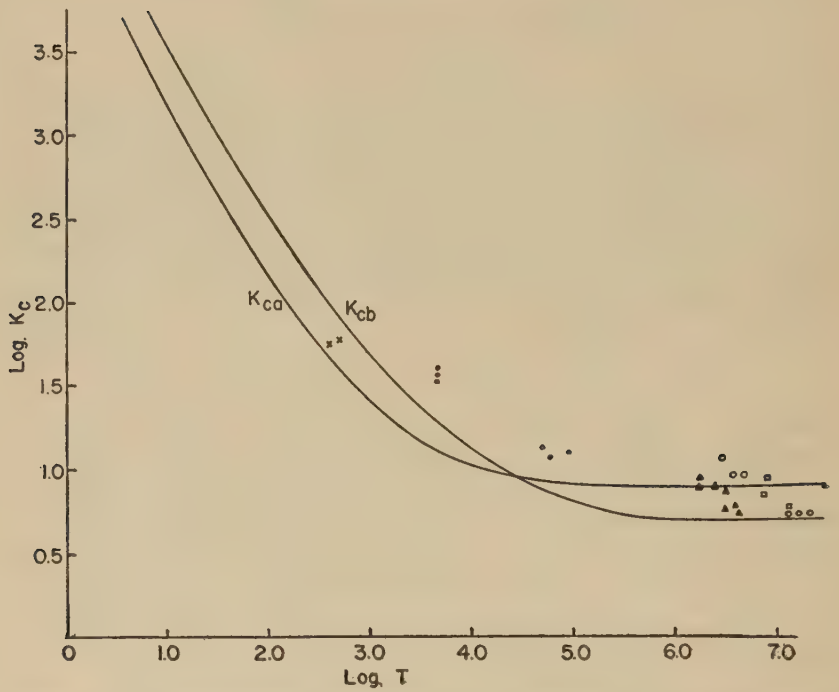

Figure 3. The variation of the critical value of K as a function of T for the symmetric convection with $l = d$. K_{ca} is for case A, K_{cb} for case B. Experimental data are the same as in Fig. 2.

As expected, the critical values of Q for this case, as given by Q_{cb} in Table IV are 2 to 3 times larger than those in Table II. This is due partly to the effect of the lateral boundaries and partly to the horizontal scale of the motion. In order to get a clearer idea of the effect of the ratio of depth to lateral extent, we may also compute the critical values of Q and K from eq. (33) by putting $l = d$. These values are given in the last two columns of Table IV as Q_{ca} and K_{ca}. Here, for values of T smaller than 2.5×10^4, Q_{cb} is larger than Q_{ca}, indicating the preponderance of the boundary effect. On the other hand, for values of T larger than 2.5×10^4, Qcb becomes smaller than Q_{ca}, indicating the difficulty of producing large scale symmetric convection in a shallow layer of fluid. We also note that the asymptotic value of K_c for case B is 4.8 as compared with the asymptotic value of 8.1 for case A. Since the ratio used in most experiments is generally between the limits of these two cases, we may take the asymptotic value of K_c to be within the limits 4.8 and 8.1. The variations of K_{ca} and K_{cb} are represented in Fig. 3.

SUMMARY OF RESULTS

The results show that the onset of symmetric convection in each case requires that the nondimensional parameter Q be above a certain critical value Q_c which increases with the rotation. Therefore, the effect of rotation is to inhibit the convection, the extent of which depends on the nondimensional parameter T. The effect of the vertical temperature distribution, represented by the parameter R, is to inhibit convection if the temperature increases upward ($R > 0$) and to facilitate convection if the temperature decreases upward ($R < 0$). In applying the results to symmetric convection in the atmosphere, the vertical temperature gradient should be replaced by the vertical gradient of the potential temperature which normally increases upward. This effect is included in equations (33) and (36). However, since it is similar to the effect of rotation, we may also consider that it is included in the effect of rotation by modifying the value of T.

For case A, the lowest critical value of Q for any given values of T and R is associated with a certain horizontal scale l_c which decreases as T increases. When T is large ($T > 5 \times 10^3$), Q_c rapidly becomes proportional to $T^{0.79}$ and to the horizontal dimension l of the cell for all values of l larger than $l_c(p_c = 4dl^{-1}Q_c\alpha T)$; thus the parameter $K_c = 4dl^{-1}Q_cT^{-1}$ rapidly approaches a constant value, showing that the onset of large symmetric convection in a shallow layer of fluid such as the atmosphere and the oceans is determined by the parameter K. This parameter may be expressed as the product of a Rossby number and Prandtl number. The asymptotic value of K for case A is 8.1.

For case B, the critical values of Q are generally 2 to 3 times larger than the minimum values obtained in case A. However, the values of Q obtained from eq. (33) by putting $l = d$ become larger than those of case B when T is larger than 2.5×10^4, showing that it is more difficult to produce large symmetric convective motions in a thin layer of fluid when the rotation rate is great.

The results obtained in this investigation may have many applications in both atmosphere and oceans, which are more nearly represented by case A. Thus we may find the minimum horizontal temperature gradient required for the onset of symmetric convection with a certain vertical dimension d at any latitude, or we may compute the maximum horizontal scale of the motion when the horizontal temperature gradient is given. A rough computation shows that meridional cells of the horizontal dimensional of 10 to 20 latitude degrees may exist near to the equator but not in middle and higher latitudes.

REFERENCES

Arakawa, H.
1940. Die Arbeiten zur allgemeinen Zirculation der Atmosphäre Von A. Oberbeck. Beitr. Geophys., *57:* 20–28.

Chandrasekhar, S.
1953. The instability of a layer of fluid heated below and subject to Coriolis forces. Proc. roy. Soc., (A) *217:* 306.

Davies. T. V.
1953. The forced flow of a rotating viscous liquid which is heated from below. Philos. Trans., (A) *246:* 81–112.

Fultz, D.
1951. Experimental analogies to atmospheric motion. Compendium of Meteorology. Amer. Met. Soc., p. 1235.

Hide, R.
1953. Fluid motions in the earth's core; and some experiments on thermal convection in a rotating fluid. Symposium on model experiments. Dept. Civil Engng. Johns Hopkins Univ., September 1–4, 1953.

Kuo, H. L.
1954. Symmetric disturbances in a thin layer of fluid subject to a horizontal temperature gradient and rotation. J. Meteor., *11:* 399–411.

Oberbeck, A.
1888. Ueber die Bewegungserscheinungen in der Atmosphäre. S. B. preuss. Akad. Wiss., 383–395, 1129–1138.

Prandtl, L.
1939. Beiträge zur Mechanik der Atmosphäre. P. Dupont, Paris, 1–32.

Sabin, B. A.
1954. A qualitative study of some of the critical parameters for the "dishpan" model of the atmosphere. Mass. Inst. of Technology (uupublished B.Sc. thesis).

Seynel, E.
1933. Ueber das Ausbeulen von rechteckigen, isotropen oder orthogonal-anisotropen platten bei Schubbeanspruchung. Ing. Archiv, *4:* 169–191.

Trefftz, E. and Fr. A. Willers
1936. Die Bestimmungen der Schubbeansprung beim Ausbeulen rechtiger platten. Z. angew. Math. Mech., *16:* 336–344.

INTERPRETATION OF SPECTROPHOTOMETER READINGS ON CHESAPEAKE BAY WATERS[1]

By

WAYNE V. BURT[2]

Chesapeake Bay Institute, The Johns Hopkins University

ABSTRACT

Numerical results of the Mie theory of scattering of light energy by suspended particles have been applied to light extinction measurements obtained from waters of Chesapeake Bay and its major tributaries. A Beckman Model DU Quartz Prism Spectrophotometer with 10 and 50 cm liquid absorption cells was used on raw and filtered samples to determine the extinction as a function of wave length. Extinction in these waters is primarily due to absorption and scattering by suspended materials. Application of theory to observed data indicates that a large share of the particles that cause the extinction are less than one micron in radius and that these particles occur in concentrations ranging from less than one to approximately 60 ppm by volume.

INTRODUCTION

This study was undertaken to determine some quantitative facts about the physical processes involved in the attenuation of light in turbid natural waters and to find out something about the materials causing the attenuation. Some 25,000 extinction readings were made aboard ship on freshly drawn samples which were collected as part of the regular survey work in the Chesapeake Bay and its tributaries. Observations covered the entire range of depths and seasons over the whole of the Bay system. The data are presented in the *Data Report* series of the Chesapeake Bay Institute.

This paper shows that the characteristic curve of extinction against the wave length of light for the visible part of the spectrum may be interpreted in terms of the Mie theory. From this interpretation estimates may be made of the size range, size distribution, and concentration of suspended materials. A second paper (Burt, 1955; see page 47 of this issue) furnishes material on the seasonal, areal, and depth distributions, as functions of the extinction measured at

[1] Contribution No. 21 from the Chesapeake Bay Institute. Results of work carried out for the Office of Naval Research of the Navy Department, the State of Maryland (Department of Research and Education), and the Commonwealth of Virginia (Virginia Fisheries Laboratory) under contract with The Johns Hopkins University.

[2] Now at the Department of General Science, Oregon State College.

several wave lengths. Further studies are being made on the relation of extinction to the absolute values of the particle distribution.

Some of the material contained in this paper is taken from Burt (1952), which contains a more complete discussion of the problem. Errors in calculation in that paper have been corrected and the material has been amended to conform with more complete and exact computations for the application of the Mie theory which have recently become available. In addition, some terminology has been changed to conform with that of Middleton (1952) and Penndorf (1953).

INSTRUMENTATION AND SAMPLING METHOD

The instrument used in this study had to supply information which would make possible a plot of extinction against wave length across the whole visible light spectrum, and furthermore, it had to be usable aboard ship. The only instrument which met these requirements is the Beckman Spectrophotometer. Methods for using the instrument as well as information on its accuracy and limitations are given by Cary and Beckman (1941), Gibson and Balcom (1947) and Caster (1951).

The instrument is designed for use on nonturbid media. Some sources of error which occur when the instrument is used to measure extinction in turbid media have been discussed and partially evaluated by Burt (1952).

Water samples were pumped aboard from desired depths through an ordinary garden hose by a rubber impeller "Jabsco" pump, and samples were drawn before they reached the pump. To minimize changes in transparency due to chemical and biological activity during storage, extinction measurements were made in the Spectrophotometer soon after the samples were drawn.

THEORY

Measurements in the Beckman Spectrophotometer eliminate the effects of the water itself, since the instrument is adjusted to read 100% transmission through a distilled water blank. Extinction measurements on both filtered ("fine" Berkefeld Filter) and unfiltered samples from Chesapeake Bay have shown that the extinction in the waters examined may be considered as being due primarily to suspended material, since the effects of filterable material are usually considerably greater than the effects of filter passing material (Burt, 1953). Clarke and James (1939) reported that filtered sea water was optically similar to distilled water. The Beckman Spec-

trophotometer reads in optical density E_λ, which is defined as the negative logarithm to the base ten of the fraction of light energy which passes through the cell. Thus

$$b_{a,p} + b_{s,p} = PE_\lambda, \tag{1}$$

where the proportionality factor P is a function of the length of the cell and of the length unit used for the partial extinction coefficients, $b_{a,p}$ and $b_{s,p}$; $b_{a,p}$ denotes the partial extinction coefficient due to absorption by suspended particles, $b_{s,p}$ that due to scattering. If centimeters are employed for the partial coefficients and if E_λ is the optical density for the 10 cm path length considered in this paper, then P has a constant value of 0.23.

In order to apply the Mie theory it is necessary to introduce the effective area coefficient K (sometimes called the scattering area ratio or the efficiency factor). It is defined as the dimensionless number by which the geometric cross-sectional area of a particle (in the plane perpendicular to the direction in which the original direct light beam is traveling) must be multiplied in order to determine its effectiveness in removing or deflecting light from a direct beam by processes of scattering and absorption; i.e., K equals the energy lost by the incident wave divided by the energy of the pencil that is geometrically obstructed by a particle. For N spherical particles per cubic centimeter with constant radius r (in centimeters), we have

$$0.23\ E_\lambda = \pi r^2\, NK. \tag{2}$$

Solving the Mie equations, we obtain values of K as a function of r, λ, and $m(1 - ik)$, the complex relative refractive index of the material in the particle relative to the suspending medium. (Here m is the refractive index, i is the $\sqrt{-1}$, and k is the bulk absorption coefficient of the material in suspension.) If the particles are in the size range of the wave length of light, or smaller (where scattering predominates over absorption), and if they are nearly transparent (at most only slightly absorbing), it can be assumed without serious error that the values of K for nonabsorbing particles of the same size and real relative refractive index m are applicable (Van de Hulst, 1946: 70; Burt, 1952: 28; Sinclair, 1951). Then

$$K = f(\alpha,m), \text{ where } \alpha = 2\pi r/\lambda. \tag{3}$$

Values of K for various values of α and for several values of m equal to or greater than 1.20 have been computed by Gumprecht and Sliepcevich (1951). If these values of K are plotted against $\alpha\ (m - 1)$ rather than α, we can draw curves of K (one for each

value of m considered) which are quite similar to each other. Van de Hulst (1946: 56–58) furnishes an equation for a curve of K vs $\alpha\ (m-1)$ for values of m close to unity which can also be superimposed on the curves for $m = 1.20$, $m = 1.33$, etc.

The limiting cases of the Mie theory $r \ll \lambda$ and $r \gg \lambda$ reduce to the two familiar results of Rayleigh's theory of scattering (Rayleigh, 1899; Stratton, 1941: 572; Sinclair, 1947; Houghton and Chalker, 1949). When $r \ll \lambda$, $K \sim (r/\lambda)^4$ and K can be readily computed for any given value of m. When $r \gg \lambda$, $K \rightarrow 2.0$.

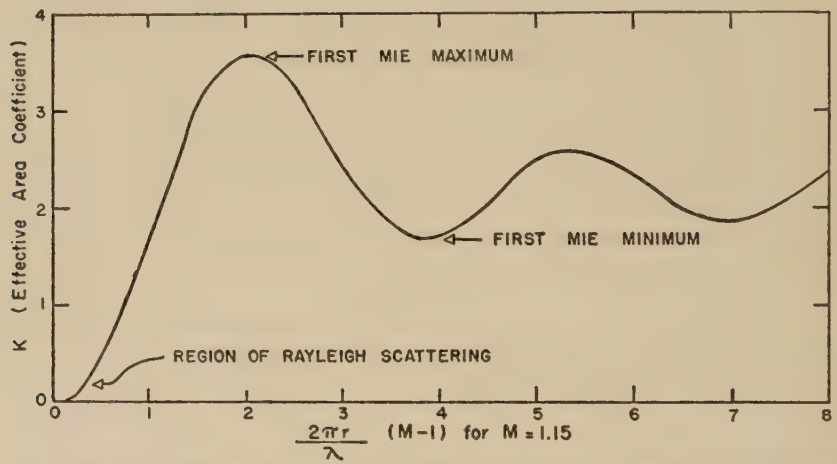

Figure 1. Effective area coefficient, K, as a function of $\alpha(m-1)$ for a relative refractive index, m, of 1.15.

The above information is sufficient to provide values of K for values of m less than 1.20. The relative refractive indices of both the organic and inorganic materials found in Chesapeake Bay waters cluster closely about 1.15 (Burt, 1952: 27). This value will be assumed for the relative refractive index of all materials in suspension.

Fig. 1 shows K as a function of $\alpha(m-1)$ for $m = 1.15$. The curve is based on the assumption that the particles are spherical, whereas those found in natural suspensions are usually not spherical. Penndorf (1953), considering theoretical work by previous investigators, concludes that the results of the Mie theory may be used for nonspherical particles without introducing an appreciable error so long as the relative refractive index is less than approximately 2.00.

The relationship shown in Fig. 1 may be replotted in a more useful form (Fig. 2). Since $m = 1.15$, $\alpha(m-1) = 0.15\alpha$, and by definition, $\alpha = 2\pi r/\lambda$. Therefore, instead of $K = f(\alpha)$, we may plot

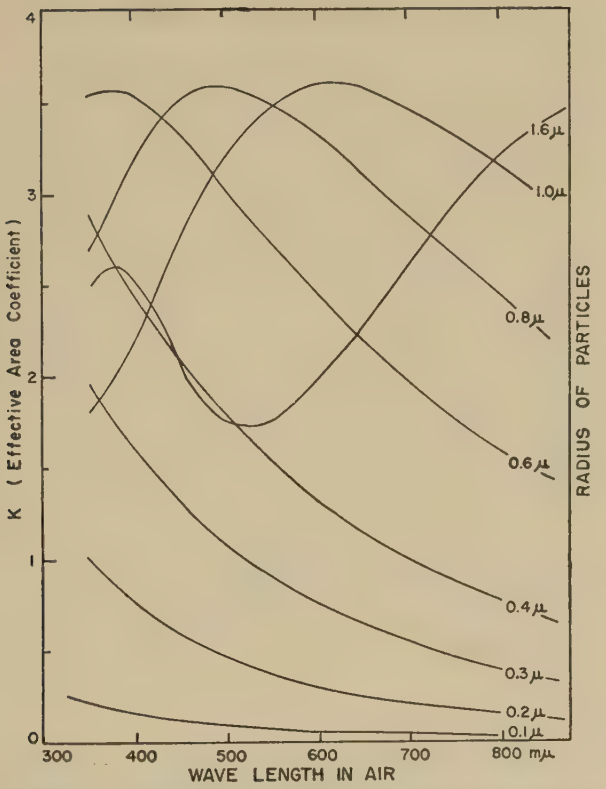

Figure 2. Variation in effective area coefficient, K, with particle radius and wave length. Relative refractive index of 1.15 in water.

$K = f(2\pi r/\lambda)$ for various values of r and λ. In applying these relationships to suspensions in water we must remember that the wave length of light in water is only ¾ of the wave length of the same wave in air and that the theoretical computations are for the wave length of light in the suspending medium. This correction has been taken into account in drawing the curves of Fig. 2; therefore they apply only to transmission through water or through a medium with a like index of refraction. In order to avoid confusion, the abscissa scale is labeled for the wave length of light in air, as on the Spectrophotometer, and thus it corresponds to the various colors usually associated with various wave lengths of light in air.

Comparison of the slopes and shapes of the curves in Fig. 2 is made easier if the ratio $K_{\lambda,r}/K_{600,r}$ is plotted against λ (Fig. 3). $K_{\lambda,r}$ is the effective area coefficient for a particular value of r as a function

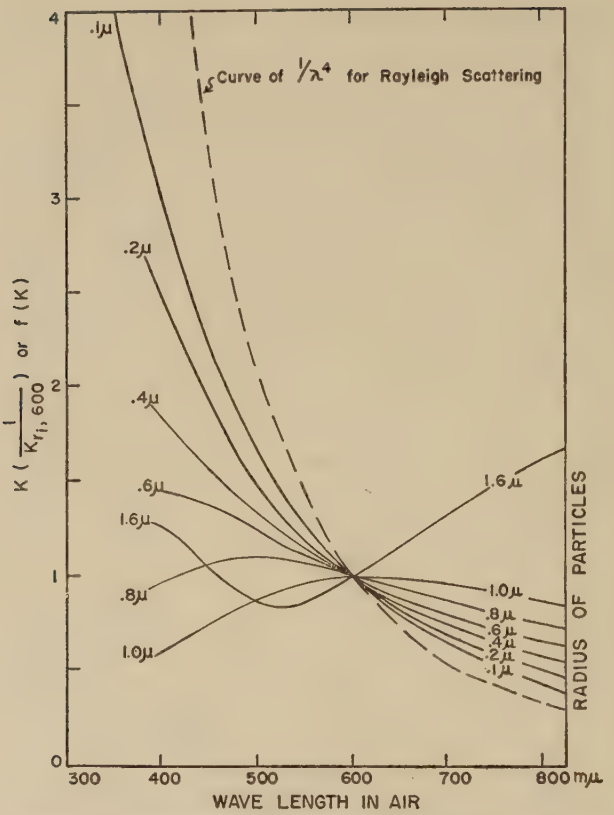

Figure 3. Variation in relative effective area coefficient, $f(K)$ with particle radius and wave length. Relative refractive index 1.15 in water.

of λ, and $K_{600,r}$ is the value of the effective area coefficient for the same value of r and $\lambda = 600\text{m}\mu$.

To illustrate the relationship between the effective area and wave length for Rayleigh scattering, the broken line in Fig. 3 was added to show that Rayleigh scattering is approached when particles have radii of less than 0.1μ. Fig. 3 also shows that in water, within the wave length band 400 to 800 mμ, the Mie scattering curves for particles smaller than 0.6μ are characteristically "J" shaped, the magnitude of the slope increasing with decreasing wave length. For particles with a radius of about 0.6μ, the first Mie maximum begins to appear at the low end of the curve; as the particle size increases this maximum appears at larger and larger wave lengths.

OPTICAL DENSITY CURVES OF NATURAL SAMPLES

From eq. (2) it is seen that the shape (relative slope and curvature) of an optical density curve (E_λ vs λ) for a suspension of completely uniform particles is dependent on the shape of the effective area coefficient curve (K vs λ) for the individual particles. In addition, this equation shows that the numerical value of E_λ at any given value of λ is directly proportional to N, the number of particles in suspension per unit volume of suspension.

To determine the radius of uniformly sized particles, each measured value of E_λ for the sample is divided by E_{600} for the sample. The result, when plotted as a curve of $f(E_\lambda)$ vs λ, is independent of concentration and as such is directly comparable to the curves of $f(K)$ vs λ in Fig. 3. The radius of the particles is determined by superimposing the $f(E_\lambda)$ curve over the $f(K)$ curves and interpolating.

The concentration of particles N may now be determined by solving (2). The value of K is taken from the curve in Fig. 2 for the proper radius at any chosen wave length for which a value of E_λ has been determined.

Comparison of the natural sample $f(E_\lambda)$ curves with the theoretical $f(K)$ curves in Fig. 3 indicates that the controlling radii vary from sample to sample between the limits of 0.1 and 0.5μ. However, close examination brings out the fact that the $f(E_\lambda)$ curves have a greater average curvature between 400 and 600 mμ than the $f(K)$ curves with the same average slope. This is indicative of an expected nonuniformity of size. The difference in shape between the observed and theoretical curves may best be accounted for by assuming that the particle size distributions of the samples are highly skewed toward the smaller particles with median values of the radius for any given distribution of less than 0.5μ.

Axford, *et al.* (1948) and Inman (1951) have reviewed the work of a number of researchers who found that the size distribution of fine sediments, natural dusts and smokes may be best approximated by some form of the highly skewed logarithmic normal curve,

$$V = be^{-c(\log r)^2}, \tag{4}$$

where V is the volume of material corresponding to any given radius r, and where b and c are constants that determine the mean radius and dispersion about the mean for any distribution.

This type of distribution function can be used to build a synthetic optical density curve comparable to the $f(K)$ curves in Fig. 3. This curve, independent of concentration, gives the theoretically expecte relationship between $f(E_\lambda)$ and λ for a suspension of particles wi t

the selected volume distribution function. The synthesis consists of making the following summation numerically by small increments:

$$f(E_\lambda) = \frac{1}{E_{600}}\left[\sum_{i=0}^{i=\infty} K_{\lambda,i}\,\pi\,N_i\,r_i^2\right], \tag{5}$$

where the factor $1/E_{600}$ adjusts the function so that $f(E_\lambda)$ is unity at a wave length of 600 mμ. The number of particles N_i that correspond to any given radius r_i is taken from the distribution function. The numerical value of the effective area coefficient $K_{\lambda,i}$ for particles of radius r_i is taken from the information upon which Figs. 1 and 2 are based.

The synthetic optical density curves resulting from the previous summation (eq. 5) for selected distributions of particles of the form shown in eq. 4 fit more nearly the shape of the $f(E_\lambda)$ curves measured from natural samples than they do the $f(K)$ curves for a single particle size. Adjustment of the mass median radius and dispersion about the median can usually be made until the theoretically derived synthetic curves fit the measured curves satisfactorily.

Figs. 4a and 4b show synthetic curves based on (4) and (5) as well as measured curves for typical natural samples. Each distribution was given a dispersion factor of four, which means that the 95th percentile of cumulative volume has a radius four times that of the mass median (50th percentile). Note that the ratio E_{400}/E_{600} or $f(E_{400})$, which we now define as S_1, increases in value with decreasing average particle size. The ratio S_1 ranges from a value of one for a distribution of large particle sizes up to a value of five for a distribution of particles so small that Rayleigh scattering applies over the whole range of particle sizes present.

A small amount of dissolved yellow substance (Burt, 1953) would tend to make measured curves diverge from the synthetic curves at the short wave lengths, as indicated in Fig. 4b. At the other end of the spectrum there is a tendency for the measured curves to be slightly higher than the synthetic curves due to the presence of large particles such as plankton which, although they are comparatively insignificant numerically, may present a relatively great net cross-sectional area. Due to the large size of plankton ($r \gg \lambda$), their effective area is constant with wave length and they could be accounted for by inserting a constant (equal to twice the cross-sectional area of the large particles per unit volume) inside the brackets and by adding it to E_{600} in eq. 5. The addition of a constant tends to raise the right end of the synthetic curves and would, for example, tend to make for better agreement between the theoretically and

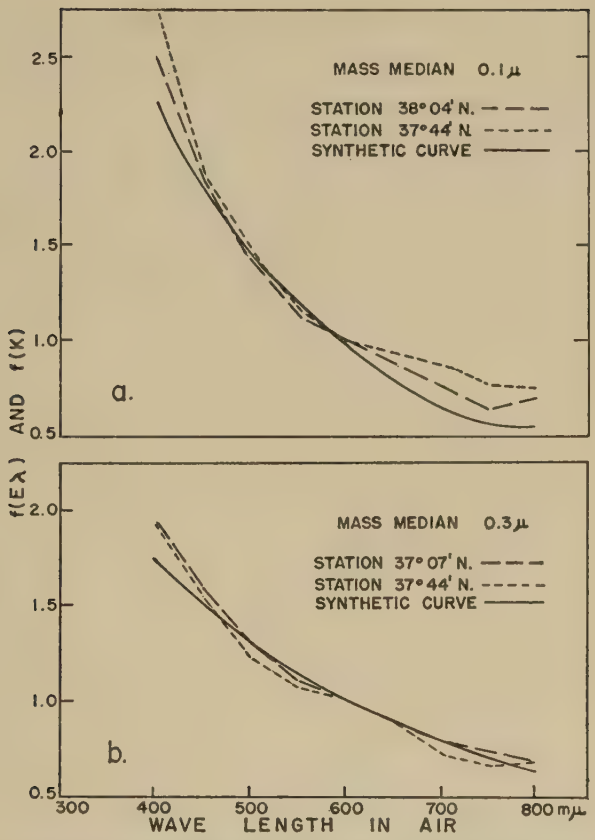

Figure 4. Comparison of synthetic log-normal distribution optical density curves which were computed from the Mie theory with those observed on Chesapeake Bay waters.

experimentally derived curves in Fig. 4a. Let us define the ratio S_2 as E_{800}/E_{600} or $f(E_{800})$. Addition of large particles to any given distribution of small particles would tend to increase the numerical value of S_2.

SIZE DISTRIBUTION

The majority of the $f(E_\lambda)$ curves for Chesapeake Bay waters can be approximated by the synthetic curve in Fig. 4b for a log-normal particle size distribution with a mass median radius of 0.3μ and a dispersion factor of four. Major discrepancies occur when the water becomes abnormally clear, at which time the $f(E_\lambda)$ curves are better represented by the synthetic curve (Fig. 4a) for a mass

median radius of only 0.1μ and a dispersion factor of four. Occasional samples were found with indications of larger mass median radii than 0.3μ, but in no case did the controlling median radius appear to exceed 0.6μ. This is evidenced by the lack of maxima on the measured optical density curves (Fig. 2).

CONCENTRATION OF SUSPENDED MATERIALS

Once the size distribution of suspended materials has been determined it is a relatively simple matter to determine the concentration, which is a linear function of the optical density (eq. 2). The volume of the suspended materials V_s per unit volume of suspension V_w is

$$V_s/V_w = (4/3) \sum_{i=0}^{i=\infty} \pi N_i r_i^3 . \tag{6}$$

Eq. 2 may be rewritten in terms of a summation for a suspension containing a distribution of different size particles as

$$E_{600} = 4.35 \sum_{i=0}^{i=\infty} K_{600,i} \pi N_i r_i^2 . \tag{7}$$

$$\frac{V_s}{V_w} = 0.37 E_{600} \frac{\sum_{i=0}^{i=\infty} \pi N_i r_i^3}{\sum_{i=0}^{i=\infty} K_{600,i} \pi N_i r_i^2} = E_{600} F \tag{8}$$

The factor F is a constant for any given size distribution of suspended particles. It is determined by setting V_s/V_w equal to unity and solving eq. 8. When the concentration is considered in units of parts per million by volume, then F has a numerical value of 13 for a log-normal distribution with a mass median radius of 0.3 and a dispersion factor of 4. This distribution gives the best fit to the average observed data of any distribution that was tried.

DISCUSSION

The primary advantage of this procedure is the relative ease with which the data can be obtained. Each determination can be carried out in less than ten minutes. Changes in the slopes of the measured optical density curves indicate changes in the particle size or size distribution, while changes in the numerical value of the optical density at a given wave length indicate changes in the concentration of suspended materials.

Since most of the errors involved, particularly those which are apt to be significant (see below), are relative, the system may be used for determination of relative size and concentration. Refinements in instrumentation, technique and theory, as well as calibration of results against those of other methods, should decrease the relative errors to a point where absolute results may be obtained.

The Beckman Spectrophotometer includes as transmitted light that portion of light which is scattered in a nearly forward direction, giving a low reading of optical density (Burt, 1952; see Gumprecht and Sliepcevich, 1953 for a discussion of the problem). The instrumental efficiency appeared to decrease with increasing wave length, thus giving the observed optical density curves greater slope than they should have. This spurious increase in slope is added to the increased slope because of dissolved coloring matter at shorter wave lengths, thus indicating smaller median particle sizes than actually occur. Some of the large particles, such as plankton with relatively small cross-sectional area per unit volume of suspended material, may be neglected by assuming the log-normal particle distribution.

The above sources of error tend toward an underestimation of the median radii by a factor of less than one-half. This upper limit of error is well defined by the fact that a maxima would occur on the observed optical density curves (Fig. 3) for larger mass median radii. The underestimation of the median radii, the instrumental efficiency, and the neglect of the large particles tend toward an underestimation of the absolute concentration by a factor which is probably greater than two in most cases and which may be as great as five.

Fig. 5 compares the results of filtering, drying, and weighing the suspended materials from 11 water samples with the results from the determination of the concentration of suspended materials by the optical method. The weighed materials were given a density of 2.65 to convert their weight to volume in ppm. The average optical density curve for a distribution with a mass median of 0.3μ and a dispersion factor of 4 was used to convert the observed optical densities to ppm by volume ($V_s/V_w = 13E_{600}$). Over the range of concentrations examined, the expected linear relationship appears to hold with the concentration as determined by weighing, being about 3.5 times the concentration as determined optically. Thus the true suspended load in ppm by volume was approximately 45 times the numerical value of the optical density for a ten cm cell path-length measured at a wave length of 600 mμ.

Observed optical densities ranged from less than 0.01 to 1.3, indicating suspended loads ranging from less than 1 ppm to approximately 60 ppm by volume.

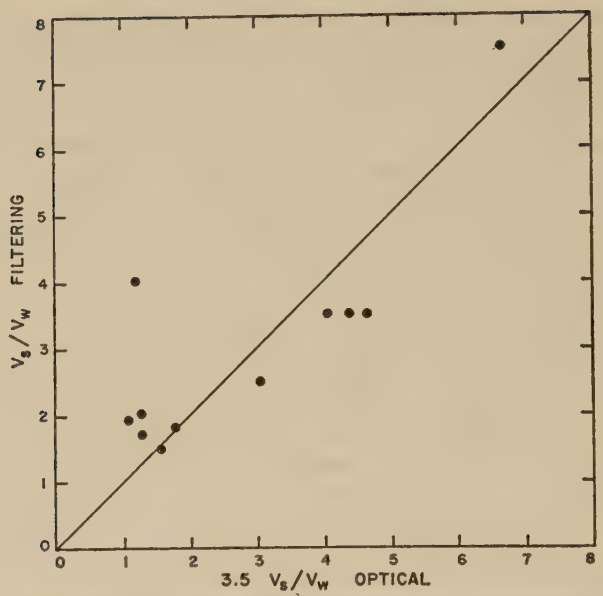

Figure 5. Comparison of the results of determining the concentration of suspended materials optically and by filtering, drying and weighing.

Joseph (1953) has shown a linear relationship of *in situ* extinction measurements over a wave length band centered about 590 mμ with the concentration of suspended material from waters of the North Sea and coastal Europe. The slope of his lines showing this relationship varied with location due to changes in the size distribution and character of the particles. For coastal waters of England and the continent respectively, Joseph's specific extinction values convert to 54 and 37 ppm by volume ($\rho = 2.65$) per unit optical density. This is in fair agreement with the above value of 45.

The Mie theory has also been applied to determine the theoretical scattering from 1 mg per liter concentrations of uniformly-sized spherical particles over the size range from very small particles up to particles with a radius of 6μ (Burt, 1954). The theoretical results compare favorably with the experimental results of Jerlov and Kullenberg (1953).

CONCLUSIONS

1. Curves representing the variation of optical density with wave length for natural water samples from Chesapeake Bay and its tributaries have a characteristic shape. Optical density, greatest at the lower end of the visible part of the spectrum, decreases in magni-

tude with increasing wave length. The rate of decrease in optical density is greatest at that part of the curve with shorter wave length.

2. Filtering removes most of the material responsible for attenuation of light energy. Dissolved coloring matter does not occur in sufficient concentrations to be of importance, and most of the attenuation (other than that due to the water itself) must be due to the absorption and scattering of light by small suspended particles.

3. The Mie theory of electromagnetic scattering and absorption by small spherical particles may be applied to the measured optical density curves in order to determine the approximate concentration and size distribution of the particles in suspension in any water sample.

4. The theory indicates that the particle size distributions are highly skewed toward small-sized particles with average radii of less than 0.6μ. Concentrations of suspended particles range from less than one to approximately 60 parts per million by volume.

ACKNOWLEDGMENT

Appreciation is due Drs. R. S. Arthur, D. Carritt, C. Eckart, G. Ewing and D. W. Pritchard and Mr. M. Pollak for suggestions, criticisms, material aid and encouragement in carrying out this research. Thanks are also due to Mrs. A. Ball and Mrs. Louise Burt.

REFERENCES

Axford, D. W. E., K. F. Sawyer and T. M. Sugden
1948. The physical investigation of certain hygroscopic aerosols. Proc. roy. Soc. London (A) *195:* 13–33.

Burt, W. V.
1952. Scattering of light in turbid water. Ph.D. thesis, Univ. Calif. Los Angeles. 64 pp.
1953. Extinction of light by filter passing matter in Chesapeake Bay waters. Science, *118:* 386–387.
1954. Specific scattering by uniform minerogenic suspensions. Tellus, *6:* 229–231.
1955. Distribution of suspended materials in Chesapeake Bay. J. Mar. Res., 14(1): 47–62.

Cary, H. H. and A. O. Beckman
1941. A quartz photoelectric spectrophotometer. J. opt. Soc. Amer., *31:* 682–689.

Caster, W. O.
1951. Variability in Beckman spectrophotometer. Analyt. Chem., *23:* 1229–1236.

Clarke, G. L. and H. R. James
1939. Laboratory analysis of the selective absorption of light by sea water. J. opt. Soc. Amer., *29:* 43–55.

Gibson, K. S. and M. M. Balcom
1947. Transmission measurements with the Beckman quartz spectrophotometer. J. opt. Soc. Amer., *37:* 593–608.
Gumprecht, R. O. and C. M. Sliepcevich
1951. Tables of light-scattering functions for spherical particles. Engrng. Res. Inst., Univ. Mich., Ann Arbor. 574 pp.
1953. Scattering of light in large spherical particles. J. phys. Chem., *57:* 90–95.
Houghton, H. C. and W. R. Chalker
1949. The scattering cross-section of water drops in air for visible light. J. opt. Soc. Amer., *39:* 955–958.
Inman, D. L.
1951. Measures for describing the size distribution of sediments. Scripps Inst. Oceanogr., Submarine Geology Rep. No. 15 (revised). 44 pp.
Jerlov, N. G. and B. Kullenberg
1953. The Tyndall effect of uniform minerogenic suspensions. Tellus, *5:* 306–307.
Joseph, Joachim
1953. Die Trübungsverhältnisse in der südwestlichen Nördsee während der "Gauss"—Fahrt im Februar/März 1952. Ber. dtsch. Komm. Meeresforsch., *13*(2): 93–103.
Middleton, W. E. K.
1952. Vision through the atmosphere. Univ. of Toronto Press, Toronto. 250 pp.
Penndorf, Rudolf
1953. On the phenomenon of the colored sun. Air Force CRC, Tech. Rep. No. 53–7, Cambridge. 41 pp.
Rayleigh, Lord
1899. On the transmission of light through an atmosphere containing small particles in suspension and on the origin of the blue of the sky. Phil. Mag., *43:* 375–384.
Sinclair, David
1947. Light scattering by spherical particles. J. opt. Soc. Amer., *37:* 475–480.
1951. Physical properties of aerosols. Unpublished report of Johns-Manville Research Center, Manville, New Jersey.
Stratton, J. A.
1941. Electromagnetic theory. McGraw-Hill, New York. 615 pp.
Van de Hulst, H. C.
1946. Optics of spherical particles. Rech. astr. Obs. Utrecht, 11 (part 1), 87 pp.

DISTRIBUTION OF SUSPENDED MATERIALS IN CHESAPEAKE BAY[1]

By

WAYNE V. BURT[2]

Chesapeake Bay Institute, The Johns Hopkins University

ABSTRACT

The distribution of suspended materials in Chesapeake Bay and its tributaries, discussed in terms of light extinction, is characterized by marked variability. There are large local time changes, seasonal and tidal, as well as large horizontal gradients. Variability in the suspended load results from varying distribution in the amount of suspended inorganic materials caused by wind mixing, tidal scouring and river discharge. Direct positive correlation between the amount of suspended materials and the diatom population was not found, though occasionally the influence of large diatom populations appears in the optical examination of raw water samples.

INTRODUCTION

In the preceding paper, Burt (1955) has shown that the optical density (extinction) curves of natural water samples (measured with the Beckman Model DU Quartz Prism Spectrophotometer) are related to the size distribution and concentration of suspended materials. The suspended load in ppm by volume for the average particle size distribution with an estimated median radius of 0.3 μ was approximately 45 times the numerical value of the optical density measured at a wave length of 600 mμ over a 10 cm path length.

The optical density is designated by E and a subscript to denote the wave length at which the measurements were made; the ratio $S_1 = (E_{400}/E_{600})$ serves as a criterion (Burt, 1955) of the coarseness of the suspended material. When S_1 is greater than the average value, the suspended material is finer than average; when less, it is coarser than average.

This paper discusses the optical density and its variability as a measure of the concentration and variability of concentration of

[1] Contribution No. 22 from the Chesapeake Bay Institute. Results of work carried out for the Office of Naval Research of the Navy Department, the State of Maryland (Department of Research and Education), and the Commonwealth of Virginia (Virginia Fisheries Laboratory), under contract with The Johns Hopkins University.

[2] Now at the Department of General Science, Oregon State College.

suspended materials. There is approximately a linear relationship between the optical density and the suspended load, but of course the exact concentration of suspended materials depends on the size distribution of the sample. It will be shown later that most of the samples appear to have little variability in the size distribution of suspended particles except in the case of the clearest samples, where the median radius of particles appears to decrease with increasing clarity of the water.

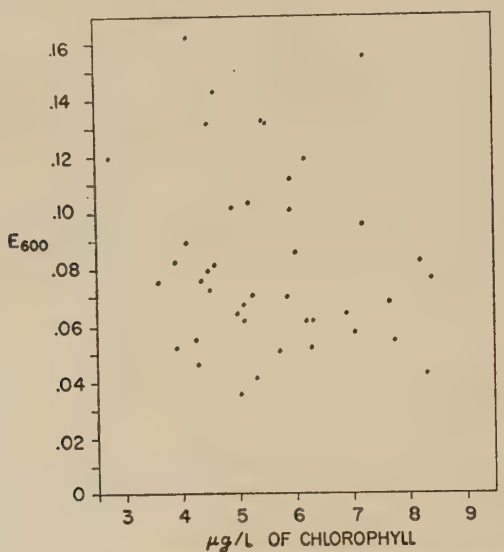

Figure 1. Plot of E_{600} against chlorophyll concentration for surface samples taken in the St. Mary's River during June and July 1951. The correlation coefficient was −0.38.

SEASONAL AND AREAL DISTRIBUTION

Discharge from the principal rivers contributes most of the inorganic material that enters Chesapeake Bay. Thus the average optical density increases in the spring months during peak flow and tends to decrease in the fall when runoff is at a minimum. However, the flow of any given river may vary widely at any time from its normal or average values.

A second source of suspended particles arises from continual production and decay of living organisms. During spring and summer the chlorophyll concentration (the only available measure of the standing crop) usually increases from regions with low average E_{600} to regions with high average E_{600}. However, there was no correlation between optical density and chlorophyll concentration for serial

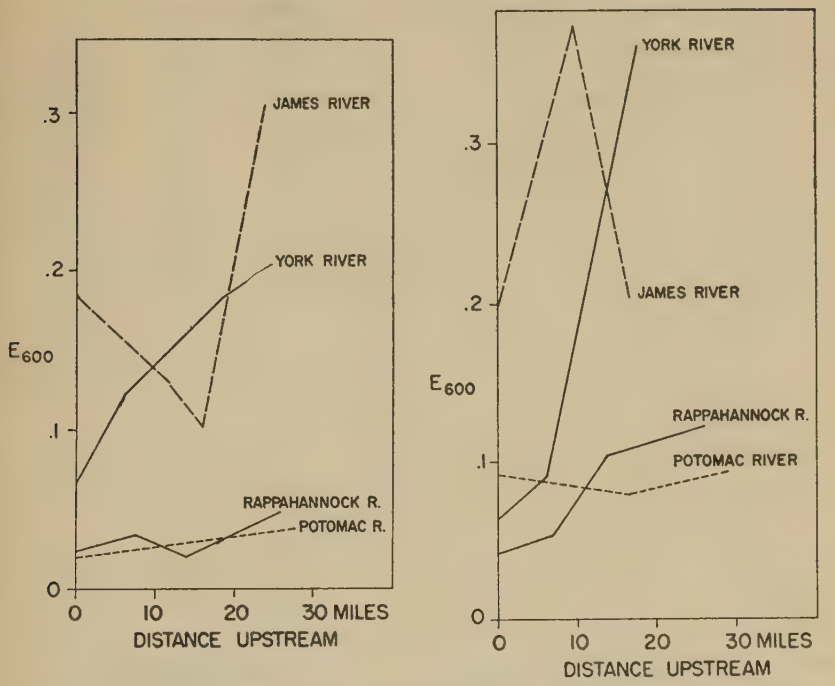

Figure 2. Increase in E_{600} with distance upstream in the main tributary rivers. Surface observations: October 1950 (left) and January 1951 (right).

observations made at a given station (see Fig. 1). Like results were obtained for similar data taken the year before in the James River. It has been suggested that the negative correlation should be expected since diatom growth is favored by clearer water.

The third source, wind mixing and tidal scouring, brings back into suspension the material which has settled to the bottom. Shallow depths, averaging approximately 20 feet, frequent cyclones, and summer thunderstorms combine to make wind mixing an important factor throughout the year except during the early fall months. On the other hand, tidal scouring is important at all times.

The annual cycle of optical density consists of high values during winter and early spring (wind mixing and runoff), relatively high but widely fluctuating values during late spring and early summer (thunderstorms, runoff, and biological production), lower but highly fluctuating values during middle and late summer (thunderstorms and biological production), and low consistent values during the early fall when all factors except tidal scouring are operating at a minimum.

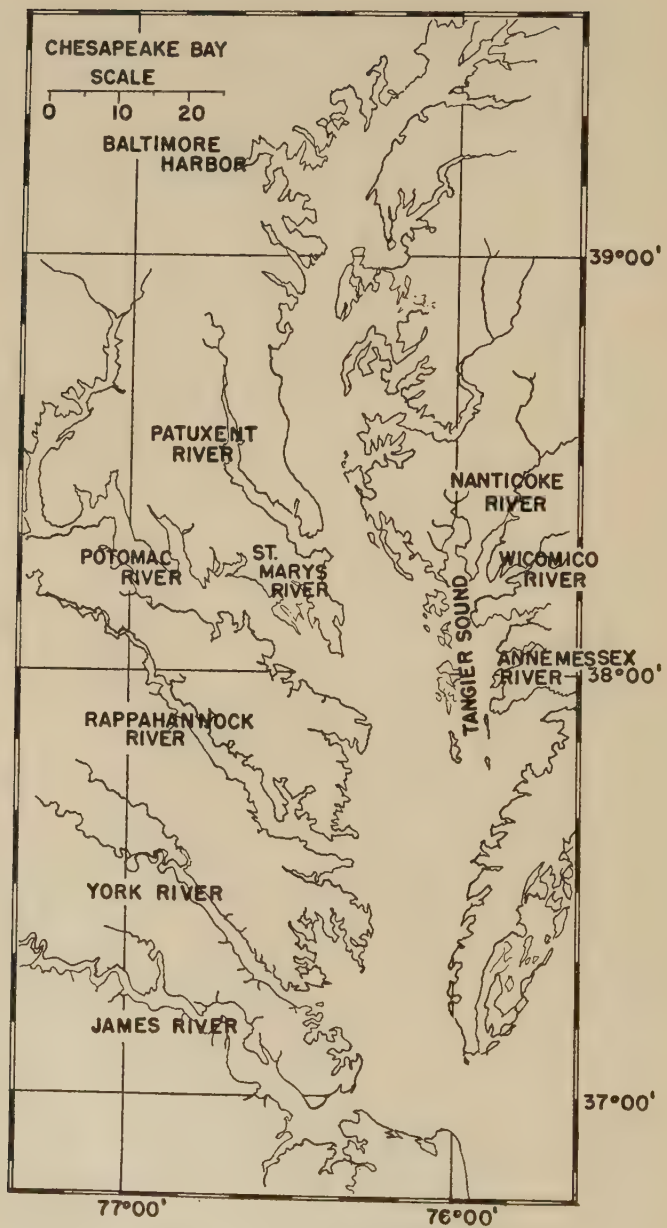

Figure 3. The Chesapeake Bay Region.

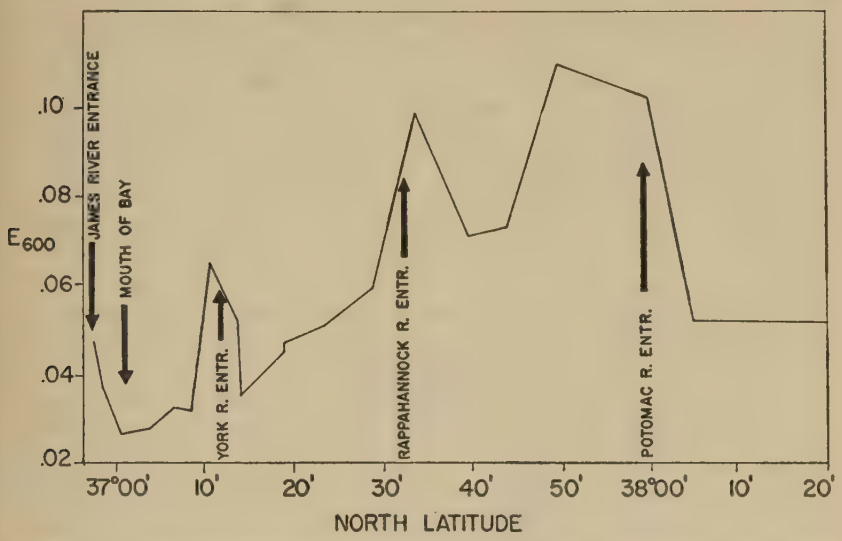

Figure 4. Variations in mid-Bay surface values of E_{600} with latitude for observations made during April 1951.

Optical density normally increases upstream in the major rivers. Absolute values of E_{600} range from extreme lows of 0.02 during the fall to more than 0.5 during spring periods with high runoff (see Fig. 2).

The optical density of surface waters in the lower part of the Bay, south of 38° 10′ N (Fig. 3), was largely influenced by that of waters from inflowing rivers with E_{600} ranging from 0.02 to 0.12. Fig. 4 gives a plot of surface E_{600} against latitude for a series of stations located in a line up the center of the lower Bay; this shows that, during times of high river outflow (spring), tongues of highly turbid water were located in the Bay off the mouth of each river. The surface waters from stations located in the center channel of the Bay were usually slightly clearer than the surface waters near the shallower edges where tidal scouring, wind mixing and local runoff have a maximum effect.

Pritchard (1952) considered the area from the mouth of the Potomac River (38° 10′ N) northward as an extension of the Susquehanna River, which provides 87 per cent of the fresh water that enters the northern half of the Bay. The deep natural channel in the center of the Bay ends abruptly at approximately 39° N (the location of the Chesapeake Bay Bridge). Above this point the Bay is shallow except for dredged navigational channels. Salinity shows an average

drop of 5 ‰ in ten miles centered at 39° N. The section of the Bay above 39° N, sometimes called the "mud flats" of the Susquehanna, acts in a number of ways as an integral part of that river. Here the optical density was uniformly high except during the fall season. It increased with increasing latitude toward the geographic mouth of the river at 39° 35′ N. The normal range of E_{600} was from 0.07 to 1.0, with occasional values as high as 1.3. $E_{600} = 1.3$ corresponds to an extinction coefficient per meter of approximately 30.0.

The part of the Bay between 38° 10′ (mouth of the Potomac) and 39° N was unique in that it usually contained clearer water than the lower part of the Bay. The optical density values were relatively constant, with E_{600} normally ranging from 0.01 to 0.1. During maximum flow of the Susquehanna, the northern boundary of this area with its large horizontal gradients of salinity and turbidity moved a few miles southward from 39° N in a manner somewhat analogous to the southward movement of an atmospheric cold front on the surface of the earth. Thus the average value of E_{600} for this area was increased materially.

Fig. 5 shows the optical front between waters of the upper Bay and mid-Bay for four different cruises. Note the horizontal change in E_{600} exceeding a factor of ten which was observed during one of the cruises.

Optical densities in the shallow sounds and wide river mouths along the eastern shore of the Bay had nearly the same values as those found in the Bay proper at the same latitude. The eastern shore rivers with their low runoff differed from the Susquehanna and the major rivers on the western shore in that the optical density values often decreased in an upstream direction.

DISTRIBUTION OF E_{600} WITH DEPTH

Twenty-six depth series were made during two cruises (fall and winter). Samples were drawn at two-foot depth intervals from the surface to 20 feet, at five-foot intervals from 20 feet to bottom. Sharp layers of increased optical density (opacity) such as those found in other regions by Whitney (1938), Pettersson (1934) and Joseph (1949) were not observed. A hydrophotometer, similar to that designed by Pettersson, was constructed in order to determine if the pumping technique was missing highly opaque layers. Ten runs were made with this instrument on the following cruise (spring). At the same time samples were drawn at two-foot depth intervals. Two of the stations contained relatively opaque layers which were equally apparent on the data obtained from either technique. From

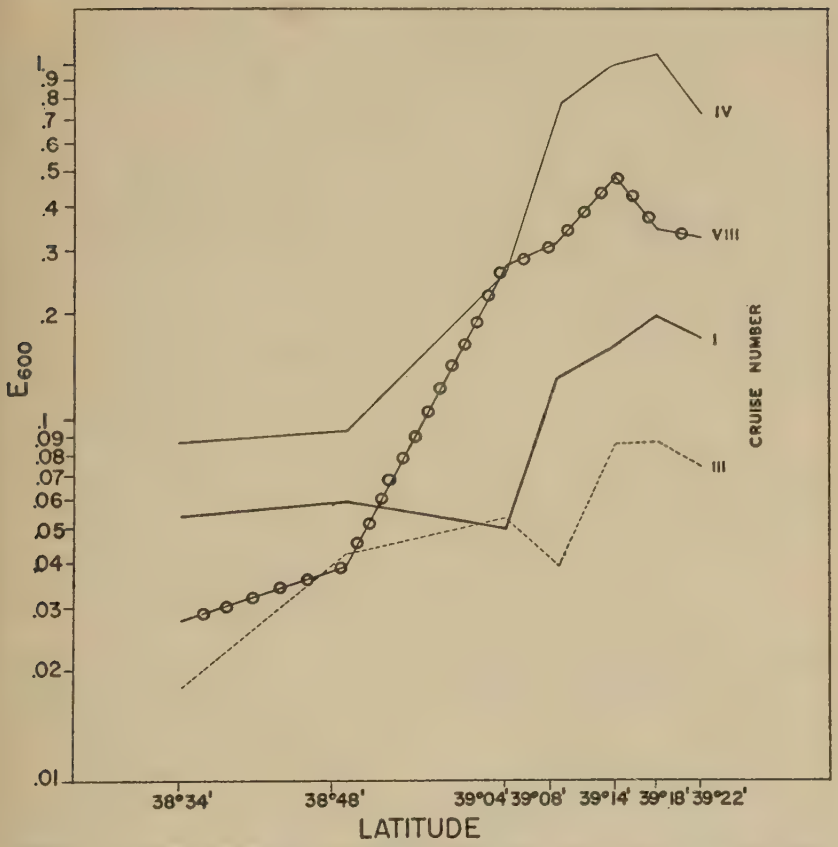

Figure 5. Optical density front observed near the site of the Chesapeake Bay bridge during four different cruises. Data were averaged when more than one station was taken at any given latitude. Interpolated values of E_{600} are presented for the earlier cruises where E_{400} and E_{700} were read.

this evidence and from the fact that the previous 26 serial observations showed no sharp discontinuities, one might assume that they do not occur normally in this region. For additional evidence, a series of more than 100 unpublished Clarke photometer observations taken by Dr. Alfred Armstrong, College of William and Mary, were examined for the presence of sharp breaks in slope. These readings were taken during all seasons over a period of four years in the lower Bay and in the James, York and Rappahannock Rivers. Only one observation indicated the presence of a thin, highly opaque layer.

The E_{600} data from surface to 20 feet were analyzed statistically for 11 stations occupied during October and November 1950 (fall)

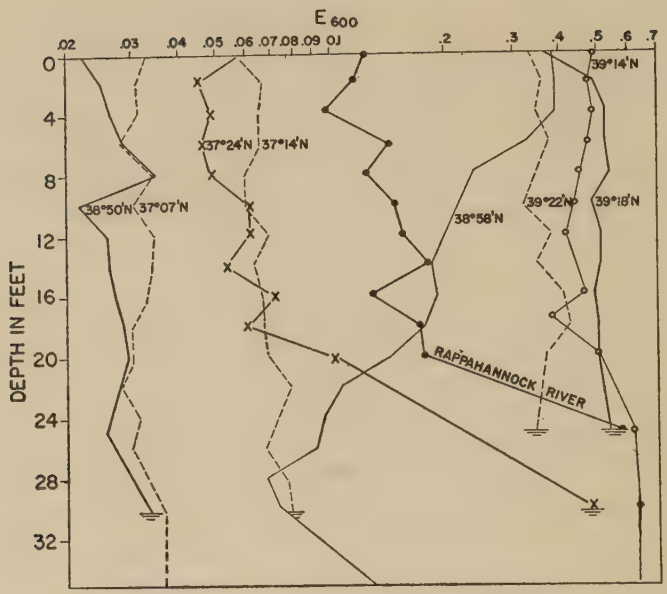

Figure 6. Change in E_{600} with depth at selected stations.

and for 13 stations occupied during January 1951 (winter). Data from one station for each period were not used because they showed obvious average increases or decreases in optical density with depth. The coefficients of variation for the various stations of the fall cruises ranged from 7 to 18%, with a mean value of 12% and a standard deviation of 4%. The variability as obtained from data of the winter cruise increased slightly; coefficients of variation ranged from 2 to 32%, with a mean value of 14% and a standard deviation of 10%.

Below a depth of 20 feet the optical density tended to remain nearly constant or to increase slowly with depth until the bottom was almost reached, at which point the optical density usually increased rapidly for the remaining depth. This latter phenomenon was more pronounced over soft muddy bottoms than over hard sandy ones. Fig. 6 shows a number of typical optical density-depth plots for stations ranging in location from the mouth to the head of the Bay.

The occasional increase in optical density with depth below 20 feet must be due to effects of settling from above and to continual tidal scouring and transport of suspended materials at these depths. The normally high turbidities just over the bottom indicated the presence of a continual stirring action.

In transition regions, the less saline surface water with high turbidity overruns the more saline water with less turbidity. This is shown in Fig. 6 for the observation taken at 38° 58′ N.

LOCAL TIME CHANGE IN OPTICAL DENSITY

One of the most striking features in the optical density distribution was the magnitude of the local time change, which was measured by taking serial observations each half hour from an anchored vessel. The suspended material appeared to occur in clouds of varying density, much the same as water, dust or haze clouds in the atmosphere. Thirteen anchor stations, located in a line running up the center of the Bay and in three of the major rivers, were made during April and May 1951. Surface and ten-foot samples were drawn at five stations for one quarter of a tidal cycle (six hours) and at the other eight stations for one half of a tidal cycle (12 hours).

Individual mean values of E_{600} averaged for all observations from each station varied from 0.017 to 0.598 and standard deviations from 0.003 to 0.165. No correlation was found between the values of the means and the coefficients of variation, which indicates that the percentage dispersion about the mean was independent of the average optical density at the station.

The values of the coefficients of variation for the different stations ranged from 5 to 38%, with an arithmetic average value of 20%. The standard deviation of the coefficients of variation was 9%. If the distributions are considered normal, this indicates that 68% of the coefficients of variation would have values between 11 and 29%, or that only 16% of the coefficients of variation are less than 11%.

The statistics on variation of E_{600} with depth which were presented above under the heading of Distribution of E_{600} with Depth were of the same order of magnitude as those presented here for the time variation within half a tidal cycle.

Except for values from one station, located in the boundary zone at 39° N, the means of the surface and ten-foot samples taken simultaneously had nearly the same numerical value; i.e., the individual values at surface and at ten feet varied about the same mean. However, the correlation between the individually paired samples taken at the same time was erratic; the correlation coefficients for the five stations were +0.30, −0.30, +0.66, +0.21 and +0.51. This is further evidence of the apparent randomness of the cloudlike distribution of suspended material in the Bay waters.

Current velocity and direction were observed at approximately hourly intervals at each anchor station (Figs. 7, 8) to ascertain whether or not certain relationships existed between observed currents (tidal

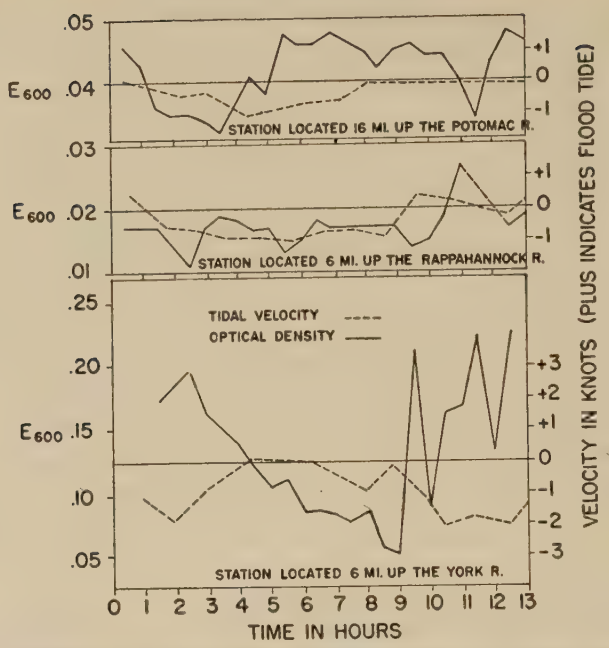

Figure 7. Variations in surface velocity and E_{600} for three river anchor stations, April 1951. E_{600} varied by a factor of four in the York River.

stage) and variations in optical density. If the average optical density increased in an upstream or up-Bay direction, then the highest optical density should occur at any station at low water, which corresponds to slack water between ebb and flood. Conversely, lowest optical densities should occur at high water, comparable to slack water between flood and ebb. The curve of the optical density should be 90° out of phase with the current velocity curve, with maximum flood occurring three hours later than maximum optical density. The curves for the data from the river stations show a slight tendency to follow the expected pattern.

Surface current and optical density data for four mid-Bay stations are plotted in Fig. 8. There is some tendency for the optical density curves to be periodic in shape, but they are almost completely out of phase with the current curves (station at 38° 48′ N) or nearly in phase (station at 38° 18′ N). These stations were located in the channel, nearly in the center of the Bay; therefore any cyclical variation in optical density due to changes in the effective tidal scouring velocities on bottom should be obscured by the time they effected the surface.

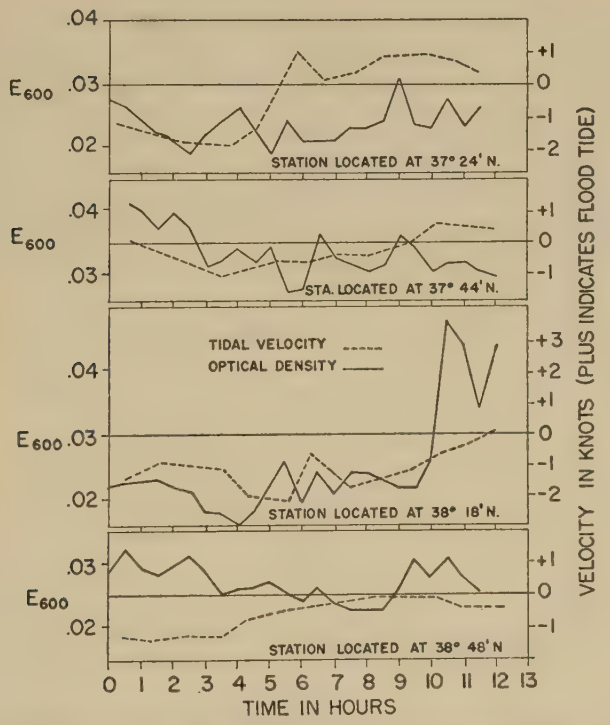

Figure 8. Variations in surface velocity and E_{600} for Bay stations, April and May 1951.

VARIATION IN MEDIAN PARTICLE RADIUS

The variation in the estimated median particle radius, $\bar{r}$, from sample to sample will be discussed in terms of the parameters $S_1 = (E_{400}/E_{600})$ and $S_2 = (E_{800}/E_{600})$. Theoretically (Burt, 1955), S_1 should increase numerically with decreasing average radius of particles in suspension while S_2 should increase numerically with an increasing proportion of suspended particles that are large in comparison to the wave length of light.

Surface samples (101) from the October and November 1950 cruise and surface samples (62) from the January 1951 cruise were analyzed statistically for variation in S_1 and S_2. These two cruises represent seasonal periods when the water was clearest (fall) and most turbid (winter). The mean value of E_{600} for the fall cruise was 0.054, which increased to 0.128 for the winter cruise. The average value of S_1 dropped from 2.05 ($\bar{r} = 0.2\mu$) for the fall to 1.71 ($\bar{r} = 0.3\mu$) for the winter. The average value of S_2 remained constant at 0.77 for both cruises.

The high average value of S_1 for the fall observations indicates the preponderance of fine suspended material in the water. This is to be expected since a minimum amount of material is being added to the water at this season from all sources except tidal scouring. Most of the larger particles have settled out, leaving a more or less permanent suspension of fine material. The numerical value of S_1 is closely related to the absolute value of E_{600} (the total amount of suspended materials). In Fig. 9, S_1 is randomly distributed between

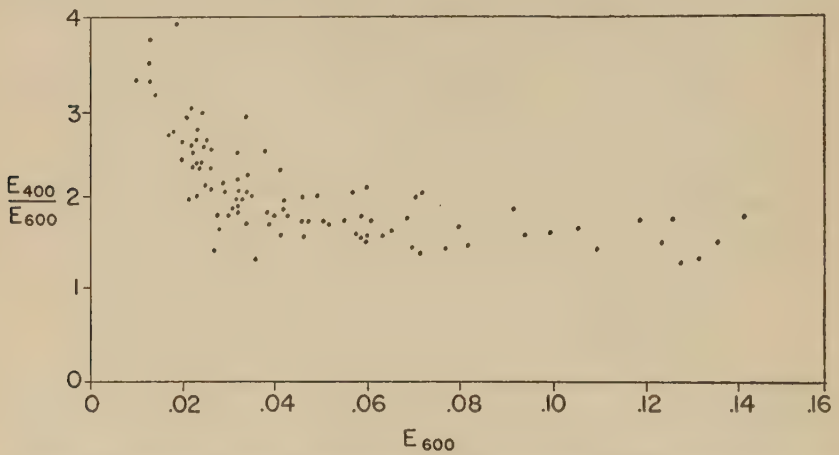

Figure 9. Relation between E_{600} and the ratio E_{400}/E_{600} for all surface samples taken during October and November 1950.

1.4 ($\bar{r} = 0.5\mu$) and 2.0 ($\bar{r} = 0.2\mu$) for values of $E_{600} > 0.04$. Below $E_{600} = 0.04$ (approximately 2 ppm by volume) the numerical values of S_1 increase rapidly such that all values of S_1 for $E_{600} < 0.02$ (less than 1 ppm by volume) have steep optical density curves with $S_1 > 2.7$ ($\bar{r} < 0.1\mu$).

The values of S_1 for the winter cruise were randomly distributed about the mean value of 1.71 independently of E_{600}. None of the winter values of E_{600} was small enough to determine whether S_1 became large as the concentration of particles became small.

No reasonable explanation was found for the constant average value of $S_2 = 0.77$ for both fall and winter cruises. S_2 was plotted against E_{600} for both cruises, but no correlation existed. The values of S_2 varied in random manner between 0.70 and 0.90 about the average, independent of the total particle concentration. A plausible explanation for this phenomenon may be that sufficiently large light particles of biological origin may have been present in enough of the fall samples to have maintained this average value of S_2.

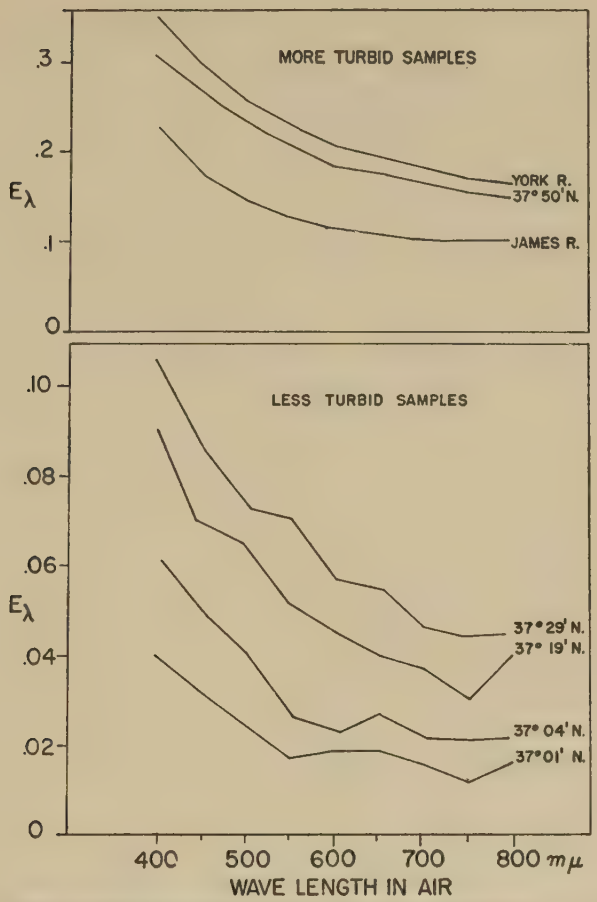

Figure 10. Diagram illustrating the tendency for optical density curves to become more regular with increasing turbidity.

IRREGULAR FEATURES IN OPTICAL DENSITY CURVES (E vs λ)

In the case of high optical density, indicating a high concentration of suspended material, the curves were usually smooth and regular. Conversely, as the optical density decreased, the curves tended to become less regular, with humps and peaks. See Fig. 10. These irregularities may be explained on the basis of one or more of the following factors: instrumental errors whose effects tend to become important as the optical density decreases, the presence of a large proportion of particles with uniform radii between 0.5μ and 5μ, and

strong absorption in small wave bands by highly colored substances in suspension.

It is difficult to show quantitatively the irregularity in optical density curves due to a suspension that contains a relatively large fraction of particles of uniform radii between 0.5μ and 5μ. According to theory, a spread of sizes in this uniform group as represented by a coefficient of variation of only 10% would tend to smooth out the effect. Although some of the irregularities may be caused by this factor, no samples indicated its presence in a clear-cut manner.

Pigmented plants constitute the only highly colored material known to be in suspension in recognizable amounts. Chlorophyll A is the most abundant pigment in plankton of these waters. To determine the magnitude of this possible source of irregularity, a number of transmission readings were made at 667 mμ, the highest wave length absorption peak for Chlorophyll A in the visible part of the spectrum. At 667 mμ, absorption peaks were superimposed on the optical density curves quite regularly during the spring cruise (May and June 1951), with a maximum value for regular stations of less than 5% of the expected reading; this was found by drawing a smooth curve through E_{600} and E_{700}. One reading taken especially for this purpose in the inner harbor at Reedville, Virginia had an extreme value of 10%. This long and narrow shallow harbor supports a high plankton bloom during this time of year due to continual fertilization from a large fleet of Menhaden fishing vessels and several Menhaden reduction plants.

Fig. 11 contains optical density plots for samples from Reedville Harbor, York River, two lower Bay locations, as well as a laboratory experiment. The experimental curve was run on the liquid from a laboratory culture of *Chlorella* which had died. Most of the particulate matter had settled out before the sample was taken. This was measured to see if a purely "biological" curve would have the same shape as those from the Bay samples. Note that the water sample taken at 60 feet in the lower Bay showed optical evidence of a recognizable amount of chlorophyll particulate matter.

Chlorophyll A has a second broad absorption band centered between 400 and 450 mμ, which is wider and somewhat stronger in optical density units for a given concentration of chlorophyll than the narrow absorption peak centered at 667 mμ. The presence of this shorter peak is easily seen on all four of the upper curves in Fig. 11. Both the 667 and 400–450 mμ peaks are absent from the York River curve taken at nearly the same time.

The above data show that, although the presence of green particulate or living organisms is easily detected by optical density measure-

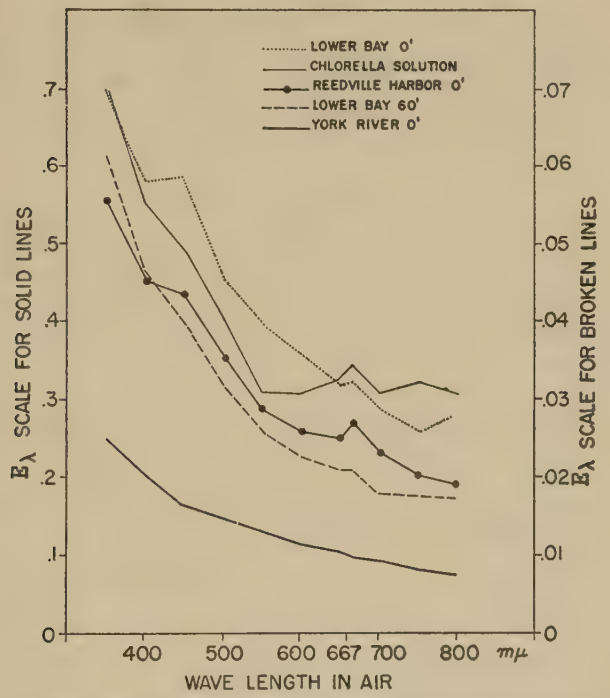

Figure 11. Optical density curves illustrating the 667mμ absorption peak due to absorption by particulate matter with a high concentration of Chlorophyll A. The solid curves are drawn to the scale of the left ordinate, while the broken and dotted curves are drawn to the expanded scale of the right ordinate.

ments at 450 or 667 mμ, it does not materially affect the over-all shape or magnitude of the optical density curves.

CONCLUSIONS

1. The distribution of suspended materials is highly variable both horizontally and vertically as well as with time.

2. Concentrations of suspended materials range from less than 1 to approximately 60 parts per million by volume.

3. Small particles occur in cloudlike distributions which may cause variations in extinction of as much as a factor of four at a given location during a single half tidal cycle.

4. Highly opaque layers did not normally occur.

5. The clearest samples contained the smallest average size particles; for the more turbid samples, no correlation was found between the average particle size and the concentration of particles.

6. No correlation was found between particle concentration and chlorophyll content for serial observations, although the presence of particles containing a high concentration of Chlorophyll A was indicated by an increased absorption at 667 mμ on the optical density curves for unfiltered samples.

ACKNOWLEDGMENT

The author wishes to thank W. B. Cronin, H. H. Whaley, R. H. Whaley, D. W. Booth, T. Hopkins, Mrs. D. Kinsman and Mrs. B. Luebberman for assistance in obtaining and analyzing the data appearing in this paper.

REFERENCES

Burt, W. V.
1955. Interpretation of spectrophotometer readings on Chesapeake Bay waters. J. Mar. Res., *14* (1): 33–46.

Joseph, Joachim
1949. Durchsichtigkeitsmessungen im Meere im ultravioletten Spektralbereich. Dtsche. Hydrogr. Z., *2* (5): 212–218.

Pettersson, Hans
1934. A transparency meter for sea water. Medd. Goteborg Hogsk. Oceanogr. Inst., *7:* 17 pp.

Pritchard, D. W.
1952. Salinity distribution and circulation in the Chesapeake Bay estuarine system. J. Mar. Res., *11:* 106–123.

Whitney, L. V.
1938. Microstratification of inland lakes. Trans. Wis. Acad. Sci. Arts Lett., *31:* 155–173.

SOME PROBLEMS IN OPTICAL OCEANOGRAPHY[1]

By

CHARLES COX AND WALTER MUNK

Scripps Institution of Oceanography

ABSTRACT

Problems involving the refraction and reflection of light from sun and sky by a *roughened* sea surface have been made accessible to numerical treatment by measurements of the probability distribution of sea surface slopes. Four cases are treated. (1) The refracted sun's glitter, as seen from beneath the surface. It is smaller but about 1000 times more luminous (neglecting absorption) than the reflected glitter, and, unlike the reflected glitter, it expands and dims as the sun sets. (2) The albedo of a rough surface to direct sunlight. It is slightly larger at high sun angles and substantially smaller at low sun angles than the albedo of a flat surface. Accordingly, more solar energy penetrates arctic waters than had been estimated previously and the amount of this additional energy depends upon wind speed. (3) The luminosity and albedo of a rough sea surface due to sky light. At the horizon a rough surface is darker than a smooth surface, thus enhancing the horizon contrast. The albedo of the sea surface to sky light varies from 5 to 10%, depending on the distribution of illumination from the sky; it is largest when the sea is flat calm. The roughening by a Beaufort 4 wind reduces the albedo by about 20%. (4) The visibility of slicks.

1. INTRODUCTION

Measurements of the probability distribution of slopes have been made by Duntley (1950), Schooley (1954), and by Cox and Munk (1954a and b). As a result of these measurements, certain oceanographic problems have become accessible to numerical treatment. In these problems we are concerned with the *average* brightness ("radiance" in optical terminology) of the sea surface due to sun or sky when viewed from above or beneath. The average is formed over sufficient time or sufficient surface area to smooth out fluctuations such as the ones that result from individual glitter sparkles of sunlight. The average is then essentially independent of time but varies smoothly with the azimuth and elevation of the portion of sea surface under consideration.

[1] Contribution from the Scripps Institution of Oceanography, New Series No. 776. This work has been sponsored in part by the Geophysics Research Directorate of the Air Force Cambridge Research Center, Air Research and Development Command, under Contract No. AF(19) 604 (1053).

Let $z(x, y)$ designate the elevation of the sea surface above a mean level and let $\partial z/\partial x = z_x$, $\partial z/\partial y = z_y$ be the corresponding slope components. We shall require the probability $p(z_x, z_y)\delta z_x \delta z_y$ that the slope components will lie within the limits $z_x \pm \frac{1}{2}\delta z_x$, $z_y \pm \frac{1}{2}\delta z_y$. As a first approximation, we find (Cox and Munk, 1954a: section 6.3) that the distribution is Gaussian,

$$p(z_x, z_y) = (\pi\sigma^2)^{-1} \exp\left[-(z_x^2 + z_y^2)/\sigma^2\right] . \tag{1}$$

The mean square slope, regardless of direction, $\sigma^2 = < z_x^2 + z_y^2 >_{AV}$, increases with the "masthead" wind speed in $m\ s^{-1}$, W, according to

$$\sigma^2 = .003 + 5.12 \times 10^{-3} W \pm .004 . \tag{2}$$

In the presence of a slick this value is reduced by a factor of two or three.

In adopting the isotropic Gaussian distribution function (1) we simplify our results at the cost of omitting certain observed effects of wind directionality. For it has been found (Cox and Munk, 1954a: sections 6.3, 6.4) that the up/downwind slope components exceed the crosswind components and that the up/downwind distribution is skewed.

2. THE GLITTER AS SEEN FROM BENEATH THE SURFACE

The same glitter pattern differs substantially when viewed from above and below the sea surface. These differences are illustrated in Fig. 1 and are described in the legend. The upper part of Fig. 1 is based on the theory of *reflected* glitter as given previously (Cox and Munk, 1954a: sections 3.1, 3.2). The theory for *refracted* glitter (lower part of Fig. 1) is developed along similar lines in the following sections.

The principal differences between the reflected and refracted glitter patterns are as follows: (1) The reflected glitter pattern is larger[2] and less luminous than the refracted pattern. (2) The reflected pattern shrinks and becomes more luminous as the sun sets; the reverse holds for the refracted pattern. (3) Both reflected and refracted patterns move toward the horizon with the setting sun, but the reflected pattern moves almost twice as fast.

In a general way these conclusions are in agreement with what has been observed. However, at ordinary diving depths the luminescence varies considerably with the passage of individual waves, whereas the patterns described here correspond to suitable time exposures. The fluctuations diminish with increasing depth, so that at a depth of, say

[2] The refracted patterns in Fig. 1 are enlarged by a factor of 2.5 relative to the reflected patterns.

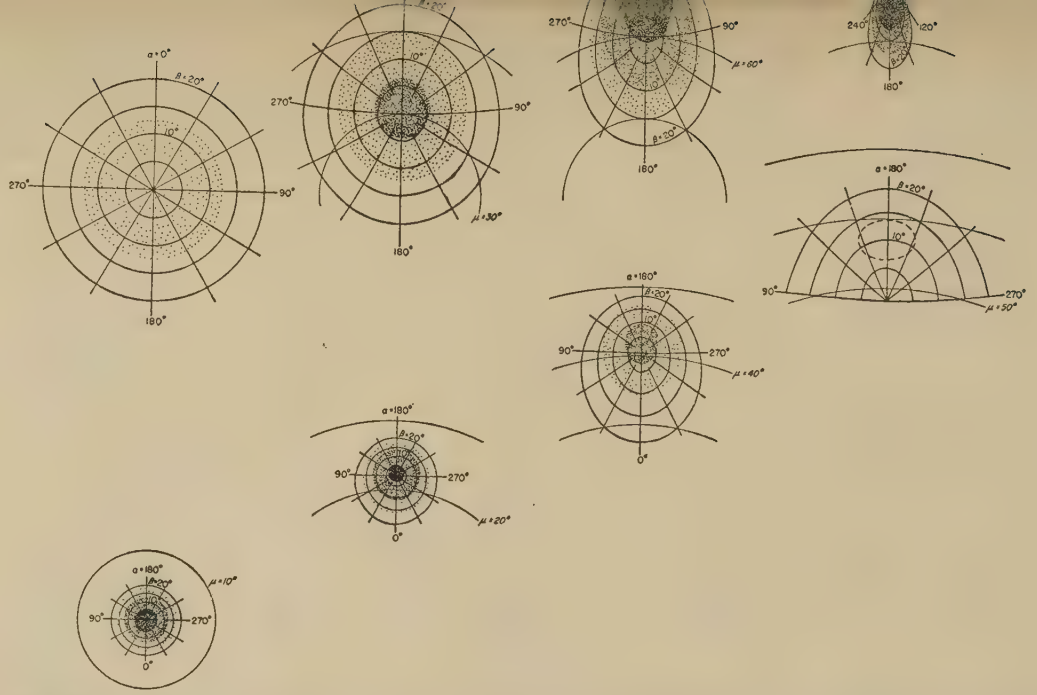

Figure 1. The glitter patterns for a Beaufort 4 wind ($W = 7\ ms^{-1}$, $\sigma = 0.2$) as seen from above the surface (Upper Four) and from beneath (Lower Four). The patterns from left to right are drawn for solar zenith angles of 0° (sun at zenith), 30°, 60°, 90° (sun at horizon). Each pattern is drawn with reference to the polar coordinates μ, the observer's zenith angle, and ν, the azimuth relative to the sun (see Fig. 2). The value $\mu = 0°$ designates a point on the surface directly beneath (above) the observer; the horizon is at $\mu = 90°$. The circular arcs in the upper patterns are drawn for $\mu = 30°, 60°, 90°$, in the lower patterns for 10°, 20°, . . . 60°, 70°. The μ-scale in the lower figure is 2.5 times the scale in the upper figures. For each diagram the radial α-lines give the azimuth of ascent, and the quasi-elliptical β-lines the tilt required for the occurrence of a highlight (Fig. 2). Shadings indicate surface luminosity. The values in units of the sun's luminosity are as follows:

shading	*none*	*light*	*medium*	*heavy*
upper figures: (parts per million)	$<.66$	.66–3.3	3.3–16.6	>16.6
lower figures: (parts per thousand)	$<.25$	.25–1.3	1.3– 6.6	>6.6

1000 feet, the observed pattern would resemble the computed pattern rather closely were it not for the effect of absorption (which we have ignored) and other difficulties.

Whitecaps have been neglected. At low sun angles the effects of multiple scattering and wave shadowing introduce a serious error into our calculation, and the angular dimension of the sun as compared to the reflected pattern should also be taken into account. All constants have been computed for an isotropic slope distribution. Under actual conditions, the most probable slope is a few degrees, not zero, and its azimuth of ascent is directed downwind. The result is an upwind displacement of the bright core of the glitter.

2.1. *The geometry of refraction.* The following derivation follows closely the derivation of the geometry of reflection attained previously (Cox and Munk, 1954a: section 3). We can therefore give an abbreviated account. All angles are defined in Fig. 2. The azimuth of ascent, α, and the tilt, β, are related to the slope components z_x, z_y according to

$$z_x = \sin\alpha \tan\beta, \quad z_y = \cos\alpha \tan\beta \,. \tag{3}$$

According to the law of refraction, a unit vector along the incident ray *minus* a vector of length n along the refracted ray[3] equals a vector normal to the refracting surface. This vector equation has the components

$$\begin{aligned} -\sin\psi - n\sin\mu\cos\nu &= -k\cos\alpha\sin\beta \\ -n\sin\mu\sin\nu &= -k\sin\alpha\cos\beta \\ -\cos\psi + n\cos\mu &= k\cos\beta \,. \end{aligned} \tag{4}$$

The factor k may be found by eliminating μ and ν. This yields

$$k = n\cos\omega_r - \cos\omega \tag{5}$$

where

$$\cos\omega = \cos\beta\cos\psi - \cos\alpha\sin\beta\sin\psi, \quad n^{-1}\sin\omega_r \sin\omega \,.$$

It can be verified that ω and ω_r are the angles of incidence and refraction with the surface normal. Solving equations (4) for μ and ν, we find the "grid" relations:

[3] The index of refraction, n, depends on the frequency of light. In the subsequent calculations we have assumed a value $n = 1.34$ corresponding to yellow light. This value is an appropriate average for phenomena depending on the total energy of sunlight.

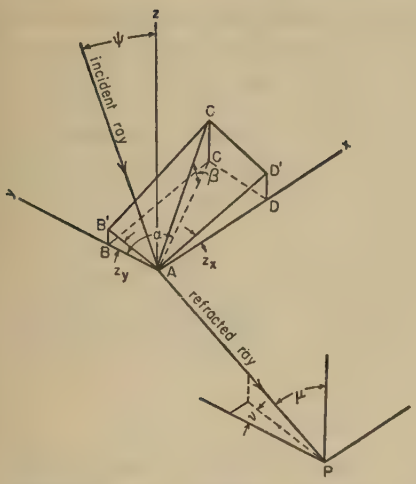

Figure 2. The coordinate system is centered at the sea surface with the z-axis vertically upward and the y-axis horizontal and toward the sun. The incident ray is refracted at A toward the observer at P, where it forms an angle μ with the vertical, and an azimuth ν to the right of the sun. Points ABCD define a horizontal plane through A, and $AB'C'D'$ a plane tangent to the sea surface. The tilt, β, is measured in the direction, AC, of steepest ascent, and this direction makes an angle α to the right of the sun.

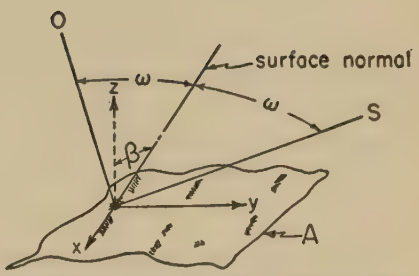

Figure 3. "A" is a unit of sea surface. The shaded portions indicate all points where the slopes lie within designated limits $z_x \pm \frac{1}{2}\delta z_x$, $z_y \pm \frac{1}{2}\delta z_y$. The average tilt in the shaded areas is β, where $\tan^2\beta = z_x^2 + z_y^2$. The y-axis is drawn away from the sun. Incident rays from the sun at O are reflected toward S. In the discussion of sky light (Sec. 4), the direction of rays is reversed. Incident rays from the sky at S are reflected toward the observer at O. In *both* cases the angle of the incident ray with the z-axis is designated by ψ and of the reflected ray by μ.

$$\begin{aligned} \cos\mu &= n^{-1}(\cos\psi + k\cos\beta) \\ \cot\nu &= \cot\alpha - (k\sin\alpha\sin\beta)^{-1}\sin\psi\,. \end{aligned} \tag{6}$$

Any point on the sea surface can be characterized by its zenith angle μ and direction ν. In the eight diagrams of Fig. 1, the angles μ, ν are represented by polar coordinates; μ is the radial distance and ν the angular coordinate. On these polar diagrams, curves of constant $\alpha(\mu, \nu)$ and $\beta(\mu, \nu)$ for various solar zenith angles ψ have been drawn according to the grid relations. An observer looking upward to a point μ, ν at the surface will see such facets highlighted that have the slope given by these curves.

2.2. *Surface radiance.* This section corresponds to the previously discussed case of reflection (Cox and Munk, 1954a: section 4). Individual highlights form distorted images of the sun. According to a general law of optics, the radiance (power per unit solid angle per

unit area normal to the beam) radiated by an image in a medium of refractive index n is (n^2) times the radiance of the object (in open space) reduced by any transmission losses of the optical system. Accordingly, the radiance within a highlight is $B' = n^2 \tau B$, where τ is the transmission of the sea surface and B is the radiance of the surface of the sun. According to Fresnel's formula for unpolarized light, $\tau = 1 - \rho$, where

$$2\rho = \sin^2(\omega - \omega_r) \csc^2(\omega + \omega_r) + \tan^2(\omega - \omega_r) \cot^2(\omega + \omega_r) . \quad (7)$$

The *total* power radiated per unit solid angle by the entire highlight is therefore $I = B' \Delta_s$, where Δ_s is the area of the highlight projected normal to the line of sight. Designating the horizontally projected area of the highlight by Δ_h, this becomes

$$I = n^2 \tau B \Delta_h \sec \beta \cos \omega_r . \quad (8)$$

The highlighted areas of the sea surface are those for which the sea surface has the appropriate tilt and azimuth of ascent to satisfy equations (6) within a small "tolerance" which allows for the fact that rays may originate at any point on the sun's face. This imposes limits on the permitted variation of α, β, or alternatively z_x, z_y, within the highlight. It may be shown that the area on the z_x, z_y-plane corresponding to the permitted variation of slopes within a highlight is

$$\delta z_x \, \delta z_y = \varepsilon k^{-2} \cos \omega \sec^3 \beta , \quad (9)$$

where ε is the solid angle subtended by the sun.[4]

The fraction of the (horizontally projected) sea surface which has slope components within the required limits $z_x \pm \frac{1}{2}\delta z_x$, $z_y \pm \frac{1}{2}\delta z_y$, is $p(z_x, z_y)\delta z_x \delta z_y$, where p is the probability distribution of slopes (Eq. 1). Hence the average power radiated by all highlights within a horizontal unit area of sea surface is $p\delta z_x \delta z_y I$. The average radiance N of the sea surface in the line of sight (power per unit solid angle per unit area *normal* to the beam) is this value multiplied by sec μ. Substituting from (8) and (9), we obtain

$$N = n^2 \tau H k^{-2} p \sec^4 \beta \cos \omega_r \cos \omega \sec \mu . \quad (10)$$

Here we have replaced $B\varepsilon$ by H, the irradiance (power per unit area) received at the sea surface from the sun.

[4] The solid angle subtended by a highlight is assumed small compared to the angle subtended by the sun. The highlighted areas are of the order of 0.1 mm², so that this assumption holds except within a few centimeters of the sea surface. In addition, the angular size of the sun is assumed to be small compared to the angular dimensions of the glitter pattern. This assumption fails for low sun angles and for very small slopes.

The simplest case is that for a point directly above the observer ($\mu = z_x = z_y = 0$) with the sun at the zenith ($\psi = 0°$). This gives

$$N_0 = \left(\frac{n}{n-1}\right)^2 \left[1 - \left(\frac{n-1}{n+1}\right)^2\right] Hp\,(0,0).$$

For a point directly *beneath* the observer, the reflected radiance under similar circumstances equals (Cox and Munk, 1954a)

$$N_0' = \frac{1}{4}\left(\frac{n-1}{n+1}\right)^2 Hp\,(0,0).$$

The ratio of refracted to reflected radiance is

$$\frac{N_0}{N_0'} = 4\left(\frac{n}{n-1}\right)^2 \left[\left(\frac{n+1}{n-1}\right)^2 - 1\right] \doteq 3000.$$

The radiance from a perfectly diffusing surface (one that scatters uniformly into a solid angle 2π) is H/π.

3. REFLECTION OF DIRECT SUNLIGHT FROM A ROUGH SEA SURFACE

The reflection of direct sunlight is an important factor in the energy budget of the ocean. Estimates based on reflection from a flat water surface are in error because the average coefficient of reflection for a rough surface differs from that for a flat surface. The difference becomes appreciable for low solar elevations.

First we consider the reflection by facets whose slopes lie within the limits $z_x \pm \frac{1}{2}\delta z_x$, $z_y \pm \frac{1}{2}\delta z_y$. Their (horizontally projected) area within a unit area A (Fig. 3) is, on the average, $p(z_x, z_y)\delta z_x \delta z_x$. The actual (tilted) area is sec $\beta p \delta z_x \delta z_y$. The projected area normal to the incoming rays from the sun is cos ω sec β $p\delta z_x \delta z_y$. The radiant flux intercepted is H cos ω sec β $p\delta z_x \delta z_y$. The reflected flux is

$$H\rho(\omega) \cos\omega \sec\beta\, p\delta z_x \delta z_y\,, \tag{11}$$

where $\rho(\omega)$ is given by Fresnel's formula (7). It is assumed that the incident light is not polarized and is reflected only once.

Equation (11) gives the reflected flux associated with slopes within the limit $z_x \pm \frac{1}{2}\delta z_x$, $z_y \pm \frac{1}{2}\delta z_y$. The total reflected flux per unit area of sea surface is then

$$H \iint \rho(\omega) \cos\omega \sec\beta\, p dz_x dz_y\,, \tag{12}$$

with the integration extending over all slopes exposed to the sun.

The radiant flux incident upon the unit area is $H \cos \psi$, where ψ is the sun's zenith angle. Consequently the fraction reflected, i. e. the *albedo*, is

$$R = \sec \psi \iint \rho(\omega) \cos \omega \sec \beta \; p dz_x dz_y \,. \tag{13}$$

For the special case of a level surface, $z_x = z_y = \beta = 0, \omega = \psi$, $\rho(z_x, z_y) = 0$ except at $z_x = 0$, $z_y = 0$. It follows that $R = \rho(\psi)$. For the general case, we make use of the law of reflection (Fig. 3)

$$\cos \omega = \cos \beta(\cos \psi + z_y \sin \psi) \,. \tag{14}$$

The quantities $F(\omega) = \rho(\omega) \cos \omega$ and $\sec \beta = (1 + z_x^2 + z_y^2)^{\frac{1}{2}}$ may now be expanded in Taylor's series in z_x, z_y around the values $z_x = z_y = 0$ for which $\beta = 0, \omega = \psi$. This yields

$$\mathrm{R} = \rho(\psi) \iint (1 + az_y + bz_y^2 + cz_x^2 + \ldots) \, p dz_x dz_y \,, \tag{15}$$

where

$$a = -F'/F, \quad b = \tfrac{1}{2} + \tfrac{1}{2}F''/F, \quad c = \tfrac{1}{2} + \tfrac{1}{2}(F'/F) \cot \psi \,. \tag{16}$$

The functions F, $F' = dF/d\omega$, $F'' = d^2F/d\omega^2$ are evaluated at $\omega = \psi$.

If all slopes are less in magnitude than $90° - \psi$, then the sea surface is everywhere exposed to the sun and the limits are $\pm \infty$. In this case

$$R = \rho(\psi) \, (1 + b < z_y^2 >_{AV} + c < z_x^2 >_{AV}) \,. \tag{17}$$

Here we have made use of

$$< z_y >_{AV} = \int_{-\infty}^{\infty}\int z_y p dz_x dz_y = 0$$

because the mean sea level is horizontal. To the present approximation the albedo depends only on the components of mean square slope along the sun's azimuth and normal to it; it does not depend on the form of $p(z_x, z_y)$. For the isotropic case, $< z_x^2 >_{AV} = < z_y^2 >_{AV} = \tfrac{1}{2} \sigma^2$, and

$$R = \rho(\psi) \, [1 + f(\psi) \, \sigma^2] \,, \tag{17a}$$

where

$$f(\psi) = \tfrac{1}{2}(b + c) = \tfrac{1}{2} + \tfrac{1}{4}(F'/F) \cot \psi + \tfrac{1}{4} F''/F \tag{17b}$$

is the "roughness" function plotted in Fig. 4. Some difficulties arise when ψ is large, and these will now be considered.

Large negative slopes in the component z_y are shadowed if they exceed $\cot \psi$. We shall allow for this "first order" hiding by setting the limits $(-\cot \psi)$ to ∞ for z_y (but $\pm \infty$ for z_x). This is equivalent to the limits 0 to 90° in the angle of incidence, ω. Because some additional slopes are hidden, the computed value of R will be too large for large ψ, but the evaluation of the "second order" hiding involves infor-

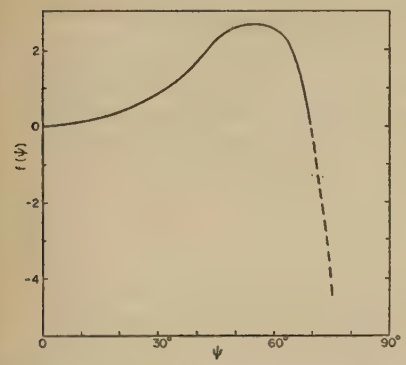

Figure 4. The roughness function $f(\psi)$ as defined in equation (17b). In the dashed portion near the horizon the function is not strictly applicable because of shadowing and multiple reflection.

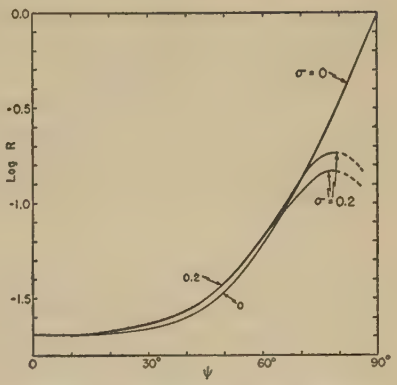

Figure 5. Reflection of solar radiation from a flat surface ($\sigma = 0°$) and a surface roughened by a Beaufort 4 wind ($\sigma = 0.2$). The albedo R varies from .02 for a zenith sun ($\psi = 0°$) to unity for the sun at the horizon ($\psi = 90°$) with the surface flat. For a rough surface, shadowing and multiple reflections become important factors when the sun is low. The lower and upper branches of the curve marked $\sigma = 0.2$ represent two assumptions regarding the effects of multiple reflection. True values are expected to lie between the indicated limits.

mation on the spectrum of ocean waves, and in the absence of such information we must restrict ourselves to the first order hiding.

The integration now yields

$$R = \rho(\psi)\ \{\tfrac{1}{2}[1 + I(k)] + \tfrac{1}{2}\pi^{-\frac{1}{2}}a\sigma e^{-k^2} + \\ + \tfrac{1}{4}\,b\sigma^2[1 + I(k) - 2\pi^{-\frac{1}{2}}\,ke^{-k^2}] + \tfrac{1}{4}\,c\sigma^2[1 + I(k)] + \ldots\} \quad (18)$$

where

$$k = \sigma^{-1}\cot\psi \quad (19)$$

and where $I(k) = 2\pi^{-\frac{1}{2}}\int_0^k e^{-t^2}dt$ is the error integral. The present approximation is adequate for large values of the dimensionless parameter k. For *very* large values, equation (18) converges on (17).

So far we have neglected multiple reflections. If the reflected ray goes toward a point *beneath* the horizon, then certainly there must be at least one further reflection. This "first order" multiple reflection requires that z_y be negative and exceed $\frac{1}{2}\cot\psi(1 - \tan^2\beta)$ in magnitude. The product of coefficients of reflection of all but the first reflection is unknown but must lie between unity and zero. In the first extreme, multiple reflections would not alter R, and equation (18)

is correct as it stands. In the latter extreme case, the integration with respect to z_y in equation (15) is between the limits $-\frac{1}{2}\cot\psi(1-\tan^2\beta)$ and $+\infty$. These can be replaced by the limits $-\frac{1}{2}\cot\psi$ and $+\infty$ because of the heavy discrimination of the exponential factor in $p(z_x z_y)$ against contributions from large β. The limits on z_x remain $\pm\infty$. The result of this integration is again equation (18) but with k now designated by

$$k = \tfrac{1}{2}\sigma^{-1}\cot\psi \tag{20}$$

rather than by the quantity in equation (19).

Fig. 5 shows the average reflectivity of the sea surface bracketed by these two expressions as compared with the reflectivity of a flat surface. At high sun elevation, the albedo of the rough surface is slightly larger; for $\psi = 40°$ the values are 2.5% for the smooth surface and 2.7% for the rough surface. At low sun elevation, increasing roughness leads to a marked decrease in albedo. The only conclusion of oceanographic consequence seems to be that in summer substantially more energy must penetrate the open stretches of the Arctic Ocean than had been estimated previously and that the amount of this additional energy depends on the wind speed.

4. REFLECTION OF SKY LIGHT FROM A ROUGH SURFACE

The radiance of the sky is due to scattering of sunlight and reflected "earth light" by air molecules (Rayleigh scattering), dust, haze, clouds, etc. This varies in a complicated and rather unpredictable way over the sky dome. We shall consider the three cases illustrated in Fig. 6:

(a) a clear tropical sky at Bocaiuva, Brazil, from measurements[5] by Richardson and Hulbert (1949);

(b) a uniform sky dome;

(c) a completely overcast sky, whose radiance can be approximated by the empirical formula (Moon and Spencer, 1942)

$$N_s(\psi) = \tfrac{1}{3}N_s(0)(1 + 2\cos\psi)\,. \tag{21}$$

To simplify subsequent calculations we shall make all quantities depend only on the zenith angle ψ. This already holds for (*b*) and (*c*), but for (*a*) the sky depends largely on zenith angle. Accordingly we have ignored the increased radiance near the sun and have based our calculations on the observed radiance along an azimuth 90° from the azimuth of the sun. In the following calculations we also assume

[5] The observations were made at 2200 feet; the sky radiance at sea level would be slightly different.

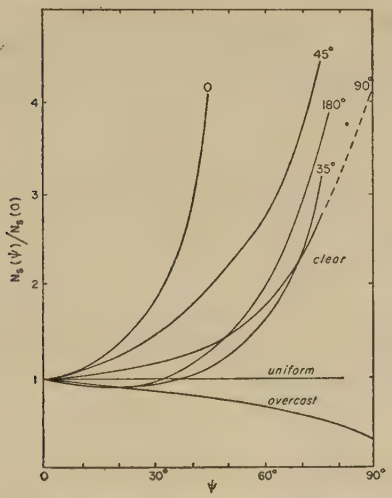

Figure 6. The radiance of the sky $N_s(\psi)$ divided by the radiance at the zenith $N_s(0°)$ as function of the zenith angle ψ. The curves for the clear sky are based on observation at Bocaiuva, Brazil, for the sun at $\psi = 60°$. They are drawn for indicated azimuths relative to the sun. Computations are based on the heavy curve marked 90°. The radiance for the overcast sky, based on the empirical law (21), applies to all azimuths.

unpolarized sky light.[6] Actually there is considerable polarization for a clear sky, and the polarization is a function of the azimuth relative to the sun.

The derivation is similar to that in the preceding section. The rays in Fig. 3 are reversed, with ψ and μ again designating the zenith angles of the incident and reflected rays. The radiant flux from a segment of sky S reflected by the unit area A toward the observer O is (in place of eq. 11)

$$N_s\, \rho(\omega)\, \cos\omega\, \sec\beta\, p\delta z_x \delta z_y\,,$$

where N_s is the radiance of the sky (power per unit solid angle per unit area normal to the beam). Summing over all *visible* slopes yields the total reflected flux from the unit area A toward the observer O,

$$\iint N_s\, \rho(\omega)\, \cos\omega\, \sec\beta\, p dz_x dz_y\,. \tag{22}$$

The radiance of the sea surface in the observer's line of sight (intensity per unit area normal to the beam) is found by dividing by $\cos\mu$:

$$N = \sec\mu \iint N_s\, \rho(\omega)\, \cos\omega\, \sec\beta\, p dz_x dz_y\,. \tag{23}$$

[6] Effectively we write $[N_{s\parallel} + N_{s\perp}]\,[\rho_\parallel + \rho_\perp]$ (or $N_s\,\rho$ in our notation) instead of $N_{s\parallel}\rho_\parallel + N_{s\perp}\rho_\perp$, where $\parallel$ $\perp$ refer to polarization in the plane of incidence, and normal to it, respectively.

For the special case of a uniform sky dome, N_s is constant, and the expression for (N/N_s) is identical with that for R in section 3. The preceding remarks on integration limits are applicable, and the results given in equations (15)–(20) and in Figs. 4 and 5 can be applied directly.

For the case where sky radiance depends on the zenith angle ψ (and ψ only), we must generalize the procedure in section 3. Writing the law of reflection in the form (Fig. 3)

$$\cos\psi = \cos^2\beta\,[(1 - \tan^2\beta)\cos\mu + 2z_y \sin\mu], \tag{24}$$

and again expanding in Taylor's series, leads to the integrals in section 3 with R now denoting $N(\mu)/N_s(\psi)$, and with a, b, c replaced by

$$\begin{aligned} a_s &= -F'/F - 2N_s'/N_s\,, \\ b_s &= \tfrac{1}{2} + \tfrac{1}{2}F''/F + 2(N_s'/N_s)(F'/F) + 2N_s''/N_s\,, \\ c_s &= \tfrac{1}{2} + \tfrac{1}{2}(F'/F)\cot\mu + 2(N_s'/N_s)\cot\mu\,. \end{aligned} \tag{25}$$

Fig. 7 shows the results for two sky conditions illustrated in Fig. 6. Directly beneath the observer ($\mu = 0°$), the rough sea may be brighter or dimmer than a smooth sea depending on the condition of the sky. A rough sea contrasts with a flat surface most markedly near the horizon, where the rough sea appears darker. If the sea were absolutely flat, then the radiance of the sea surface just beneath the horizon would equal the radiance of the sky just above it, and there would be no visible horizon.

The albedo of the sea surface exposed to sky light is the ratio of reflected to incident flux. The reflected flux from a unit area is $N(\mu)\cos\mu$ (compare equations 22 and 23) and the total reflected flux is $2\pi\int_0^{\frac{1}{2}\pi} N(\mu)\cos\mu\sin\mu\,d\mu$. Similarly, the total incident flux is $2\pi\int_0^{\frac{1}{2}\pi} N_s(\psi)\cos\psi\sin\psi\,d\psi$. Hence the albedo is given by

$$R = \int_0^{\frac{1}{2}\pi} N(\mu)\sin 2\mu\,d\mu \Big/ \int_0^{\frac{1}{2}\pi} N_s(\psi)\sin 2\psi\,d\psi\,. \tag{26}$$

TABLE I. Albedo of Sea to Sky Light

Sea / Sky	*Smooth* ($\sigma = 0$)	*Rough* ($\sigma = 0.2$)
Clear	.100	.071 – .088
Uniform	.066	.050 – .055
Overcast	.052	.043 – .044

The albedo has been evaluated numerically for a smooth and rough sea surface for each of the three sky conditions shown in Fig. 6. In the case of the rough surface, the integration was carried out along both branches of the curve $\sigma = 0.2$ in Fig. 7; the correct values are

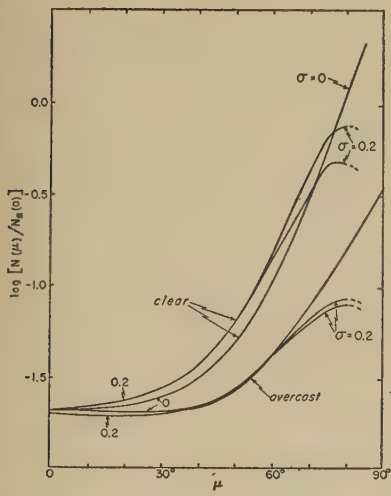

Figure 7. The radiance of the sea surface, $N(\mu)$, divided by the sky radiance at the zenith, $N_s(0°)$, as a function of the vertical angle μ. The curves are computed for a flat ($\sigma = 0$) and rough ($\sigma = 0.2$) surface for each of the three sky conditions illustrated in Fig. 6. The two branches for the curves marked $\sigma = 0.2$ again indicate the upper and lower limits inherent in equations (19) and (20).

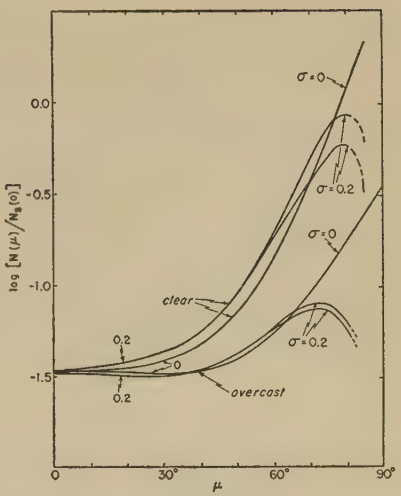

Figure 8. The radiance of a slick sea surface (see legend of Fig. 7).

believed to lie within the indicated limits. Compared to a flat sea, the albedo is reduced by about 20% in the presence of a Beaufort 4 wind, due largely to the hiding of effectively reflecting slopes and to subsequent darkening of the sea surface near the horizon.[7]

For the uniform sky, Schmidt (1915) had previously obtained a theoretical value of 0.17. Measurements by Neiburger (1948) and

[7] Note added in proof: Burt (1954) has calculated the albedo of the sea surface to direct sunlight and diffused light by methods similar to ours. However, there are two important differences. Burt made no allowance for multiple reflections but he allowed for shadowing by assuming the *same* distribution of slopes in the shadowed and unshadowed areas. For very low sun elevations he obtains 100% effective reflectivity regardless of surface roughness, whereas our approximation indicates a lowering of reflectivity which increases in magnitude with increasing roughness. Applied to the reflection of skylight, Burt's result implies that there would be no contrast at the horizon, while in fact the sea is darker than the sky, particularly on windy days. Fortunately the albedo to skylight is little effected by any of these assumptions. For $\sigma = 0.2$, Burt obtains $R = .058$ (clear sky), .048 (overcast), while our values are .050 — .055 (clear), .043 — .044 (overcast).

Burt (1953) under an overcast sky gave only 0.10. Burt subsequently noticed that Schmidt had omitted cosine terms in his flux intergration. The correct integration, already carried out by Judd (1942), gave a value of 0.066. Whereas initially the theoretical value had been too high, it was now too low with the discrepancy almost as bad. The values in Table I show that allowance for surface roughness does not help. The explanation seems to be the one offered by Neiburger (in press): a reflection from bubbles and particles in the water in addition to the reflection at the surface. The average reflection due to internal scattering measured by Powell and Clarke (1936) is 0.3, and this brings observation and theory into reasonable accord. Our measurements (Cox and Munk, 1954a) also indicate that the scattered intensity can be an appreciable fraction of the reflected intensity.

5. VISIBILITY OF SLICKS

As an application of the preceding section we may consider the contrast of slick streaks on a roughened water surface.

A slick is caused by the presence on the sea surface of a thin layer of organic matter. Natural slicks are often thin compared to the wave length of light, and the reflection coefficient of a slick surface is practically the same as that of an uncontaminated surface. The thin layer becomes visible because the rms slope is substantially smaller there than elsewhere. This reduction is accomplished, at least in part, by the viscous dissipation of wavelets against the quasi-inextensible surface film. The reduction in slope in a good sized slick may be achieved by a factor of 1.5 to 2 (Cox and Munk, 1954b).

A slick lying *within* the sun's glitter pattern has a larger luminosity near the glitter center and a smaller luminosity near the outer edges than the uncontaminated water surface. This has already been discussed (Cox and Munk, 1954b) and an example is shown in fig. 2 of that paper. The visibility of thin (natural) slicks *outside* the sun's glitter can be discussed with reference to Fig. 7. To an observer looking steeply downward (small μ), the slick (small σ) appears dark under a clear sky, light under an overcast sky. Near the horizon the slick is always light. The contrast required for the visibility of large slicks is of the order of 2% ($\sim$ 0.01 on the logarithmic scale in Fig. 7), and we may expect adequate contrast for visibility even when the winds are light. In searching for thin slicks one should concentrate on an area well toward the horizon in clear weather.

The situation is different in the case of freshly spread slicks of mineral oil. The presence of interference colors demonstrates a thickness larger than a wave length of light. Suppose the index of refraction is that of light oil, $n = 1.45$, as compared to 1.34 for water.

For normal incidence the reflectivities are

$$(n - 1)^2 (n + 1)^{-2} = 0.034 \text{ for air-oil interface,}$$
$$= 0.020 \text{ for air-water interface.}$$

Multiple reflections within the oil layer increase the effective reflectivity to 0.036, 1.8 times that of an uncontaminated surface. The ratio is smaller for glancing incidences. It equals 1.6, 1.3, 1.0 for angles of incidence 30°, 60°, 90°.

These coefficients have been taken into account in Fig. 8. The visibility of thick (artificial) slicks can be estimated by comparison with Fig. 7. Suppose we compare the oily smooth surface (Fig. 8, $\sigma = 0$) with the uncontaminated rough surface (Fig. 7, $\sigma = 0.2$). The slicks are brighter, and the contrast is most marked directly beneath the observer ($\mu = 0°$).

Some remarkable photographs of slick bands have been published by Ewing (1950). The surprising aspect is that these bands are due to *internal* waves. These are made visible by a curious chain of events: the orbital motion of the internal waves converges at the troughs and the oils resulting from biological activity are squeezed into a surface-active film under tension, as shown by Ewing. This film, by virtue of its resistance to stretching, imposes a horizontally quasi-rigid boundary against which short wavelets generated by local winds dissipate most of their energy. The resulting decrease in mean square slope affects the average reflectivity and also the segment of sky that is mirrored in the trough zones; both of these effects produce a brightness contrast between the slicks and the surrounding ruffled water. It would seem that it is virtually impossible to predict the devious means by which nature chooses to reveal herself to the astute observer!

REFERENCES

Burt, W. V.

1953. A note on the reflection of diffuse radiation by the sea surface. Trans. Amer. geophys. Un., *34:* 199–200.

1954. Albedo over wind-roughened water. J. Meterol., *2:* 283–290.

Cox, Charles and W. H. Munk

1954a. The measurement of the roughness of the sea surface from photographs of the sun's glitter. J. opt. Soc. Amer., *44:* 838–850.

1954b. Statistics of the sea surface derived from sun glitter. J. Mar. Res. *13:* 198–227.

Duntley, S. Q.

1950. The visibility of submerged objects: Part I, Optical effects of water waves. Visibility Laboratory, Mass. Inst. Techn. Report, Dec. 15, 1950, or U. S. Office of Naval Research Report No. N5 ori-07831.

Ewing, Gifford

1950. Slicks, surface films and internal waves. J. Mar. Res., *9*: 161–187.

Judd, D. B.
1942. Fresnel reflection of diffusely incident light. J. Res., Nat. Bur. Stand., *29:* 329–332. Research Paper 1504.
Moon, Parry and D. E. Spencer
1942. Illumination from a non-uniform sky. Ill. Eng., *37*; 707–726.
Neiburger, Morris
1948. The reflection of diffuse radiation by the sea surface. Trans. Amer. geophys. Un., *29:* 647–652.
1954. A note on the reflection of diffuse radiation by the sea surface. Trans. Amer. geophys. Un. (in press).
Powell, W. M. and G. L. Clarke
1936. The reflection and absorption of daylight at the surface of the ocean. J. opt. Soc. Amer., *26:* 111–120.
Richardson, R. A. and E. O. Hulburt
1949. Sky brightness measurements near Bocaiuva, Brazil. J. geophys. Res., *54:* 215–227.
Schmidt, Wilhelm
1915. Strahlung and Verdunstung an freien Wasserflächen; ein Beitrag zum Warmehaushalt des Weltmeers und zum Wasserhaushalt der Erde. Ann. Hydrogr., Berl., *43:* 111–124.
Schooley, A. H.
1954. A simple optical method for measuring the statistical distribution of water surface slopes. J. opt. Soc. Amer., *44:* 37–40.

NOTES ON THE PRECISION OF A MODIFIED ROUTINE NITRATE-NITRITE ANALYSIS

By

KENNETH T. MARVIN

U. S. Fish and Wild Life Service
Fort Crockett, Galveston, Texas

ABSTRACT

Factors responsible for difficulties in using the strychnidine method for an analysis of nitrate-nitrite content of sea water have been investigated. It has been demonstrated that their effects can be minimized and that the ease of analysis is materially increased by certain modifications, one of which is the adjustment of the concentration of nitrate by dilution to bring the optical density within the best working range of the photometer used. The largest single source of error was found to be variation in the rate of heat formation during the mixing of the sample and reagent, which could be minimized by following the mixing procedure recommended. It is believed that this work offers improved precision without affecting the value of the technique as a rapid routine method for large-scale investigations.

In using the strychnidine method for analysis of nitrate-nitrite in sea water, we experienced many of the same difficulties encountered by other operators. In an effort to minimize these difficulties, a modified method has been developed which is now employed in the laboratory of the Gulf Fishery Investigations. Actually, it is a modified version of the analysis prescribed by Zwicker and Robinson.[1]

This modification controls color densities of the reagent-sample mixture so that the range of concentrations found in sea water can be determined by using 3 ml micro cells (cylindrical cell 6.75 cm long and 1.19 cm inside diameter) in a Fisher A. C. Electrophotometer. The mixture is obtained by diluting the water sample with two parts of distilled water and then adding this diluted sample to an equal volume of a reagent consisting of 0.3 millimole of strychnidine per liter of concentrated sulfuric acid.

[1] Zwicker, B. M. G. and R. J. Robinson. 1944. The photometric determination of nitrate in sea water with a strychnidine reagent. J. Mar. Res., *5:* 214–231. They used the Zeiss-Pulfrich photometer equipped with 0.1–15 mm variable depth cell. Their procedure was as follows:

Equal volumes of reagent and sample were carefully mixed in aged pyrex tubes by four careful but rapid transfers from one to the other. The hot mixtures were immediately placed in the dark for three to five hours. Measurements were then made with a photometer.

This reagent is suitable for determining concentrations found in waters which range from 0 to about 45 microgram atoms of NO_3-NO_2 nitrogen/liter (μg-at NO_3-NO_2-N/l). The -log T readings for this range cover practically the entire scale of the electrophotometer and at the same time permit the use of a calibration curve having the best possible slope. Thus, maximum efficiency of the photometer is achieved. At concentrations above 45 μg-at/l, the slope flattens too much for use.

The dilution of samples does not necessarily mean that all errors will be increased proportionally. Actually, the dilution moves the concentration of many samples to a more sensitive region of the NO_3-NO_2 calibration curve.

Zwicker and Robinson recommended that the strength of the reagent and the depth of the cell be dependent upon the range of NO_3-NO_2 concentration in the sample in order to utilize the optimum operating conditions of reagent and photometer.[2] In our routine sampling of hundreds of water samples having the range of NO_3-NO_2 concentration found in the Gulf, their recommendation would be impractical since it would necessitate a preliminary investigation of all samples to approximate the magnitude of the NO_3-NO_2 concentration.

A chemist and his helper can easily run 200 determinations in an eight-hour period when employing our modification, which is as follows:

1. With a 1 ml pipette, transfer 1 ml of sample which has had no preliminary preparation, such as filtration, etc., into each of two 10 ml pyrex test tubes (for duplicates).

2. With a 3 ml automatic pipette, add 2 ml of distilled water to each of the 10 ml tubes.

3. Using a 5 ml automatic pipette, add 3 ml of strychnidine reagent to each tube. To prevent boiling during this addition, tilt the tube to about a 45° angle and allow the reagent to run down the inside so that it forms a layer under the water sample. It is important that this step be performed with great care to avoid unnecessary mixing of reagent and sample.

4. With the aid of a 15 ml pyrex tube, mix by gently pouring the contents of each tube into the mixing tube and back again only once. It is suggested that about 15 mixing tubes be used in rotation and that each tube be allowed to drain after use.

[2] Their recommended procedure for the Zeiss-Pulfrich photometer follows:

NO_3 *range* (µg-at/l)	*Strychnidine* (millimoles/l)	*Sample* (ml)	*Size of Test Tube* (mm)	*Standing Time* (hours)	*Thickness of Cell* (stratum, mm)
0.2–4	0.10	14	20 ×155	4–24	50
2.5–10	0.10	3	13 ×100	2–28	10
5–15	0.50	3	13 ×100	2–5	5
1.2–40	1.0	3	13 ×100	2–5	2
2.5–75	5.0	3	13 ×100	2–4	1

5. Store samples in darkness for four hours.

6. Check color density with the Fisher A. C. Electrophotometer by using 3 ml micro cells and 525 mμ "B" filter.

7. Check the results against standard controls which are run with the samples and which are interspersed among them during the reading of color densities.

ESTIMATE OF PRECISION OF THE METHOD

An estimate of precision was obtained by running a series of checks within the range of values that are possible with a Fisher A. C. Electrophotometer equipped with a 3 ml micro cell and with a reagent containing 0.3 millimole of strychnidine in a liter of concentrated sulfuric acid. This range includes concentrations from 0 to 15 μg-at/l of nitrate.

The range was covered in 1 μg-at/l steps. Approximately 50 replicate determinations were made on each of the 16 concentrations that were checked. Color density differences between samples and distilled water were read directly from the electrophotometer in -log T units after which they were converted to μg-at/l units by assuming a constant slope between two adjacent sets of standards. An estimate of precision for the concentrations tested is tabulated in column 4 of Table I.

TABLE I. Statistics Pertaining to NO_3-NO_2 Analyses at Various Concentration Levels

Concentration level	N	$\bar{X}$	S	l_1	l_2
0	55	0.000	0.1551	−0.0558	0.0558
1	52	1.004	0.1171	0.9606	1.0474
2	55	1.987	0.1156	1.9454	2.0286
3	52	2.988	0.1131	2.9461	3.0299
4	51	4.022	0.1640	3.9605	4.0835
5	56	4.993	0.2463	4.9052	5.0808
6	53	6.030	0.0799	6.0007	6.0593
7	55	6.980	0.2791	6.8796	7.0804
8	56	8.014	0.1939	7.9449	8.0831
9	53	9.002	0.3054	8.8899	9.1141
10	51	9.998	0.3465	9.8682	10.1278
11	43	11.040	0.2927	10.9197	11.1603
12	54	12.030	0.3937	11.8869	12.1731
13	53	13.028	0.3478	12.9003	13.1557
14	46	13.974	0.3022	13.8540	14.0940
15	57	14.974	0.3807	14.8396	15.1084

N—Number of replicates.

$\bar{X}$—Average of replicates in μg-at NO_3-NO_2-N/l.

S—Standard deviation.

l_1; l_2—Fiducial limits of $\bar{X}$ at a probability level of .01.

In the modified routine analysis, the precision would be approximately one-third that shown in column 4 of Table I because all samples are diluted with two parts of water; hence, the standard deviation of the sets would be increased by three. Also, the difference in error of the two methods due to volumetric difference would have to be included. This, as shown in Table II, is negligible. Based on these facts, Table III has been constructed to show the precision that can be expected from routine analysis.

TABLE II. Precision of Volumetric Measurements

No. 1 *Steps involved in routine analysis.*

1.—1 ml sample delivery using 1 ml pipette.
2.—2 ml H_2O delivery using 3 ml automatic pipette.
3.—3 ml reagent delivery using 5 ml automatic pipette.

Step	1	2	3
N	31	33	30
S^2	2.35×10^{-5}	6.36×10^{-5}	1.69×10^{-4}

$$S^2 \text{ due to volumetric deviation} = \frac{2.35 \times 10^{-5}}{6} + \frac{6.36 \times 10^{-5}}{3} + \frac{1.69 \times 10^{-4}}{2} = 1.096 \times 10^{-4}.$$

S due to volumetric deviation = .0105.

No. 2 *Steps involved in estimating precision.*

1.—3 ml sample delivery using 5 ml automatic pipette.
2.—3 ml reagent delivery using 5 ml automatic pipette.

Step	1	2
N	20	30
S^2	6.42×10^{-5}	1.69×10^{-4}

$$S^2 \text{ due to volumetric deviation} = \frac{6.42 \times 10^{-5}}{2} + \frac{1.69 \times 10^{-4}}{2} = 1.166 \times 10^{-4}.$$

S due to volumetric deviation = .0108.

N—Number of replicates. S^2—Variance. S—Standard deviations..

ESTIMATE OF PRECISION OF EACH STEP IN THE NITRATE DETERMINATION

The precision of the modified technique was estimated by determining the accuracy that could be expected from each individual step. Experiments were conducted in which the various steps of the technique were deliberately varied to considerable extents. The effects of these alterations on the final nitrate concentration were then ascertained.

Human and instrumental errors introduced in reading color density differences were estimated by measuring the deviation that occurred in reading sets of replicates from a series of standards. A standard was made up and a portion poured off and checked in the photometer.

TABLE III. STATISTICS PERTAINING TO ROUTINE NO_3-NO_2 ANALYSIS

Concentration Level	*N*	S^2	$\bar{X}$	S_1^2	S_2^2	$S^2-(S_1^2+S_2^2)$	l_1	l_2
0	55	0.2406	0.000	0.0036	0.0001	0.2369	−0.0558	0.0558
3	52	0.1234	3.012	0.0036	0.0001	0.1197	2.8818	3.1422
6	55	0.1202	5.964	0.0036	0.0001	0.1165	5.8362	6.0858
9	52	0.1153	8.964	0.0049	0.0001	0.1103	8.8383	9.0897
12	51	0.2423	12.066	0.0049	0.0001	0.2373	11.8815	12.2505
15	56	0.5461	14.979	0.0081	0.0001	0.5379	14.7156	15.2424
18	53	0.0574	18.090	0.0121	0.0001	0.0452	18.0021	18.1779
21	55	0.7013	20.940	0.0289	0.0001	0.6723	20.6388	21.2412
24	56	0.3385	24.042	0.1521	0.0001	0.1863	23.8347	24.2493
27	53	0.8394	27.006	0.0625	0.0001	0.7768	26.6697	27.3423
30	51	1.0854	29.994	0.1156	0.0001	0.9697	29.6046	30.3834
33	43	0.7720	33.120	0.1849	0.0001	0.5870	32.7591	33.4809
36	54	1.3912	36.090	0.2704	0.0001	1.1207	35.6607	36.5193
39	53	1.0952	39.084	0.3600	0.0001	0.7351	38.7009	39.4671
42	46	0.8217	41.922	0.2304	0.0001	0.5912	41.5620	42.2820
45	57	1.3003	44.922	0.3025	0.0001	0.9977	44.5188	45.3252

Concentration Level—Approximate Concentration in μg-at NO_3-N/l Tested.

N—Number of replicates.

$\bar{X}$—Average of replicates expressed in μg-at NO_3-N/l.

S^2—Variance.

S_1^2—Variance due to instrumental and operational deviation.

S_2^2—Variance due to volumetric deviation assuming all deviations are accumulative.

l_1; l_2—Fiducial limits of $\bar{X}$ at a probability level of .01.

The sample was then removed from the instrument and poured back into the original batch of standard. This cycle was repeated approximately 50 times for each concentration. Instrumental and operational errors were based on deviation in these sets of readings. The standards used for this check consisted of various dilutions of a nonfading red compound (red ink). This eliminated possible deviation due to color fading during the time required to read a set of replicates. The results, tabulated in column 5 of Table III are also presented in Fig. 1.

The errors involved in pipette deliveries result from variations in measuring: 1 ml of sample with a 1 ml pipette, 2 ml of distilled water with a 3 ml automatic pipette, and 3 ml of reagent with a 5 ml automatic pipette. The variation that can be expected with these three instruments was estimated by measuring equivalent amounts of distilled water for the 1 and 2 ml measurement and of sulfuric acid for the 3 ml reagent measurement, after which the accuracy of each measurement was determined by weight on an analytical balance having a sensitivity of approximately 1/10 mg.

The results of this check are given in Table II and in column 6 of Table III. The effect of deviations in sample and reagent measurements on the final nitrate concentration was determined by running several series of checks in which variations were deliberately intro-

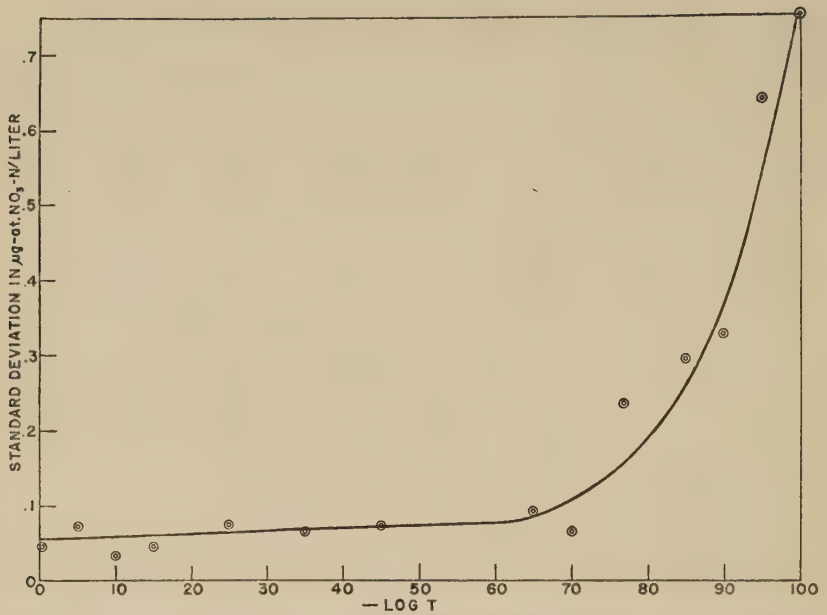

Figure 1. Deviation in NO_3 concentration caused by instrumental and operational errors.

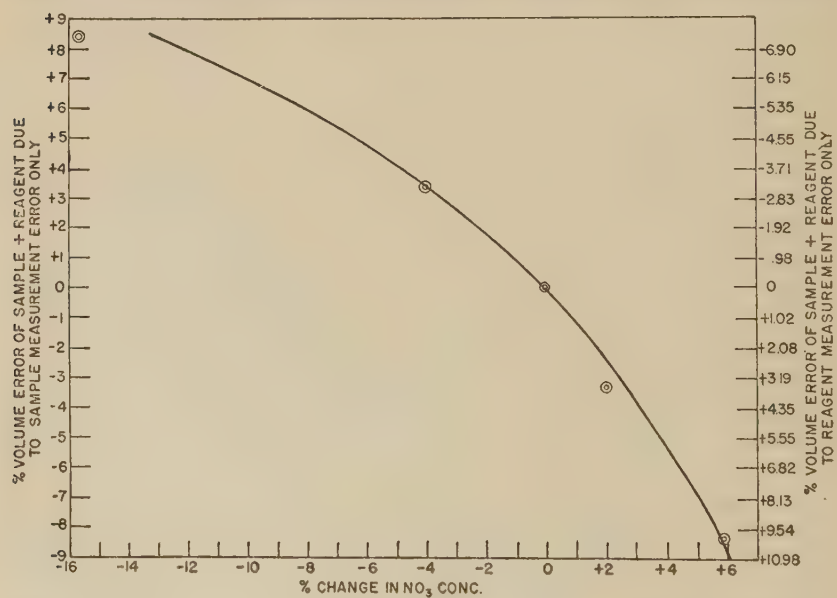

Figure 2. Per cent errors in NO_3 concentration caused by volumetric deviations.

duced. The results, which show variation in nitrate concentration vs. variations in sample and reagent measurements, are presented in Fig. 2.

We found that variation in the rate of heat formation during the mixing of the sample and reagent is the greatest single factor that affects the precision of the results. Investigation has shown that the degree of variation in color formation of replicate samples is dependent on the rate of removal of the heat produced during the mixing opera-

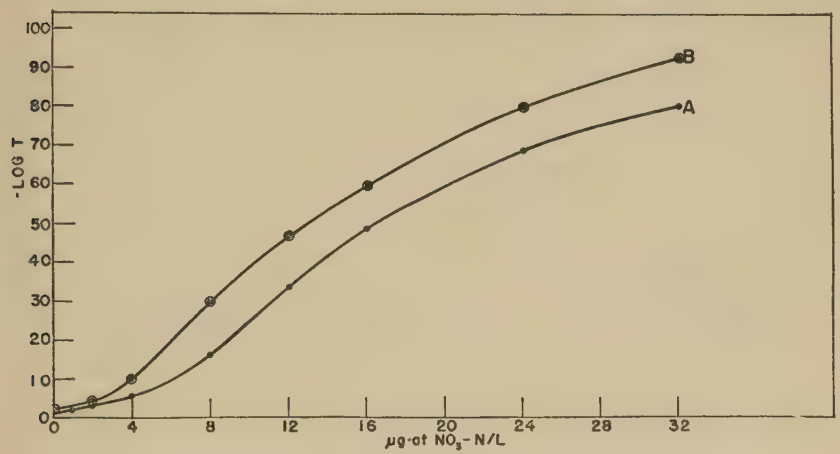

Figure 3. NO_3 calibration curve showing effect of rate of heat formation on color development. *A*—high rate of heat formation. *B*—low rate of heat formation.

tion. A high rate of increase in temperature results in a minimum color density, whereas a low rate of increase results in a maximum color density. By standardizing the mixing operation, it has been possible to reduce greatly the variability due to heat, thereby increasing the precision of the method.

The effects of high and low rates of heat formation are demonstrated in two calibration curves, *A* and *B* of Fig. 3. Both curves were made from a single set of standard samples and from the same batch of reagent. The determination of values for the two curves was based on the average of 10 replicates run alternately to minimize errors due to time difference. A maximum rate of heating was obtained by mixing the samples and reagent rapidly (see Curve *A*). A minimum rate was obtained by carefully adding reagent to sample in such a way that two distinct layers were formed. These were then mixed by pouring them into a "mixing" tube and back into the original tube; thus, the mixture was poured only twice, from original tube to mixing tube and back again.

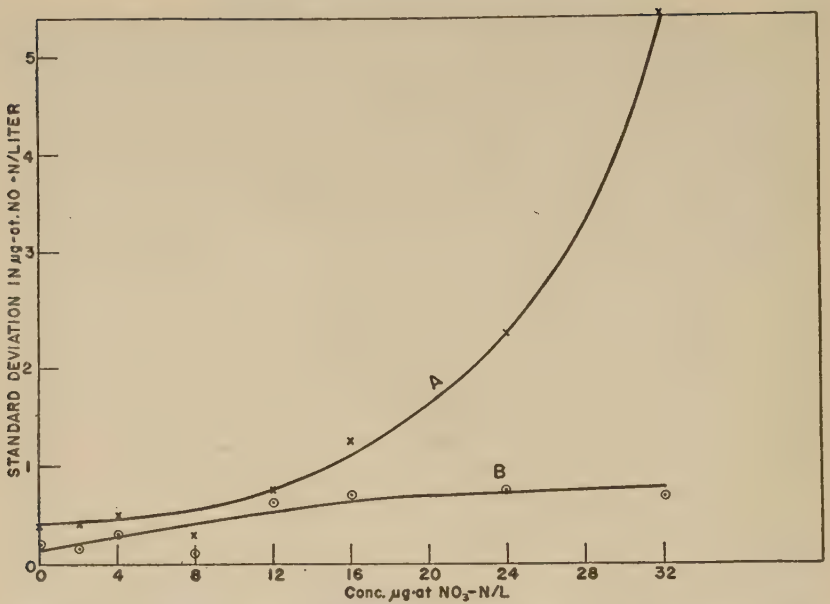

Figure 4. Comparison of standard deviations at various NO_3 concentration levels: *A*, when rate of heat formation during the mixing of reagent and sample is high; *B*, when the rate of heat formation is low.

The range of values represented by the horizontal distance between curves *A* and *B* represents the deviation that could occur within a set of replicate samples if an operator were unfamiliar with the relationship that exists between rate of heat formation and color formation. A comparison of the standard deviation of the two sets is shown in Fig. 4.

The low degrees of variation exhibited by *B*, as compared to *A*, indicate that careful mixing is necessary if good precision is to be maintained.

DISCUSSION

The entire check on precision of the method could not be completed during one session. Had it been possible, then the average of the 16 sets could have been used in the construction of a calibration curve, thus eliminating the necessity of arriving at slope values by assuming straight line relationships between two sets of values. The fact that all 16 points do not form a smooth curve emphasizes the importance of including a set of standards with every run of samples. We found that there was considerable day-to-day variation in the density of color formation, probably due to temperature difference, methods of

mixing sample and reagent, and other conditions that would be difficult to control.

A four-hour color development time was allowed for all determinations. This time was based on a check of color density vs. time for concentrations of 0, 6, 18, 25, 30, and 45 μg-at NO_3-N/l. Results show that rate of development at 30° C became minimal between the fourth and fifth hour. The room temperature during the experiments was approximately 30° ± 2° C.

The final nitrate concentration varies almost directly with the deviations normally expected in the measurement of sample, reagent, and distilled water. This is illustrated in Fig. 2, in which volumetric errors have been deliberately introduced. This direct relationship was assumed to be the case.

A large percentage of the total deviation incurred in the modified technique cannot be accounted for by instrumental, operational, or volumetric errors. The data in columns 3 and 7 of Table III demonstrate that variation in rate of heat formation during the mixing of sample and reagent probably accounts for a large percentage of this difference even though efforts were made to minimize this effect.

THE SEASONAL OSCILLATION IN SEA LEVEL[1]

By

JUNE PATTULLO, WALTER MUNK,
ROGER REVELLE, ELIZABETH STRONG

Scripps Institution of Oceanography

ABSTRACT

On the basis of all available tide gauge records, bathythermograms, and Nansen bottle casts, we have compiled, on a global scale, monthly departures of *recorded* and *steric* sea levels from their annual means. The steric fluctuation is defined in terms of the seasonal fluctuation in specific volume. The results are given in the appendices and in three charts, together with error estimates. In general, the departures are comfortably above the uncertainties introduced by year to year variations and by the effects of local topography.

Recorded and steric departures agree remarkably well in low and temperate latitudes (conditions are *isostatic*). In these regions the steric levels are associated largely with temperature fluctuations in the upper 100 m. In high latitudes conditions are indeterminate.

Pronounced semiannual fluctuations are found along the west coast of South Africa, in Indonesia, in corresponding regions of the Labrador and Oyashio currents, and in the Gulf of Mexico and adjoining Gulf Stream stations (but not in the Kuroshio!). Elsewhere the oscillations are largely annual in character, with low sea level in each hemisphere during its spring and with high level during the fall. Recorded amplitudes vary from a few centimeters in the tropics to a few decimeters at higher latitudes; they exceed one meter in the Bay of Bengal. Atmospheric pressure effects and long period astronomic tides account for only a small part of the recorded fluctuations.

1. INTRODUCTION

The noteworthy compilation of 10^5 mean monthly heights of sea level from nearly all existing tide gauge stations, prepared by Proudman under the auspices of the Union Géodésique et Géophysique Internationale (UGGI, 1940, 1950), makes it possible to view the seasonal oscillation in sea level on a global scale. Numerous investigations have dealt with single stations or with small groups of stations.

[1] Contribution from Scripps Institution of Oceanography, New Series No. 780. This compilation has been made possible by a grant-in-aid from the Institute of Geophysics, and by the support of the Office of Naval Research. We have also received substantial assistance from the Woods Hole Oceanographic Institution and the Hydrographic Office, U. S. Navy. We are especially indebted to Mrs. Jack Ludwick, Miss Evangeline P. Tollios, Mr. Gordon Groves and Mr. Heber Blair for their help.

But it appears to be typical of meteorological and oceanographic phenomena that the larger the area under consideration the simpler they are. We believe, therefore, that an investigation on a global scale, although offhand more ambitious, is actually less so. It certainly is the more rewarding at this time.

For comparison we have also computed oscillations in the height of the sea surface arising from the seasonal variation in specific volume. These are called *steric* oscillations.[2] The steric sea level is high when the water is warm, low when it is cold. Conversely, a high steric level corresponds to a low value of salinity. The source of data consists of bathythermograms and, to a much lesser extent, Nansen bottle casts. For all oceans, information is now on file at the U. S. Navy Hydrographic Office for 5×10^5 bathythermograph casts and for 2×10^5 Nansen bottle casts. Although these numbers are impressive, the observations are so scattered in time and place that the seasonal changes in specific volume could be computed for only 69 areas, barely enough to indicate some global characteristics.

A comparison of recorded and steric fluctuations in sea level puts the problem on a much more definitive basis than would be possible with either set of data by itself. In some regions the two fluctuations resemble one another more closely (correlation 0.90 off Hawaii and Japan, 0.85 off Cape Hatteras) than any other sets of independent oceanographic observations known to us.

During the last few years some progress has been made in accounting for the mean ocean circulation in terms of the distribution of wind stress over the seas. The next problem is to account for departures from the mean circulation. This is much more difficult. The observed seasonal variations in sea level will have to provide much of the necessary empirical guidance for such an undertaking. We therefore present the following description even though we have not been able to explain it. A complete explanation probably involves the solution of most of the important unsolved problems in dynamic oceanography.

2. THE RECORDED SEA LEVEL

2.1 *Sources of tide gauge data.* The principal sources are the two publications prepared by Proudman and others (UGGI, 1940, 1950). Additional data were obtained from the U. S. Coast and Geodetic

[2] The steric oscillations are nearly equal in magnitude to those in dynamic height, so that for traditional reasons the term *dynamic oscillations* would appear to be appropriate. But dynamic height has dimensions of work rather than length, and dynamic oscillation seems to us a poor adaptation of a poor term.

Survey, the Geographical Survey Institute of Japan (1950) and a few other sources. A footnote in Appendix I indicates if part or all of the data for a station are from a source other than the two UGGI publications. Some published stations were omitted because the data were too incomplete. Here it must be admitted that our standards were more exacting where more observations were available. For example, the Arctic and Antarctic stations were included in spite of the fact that the observations were scanty.

Appendix I lists the latitude and longitude of each station as given in the above references. The inclusive dates for the calendar years for which data are available are also given. When two calendar years represent data for 13 months or less, the inclusive months are indicated. The figure in parentheses following the dates indicates the number of years for which data are incomplete. The next column gives the total number of calendar years represented, except in cases where data for 13 months or less were available. This is considered as one year even though the observations may have extended through two calendar years. For example:

Years	*Total years*	
1931–39 (1)	9	Data from 1931 (incl) to 1939 (incl) but one year incomplete. Hence 9 years of data.
1935–41, 1943–46 (1)	11	Data from 1935 (incl) to 1941 (incl) and 1943 (incl) to 1946 (incl), with one year incomplete for latter period. Hence 11 years of data for both periods.
June 1941–May 1942 (2)	1	Data from June 1941 (incl) to May 1942 (incl), both years incomplete. Hence *one* total year by above rule.

2.2 *Normal monthly values.* The standard procedure is to take hourly readings of tide records. The published monthly value for, say January 1950, is a straight average of all hourly readings during January 1950. The figure appearing in the January column of Appendix I represents an average value for all Januaries for which sea level was reported at the particular station under consideration. Similar calculations of "normal monthly" values were made for all other months of the year. The mean value of the monthly means has been subtracted, so that the numbers in the appendix represent departures from an annual mean.

For stations with data for only part of a year among a group of stations with data for all 12 months, the reference level was adjusted so that the mean value of the available monthly means equalled the mean departure for the same months in the remaining stations of the group.

2.3 *Group averages.* The seasonal curve was drawn for each station. *Adjoining stations that showed similar behavior* were then combined into groups. Altogether there are:

419 stations
92 station groups
an average of 4.6 stations per group
an average of 20.6 years of record per station
longest record (133 years) is from Swinemunde, Germany.

The problem as to how individual stations should be combined to form group averages requires consideration. There are two obvious procedures. We could form an *average of stations*, assigning to each station equal weight; or we could form an *average of years*, lumping all data within the group together without regard to station. The former procedure would come close to giving us the geographic average we really want, except that the stations are never distributed too well throughout the area under consideration. The latter procedure leads to a minimum standard deviation in the group average.

The two procedures outlined above correspond to weighting each station average by

$$1 \text{ (or } n^0), \qquad n \text{ (or } n^1) \tag{1}$$

respectively, where n is number of years of record. We have chosen a *root-weighted* average as a compromise.[3] Each station is weighted by the nearest integral number to

$$n^{\frac{1}{2}}. \tag{2}$$

In this way the group averages in Charts 1 to 3 and in Appendix I have been computed.

2.4 *Discussion of errors.* The monthly departures for each group (Charts 1–3) are estimates of normal seasonal conditions in the general area occupied by the stations in the group. In regions where the records are short and the stations few, there is doubt regarding the significance of secondary peaks or even of principal features. An estimate of the uncertainty of the plotted normal departures is therefore essential. It should be emphasized, of course, that the changes from year to year which give rise to this uncertainty are themselves of interest. But this is another story.

2.41 *Time variance.* The seasonal departures differ considerably from one year to the next, due largely to anomalies in weather (atmos-

[3] A better procedure is to use the "semiweighted" mean (Cochran, 1954), which Mr. Theodore Widrig called to our attention after the computations had been nearly completed.

phere and ocean). The fact that neighboring stations show similar anomalies in a given year eliminates observational error as an important factor. The compilation in Table I gives the standard deviation, ϵ, of a monthly departure from the annual average, taken year by year. The first line, for example, contains the standard deviation of the following 45 numbers: Göteborg, Jan. 1902 minus annual 1902, Jan. 1903 minus annual 1903, ..., Jan. 1946 minus annual 1946. In Table I we have selected stations with many years of record in both hemispheres and all major oceans, and, except in four instances, we have ignored the first ten years to give the station a chance to "settle down."

TABLE I. Standard deviation per year, ϵ, for stated months

Group	*Station*	*Month*	*Years*	*n*	ϵ(*cm*)
3	Göteborg	Jan.	1902–46	45	11.6
3	Göteborg	Feb.	1902–46	45	10.9
3	Göteborg	April	1902–46	45	7.1
3	Göteborg	July	1902–46	45	5.2
3	Göteborg	Oct.	1902–46	45	11.1
21	La Plata*	April	1916–34	19	8.0
21	Buenos Aires	April	1915–46	31	6.3
21	Puerto de Colonia*	April	1938–46	9	8.2
21	Montevideo*	April	1938–46	9	6.2
21	Puerto de Punta del Este*	April	1938–45	8	9.3
8	Brest	April	1874–1943	70	6.2
30	Baltimore	April	1912–46	35	4.2
44	San Francisco	April	1907–46	40	5.2
49	Honolulu	April	1915–46	32	5.5
69	Hososima	April	1910–49	40	3.4
83	Bombay	April	1888–1946	59	4.3

* *All* years on record were used.

At Göteborg the standard deviation is small in spring and summer, large in fall and winter. For Group 21, which is a typical group according to the statistical summary in Section 2.3, the standard deviation for April varies from 6.2 at Montevideo to 9.3 at Puerto de Punta. Applying Bartlett's χ^2-test (Cochran, 1954), we obtain $\chi^2 = 35$ for Göteborg, and $\chi^2 = 2.9$ for Group 21, both with four degrees of freedom. The 5% significance level is at $\chi^2 = 9.5$. Thus the seasonal variation in ϵ at Göteborg is significant, whereas the variation between the different stations in Group 21 is probably not.

The mean April deviation for all stations in Table I is 6.15 cm.

A value of

$$\varepsilon = 6 \text{ cm} \tag{3}$$

will be taken as representative of the standard deviation of a monthly value for all months and all stations. The standard deviation of the normal monthly mean value based on n years of record is therefore

$$\varepsilon n^{-\frac{1}{2}}. \tag{4}$$

Since the annual variation in sea level has a double amplitude of the order of 20 cms, something like a decade of record is required to suppress the "noise level" at any one station to 10 per cent of the signal strength.

It can be verified that the standard deviation of the root-weighted group average is

$$\frac{1}{m^{\frac{1}{2}} < n^{\frac{1}{2}} >} \varepsilon = k\varepsilon, \tag{5}$$

where m is the number of stations comprising the group and where $< n^{\frac{1}{2}} >$ is the average value of $n^{\frac{1}{2}}$ for the m stations. Thus, for a group of four stations with records of 1, 4, 9, 16 years respectively, we have

$$k = \frac{1}{2\,(1 + 2 + 3 + 4)} = 0.2\,.$$

2.42 *Geographic variance.* An additional uncertainty arises from the location of stations. Suppose that sea level varies erratically from bay to bay, from headland to headland. Then if each station in a group had been located one mile from its actual location, the resulting group average would have been different. Even if all records were exceedingly long so that the time-variance at each station was negligible, still there would be uncertainty as to the extent to which the computed group average is representative of the general area under consideration.

Two extreme cases are here considered. If departures at neighboring stations show no correlation, i.e., the departures are *incoherent*, then the total variance is the sum of the time variance and the geographic variance. If, however, the departures are *coherent* and the stations uniformly spaced, then the geographic variance does not contribute to the uncertainty of the group average. As an example of this latter case, consider a linear rise in sea level from station to station along a coastline. Then the station average gives the precise value for *average* sea level in the area. Shifting all the stations, or expanding the distance between them, would hardly affect the computed average. From the standpoint of variance the incoherent

case may become the coherent case if the station spacing is sufficiently reduced.

The geographic variance has been estimated as follows. Let δ_i^2 be the mean square deviation of the 12 normal monthly values at the i^{th} station from the corresponding group averages. The root-weighted variance for all m stations in a group is

$$\delta^2 = \frac{\sum_{i=1}^{m} n_i^{\frac{1}{2}} \delta_i^2}{\sum_{i=1}^{m} n_i^{\frac{1}{2}}}.$$

This is taken as the geographic variance per station. The variance of the group average is then $m^{-1}\delta^2$.

In Appendix I the value of k precedes the uncorrected averages for each group, and $m^{-\frac{1}{2}}\delta$ (in cm) precedes the corrected averages. On Charts 1–3 the numbers following each group number give (in cm)

$$k\varepsilon \text{ and } \sqrt{k^2\,\varepsilon^2 + m^{-1}\,\delta^2} \text{ for } \varepsilon = 6.0 \text{ cm}. \qquad (6)$$

These are low and high estimates of the standard deviation, corresponding (more or less) to coherent and incoherent groups of stations. But there are some difficulties inherent in this procedure, and it is not clear where the best estimate of variance lies.

As an example, consider the three neighboring groups

No.	*Locality*	k	$k\varepsilon$ *cm*	$m^{-\frac{1}{2}}\delta$ *cm*	*Limits of standard deviation* *cm*
7	North Sea (South)	0.04	0.24	0.40	0.2—0.4
8	English Channel	0.14	0.84	1.93	0.8—2.1
9	Bay of Biscay	0.36	2.16	2.11	2.2—3.0

The increasing irregularity of the curves toward the south, as seen on Chart 1, is related to the decrease in the number of observations.

2.43 *Suppression of the astronomic tides.* Short period astronomic tides are larger than the seasonal variation. However, the combination of hourly values into monthly averages for a given year and of corresponding values for several years into the "normal" monthly values suppresses the short astronomic tides. But the elimination is not complete. We shall consider briefly the extent to which spurious fluctuations in the mean monthly values can be attributed to the tidal residues.[4]

[4] We are indebted for this method of treatment to Mr. Gordon Groves.

Let t designate time in mean solar hours and $y(t + 1^h)$, $y(t + 2^h)$, . . . $y(t + i^h)$, . . . $y(t + N^h)$ the tidal heights at $(t + 1^h)$, $(t + 2^h)$, . . . $(t + i^h)$, . . . $(t + N^h)$. This includes all hourly values from the first to last ($N'th$) hourly tidal height during the month.

For a pure harmonic constituent of speed σ(in hours^{-1}) and of unit amplitude,

$$y(t) = \cos(\sigma t - \eta) . \tag{7}$$

The monthly average is then

$$(1/N) \sum_{i=1}^{N} y(t + i) = f \cos(\sigma t - \eta + \tfrac{1}{2}\sigma N + \tfrac{1}{2}\sigma) , \tag{8}$$

where

$$f = N^{-1} \csc \tfrac{1}{2}\sigma \sin \tfrac{1}{2}\sigma N . \tag{9}$$

Table II gives the values of f for the principal tidal constituents for months of all possible lengths.

TABLE II. ATTENUATION FACTOR f

Constituent	*28 days*	*29 days*	*30 days*	*31 days*
M_2	.0019	.0006	−.0006	−.0016
S_2	.0000	.0000	.0000	.0000
N_2	−.0016	.0003	.0021	.0035
K_2	.0027	.0027	.0026	.0026
K_1	.0027	−.0027	.0027	−.0027
O_1	.0010	.0016	−.0040	.0060
P_1	−.0027	.0027	−.0027	.0027
Mf	.0242	.0564	.0837	.1050
MSf	−.0537	−.0183	.0156	.0466
Ssa	.9618	.9591	.9562	.9533
Sa	.9903	.9897	.9890	.9882

The contribution from any one semidiurnal or diurnal species is less than 1% of its amplitude. The total contribution depends on the actual amplitudes and relative phases. If all constituents are in phase in the monthly average, the total contribution to the monthly mean may reach as much as 1 cm at stations with extreme tides. On the average the contribution will be of the order of a millimeter.

The effect of the fortnightly tides is larger. The Mf constituent has an amplitude of the order of 5 cm, and the contribution to the monthly means will be of the order of several millimeters. At stations with large shallow water effects, the distortion of the primary constituents, M_2 and S_2, gives rise to a fortnightly constituent with

the same period as the astronomic constituent MSf. Here the contribution to the monthly means may exceed a centimeter. The semiannual and annual constituents appear in the monthly averages with nearly, but not quite, their full amplitude.

The preceding discussion refers to any particular monthly mean in a single year. Consider now the contribution of the tidal constituents to an average over n years of this monthly mean. The arguments of the lunar constituents, M_2 N_2 O_1 Mf MSf, depend on the position of the moon, and their phase in any given monthly average will not vary in a simple manner from one year to the next. The cosine in equation (7) will take up in successive years scattered values between -1 and $+1$. Though the process is not random, strictly speaking, we might expect the lunar contribution to the monthly means to be of the order of $fn^{-\frac{1}{2}}$.

On the other hand, the solar constituents, K_2 K_1 P_1, have approximately the same argument at the beginning of a given month, regardless of the year, and the contribution to any monthly mean is given by equation (8) no matter how many years of record are averaged. The value must lie between $-f$ and $+f$, and if necessary it can be computed from the known values of σ, N, and η. There is a slight attenuation because the phase varies somewhat from year to year. We can compute an upper limit to the attenuation by considering K_2, whose argument shows the greatest variation (i.e., 40°; see Schureman, 1941: table 15), and by assuming that this argument at 0000 1 Jan. is with equal frequency at the extreme values of the 40° range. Then, since amp $\frac{1}{2}$ [cos $(x + 40°)$ + cos x] = 0.94, the reduction achieved by averaging over many years is only 6%. A slightly greater reduction is achieved for February because of the leap year variation in N.

The contribution from astronomic tides to the monthly means can be summarized as follows. For short records, say n less than 10 years, the principal factor is a nearly random contribution from fortnightly tides amounting to 0.1 $n^{-\frac{1}{2}}$ to 0.5 $n^{-\frac{1}{2}}$ cm. For longer records a nearly systematic contribution from solar constituents becomes predominant, and this is nearly independent of n. A typical value for K_1 is 0.1 cm. All these values are small compared to the observed standard deviation of about $6n^{-\frac{1}{2}}$ cm (Section 2.4$_1$), and it may be concluded that the present method of forming straight monthly averages is adequate. It should be pointed out, however, for the benefit of future oceanographers, that after a thousand years or so better methods for eliminating the solar constituents will become worthwhile.

3. THE STERIC SEA LEVEL

Wherever observations are adequate we have attempted to compute the seasonal departures in sea level arising from seasonal departures in specific volume. The resulting "steric sea levels," summarized in Appendix II, are shown in red on Chart 1. The selection and analysis of a large part of the observations have been made possible only by the help and active participation of the U. S. Navy Hydrographic Office and the Woods Hole Oceanographic Institution.

3.1 *Sources of data.* There are three sources of data:
(1) A few *analyses of seasonal variation* in temperature (and/or salinity) are available in journals and technical reports. They will be referred to under the author's name.
(2) *Bathythermograms* on file at Woods Hole and at Scripps Institution are referred to as WHOI and SIO.
(3) *Serial hydrographic observations* were provided by the Hydrographic Office, U. S. Navy (HYDRO).

Calculations have been made for 69 areas. The information given for each area in Appendix II is illustrated by the following examples:

No.	*Locality*	*Latitude*	*Longitude*	*BTs/Mo.*	*NB*	*Principal Source*
6	Off Gibraltar	32°–37° N	010°–015° W	104[1]	0[2]	WHOI
24	Aleutian Is.	52°–53° N	179° E–180°	8	1	Pattullo (1950)
3	North Sea	55°–60° N	005°–010° E	57[1]	unk.	Dietrich (1950)
55	Kuroshio[3]	unknown		unknown		Koenuma (1939)
		34°–35° N	139°–140° E	0	118	Japanese
		37°–38° N	142°–143° E	0	216	JAP-HYDRO

All observations for No. 6 were taken off Gibraltar between 32° and 37° N and 010° and 015° W. An average of 104 bathythermograms per month were available, but according to footnote 1 (App. II) some temperatures from reversing thermometers were included. The column under *NB* (Nansen bottle) indicates that no serial Nansen bottle observations were used. According to footnote 2, salinity was deduced from a *T-S* scatter diagram. Bathythermograms on file at the Woods Hole Oceanographic Institution are the principal source of data. In No. 24, the analysis was based on an average of 8 bathythermograms per month and 1 serial Nansen bottle cast. In No. 3 the principal source is an analysis by Dietrich based on an unknown number of Nansen bottle serial observations; however, some additional data consisting largely of bathythermograms have been used. No. 55 represents a special case. Here we have combined

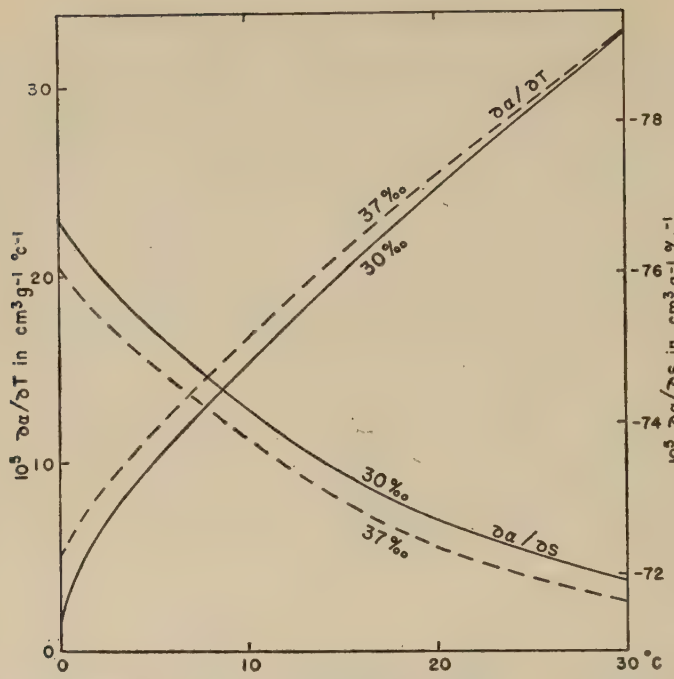

Figure 1. Thermal expansion, $\partial\alpha/\partial T$, and haline expansion, $\partial\alpha/\partial S$, of sea water at atmospheric pressure, as functions of temperature in °C for salinities S = 30°/oo and 37°/oo.

a temperature analysis by Koenuma with an assortment of Japanese serial observations.

3.2 *Thermal and haline effects.* From the available data we gain information concerning variations in the temperature and salinity fields with time of year at various depths (or pressures). For any depth let $\Delta T = T - \overline{T}$, $\Delta S = S - \overline{S}$ designate the monthly departures in temperature and salinity from their annual means, $\overline{T}$, $\overline{S}$. For small values of ΔT and ΔS the corresponding departure in specific volume is given by $\Delta\alpha = \alpha(T,S,p) - \alpha(\overline{T},\overline{S},p) = (\partial\alpha/\partial T)\Delta T + (\partial\alpha/\partial S)\Delta S + \ldots$, where $\partial\alpha/\partial T$ and $\partial\alpha/\partial S$ are to be evaluated at $\overline{T}$, $\overline{S}$, p. But the explicit dependence of $\partial\alpha/\partial T$, $\partial\alpha/\partial S$ on pressure can be neglected, and accordingly in all numerical work we have read $\partial\alpha/\partial T$ and $\partial\alpha/\partial S$ as functions of $\overline{T}(p)$, $\overline{S}(p)$, 0 (Fig. 1).

The "thermal" and "haline" departures are now defined by

$$z_T = g^{-1}\int_{p_a}^{p_0}(\partial\alpha/\partial T)\,\Delta T\,dp\,, \quad z_S = g^{-1}\int_{p_a}^{p_0}(\partial\alpha/\alpha S)\,\Delta S\,dp\,. \quad (10)$$

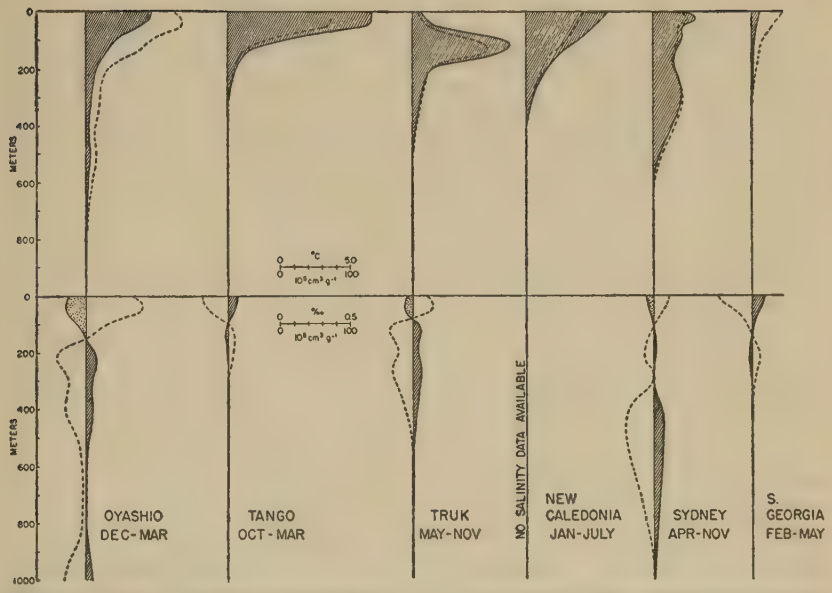

Figure 2. Top. Ranges of temperature, ΔT, in °C (dashed lines, upper scale), and the resulting ranges of specific volume, $(\partial\alpha/\partial T)\Delta T$, in cm³ g⁻¹ (solid lines, lower scale) between months of maximum and minimum steric departures. Bottom. Ranges of salinity, ΔS, in °/₀₀ (dashed lines, upper scale), and the resulting ranges of specific volume $(\partial\alpha/\partial S)\Delta S$, in cm³ g⁻¹ (solid lines, lower scale) between months of maximum and minimum steric departures.

The steric departures equal

$$z_a = g^{-1} \int_{p_a}^{p_0} \Delta\alpha \, dp \,. \tag{11}$$

Here p_a is the atmospheric pressure and p_0 the pressure to which the integration has been carried, presumably the pressure where all seasonal effects vanish.

3.21 *Thermal departures* have been computed for 69 localities. More than half of these are based on bathythermograph observations, which usually extend to only 450 feet (135 m). It was therefore necessary to augment the bathythermograph data by Nansen bottle temperature measurements and some subjective interpolation.

Fig. 2 shows some seasonal differences in ΔT and $(\partial\alpha/\partial T)\Delta T$. At most localities these quantities are large only in the upper few hundred meters or upper 10% of the sea. However, five southern hemisphere areas showed appreciable temperature variations as deep as 600 or 800 m. All of these were near the southern tips of the southern continents—Africa, South America, and Australia.

3.22 *Haline departures.* Only 30 areas were found with enough serial observations for computation of z_S. A third of these is in the western North Pacific; another third is south of Lat. 30° S. Only one satisfactory sample is from the cold Subarctic water of the northern hemisphere. This constitutes a far less satisfactory set of data than was available for z_T. It will be noted from Fig. 2 that ΔS usually changes sign with depth and that it extends deeper than ΔT.

3.23 *Steric departures* were computed in the usual way (LaFond, 1951) according to equation (11). Except for second and higher order terms they equal the sum of the thermal and haline departures.

3.3 *Discussion of errors.* It is difficult to give a rigorous discussion of errors when the original body of data has undergone subjective treatment. Nevertheless it seems desirable to make a rough estimate.

3.31 *Thermal errors.* Robinson (1951, 1952) has computed the standard deviation, s, of sea water temperatures from a normal monthly mean. Taking all available data, possibly from different years, which were collected during a specified month at a specified depth and location, she finds a value of 0.8°C to be representative of the upper 400 feet. Although we might expect that most of the variation takes place in this upper layer, let us assume this value to be representative all the way down to 400 m.

Suppose that this average is based on n' observations and that the deviations for any one bathythermogram are the same at all depths. Then the standard deviation of the mean temperature is $s(n')^{-\frac{1}{2}}$ and of the computed mean sea level departure $s\ (n')^{-\frac{1}{2}}\ (\partial\alpha/\partial T)\ h$. Typical numerical values are $s = 0.8°$ C, $n' = 25$ (the median for our data), $\partial\alpha/\partial T = 1.5 \times 10^{-4}$ cm^3 g^{-1} $°C^{-1}$, and $h = 400$ m. The foregoing formula then gives the value 1.0 cm.

A second estimate has been made by computing z_T for each of 100 bathythermograms taken in August 1943–48 at Weather Station "Nan," 30° N, 140° W, No. 31. The standard deviation per year is $\epsilon' = 2.9$ cm and per five-year average $2.9 \times 5^{-\frac{1}{2}} = 1.3$ cm. The value of ϵ' is roughly half of ϵ, the value adopted in Section 2.41 as representative of the standard deviation of the recorded departures.

For the three years 1943–46 the tide gauge and steric sea level records at Hawaii overlap (recorded group 49, steric group 35). For these three years we find $\epsilon = 2.9$ cm, $\epsilon' = 3.5$ cm. There is no evidence here for a difference between the standard deviations of recorded and thermal departures, but obviously the data are far from conclusive. The thermal departures appear smoother on Chart 1. This is due, at least in part, to the fact that they were computed from smoothed temperature

data, whereas the recorded departures are drawn through each point without smoothing.

There are also systematic errors. Neglect of the direct pressure effect on $\partial\alpha/\partial T$ leads to a computed amplitude about 5% too small. Furthermore, we have neglected second and higher order terms. The ratio of these to the first order terms is of the order

$$\frac{(\partial^2\alpha/\partial T^2)\,(\Delta T)^2}{(\partial\alpha/\partial T)\,\Delta T} = \frac{(\partial^2\alpha/\partial T^2)\,\Delta T}{\partial\alpha/\partial T} = \frac{(10^{-5}\text{cm}^3\,g^{-1}\,°\text{C}^{-2})\,(1\,°\text{C})}{1.5\times 10^{-4}\text{cm}^3\,g^{-1}\,°\text{C}^{-1}} = \frac{1}{15}.$$

This will make the computed sea levels too low in both extreme seasons but it will leave the ranges almost unaffected.

3.32 *Haline errors.* We have not been able to find a study of salinity variability that is comparable to Mrs. Robinson's work on temperature. Our data, though not rigorously analyzed by statistical methods, suggest a value of about 0.10‰ for the standard deviation. On an average there are eight observations per month, and our estimate of the error following Section 3.31 is then 2 cm. But now there are additional uncertainties associated with the fact that the contributions from some depths cancel those from other depths (Fig. 2), so that the final value represents a difference of two uncertain quantities. Only at stations with rather large haline departures can the computed values of z_S be considered significant.

Systematic errors in haline departure are quite small. The effect of pressure on $\partial\alpha/\partial S$ again leads to a computed amplitude that is too small, but by less than 2%. The ratio of the second order to the first order term is less than 0.001.

4. ATMOSPHERIC PRESSURE

The last three lines for each group of stations in Appendix I give a correction for the isostatic yielding of the ocean surface to the fluctuating atmospheric pressure. On first consideration, the only requirement seems to be that the sea surface be depressed by 1 cm for every rise in pressure[5] by 1 mb in the general area of the group of tide stations. This has been done in previous investigations. But this procedure does not take into account a surprisingly large annual change in the mean pressure over all oceans, from 1012 mb in December to 1014 mb in July, due principally to a shift in air mass toward Siberia in winter. It is clear that no correction would be required if the annual change in pressure were uniform over all oceans.

[5] The pressure exerted by 1 cm of sea water is 1.005 mb.

Let P_g designate the mean monthly pressure in the general vicinity of the group of tide gauge stations and P_0 the mean pressure over all oceans for the same month (Table III). Then $c' = P_g - P_0$ represents the amount by which the water surface in this area is depressed relative to mean global sea level. The recorded sea level has to be

TABLE III. Example of Pressure Correction

	J	*F*	*M*	*A*	*M*	*J*	*J*	*A*	*S*	*O*	*N*	*D*
P_g − 1000 mb	6.5	8.0	9.0	9.5	14.5	14.0	11.5	10.0	10.5	8.5	7.0	7.0
P_0 − 1000 mb	12.4	12.4	12.8	12.8	12.8	13.5	14.0	13.3	13.4	12.8	12.6	11.9
$P_g - P_0$	−5.9	−4.4	−3.8	−3.3	1.7	0.5	−2.5	−3.3	−2.9	−4.3	−5.6	−4.9
c (cm)	−2.7	−1.2	−0.6	−0.1	4.9	3.7	0.7	−0.1	0.3	−1.1	−2.4	−1.7

raised by this amount to correct for the effect of atmospheric pressure. Since the base level is arbitrary, it is more convenient to use the correction factor $c = c' - \overline{c'}$, whose mean annual value is zero. These four steps are illustrated in Table III. In Appendix I the last four lines for each station group designate z, P_g − 1000 *mb*, c, and $z + c$. The quantities z, c, and $z + c$ have a zero annual mean. The second line in Table III designates the mean pressure over all oceans, and of course it is the same for all tide groups. The average was formed on the basis of values for each 5° quadrangle between 90° N and 10° N (U. S. Department of Commerce, 1946) and for each 10° quadrangle between 10° N and 60° S (Bartholomew and Herbertson, 1899). These two references were also the source of the P_g values.

The foregoing isostatic adjustment for atmospheric pressure changes would be invalid for quick changes in pressure. There simply would not be time for the water to move. Various theoretical models yield time constants short compared to a year. Empirical evidence (to be published shortly by Mr. Gordon Groves) indicates that sea level yields virtually isostatically to atmospheric pressure disturbances with dimensions of several thousand miles and a time scale of several days. We are satisfied that the isostatic adjustment to atmospheric pressure is a suitable approximation for the annual term.

We have made no allowance for wind stress. Changes in wind accompany changes in pressure, and the wind effect is likely to be larger and opposite in sign to the pressure effect. This may account for the fact that in some cases the variation in sea level, corrected for atmospheric pressure, is actually larger than the uncorrected variation (see Section 6.6).

5. LONG PERIOD ASTRONOMIC TIDES

In this section we consider the extent to which astronomic tides of annual and semiannual period contribute to the recorded monthly departures. Rayleigh has shown (Lamb, 1932) that tides in the actual oceans[6] with periods long compared to a day have nearly the values given by the equilibrium theory. For the solar annual (Sa) and the solar semiannual (Ssa) species, these values are (Doodson and Warburg,[7] 1941)

$$z = [0.16 \cos (\odot - 282°) + 0.98 \cos 2\odot] (1 - 3 \sin^2 \phi) , \quad (12)$$

where ϕ is latitude and $\odot$ the sun's longitude (March 21: $\odot = 0, 2\pi$; June 21: $\odot = \frac{1}{2}\pi$, etc.).

The above formula must be corrected for the elastic yielding of the crust (relative to which sea level is measured) and for the gravitational attraction of the tidal bulge on itself by multiplying by a factor (Jeffreys, 1952: 204)

$$1 + k - h = 0.69 , \quad (13)$$

where k and h are "Love's numbers."[8] In addition, we must superpose a uniform tide z' over all oceans so that the total tidal volume

$$\int_{ocean} z (\odot, \phi) \, d\sigma + z' (\odot) \int_{ocean} d\sigma$$

vanishes in spite of the irregular distribution of land and sea. When this is done, the expression $(1 - 3 \sin^2 \phi)$ in equation (12) is replaced by

$$3(1 - D/C) - 3 \sin^2 \phi = 0.91 - 3 \sin^2 \phi , \quad (14)$$

where $C = \int\int \cos \phi \, d\phi d\theta = 8.79$ and $D = \int\int \cos^3 \phi \, d\phi d\theta = 6.11$ are integrals over such ranges of latitude ϕ and longitude θ as are covered by oceans. The values were obtained by Munk and Revelle (1952: 333) by numerical integration.

Applying these two factors to the above formula for the equilibrium tide gives

$$z = [0.11 \cos (\odot - 282°) + 0.68 \cos 2\odot] (0.91 - 3 \sin^2 \phi) . \quad (15)$$

[6] In the case of an ocean covering the entire globe, this result probably does not hold (Lamb, 1932: 362; Jeffreys, 1952: 371).

[7] The numerical results follow from equations (4.3a for sun), (4.3b), (7.10a), and Table 7.17, setting $p = 282°$ and writing $\odot$ for h.

[8] This k is used in accordance with convention. It is not the k used in other sections of this paper.

An observational test of this formula is impossible because the meteorological effects of annual and semiannual period far outweigh the astronomic effects. The only long period tide for which the astronomic factors predominate is the lunar fortnightly tide, and here at least an expression analogous to (15) agrees roughly with the results of observations. Fig. 3 shows the height of the combined annual and semiannual tides according to equation (15). The maximum tidal range is 3.2 cm between March 20 and June 21 at latitude 90°. This value is much smaller than a typical value for the recorded range.

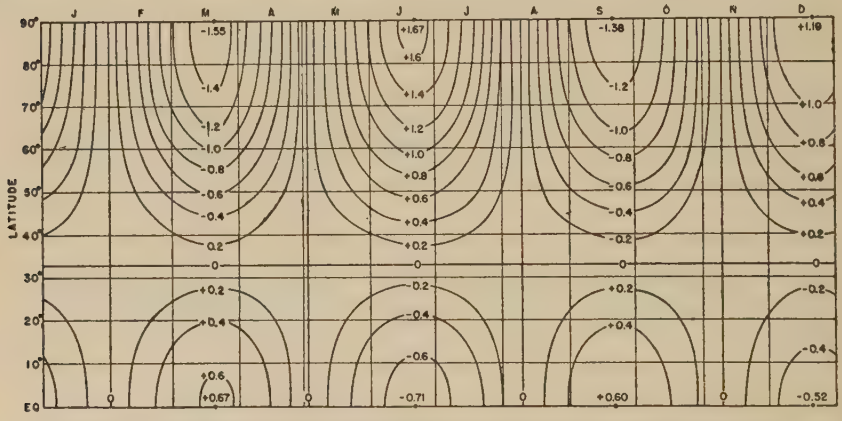

Figure 3. Long period tides in centimeters as a function of latitude and month.

6. DISCUSSION

This is a presentation of data so combined and so plotted as to give a global summary of seasonal oscillation in sea level. No hypothesis is offered as to the causes of the observed oscillation.

6.1 *The data.* The geographic distribution of stations gives a remarkably good picture of the geographic extent of western civilization, but it is hardly a desirable distribution from our point of view (see Chart 1). More than one third of the stations are around the shores of northern Europe and the British Isles. Some 72% of the tide gauge groups, 75% of the steric height summaries, 79% of the tide stations, and 92% of the tide station-years are from the northern hemisphere. Most of the sea level observations refer to shores of larger land masses. Sea level data in midocean are available for five island groups in the Atlantic and for ten islands in the Pacific. Vast areas of the North Atlantic and Pacific are without any midocean observations whatsoever, and one must beware lest the aversion of coral for cold water become the basis of a hypothesis for seasonal changes in sea level.

Comparison of the recorded and steric sea level observations is made difficult by the fact that these are for the most part neither synchronous nor adjacent. Moreover, different methods of averaging had to be used for these two kinds of observations; the steric departures show the result of smoothing whereas the recorded departures do not.

In this kind of study, questions concerning the reliability, even the reality, of the results are paramount. We have attempted to estimate the standard errors of the results obtained.

6.2 *Description of recorded sea levels.* The seasonal range varies from a few centimeters at several island stations in low latitude to 165 cm in the Bay of Bengal. Large seasonal changes are found in the monsoon regions of the western Pacific and Indian Ocean, in the Red Sea and the Persian Gulf, the west coast of Mexico and Central America, the North Atlantic north of 60°, the Gulf of Alaska, and the Sea of Japan. In general, amplitudes are smaller in the southern than in the northern hemisphere.

Fig. 4 is a synopsis of North Atlantic and North Pacific observations. Two zones of high annual activity correspond quite well to the subtropical and subpolar gyres of ocean circulation (Munk, 1950). In either zone the double-amplitude reaches close to a foot. In the subtropical zone, the high is in September, the low in March; in the subpolar zone the extremes occur three months later. There is an indication of an oscillation in the equatorial gyre which is roughly in phase with the subtropical gyre though only half as large.

Sea level in both hemispheres is generally low in their respective spring seasons and high in the fall. An exception occurs at the Great Australian Bight, where sea level is highest during the southern winter and lowest in summer. The boundary between the northern and southern types does not always follow the geographic equator; it lies north of it in the western Pacific and western Indian Ocean. The intrusion of the southern type into the Gulf of Siam is particularly striking (Chart 3).

In most regions the oscillation is annual in character. Pronounced semiannual oscillations in sea level occur off the west coast of India, in Indonesia, off the west coast of Africa, in the Labrador Current region of the western North Atlantic and the corresponding Oyashio region of the western North Pacific, and in the Gulf of Mexico and adjoining Gulf Stream stations (but not in the corresponding region of the Kuroshio!). A few curves on Chart 1 have even shorter period oscillations, but their reality is doubtful.

6.3 *Marginal seas.* In the Baltic (Chart 2), the Mediterranean, the North Sea, Hudson Bay, the Gulf of California, and the Sea of Japan, the annual variation in sea level corresponds closely to that

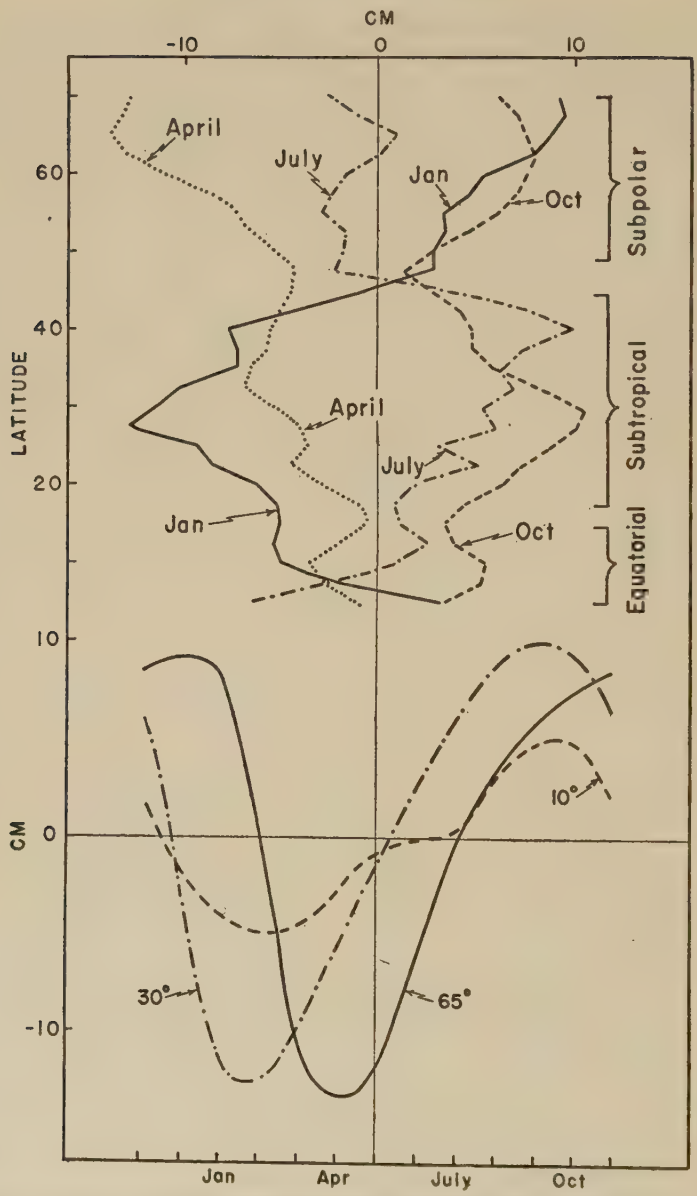

Figure 4. Upper. Recorded departures from mean sea level as a function of latitude for each of four months. Lower. Average recorded departures from mean sea level as a function of month. Each curve represents a ten-degree belt of latitude.

in the adjacent oceans at about the same latitude. Seasonal departures throughout these complex inland bodies of water are remarkably uniform. In the Red Sea the times of maximum and minimum sea level are similar to those in the western Indian Ocean, but the range is greater. The Persian Gulf is unlike any other region, and there are many complexities in the East Indies, corresponding to the complex topography and current systems of this region (see Chart 3). Striking double maxima in the Gulf of Mexico have already been referred to. Data for the Arctic Sea are completely inadequate.

6.4 *Description of steric sea levels.* The steric level is nearly equal to the algebraic sum of the thermal and haline departures. These two kinds of departures have quite different characteristics.

The average range of thermal departures is 11 cm. Maximum ranges of 25 cm are observed in the Sea of Japan and north of Bermuda. Small thermal departures are observed in some equatorial and most polar regions.

The haline departures do not tend to cluster around a mean value. Two-thirds of the z_S computations yield virtually negligible ranges—5 cm or less. The haline departures are consistently small around Bermuda and in the vast oceanic area east and southeast of Japan. Appreciable values of z_S occur: (a) at one location in the Bay of Bengal (a range of 41 cm); (b) at the five southern hemisphere localities that show deep thermal variations; and (c) along the continental slope off eastern Asia, from Formosa to Hokkaido.

On the whole, steric departures are in phase with recorded departures. In equatorial latitudes the steric departures are largely thermal and relatively small. The considerable irregularity from place to place prevents one from making any easy generalization, but recorded and steric departures may not be far out of line here.

In subtropical latitudes the steric departures are mostly thermal and quite large. On the average they agree well with the recorded departures.

In subpolar latitudes the thermal departures are small and the recorded departures large. Unfortunately the rôle of salinity remains in doubt. Where salinity observations are available, the water is shallow. Deep salinities are available for only the Oyashio (steric No. 58), which has abnormally small recorded departures. But there, at least, the haline departures are equivalent to the thermal departures, and together they lead to a fair agreement between steric and recorded departures. This suggests that in subpolar latitudes as well there may be agreement between recorded and steric departures. In order for this to be true there must be large and

deep seasonal changes in salinity of the required amount, and as a consequence the haline departures must be large compared to the thermal departures. Observations will tell.

6.5 *Astronomic tides.* Comparison of Fig. 3 with Chart 1 shows that at all latitudes the long period astronomic tides are much smaller than the recorded departures in sea level.

6.6 *Atmospheric pressure effects.* In general, changes in atmospheric pressure exert an effect which is small compared with the observed departures in sea level. In most cases the effect of "correcting" for pressure is a small reduction in range; the average reduction for all stations is 1.6 cm. The groups where the pressure correction is most prominent are illustrated in Fig. 5. Column 1 contains all groups where the pressure correction *decreases* the range by more than 10 cm. All but one of these groups are in the seas surrounding Japan. Group 36 is off southern Greenland, near the center of the Icelandic low. Column 2 contains all cases where the range is *increased* appreciably. These groups are generally of southern hemisphere type, although a few are actually north of the equator. They occur off the southeast coasts of Africa, Australia, and New Zealand. The anomalous member of this set, No. 61, is located in the East China Sea. Column 3 illustrates stations where the phase is changed. Most of these have either rather small amplitudes or multiple maxima and minima, and the change of phase occurs when one of these extrema is accentuated by the correction. This class lacks geographical coherence.

6.7 *Isostasy.* In many regions the recorded departures nearly equal the steric departures plus the departures in atmospheric pressure. In such regions the total weight of water and air per unit area tends to remain nearly constant throughout the year, so that a pressure recorder at the sea bottom would show very small seasonal fluctuations. In analogy with geologic usage, this condition will be called *isostatic.* For oceanographic usage we suggest, as a strict definition, that conditions be called isostatic if the *hydrostatic* pressure due to atmosphere and ocean at a point on the deep sea floor does not change with time. Under such isostatic conditions the *measured* pressure at this point would remain nearly constant, varying only in response to accelerations in the fluid motion. Astronomic tides give rise to small departures from isostasy both because of changes in g and in water mass per unit area. In an isostatic region, surfaces of constant pressure coincide at depth with surfaces of constant gravitational potential.

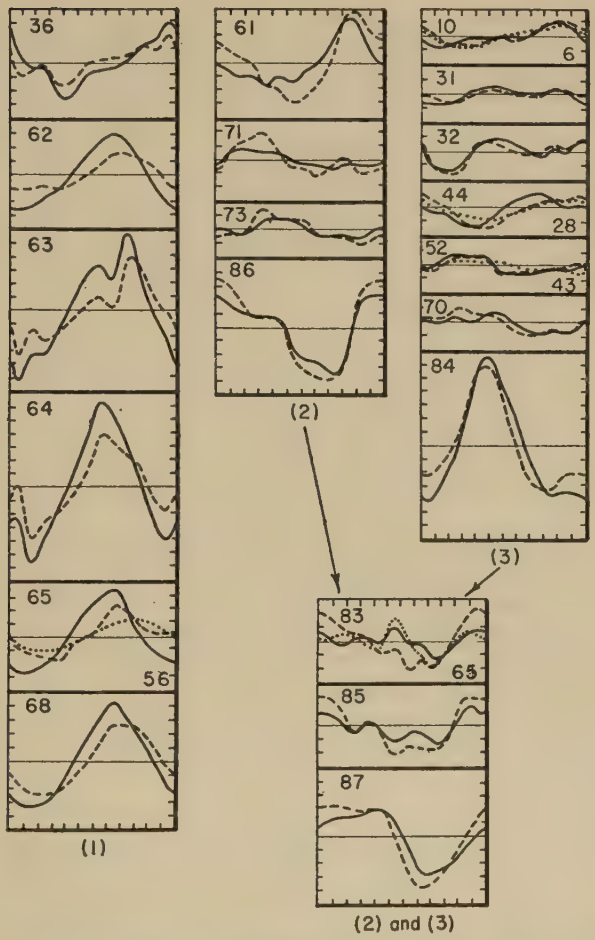

Figure 5. Groups for which the atmospheric pressure effect is most pronounced. Solid curves are recorded levels; dashed curves are the levels "corrected" for atmospheric pressure; dotted curves are steric levels. Column (1) includes all cases where the pressure correction decreases the range by more than 10 cm; column (2) where it increases the range by more than 5 cm; and column (3) where the time of maximum or minimum is changed by three months or more. Groups 83, 85 and 87 belong to both columns (2) and (3).

Nomitsu and Okamoto (1927) noted the close correspondence between recorded and steric levels off Japan, and LaFond (1939) demonstrated a similar correspondence off southern California, but the widespread occurrence of quasi-isostatic conditions emerges as a primary result of the present study.

Since the effects of atmospheric pressure are usually small, the latitude dependence of isostasy can be inferred from Section 6.4. Outstanding examples of isostasy are found near the Azores, Bermuda, Hawaii, off California, along the coasts of Japan and even in the high annual tide of the Bay of Bengal. In some of these cases the atmospheric pressure correction enters as an important factor (Fig. 5).

There are a number of regions where, for one reason or another, the situation is indeterminate. For example, in the area of the Florida Current the recorded levels are from the western side while the steric (thermal) levels are from the eastern side of the stream; the shallow depth along the western side does not permit the calculation of steric levels. A similar situation exists off Nova Scotia and off the west coast of Florida. The degree of isostatic adjustment in the southern hemisphere cannot be determined from the available data, but there is no evidence against isostatic adjustment at low latitudes; possibly there is an indication of isostasy as far south as 60° S, off the Palmer Peninsula (recorded level group 90 and steric level group 69).

In spite of quite a number of thermal calculations, little can be said about isostasy in the Arctic and Subarctic waters of the northern hemisphere. The thermal departures alone are definitely neither large enough nor of the right phase for isostasy. The only Subarctic locality *in deep water* with salinities as well as temperatures, off Hokkaido, exhibits isostasy effected by deep changes in salinity. Other cold-water localities (Korea, Norwegian Sea, Barents Sea, etc.) are on the continental shelves, where deep-level compensation is impossible.

6.8 *Relative and absolute currents.* It is emphasized in oceanographic textbooks that the standard computation of currents from dynamic topography can yield only relative values. Yet, in the few instances where comparison with actual current measurements have been made, the relative and absolute currents have agreed rather well. There is harmony between these findings and the widespread occurrence of isostatic conditions. For in isostatic regions, *seasonal changes* in absolute current can be determined from measurements of dynamic height. Our study can give no evidence concerning the mean conditions.

6.9 *The International Geophysical Year.* The principal shortcomings of the present data could be overcome by making synchronous and adjacent observations of recorded and steric levels, with emphasis on (1) island stations near deep water in the southern hemisphere, and (2) Subarctic waters, where recorded departures are large and

thermal departures are not. A single year's observations should be sufficient to clarify many of the uncertainties that now remain. It is hoped that this might be accomplished during the forthcoming International Geophysical Year.

REFERENCES

Bartholomew, J. G. and A. J. Herbertson

1899. Atlas of Meteorology, in Bartholomew's Physical Atlas. Roy. Geogr. Soc., Edinburgh, vol. 3, 40 pp., 34 plates.

Cochran, W. G.

1954. The combination of estimates from different experiments. Biometrics, *10:* 101–129.

COEC, Comité Central d'Océanographie et d'Étude des Côtes

1951. Annex to documentation. Bulletin d'Information 111^{éme} Année (3): 106–112. Mars.

Conseil Permanent International pour l'Exploration de la Mer

1904. Bulletin des résultats acquis pendant les courses périodiques, 1903–1904. Bull. Cons. Explor. Mer, Teil B, 34 pp. Copenhague.

CSIRO, Commonwealth Scientific and Industrial Research Organization

1952, 1953. Oceanographical station list of investigations made by the Div. of Fisheries, CSIRO, Melbourne, Australia, vol. 1–3, 14, 17.

Deacon, G. E. R.

1933. A general account of the hydrology of the South Atlantic Ocean. 'Discovery' Rep., *7:* 173–238.

Dietrich, Gunter

1950. Die natürlichen Regionen von Nord- und Ostsee auf hydrographische Grundlagen. Kieler Meeresforsch., *7* (2): 35–69.

Discovery Reports

1929. Station list, 1925–1927. *1:* 1–138.
1932. Station list, 1929–1931. *4:* 1–230.
1941. Station list, 1931–1933. *21:* 1–226.
1942. Station list, 1933–1935. *22:* 1–196.
1945. Station list, 1935–1937. *24:* 1–196.
1949. Station list, R.R.S. William Scoresby, 1931–1938. *25:* 144–280.

Doodson, A. T. and M. D. Warburg

1941. Admiralty manual of tides. H. M. Stationery Office, London. 270 pp.

Fuglister, F. C.

1947. Technical report on the hydrography of the western Atlantic. No. 4. The hydrography of the northwestern Sargasso Sea. Woods Hole Oceanogr. Inst., 13 pp., 33 figures.

Geographical Survey Institute, Ministry of Construction, Japan

1950. Tidal record, 1930–1949. 24 pp.

Helland-Hansen, B.

1930. Physical oceanography and meteorology. Rep. Sars N. Atlantic Deep-Sea exped., *1, 2:* 115, 107 pp.

HYDRO, Hydrographic Office, U. S. Navy
Microfilm of oceanographic data taken by the Armauer Hansen in the Mediterranean Sea, 1931, and the Norwegian Sea, 1935–1936; also numerous Arctic expeditions by various vessels. Received from Dr. Håkon Mosby, Univ. of Bergen, Bergen, Norway. (On file at Hydrographic Office, Washington, D. C.)

Hydrographic Office, U. S. Navy
1934. Dynamic oceanographic data for central eastern Pacific Ocean, collected by the USS Hannibal and Yacht Valero III, and surface temperature and salinity data for eastern Pacific Ocean, collected by U. S. Naval Vessels. Publ. U. S. Navy Hydrogr. Off., No. 212. 53 pp.

Japanese Hydrographic Department
1924–1935. Bulletin of the hydrographic department of the Imperial Japanese Navy. *6* through *14*. Tokyo.

JAP-HYDRO
Monthly averages of temperature and salinity, compiled and provided by the U. S. Navy Hydrographic Office from Japanese serial observations.

Jeffreys, Harold
1952. The Earth. Cambridge University Press, London. 392 pp.

Koenuma, K.
1939. On the hydrography of the southwestern part of the North Pacific and the Kuroshio. Mem. Mar. Obs. Kobe, *7:* 41–114.

Lafond, E. C.
1939. Variations of sea level on the Pacific Coast of the United States. J. Mar. Res., *2:* 17–29.

Lafond, E. C. and R. Prasada Rao
1954. Changes in sea level at Visakhapatnam on the east coast of India. Mem. Andhra Univ., Oceanogr., *1*, Waltair, India.

Lamb, Horace
1932. Hydrodynamics. Cambridge University Press, London. 738 pp.

Leipper, D. F. and E. R. Anderson
1950. Sea temperature, Hawaiian Island area. Pacif. Sci., *4:* 228–248.

Leipper, D. F. and William Wood
1947. Temperature and salinity of Philippine waters. Oceanogr. Rep. Scripps Inst. Oceanogr., No. 4. 47 pp.

Mao, Han Lee and Kozo Yoshida
1953. Physical oceanography in the Marshall Islands area 28° N–5° S, 155° E–175° E. Scripps Inst. Oceanogr., Univ. Calif., Ref. 53–27.

Munk, W. H.
1950. On the wind-driven ocean circulation. J. Met., *7:* 79–93.

Munk, W. H. and Roger Revelle
1952. On the geophysical interpretation of the irregularities in the rotation of the earth. Geophys. Suppl. M.N.R.A.S., *6* (6): 331–347.

Nomitsu, Takaharu and Motojiro Okamoto
1927. The causes of the annual variation of the mean sea level along the Japanese Coast. Mem. Coll. Sci. Kyoto, (A) *10* (3): 125–161.

Pattullo, June G., J. D. Cochrane and W. V. Burt
1950. Sea temperature in the Aleutian Island area. Oceanogr. Rep. Scripps Inst. Oceanogr., No. 24. 6 pp., 34 figures.
Robinson, Margaret K.
1951. Sea temperature in the North Pacific area 20°–40° N, 125°–155° W. Scripps Inst. Oceanogr., Univ. Calif., Ref. 51–20. 13 pp., 36 figures.
1954. Sea temperature in the Marshall Islands area. Prof. Pap. U. S. Geol. Surv., 260-D.
In press. Sea temperature in the Gulf of Alaska. Bull. Scripps Inst. Oceanogr.
Schureman, Paul
1941. Manual of harmonic analysis and prediction of tides. U. S. Govt. Printing Office, Washington, D. C. 317 pp.
SIO, Scripps Institution of Oceanography, University of California
Bathythermograms on file. La Jolla, Calif.
Skogsberg, Tage
1936. Hydrography of Monterey Bay, California. Thermal conditions, 1929–1933. Trans. Amer. phil. Soc., N.S. *29:* 1–152.
UGGI, Union Géodésique et Géophysique Internationale
1940. Monthly and annual mean heights of sea level, up to and including the year 1936. Publ. Sci. Ass. Océanogr. Phys., No. 5. 255 pp.
1950. Monthly and annual mean heights of sea level, 1937–1946, and unpublished data for earlier years. Publ. Sci. Ass. Océanogr. Phys., No. 10. 82 pp.
U. S. Coast and Geodetic Survey
Unpublished monthly averages of mean sea level, prepared by and on file at USCGS, Washington, D. C.
U. S. Department of Commerce
1946. Normal weather maps, northern hemisphere sea level pressure. Weather Bureau, U. S. Dept. of Commerce., April.
Von Drygalski, Erich
1926. Ozean und Antarktis meereskundliche Forschungen und Ergebnisse. Dtsch. Südpolar-Exped., 1901–1903. *7* (5). 181 pp.
WHOI, Woods Hole Oceanographic Institution
Unanalyzed averages of temperatures and salinities at selected depths from 0 to 400 meters. On file at W.H.O.I, Woods Hole, Mass.
Worthington, L. V.
1953. Oceanographic results of Project Skijump I and Skijump II in the Polar Sea, 1951–1952. Trans. Amer. geophy. Un., *34* (4): 543–551.

As this paper went to press our attention was directed to a recent study by Eugénie Lisitzin, Les Variations Annuelles du Niveau des Océans, Bulletin d'Information, Comité Central d'Océanographie et d'Études des Côtes, No. 6, June 1955. Dr. Lisitzin studied the annual term on the basis of 140 selected stations distributed over all oceans. She has noted the phase reversal between northern and southern hemispheres as well as the three months phase lag in the subpolar regions relative to the subtropical regions. We pointed out this feature for the northern hemisphere only, but Dr. Lisitzin has found evidence for this in the southern hemisphere as well.

APPENDIX I

1. ATLANTIC (ARCTIC SECTOR): Barents Sea

Station	Latitude	Longitude	Years	Total Years	J	F	M	A	M	J	J	A	S	O	N	D
Liinahamari (Fi)	69°39N	31°22E	1931–39(1)	9	7.5	4.0	−7.4	−12.1	−13.0	−5.4	−4.5	−1.5	4.8	8.8	9.7	8.8
Vardö (No)	70°22N	31°06E	1880–85(3)	6	14.8	5.8	−6.4	−18.9	−15.7	−7.1	−1.2	1.2	0.3	3.0	11.9	11.7
Berlevåg (No)	70°51N	29°06E	1939–41(1), 1942–43(1)	5	5.9	7.3	−7.5	−5.5	−11.8	−6.1	−7.7	−3.5	3.2	5.0	7.7	13.2
				k = .22	9.1	5.5	−7.1	−12.2	−13.4	−6.1	−4.5	−1.3	3.1	6.1	9.8	10.9
				P_g	8.0	6.5	8.0	11.0	14.0	12.5	12.0	11.0	9.5	8.0	6.5	8.0
				c	−1.1	−2.6	−1.5	1.5	4.5	2.3	1.3	1.0	−0.6	−1.5	−2.8	−0.6
				±1.39	8.0	2.9	−8.6	−10.7	−8.9	−3.8	−3.2	−0.3	2.5	4.6	7.0	10.3

2. ATLANTIC: Norway, West

Andenes (No)	69°19N	16°09E	1938–46(3)	9	6.4	5.2	−2.6	−6.9	−14.5	−8.4	−12.6	−3.0	1.9	9.6	11.0	13.7
Narvik (No)	68°26N	17°25E	1928–39(3)	12	8.7	−1.6	−6.0	−16.8	−14.1	−6.2	0.5	−2.6	1.2	10.9	14.9	11.6
Kabelvaag (No)	68°13N	14°30E	1880–85(3)	6	13.5	8.5	−7.3	−14.1	−6.0	−8.6	−4.2	−3.4	−3.8	2.0	9.3	14.5
Trondhjen (No)	63°26N	10°22E	1872–74(3), 1877–78 (2), 1880–81(2)	7	18.9	1.8	−10.1	−16.5	−7.7	−3.3	−5.9	−9.8	−3.9	9.0	15.8	11.3
Heimsjöen (No)	63°26N	9°07E	1935–41, 1943–46(1)	11	8.6	5.1	−8.0	−8.1	−15.1	−5.1	−6.1	−1.7	2.9	11.1	3.6	12.3
Kjöllesdal (No)	61°55N	5°38E	1935–41(2), 1943(1), 1945–46(1)	10	4.3	−0.5	−7.6	−9.2	−14.9	−4.8	−0.9	0.3	5.0	9.6	11.1	7.6
Bergen (No)	60°24N	5°18E	1883–89(2), 1928–40, 1944(1), 1946	22	8.4	−1.3	−7.1	−13.9	−13.8	−6.9	−0.7	1.8	2.5	11.0	11.6	8.8
Stavanger (No)	58°58N	5°44E	1881–85(5), 1928–39(1)	17	4.4	−4.2	−8.5	−9.3	−13.2	−2.6	0.1	3.3	2.1	9.8	15.3	2.6
				k = .10	8.7	0.9	−7.2	−11.8	−12.8	−5.6	−3.3	−1.3	1.4	9.6	11.8	9.7
				P_g	6.5	8.0	9.0	9.5	14.5	14.0	11.5	10.0	10.5	8.5	7.0	7.0
				c	−2.7	−1.2	−0.6	−0.1	4.9	3.7	0.7	−0.1	0.3	−1.1	−2.4	−1.7
				±1.13	6.0	−0.3	−7.8	−11.9	−7.9	−1.9	−2.6	−1.4	1.7	8.5	9.4	8.0

3. ATLANTIC: Skagerrak, Kattegat, and Eastern North Sea

Tregde (No)	58°00N	7°34E	1935–40, 1942–43(1), 1945–46	10	1.5	1.0	−8.5	−6.4	−8.5	−4.1	0.2	1.6	5.3	6.1	8.1	4.2
Nevlunghavn (No)	58°58N	9°53E	1935–41(2), 1943–46	11	−0.6	−1.3	−9.9	−8.9	−11.0	0.7	4.7	5.0	6.1	4.5	9.1	1.9
Oscarsborg (No)	59°41N	10°37E	1872–82(4)	11	−5.0	−13.0	−15.6	−15.2	−9.5	2.7	10.7	13.7	15.4	8.6	5.5	2.0
Oslo (No)	59°54N	10°45E	1885–90(1), 1928–46(1)	25	−0.1	−8.5	−11.3	−12.6	−11.9	0.8	8.3	9.0	7.7	10.0	6.9	1.2
Strömstad (Sw)	58°57N	11°11E	1900–23, 1925–40, 1946(1)	41	1.4	−4.3	−10.5	−10.6	−8.4	−0.2	4.9	7.5	4.5	4.0	6.7	4.7
Smögen (Sw)	58°22N	11°13E	1911–46	36	5.0	−2.8	−5.1	−6.4	−5.0	−2.1	1.1	2.6	2.1	3.6	2.9	3.9
Bäckevik (Sw)	58°22N	11°15E	1895–1928	34	1.8	−2.8	−9.5	−10.8	−8.0	−1.6	4.1	7.2	5.4	4.0	5.6	4.9
Göteborg (Sw)	57°43N	11°57E	1887–1900, 1902–46	59	0.6	−3.8	−9.3	−11.5	−9.4	−1.6	4.6	8.2	6.8	6.0	5.6	4.0
Varberg (Sw)	57°06N	12°13E	1887–1946	60	0.0	−4.3	−9.5	−10.4	−9.6	−1.6	4.7	8.2	7.1	6.7	5.1	3.6
Frederikshavn (De)	57°26N	10°34E	1893–1946(1)	54	1.7	−3.5	−9.6	−9.5	−10.4	−1.4	4.0	6.1	5.1	5.7	6.8	5.1
Hirtshals (De)	57°36N	9°57E	1892–1946(4)	55	1.2	−3.6	−10.7	−9.9	−11.0	−0.8	5.3	7.4	6.1	6.5	5.0	4.3
Esbjerg (De)	55°28N	8°27E	1889–1946(1)	58	5.2	−2.6	−10.7	−13.9	−16.1	−7.0	0.7	6.4	6.5	10.5	10.8	10.8
Bremerhaven (Ge)	53°34N	8°34E	1898–1943	46	−0.2	−4.5	−9.9	−6.5	−9.1	−0.2	4.4	6.7	5.1	5.1	5.1	3.4
				k = .05	1.2	−4.0	−9.8	−10.2	−9.9	−1.6	4.2	6.9	6.1	6.3	6.3	4.5
				P_g	13.0	13.0	12.5	12.0	14.0	14.0	13.5	13.5	15.0	13.0	13.0	13.0
				c	0.2	0.2	−0.7	−1.2	0.8	0.1	−0.9	−0.2	1.2	−0.2	0.0	0.7
				±.64	1.4	−3.8	−10.5	−11.4	−9.1	−1.5	3.3	6.7	7.3	6.1	6.3	5.2

4a. ATLANTIC: Sweden, East

Mem (Sw)	58°29N	16°25E	1887–1924	38	2.9	2.0	−4.7	−9.7	−9.7	−5.3	3.7	9.7	4.8	0.4	−1.1	6.4
Nedre Nyköping (Sw)	58°45N	17°01E	1909–20	12	6.8	−0.7	−9.4	−9.3	−9.6	−2.4	3.5	7.8	7.1	−0.4	−0.8	7.6
Landsort (Sw)	58°45N	17°52E	1887–1946	60	2.3	−0.3	−9.6	−12.0	−12.5	−3.6	5.5	9.2	7.2	4.6	2.0	6.6
N. Södertälje (Sw)	59°12N	17°38E	1869–1946	78	3.3	−1.2	−8.6	−12.3	−12.3	−2.7	5.7	8.8	7.0	4.3	2.5	5.6
Stockholm (Sw)	59°19N	18°05E	1889–1946	58	3.3	0.6	−8.9	−10.5	−12.2	−3.7	5.2	9.0	6.8	4.1	1.9	5.0
Grönskär (Sw)	59°17N	19°02E	1922–30	9	4.0	−9.1	−20.0	−17.8	−13.6	1.8	7.2	10.9	8.3	10.2	12.7	5.1
Björn (Sw)	60°38N	17°58E	1892–1946	55	4.4	0.3	−9.8	−11.5	−13.7	−5.1	4.2	8.3	7.2	4.6	3.5	7.1
Nedre Gävle (Sw)	60°41N	17°10E	1896–1946	51	5.7	−1.1	−9.3	−11.6	−12.3	−5.8	4.8	8.4	6.1	4.0	2.7	8.2
Draghällan (Sw)	62°20N	17°28E	1898–1946	49	6.3	0.4	−10.1	−12.1	−13.4	−5.6	4.2	8.0	9.7	3.3	3.0	6.4
Ratan (Sw)	64°00N	20°55E	1892–1946	55	6.9	1.8	−9.4	−12.0	−14.6	−6.2	2.2	6.4	6.8	4.3	5.4	8.0
				k = .05	4.4	−0.2	−9.4	−11.7	−12.5	−4.2	4.6	8.6	7.1	3.9	2.9	6.6
				P_g	14.0	13.5	13.0	12.5	14.0	14.0	12.5	12.5	15.5	14.0	14.0	13.5
				c	0.8	0.3	0.4	−1.1	0.4	−0.3	−2.3	−1.6	1.3	0.4	0.6	0.8
				±.57	5.2	0.1	−9.0	−12.8	−12.1	−4.5	2.3	7.0	8.4	4.3	3.5	7.4

4b. ATLANTIC: Gulf of Bothnia, North

Station	Latitude	Longitude	Years	Total Years	J	F	M	A	M	J	J	A	S	O	N	D
Furuögrund (Sw)	64°55N	21°14E	1916–46	31	8.8	−2.0	−12.3	−11.6	−10.5	−5.2	0.9	4.4	5.6	5.8	8.7	7.2
Kemi (Fi)	65°44N	24°33E	1920–44(3)	25	9.3	−3.0	−11.7	−16.6	−16.5	−5.4	2.7	6.4	6.0	7.6	11.7	9.8
Toppila (Fi)	65°02N	25°26E	1889–1944(6)	56	9.5	2.8	−8.4	−12.8	−14.9	−6.8	1.4	4.6	6.1	4.0	6.0	8.9
Hornankallio (Fi)	64°42N	24°30E	1922–44(1)	23	8.8	−1.9	−14.4	−15.5	−18.2	−4.9	2.9	5.8	6.5	9.4	11.3	9.9
				k = .09	9.1	−0.7	−11.4	−13.9	−14.8	−5.7	1.9	5.2	6.0	6.4	9.1	8.9
				P_g	8.0	9.5	11.0	11.0	14.0	12.5	11.0	11.0	11.0	11.0	9.5	11.0
				c	−2.4	−0.9	0.2	0.2	3.2	1.0	−1.0	−0.3	−0.4	0.2	−1.1	1.1
				±.86	6.7	−1.6	−11.2	−13.7	−11.6	−4.7	0.9	4.9	5.6	6.6	8.0	10.0

4c. ATLANTIC: Gulf of Bothnia, East

Ykspihlaja (Fi)	63°50N	23°02E	1889–1924	36	6.4	3.2	−7.8	−14.0	−13.3	−5.8	3.1	7.4	8.4	2.2	2.7	7.5
Leppäluoto (Fi)	63°42N	22°42E	1914–44(2)	31	7.0	−1.9	−12.8	−13.8	−16.5	−3.5	2.9	5.9	7.4	7.9	6.8	10.2
Vaasa (Fi)	63°07N	21°36E	1883–1921(2)	39	6.7	3.9	−8.1	−14.5	−14.9	−7.8	2.0	6.6	7.4	3.6	3.3	11.4
Vaskiluoto (Fi)	63°06N	21°34E	1922–44	23	6.3	−3.8	−13.1	−14.2	−15.8	−2.8	4.6	7.3	6.8	8.9	8.7	7.1
Rönnskär (Fi)	63°04N	20°48E	1867–1910, 1920–36	61	7.8	1.1	−9.6	−16.2	−15.1	−6.1	3.3	7.1	6.1	6.8	6.5	7.8
Kaskinen (Fi)	62°23N	21°13E	1926–44(3)	19	3.9	0.1	−11.2	−10.7	−15.9	−4.7	4.7	6.5	4.9	8.8	7.9	6.1
Sälgrund (Fi)	62°20N	21°12E	1919–28(1)	10	12.3	−1.5	−12.1	−17.6	−13.0	−0.2	4.4	9.5	9.6	3.7	2.9	2.1
Reposaari (Fi)	61°37N	21°27E	1889–1926	38	7.1	3.0	−7.3	−12.9	−14.2	−6.4	2.1	7.7	7.9	2.0	2.7	7.9
Mäntyluoto (Fi)	61°36N	21°29E	1910–44(2)	35	4.7	−2.2	−10.0	−11.9	−14.3	−3.0	3.7	6.5	6.7	6.0	6.2	7.2
Säppi (Fi)	61°29N	21°20E	1919–36(2)	18	8.7	−4.6	−15.3	−15.9	−16.2	−2.8	5.3	10.4	6.5	10.7	8.4	4.9
Rauma (Fi)	61°08N	21°29E	1933–44	12	−0.3	0.5	−8.0	−8.3	−14.1	−4.9	5.1	7.2	5.7	6.8	4.8	5.5
				k = .06	6.5	0.1	−10.3	−13.8	−14.9	−4.8	3.5	7.3	7.0	5.9	5.5	7.5
				P_g	12.5	12.5	12.5	12.5	14.0	14.0	11.0	11.0	14.0	12.5	12.5	12.5
				c	0.4	0.4	0.0	0.0	1.5	0.8	−2.7	−2.0	0.9	0.0	0.2	0.9
				±.61	6.9	0.5	−10.3	−13.8	−13.4	−4.0	0.8	5.3	7.9	5.9	5.7	8.4

4d. ATLANTIC: Gulf of Bothnia, Southeast														
Lyökki (Fi)	60°51N	21°11E	1858–1936(1)	79	5.9	0.6	−11.5	−14.5	−13.8	−4.9	4.5	8.5	7.6	5.7	5.5	5.8
Lypyrtti (Fi)	60°36N	21°14E	1858–1936(1)	79	5.3	−2.2	−10.2	−14.4	−13.7	−3.4	4.6	8.5	7.2	5.4	5.7	7.0
Ruissalo (Fi)	60°25N	22°06E	1922–44(1)	23	7.4	−11.6	−23.4	−23.7	−24.4	−0.4	10.9	14.4	12.0	16.1	13.4	9.1
Heligman (Fi)	60°12N	19°18E	1920–36(1)	17	7.3	−3.8	−14.0	−14.8	−16.0	−2.9	5.2	9.6	6.0	10.3	9.0	4.2
Strömma (Fi)	60°11N	22°53E	1899–1936(1)	38	7.3	0.0	−11.4	−13.4	−14.1	−5.5	3.5	9.3	7.1	5.7	5.3	6.6
Lemström (Fi)	60°06N	20°01E	1889–1936	48	5.0	1.9	−9.8	−13.0	−14.5	−6.0	4.0	9.2	7.8	4.9	3.8	6.4
Lohm (Fi)	60°06N	21°40E	1920–27(1)	8	11.0	−6.7	−12.5	−14.2	−13.2	1.7	3.9	9.1	10.1	6.0	5.5	−1.2
Degerby (Fi)	60°02N	20°23E	1924–44	21	3.0	−2.4	−10.3	−18.7	−13.9	−2.5	6.9	8.3	7.6	9.8	6.9	4.9
Kobbaklintar (Fi)	60°02N	19°53E	1921–24, 1926–36	15	4.3	−6.2	−15.0	−15.0	−15.2	−2.6	7.2	10.6	5.2	11.7	10.3	4.8
Jungfrusund (Fi)	59°57N	22°22E	1858–1934	77	4.8	−0.3	−10.9	−13.9	−12.6	−3.8	5.5	8.9	7.7	4.5	5.0	5.2
Hanko (Fi)	59°49N	22°58E	1897–1903, 1921–39, 1942–44(1)	29	4.3	0.7	−10.5	−11.6	−13.7	−4.3	4.4	6.3	5.7	7.7	7.2	4.0
Utö (Fi)	59°47N	21°22E	1866–1936(2)	71	4.1	0.2	−10.5	−13.8	−13.9	−4.2	4.8	8.7	7.5	5.1	5.2	6.9
				k = .05	5.5	−1.7	−12.0	−14.8	−14.7	−3.7	5.3	9.1	7.6	7.1	6.4	5.7
				P_g	12.5	12.5	12.5	12.0	14.0	13.0	11.0	11.0	14.0	12.5	12.5	12.5
				c	0.5	0.5	0.1	−0.4	1.6	−0.1	−2.6	−1.9	1.0	0.1	0.3	1.0
				±.71	6.0	−1.2	−11.9	−15.2	−13.1	−3.8	2.7	7.2	8.6	7.2	6.7	6.7
4e. ATLANTIC: Gulf of Finland														
Russarö (Fi)	59°46N	22°57E	1866–1924, 1926–36(3)	70	4.4	−0.2	−9.6	−14.1	−12.7	−4.1	4.6	8.4	7.1	4.9	5.0	6.6
Tvärminne (Fi)	59°51N	23°15E	1921–36	16	5.0	−5.4	−14.2	−13.0	−15.8	−3.3	5.9	9.8	6.5	12.0	8.1	3.9
Skuru (Fi)	60°06N	23°33E	1900–36	37	3.4	−6.7	−11.0	−11.2	−11.2	−2.9	5.6	10.7	7.2	5.2	4.9	6.2
Helsinki (Fi)	60°09N	24°58E	1857–62(1), 1879–1944	72	4.1	−1.3	−10.1	−13.7	−13.1	−4.4	5.4	9.1	7.7	5.4	4.4	6.9
Söderskär (Fi)	60°07N	25°25E	1866–1936	71	3.5	−0.9	−11.4	−14.9	−13.0	−3.1	5.5	9.1	8.4	5.3	5.4	6.1
Kotka (Fi)	60°27N	26°57E	1908–12, 1914–27	19	7.3	−1.3	−16.1	−14.0	−12.0	−2.1	1.6	8.6	12.0	5.2	5.8	4.6
Hamina (Fi)	60°34N	27°11E	1928–44(1)	17	0.7	−4.7	−10.3	−11.0	−15.9	−2.4	6.7	8.1	6.7	9.3	6.6	5.8
Viipuri (Fi)	60°42N	28°44E	1889–1939(1), 1943–44(2)	53	3.3	−0.6	−13.3	−15.9	−15.9	−4.5	5.1	9.7	10.3	7.1	8.4	6.0
Koivisto (Fi)	60°21N	28°37E	1922–39(4)	18	3.5	−8.6	−16.5	−17.6	−15.0	−2.2	4.3	7.9	6.5	13.5	9.1	15.1
Suursaari (Fi)	60°05N	26°59E	1920–36(2)	17	3.4	−7.1	−13.4	−15.3	−13.6	1.7	9.1	11.5	8.2	10.6	4.8	0.5
Tallinn (Es)	59°27N	24°48E	1928–38	11	1.8	−1.6	−10.0	−11.9	−17.1	−4.2	8.1	8.8	5.1	12.3	8.7	0.2
				k = .05	3.7	−2.9	−12.0	−14.0	−13.8	−3.1	5.5	9.2	7.9	7.4	6.2	5.9
				P_g	13.5	13.0	13.0	12.5	15.0	12.5	10.5	11.0	13.5	13.5	13.0	13.0
				c	1.2	0.7	0.3	−0.2	2.3	−0.9	−3.4	−2.2	0.2	0.8	0.5	1.2
				±.62	4.9	−2.2	−11.7	−14.2	−11.5	−4.0	2.1	7.0	8.1	8.2	6.7	7.1

4f. ATLANTIC: Baltic Sea, Northeast

Station	Latitude	Longitude	Years	Total Years	J	F	M	A	M	J	J	A	S	O	N	D
Vilsandi (Es)	58°23N	21°49E	1928–38(1)	11	1.6	−3.9	−12.4	−11.1	−15.1	−2.6	1.0	10.0	6.0	14.0	11.1	1.6
Kolkasrags (La)	57°48N	22°38E	1884–93, 1901–13, 1925–36(1)	35	2.7	−1.2	−13.5	−15.1	−14.1	−3.2	6.1	11.2	7.7	7.4	4.7	7.1
Mērsrags (La)	57°20N	23°07E	1929–36	8	−2.0	−6.5	−13.7	−11.4	−14.0	−3.0	10.0	13.7	5.6	14.9	6.1	0.8
Daugavgrīva (La)	57°03N	24°02E	1872–1917, 1922–38(2)	63	−0.8	−3.3	−9.4	−8.2	−8.8	−0.9	7.4	10.5	8.1	2.8	1.3	1.7
Dzirnupe (La)	57°01N	24°07E	1931–36	6	−5.7	0.5	−12.6	−2.2	−9.4	−5.2	7.6	11.2	5.6	13.3	−2.6	−0.6
Andrejosta (La)	56°58N	24°06E	1930–36	7	−3.5	−3.7	−9.9	3.0	−5.6	−8.6	4.3	10.2	0.1	10.8	5.3	−2.4
Ainaži (La)	57°53N	24°20E	1930–36	7	2.8	−1.1	−14.4	−14.4	−17.3	−6.9	7.7	13.4	3.9	16.5	7.9	2.0
Salacgriva (La)	57°45N	24°22E	1929–36	8	−3.9	−7.1	−4.2	−6.2	−16.2	−5.4	8.0	11.3	3.5	15.5	5.8	−0.8
				k = .09	−0.5	−3.2	−11.1	−9.1	−12.2	−3.8	6.6	11.3	5.8	10.0	4.6	1.9
				P_g	14.0	14.0	14.0	12.5	14.0	14.0	11.0	11.0	14.0	14.0	14.0	14.0
				c	1.1	1.1	0.7	−0.8	0.7	0.0	−3.5	−2.8	0.1	0.7	0.9	1.6
				±1.16	0.6	−2.1	−10.4	−9.9	−11.5	−3.8	3.1	8.5	5.9	10.7	5.5	3.5

4g. ATLANTIC: Baltic Sea, Southeast

Station	Latitude	Longitude	Years	Total Years	J	F	M	A	M	J	J	A	S	O	N	D
Ventspils (La)	57°24N	21°33E	1873–1913, 1920–36(3)	58	2.8	−2.3	−9.2	−13.1	−12.9	−3.8	5.5	10.4	7.5	5.4	5.1	4.8
Pāvilosta (La)	56°54N	21°11E	1930–36	7	1.8	1.9	−13.1	−11.9	−16.6	−8.4	6.0	11.7	3.2	14.7	8.8	1.7
Liepāja (La)	56°32N	20°59E	1865–93, 1896–1913, 1921–38	65	0.9	−3.4	−10.3	−13.4	−11.1	−2.8	6.4	8.7	8.6	5.6	5.5	5.0
Pape (La)	56°09N	21°02E	1930–36	7	1.2	1.8	−12.5	−12.3	−17.3	−9.3	6.1	12.0	3.2	16.3	9.0	1.7
Klaipeda (Li)	55°42N	21°08E	1937–38	2	−6.5	−4.5	6.5	13.0	−10.5	−2.5	9.5	−2.5	4.5	1.5	7.0	−15.5
Memel (Ge)	55°43N	21°07E	1898–1919	22	6.1	3.9	−19.0	−4.1	−12.0	−6.7	3.5	10.4	8.6	−1.0	1.3	9.5
Pillau (Ge)	54°38N	19°54E	1898–1943(1)	46	−0.5	−2.2	−10.1	−8.2	−10.8	−3.9	7.8	11.8	9.1	3.7	0.6	2.7
Hel (Po)	54°36N	18°48E	1931–38	8	−4.8	2.0	−6.9	−5.8	−11.0	−4.3	8.5	11.1	6.2	9.8	1.5	−6.5
Gdynia (Po)	54°32N	18°33E	1931–38	8	−3.2	2.5	−8.3	−17.5	−10.6	−3.6	8.4	10.2	7.7	11.0	3.8	−0.6
				k = .08	0.8	−0.5	−10.7	−10.2	−12.3	−4.7	6.4	10.2	7.3	6.5	4.1	2.9
				P_g	15.5	15.5	15.5	12.5	14.0	13.5	12.5	12.5	15.0	15.0	15.0	14.0
				c	1.8	1.8	1.4	−1.6	−0.1	−1.3	−2.8	−2.1	0.3	0.9	1.1	0.8
				±1.13	2.6	1.3	−9.3	−11.8	−12.4	−6.0	3.6	8.1	7.6	7.4	5.2	3.7

4h. ATLANTIC: Baltic Sea, Central													
Limhamn (Sw)	55°35N	12°56E	1928–36(1)	9	−2.2	−3.4	−12.9	−10.8	−11.0	−3.3	7.8	10.1	6.6	13.0	5.2	1.4
Klagshamn (Sw)	55°31N	12°55E	1929–46(1)	18	−0.9	−3.4	−6.5	−3.7	−6.4	−1.9	6.4	8.2	5.1	5.6	0.9	−3.7
Ystad (Sw)	55°25N	13°49E	1887–1946	60	−0.7	−0.6	−7.0	−7.9	−8.2	−2.9	6.3	7.1	6.0	4.7	0.5	3.1
Kungsholms Fort (Sw)	56°06N	15°35E	1887–1946	60	4.4	−0.3	−8.7	−7.7	−10.7	−3.3	4.8	7.8	6.3	4.1	0.4	3.4
Ölands n. udde (Sw)	57°22N	17°06E	1923–46	24	0.2	−2.8	−11.4	−9.8	−11.8	−1.6	6.7	9.0	7.4	8.5	4.4	1.7
Stolpmünde (Ge)	54°35N	16°51E	1911–43	33	0.1	−3.4	−9.6	−8.1	−10.2	−0.7	6.9	9.9	9.0	6.3	−3.0	3.3
Swinemünde (Ge)	53°56N	14°17E	1811–1943(3)	133	−0.3	−2.8	−5.1	−5.7	−6.4	−0.6	7.1	7.9	5.6	0.3	−0.5	0.1
Arkona (Ge)	54°41N	13°26E	1882–1935(6)	54	−1.5	−0.6	−7.0	−8.3	−8.1	−2.3	4.6	7.7	6.5	4.5	1.2	3.4
				k = .05	0.1	−1.9	−7.8	−7.5	−8.7	−1.9	6.2	8.2	6.5	4.7	0.6	1.8
				P_g	15.5	14.5	13.5	12.5	14.0	14.0	13.0	13.0	15.5	14.0	14.0	13.5
				c	1.9	1.0	−0.4	−1.5	0.0	0.3	−2.2	−1.4	0.9	0.0	0.2	0.5
				±.65	2.0	−0.9	−8.2	−9.0	−8.7	−1.6	4.0	6.8	7.4	4.7	0.8	2.3
4i. ATLANTIC: Baltic Sea, West																
Warnemünde (Ge)	54°11N	12°05E	1882–1943(3)	62	−3.3	−3.3	−5.3	−5.3	−4.5	1.2	6.3	8.6	6.3	3.0	−1.8	−1.9
Wismar (Ge)	53°54N	11°28E	1882–1943(4)	62	−4.7	−2.6	−6.8	−4.2	−3.1	2.0	6.9	7.9	6.4	2.2	−2.9	−1.3
Travemünde (Ge)	53°58N	10°53E	1855–1943(2)	89	−2.8	−2.0	−3.3	−2.6	−2.1	0.3	3.2	3.9	3.7	4.5	−1.8	−1.0
Marienleuchte (Ge)	54°30N	11°15E	1882–1943(4)	62	−3.3	−1.8	−5.5	−5.1	−4.4	0.3	5.3	7.0	5.7	3.3	−1.8	−0.1
Gedser (De)	54°34N	11°58E	1898–1946	49	−2.5	−2.6	−6.3	−5.2	−4.3	−0.8	5.7	7.9	6.4	3.7	−2.2	0.2
København (De)	55°41N	12°36E	1889–1946(1)	58	−0.8	−3.0	−8.4	−8.0	−8.2	−1.7	5.9	8.1	7.2	5.1	2.2	1.7
Hornbaek (De)	56°06N	12°28E	1898–1946(1)	49	−1.4	−4.9	−10.6	−9.4	−8.7	0.9	7.2	9.2	7.5	6.4	3.6	−0.2
Korsor (De)	55°20N	11°08E	1897–1946	50	−1.3	−2.7	−6.8	−6.3	−5.9	−1.6	4.3	6.3	5.7	4.8	1.7	1.9
Slipshavn (De)	55°17N	10°50E	1896–1946(1)	51	4.8	−2.7	−6.8	−6.6	−6.9	−4.4	3.7	5.5	5.1	4.5	2.8	1.1
Fredericia (De)	55°34N	9°46E	1889–1946(3)	58	−0.2	−2.3	−5.7	−5.8	−6.0	−2.4	2.2	4.1	4.6	5.5	3.8	2.6
Aarhus (De)	56°09N	10°13E	1888–1946(1)	59	5.2	−3.8	−7.0	−7.9	−8.4	−2.8	2.1	4.2	4.1	6.0	4.6	3.3
				k = .04	−0.9	−2.9	−6.5	−6.0	−5.6	−0.8	4.8	6.5	5.7	4.4	0.7	0.5
				P_g	15.5	14.0	12.5	12.5	14.0	14.0	14.0	13.5	15.5	14.0	13.5	13.5
				c	2.1	0.6	−1.3	−1.3	0.2	−0.5	−1.0	−0.8	1.1	0.2	−0.1	0.6
				±.57	1.2	−2.3	−7.8	−7.3	−5.4	−1.3	3.8	5.7	6.8	4.6	0.6	1.1
4. ATLANTIC: Baltic Sea Summary																
				k = .02	3.0	−1.7	−9.9	−11.1	−11.7	−3.3	5.0	8.3	6.8	5.9	4.0	4.4
				c	0.8	0.6	0.2	−0.8	1.1	−0.1	−2.3	−1.7	0.6	0.4	0.2	0.9
				±.24	3.8	−1.1	−9.7	−11.9	−10.6	−3.4	2.7	6.6	7.4	6.3	4.2	5.3

Station	Latitude	Longitude	Years	Total Years	J	F	M	A	M	J	J	A	S	O	N	D
5. ATLANTIC: North Sea, West																
Aberdeen (Sc)	57°09N	2°05W	1862–1913	52	6.1	0.0	−6.1	−9.2	−9.2	−6.1	−3.1	0.0	0.0	6.1	9.2	12.2
Dundee (Sc)	56°27N	2°58W	1897–1912	16	6.7	1.1	−5.3	−8.8	−10.7	−8.3	−6.4	−0.7	−0.3	8.0	10.9	13.8
Dunbar (Sc)	56°00N	2°31W	1913–46(1)	34	3.1	−2.1	−5.5	−7.0	−7.9	−4.3	−0.9	1.2	2.4	6.4	7.6	6.1
Felixstowe (En)	51°56N	1°19E	1918–46(6)	29	−2.4	−4.6	−4.9	−3.4	−5.2	−1.8	0.6	2.7	4.3	6.4	5.2	2.4
				k = .09	3.5	−1.4	−5.5	−7.2	−8.2	−5.0	−2.3	0.8	1.6	6.7	8.2	8.6
				P_g	14.0	13.0	12.5	12.5	14.0	15.5	15.5	14.0	15.5	12.5	12.5	11.5
				c	0.9	−0.1	−1.0	−1.0	0.5	1.3	0.8	0.0	1.4	−1.0	−0.8	−0.9
				±1.15	4.4	−1.5	−6.5	−8.2	−7.7	−3.2	−1.5	0.8	3.0	5.7	7.4	7.7
6. ATLANTIC: Irish Sea																
Dublin (Ei)	53°21N	6°13W	1938–46	9	3.4	−5.5	−5.2	−5.2	−2.7	−3.1	0.0	−0.9	0.3	7.9	9.4	3.1
Douglas (En)	54°09N	4°28W	1938–46	9	3.7	−4.0	−6.1	−8.5	−6.4	−2.7	−1.2	−0.9	0.3	5.5	12.8	8.8
Liverpool (En)	53°25N	3°00W	1918, 1920, 1924, 1930, 1934–46	17	8.1	−4.7	−8.1	−7.9	−8.0	−3.9	−2.8	−0.6	4.9	8.3	7.8	6.6
Holyhead (En)	53°19N	4°37W	1838–39(2), 1846–47(2), 1938–46(2)	13	8.2	−1.6	−7.4	−8.6	−7.4	−4.3	−4.3	0.5	2.4	8.2	10.0	3.9
Milford Haven (En)	51°42N	4°57W	1886–92	7	−0.2	−11.1	−4.4	−5.9	−1.4	−3.2	0.8	4.4	−1.7	6.0	9.3	7.8
Avonmouth (En)	51°30N	2°43W	1925–46	22	5.4	0.5	−6.3	−6.6	−6.3	−4.5	−0.5	−1.7	3.7	6.8	8.7	1.0
Newlyn (En)	50°06N	5°33W	1916–46	31	1.8	−6.4	−1.1	−3.5	−2.6	−3.7	−2.8	−0.5	0.2	6.2	8.7	3.5
				k = .10	4.4	−4.4	−5.3	−6.4	−5.1	−3.7	−1.7	−0.1	1.6	7.0	9.3	4.5
				P_g	14.0	14.0	13.0	14.5	15.0	17.0	15.5	15.0	16.0	13.5	13.0	12.0
				c	0.1	0.1	−1.3	0.2	0.7	2.0	0.0	0.2	1.1	−0.8	−1.1	−1.4
				±.81	4.5	−4.3	−6.6	−6.2	−4.4	−1.7	−1.7	0.1	2.7	6.2	8.2	3.1
7. ATLANTIC: North Sea, South																
Delfzijl (Ne)	53°20N	6°56E	1865–1946	82	0.3	−3.7	−6.8	−8.0	−8.2	−1.8	2.1	4.5	4.6	6.3	6.6	4.7
Terschelling (Ne)	53°22N	5°13E	1921–46	26	1.2	−4.8	−9.6	−8.4	−9.2	−3.5	1.1	3.3	5.2	10.3	9.4	4.5
Harlingen (Ne)	53°10N	5°25E	1865–1946	82	0.9	−3.6	−7.6	−9.0	−9.9	−3.8	1.6	4.9	5.5	7.6	7.3	6.1
Den Helder (Ne)	52°58N	4°45E	1865–1946	82	1.7	−2.8	−7.1	−8.6	−9.0	−4.2	0.3	1.0	4.6	8.0	8.9	7.3
Ijmuiden (Ne)	52°28N	4°35E	1871–1946	76	0.4	−5.2	−7.3	−7.6	−7.8	−2.7	1.8	4.3	4.6	7.3	7.1	5.1

Hoek van Holland (Ne)	51°59N	4°07E	1864–1946	83	−1.3	−4.1	−5.7	−6.0	−6.4	−1.8	1.6	3.7	3.9	6.3	5.9	3.7
Maassluis (Ne)	51°55N	4°15E	1848–1936	89	0.4	−1.5	−3.7	−5.3	−6.5	−1.9	1.2	2.4	1.8	4.6	4.3	4.4
Hellevoetsluis (Ne)	51°49N	4°08E	1861–1946	86	−2.2	−4.5	−5.6	−5.6	−6.0	−1.7	1.8	3.4	3.1	4.8	5.1	7.2
Brouwershaven (Ne)	51°44N	3°54E	1872–1946	75	−2.1	−5.4	−6.0	−5.5	−5.2	−1.2	2.2	4.1	4.3	6.3	5.5	2.8
Zierikzee (Ne)	51°38N	3°55E	1872–1946	75	−2.7	−5.2	−5.7	−5.2	−4.8	−0.9	2.4	4.2	3.9	5.7	5.4	2.5
Vlissingen (Ne)	51°27N	3°36E	1862–1946	85	−2.4	−4.7	−5.3	−4.6	−4.5	−1.2	2.0	3.8	3.9	6.0	4.7	2.2
				k = .04	−0.6	−4.1	−6.3	−6.6	−7.0	−2.2	1.7	3.6	4.1	6.5	6.2	4.6
				P_g	14.0	14.0	13.0	13.0	14.0	15.0	15.0	14.5	17.0	14.0	14.0	14.0
				c	0.2	0.2	−1.2	−1.2	−0.2	0.1	−0.4	−0.2	2.2	−0.2	0.0	0.7
				±.40	−0.4	−3.8	−7.5	−7.8	−7.2	−2.1	1.3	3.4	6.3	6.3	6.2	5.3
				8. ATLANTIC: English Channel												
Zeebrugge (Be)	51°21N	3°12E	Aug. 1942–July 1943(2)	1	1.6	3.2	−11.4	−3.0	−12.4	−6.6	0.8	−5.3	5.9	14.1	3.4	9.3
Antwerpen (Be)	51°14N	4°25E	1937–38, 1943–44(2)	4	8.2	7.5	−2.7	−1.4	−4.2	−7.4	−1.9	1.3	−0.6	2.3	6.3	−7.8
Ostende (Be)	51°14N	2°55E	1937–38, 1943–Jan. 1944(1)	3	6.4	−0.1	−4.6	−3.0	−5.8	−2.1	−1.0	0.8	−0.1	2.8	9.9	−0.5
Nieuport (Be)	51°09N	2°43E	1943	1	6.5	4.0	−5.2	1.4	−8.9	−8.9	−3.9	4.4	−0.8	2.7	13.5	−6.6
Dunkerque (Fr)	51°03N	2°22E	1942	1	−12.9	−14.8	−10.6	−8.3	0.9	−4.4	4.1	2.5	7.6	15.5	8.5	11.6
Calais (Fr)	50°58N	1°51E	June 1941–May 1942(2)	1	−10.2	−9.2	2.5	−23.8	−12.3	3.6	7.6	12.4	0.9	15.6	5.8	7.4
Boulogne (Fr)	50°44N	1°35E	1942	1	−12.5	−22.9	−8.9	−0.9	2.2	−5.2	41.0	15.1	−1.7	5.5	−13.2	1.2
Dieppe (Fr)	49°56N	0°21E	1942	1	−7.7	−18.0	−7.3	−7.8	0.2	−6.1	0.6	2.9	16.6	18.8	−0.4	8.6
Fecamp (Fr)	49°46N	0°21E	1942	1	−7.8	−15.9	−5.1	−6.5	2.1	−2.4	2.4	2.2	9.8	11.6	−1.2	10.9
Le Havre (Fr)	49°29N	0°06E	Dec. 1941–Nov. 1942(2)	1	−25.4	−4.4	15.9	2.7	0.6	5.5	10.1	−5.3	9.3	13.0	0.1	−22.3
Cherbourg (Fr)	49°39N	1°37W	1943	1	−31.9	−40.1	−21.8	−18.8	17.3	10.0	12.1	12.0	19.2	19.7	2.9	19.9
Guernsey (Fr)	49°27N	2°31W	1943	1	−11.7	−40.8	−35.8	−33.9	−8.6	10.7	15.9	21.3	22.0	31.6	21.8	8.0
Jersey (Fr)	49°14N	2°12W	Sept. 1943–Apr. 1944(2)	1	−7.1	−8.1		1.0					4.5	14.3	5.1	−9.6
St. Malo (Fr)	48°38N	2°02W	June 1942–May 1943(2)	1	14.7	−13.7	−9.9	−13.1	−9.8	13.9	3.2	0.4	1.5	5.2	−3.5	11.3
Lizardrieux (Fr)	48°47N	3°06W	1942	1	0.3	−10.1	−1.0	−6.8	−1.9	−7.9	−2.9	4.2	10.9	12.5	−3.5	6.6
Brest (Fr)	48°23N	4°29E	1807–35, 1846–56, 1861–1943	123	0.8	−2.0	−3.1	−3.1	−2.6	−3.7	−3.1	−1.7	0.6	6.4	6.8	4.5
				k = .14	−2.4	−7.1	−5.3	−5.7	−2.9	−2.1	1.9	1.9	4.0	9.3	5.2	3.2
				P_g	17.0	18.5	14.0	14.0	14.0	17.0	17.0	16.0	18.0	15.0	15.0	14.0
				c	1.7	3.2	−1.7	−1.7	−1.7	0.6	0.1	−0.2	1.7	−0.7	−0.5	−0.8
				±1.93	−0.7	−3.8	−7.0	−7.4	−4.6	−1.5	2.0	1.7	5.7	8.6	4.7	2.4

9. ATLANTIC: Bay of Biscay

Station	Latitude	Longitude	Years	Total Years	J	F	M	A	M	J	J	A	S	O	N	D
Lorient (Fr)	47°45N	3°21W	1942	1	−12.1	−8.5	2.3	3.0	3.4	−1.2	7.2	−3.2	−1.8	3.5	−2.7	9.9
St. Nazaire (Fr)	47°16N	2°12W	Apr. 1941–Mar. 1942(2)	1	−3.1	−8.8	6.9	2.2	−2.2	5.2	3.8	3.1	−8.1	−4.9	11.6	−5.9
La Pallice (Fr)	46°10N	1°13W	1942	1	−11.1	−15.3	−0.8	−1.5	4.8	1.4	−3.7	0.7	7.6	12.2	−0.2	6.1
Le Verdon (Fr)	45°33N	1°04W	1941–42(1)	2	−7.9	−11.9	4.5	5.5	2.9	1.0	−6.3	2.5	5.6	6.3	2.5	−4.3
St. Jean-de-Luz (Fr)	43°24N	1°41W	1942–44(3)	3	−5.6	−5.2	−4.2	−2.3	−5.4	15.9		−1.5	−0.2	9.7	−0.9	−0.2
				k = .36	−7.6	−9.2	0.8	0.8	−0.3	6.4	0.2	0.0	0.5	6.1	1.6	0.9
				P_g	18.5	18.5	15.5	15.5	15.5	18.5	17.5	17.0	18.0	15.5	15.5	17.0
				c	2.1	2.1	−1.3	−1.3	−1.3	1.0	−0.5	−0.3	0.6	−1.3	−1.1	1.1
				±2.11	−5.5	−7.1	−0.5	−0.5	−1.6	7.4	−0.3	−0.3	1.1	4.8	0.5	2.0

10. ATLANTIC: Iberian Peninsula

Cascais (Po)[1]	38°41N	9°25W	1917–46(2)	30	−3.6	−5.2	−0.9	−0.5	−0.6	−1.9	−1.2	0.9	2.7	6.5	4.8	−0.5
Lagos (Po)[1]	37°06N	8°40W	1908–46(8)	39	−4.3	−5.3	−3.4	−3.3	−3.1	0.7	0.1	1.9	4.0	6.5	5.4	0.6
Cadiz (Sp)	36°30N	6°18W	1916–19(4)	4	0.7	0.5	−3.5	2.3	0.8	1.6	−2.5	−7.3	−2.9	−1.0	7.4	3.5
				k = .13	−3.3	−4.4	−2.5	−1.4	−1.5	−0.1	−0.8	0.1	2.4	5.7	5.5	0.7
				P_g	23.0	20.0	18.5	17.0	17.0	18.5	18.5	18.5	18.5	18.0	18.5	21.0
				c	4.6	1.6	−0.3	−1.8	−1.8	−1.0	−1.5	−0.8	−0.9	−0.8	−0.1	3.1
				±1.10	1.3	−2.8	−2.8	−3.2	−3.3	−1.1	−2.3	−0.7	1.5	4.9	5.4	3.8

11a. ATLANTIC: Mediterranean, North

Alicante (Sp)	38°20N	0°29W	1916–20	5	−5.2	−6.0	−3.4	−3.2	−2.0	−4.9	1.6	3.4	3.2	6.4	8.4	1.5
Marseille (Fr)	43°18N	5°21E	1885–1946(1)	62	−1.4	−2.3	−2.5	−1.5	−1.4	−1.8	−2.6	−2.3	−1.1	4.8	7.8	3.9
Porto Maurizio (It)	43°52N	8°01E	1896–1922(4)	27	−3.0	−4.0	−2.9	−1.6	−1.9	−0.2	−0.3	0.3	0.6	4.3	6.1	2.8
Genova (It)	44°25N	8°55E	1883–1910, 1928–45(4)	46	−2.9	−2.0	−0.3	0.8	−3.2	−1.9	1.2	1.2	−2.3	3.4	4.1	2.3
Livorno (It)	43°32N	10°18E	1896–1911	16	−5.7	−4.1	−2.5	−0.9	−0.4	0.8	−1.4	−0.7	0.0	5.0	6.0	4.3
Civitavecchia (It)	42°03N	11°49E	1896–1922(6)	27	−1.3	−1.8	−1.9	−0.5	−2.1	−2.2	−2.6	−1.8	−0.7	3.9	6.5	4.5
Napoli (Arsenale) (It)	40°52N	14°16E	1899–1922(13)	24	−1.5	−1.2	−2.0	−1.2	−2.4	−1.0	−1.8	−0.6	−0.8	3.4	5.9	3.7
Napoli (Mandraccio) (It)	40°52N	14°16E	1896–1922(9)	27	−1.9	−3.1	−2.4	−0.6	−1.5	−1.1	−1.8	−0.5	−1.1	3.8	6.3	4.5
Messina (Si)	38°12N	15°34E	1897–1923(3)	27	−0.1	−0.7	−2.9	−1.4	−3.1	−2.4	−2.7	−0.8	−1.0	3.7	6.5	5.4
				k = .06	−2.2	−2.5	−2.2	−0.9	−2.0	−1.5	−1.3	−0.5	−0.7	4.1	6.3	3.7
				P_g	20.0	17.0	15.5	14.0	15.5	15.5	15.5	15.5	17.0	17.0	15.5	17.0
				c	4.2	1.2	−0.7	−2.2	−0.7	−1.4	−1.9	−1.2	0.2	0.8	−0.5	1.7
				±.39	2.0	−1.3	−2.9	−3.1	−2.7	−2.9	−3.2	−1.7	−0.5	4.9	5.8	5.4

11b. ATLANTIC: Mediterranean, Sardinia														
La Maddalena (Sa)	41°14N	9°22E	1896–98, 1900–13(7)	17	−6.7	−7.3	−5.4	−3.3	−1.8	1.3	2.3	4.8	3.8	6.2	4.6	1.7
Cagliari (Sa)	39°12N	9°10E	1896–1934(12)	39	−6.8	−5.7	−5.6	−3.8	−2.6	−0.1	1.7	4.7	4.9	6.6	6.0	1.1
				k = .14	−6.8	−6.3	−5.5	−3.6	−2.3	−0.5	1.9	4.7	4.5	6.4	5.4	1.3
				P_g	18.5	15.5	14.0	13.0	14.0	14.0	15.0	14.0	15.5	15.5	15.5	17.0
				c	3.9	0.9	−1.0	−2.0	−1.0	−1.7	−1.2	−1.5	−0.1	0.5	0.7	2.9
				±.32	−2.9	−5.4	−6.5	−5.6	−3.3	−2.2	0.7	3.2	4.4	6.9	6.1	4.2
11c. ATLANTIC: Mediterranean, Sicily														
Mazara del Vallo (Si)	37°40N	12°34E	1909–16(2)	8	2.0	−1.8	−1.2	−5.8	−4.8	−3.8	−4.9	−2.9	−0.7	4.6	11.6	7.5
Palermo (Si)	38°08N	13°20E	1896–1922(11)	27	−0.7	−1.6	−3.1	−1.6	−2.8	−1.9	−2.2	−0.7	0.8	5.2	6.3	2.9
Catania (Si)	37°30N	15°08E	1896–1920(9)	25	−1.5	−1.1	−3.0	−3.2	−4.1	−2.3	−0.7	1.6	1.1	3.6	5.7	4.5
				k = .13	−0.4	−1.4	−2.6	−3.2	−3.8	−2.5	−2.2	−0.3	0.6	4.4	7.3	4.6
				P_g	17.0	15.5	14.0	14.0	14.0	14.0	14.0	14.0	15.5	16.0	15.5	17.0
				c	2.4	0.9	−1.0	−1.0	−1.0	−1.7	−2.2	−1.5	−0.1	1.0	0.7	2.9
				±.77	2.0	−0.5	−3.6	−4.2	−4.8	−4.2	−4.4	−1.8	0.5	5.4	8.0	7.5
11d. ATLANTIC: Mediterranean, Adriatic														
Taranto (It)	40°26N	17°16E	1906–11	6	−7.5	−0.5	−3.1	−1.9	1.9	0.9	−0.8	1.3	3.0	0.3	4.0	3.0
Ancona (It)	43°35N	13°29E	1896–1910(7)	15	−2.2	−0.4	−3.6	−1.6	−2.0	−1.5	−3.4	−3.3	−2.9	5.5	7.6	7.3
Porto Corsini (It)	44°30N	12°17E	1896–1922(3), 1937–42	33	−1.7	−2.1	−3.2	−0.1	−2.1	−1.0	−3.4	−3.2	−2.8	4.7	8.7	5.6
Venezia (Diga Sud di Lido) (It)	45°21N	12°23E	1917–34	18	−2.6	−6.1	−5.2	−0.4	−2.8	−0.3	−0.7	−1.1	−0.6	6.5	9.3	4.3
Venezia (Arsenale) (It)	45°24N	12°21E	1889–1913(7)	25	−4.1	−5.8	−2.7	−1.1	−0.4	0.0	−1.3	−1.3	−0.7	6.8	6.7	3.4
Venezia (S. Stefano) (It)	45°25N	12°20E	1896–1920(4)	25	−4.4	−5.3	−3.2	−0.1	−0.8	0.3	−1.3	−2.0	−1.4	5.5	7.1	5.4
Trieste (It)	45°39N	13°46E	1905–14, 1920–22, 1927–36(2)	23	−5.4	−8.0	−4.7	−0.3	−0.2	1.4	−0.4	−0.4	−0.2	5.7	9.5	3.8
Pola (It)	44°52N	13°51E	1897–1910, 1912–13	16	−5.4	−2.0	−3.7	−1.5	−1.3	0.6	−1.6	−1.7	−1.0	5.1	7.2	5.1
Bakar (Yu)	45°18N	14°32E	1930–38(2)	9	−10.1	−8.7	−9.7	−8.5	−9.0	−8.8	9.8	8.4	1.4	9.2	12.0	8.0
Split (Yu)	43°30N	16°27E	1930–38(2)	9	2.4	2.8	0.9	1.6	0.1	−1.7	−2.3	−3.2	−11.8	4.6	9.6	−3.2
				k = .08	−3.9	−3.9	−3.8	−1.1	−1.6	−0.8	−0.9	−1.1	−1.7	5.6	8.2	4.5
				P_g	17.0	15.5	15.5	13.5	14.0	14.0	14.0	14.0	15.5	17.0	17.0	17.0
				c	2.1	0.6	0.2	−1.8	−1.3	−2.0	−2.5	−1.8	−0.4	1.7	2.1	2.6
				±.82	−1.8	−3.3	−3.6	−2.9	−2.9	−2.8	−3.4	−2.9	−2.1	7.3	10.3	7.1

11e. ATLANTIC: Mediterranean, East

Station	Latitude	Longitude	Years	Total Years	J	F	M	A	M	J	J	A	S	O	N	D
Port Said (Su)	31°15N	32°18E	1923–46(1)	24	−2.1	−5.2	−9.4	−10.1	−7.8	−1.6	6.6	10.3	7.3	4.3	5.4	2.3
				k = .20												
				P_E	17.6	16.6	14.5	12.5	13.2	11.8	9.1	9.8	13.5	14.5	16.6	16.9
				c	4.2	3.2	0.7	−1.3	−0.6	−2.7	−5.9	−4.5	−0.9	0.7	3.0	4.0
					2.1	−2.0	−8.7	−11.4	−8.4	−4.3	0.7	5.8	6.4	5.0	8.4	6.3

11. ATLANTIC: Mediterranean Sea Summary

				k = .04	−3.0	−3.3	−3.4	−1.9	−2.4	−1.2	−0.6	−0.1	−0.1	4.9	7.0	3.8
				c	3.4	1.4	−0.4	−1.7	−0.9	−1.9	−2.7	−2.1	−0.3	0.9	1.2	2.8
				±.36	0.4	−1.9	−3.8	−3.6	−3.3	−3.1	−3.3	−2.2	−0.4	5.8	8.2	6.6

12. ATLANTIC: Azores

Horta (Az)	38°32N	28°38W	1905–38(7), 1945	35	0.0	−1.9	−4.0	−3.6	−2.7	−0.5	1.1	2.7	3.2	3.0	1.6	0.7
Angra do Heroismo (Az)	38°38N	27°12W	1933–37(1)	5	−0.9	−2.9	−3.6	−6.1	−1.5	−2.8	−0.5	0.5	3.2	4.6	5.3	4.2
Ponta Delgada (Az)[2]	37°44N	25°40W	1924, 1930–51(4)	23	0.0	−2.9	−3.8	−3.6	−4.3	−1.6	0.5	2.5	4.1	4.1	2.7	2.4
				k = .07	−0.1	−2.4	−3.9	−4.0	−3.1	−1.3	0.6	2.3	3.5	3.7	2.6	1.9
				P_E	17.0	14.0	15.0	15.5	17.0	17.0	18.5	18.5	18.5	18.5	17.0	17.0
				c	0.5	−2.5	−1.9	−1.4	0.1	−0.6	0.4	1.1	1.0	1.6	0.3	1.0
				±.46	0.4	−4.9	−5.8	−5.4	−3.0	−1.9	1.0	3.4	4.5	5.3	2.9	2.9

13. ATLANTIC: Canary Islands

Santa Cruz de Tenerife (CI)	(a)[2,3]	28°29N	16°14W	1927–36(1), 1940–46(1)	17	−7.3	−6.2	−4.4	−1.9	−2.0	0.4	4.5	6.8	6.1	5.8	1.0	−2.9
	(b)[2,3]	28°29N	16°14W	1926–36(3), 1940–46(1)	18	−7.8	−6.7	−4.7	−1.8	−1.5	0.8	5.1	7.1	6.1	6.1	1.2	−3.8
					k = .17	−7.6	−6.4	−4.6	−1.8	−1.8	0.6	4.8	7.0	6.1	6.0	1.1	−3.4
					P_E	22.5	20.0	18.5	18.5	17.0	17.0	17.0	17.0	17.0	17.0	18.5	21.5
					c	4.4	2.0	0.1	0.1	−1.4	−2.1	−2.6	−1.9	−2.0	−1.4	0.3	4.0
					±.17	−3.1	−4.4	−4.5	−1.7	−3.2	−1.5	2.2	5.1	4.1	4.6	1.4	0.6

14. ATLANTIC: Cape Verde Islands														
Porto Grande (CVI)[2] (St. Vincent)	16°53N	25°00W	1947–50											
				4	−3.3	−3.9	−2.1	−0.3	0.3	−0.1	0.2	1.4	1.7	2.0	2.6	1.2
				k = .50												
				P_g	17.0	17.0	16.5	16.0	16.0	16.5	16.5	15.0	15.5	15.5	15.5	16.0
				c	1.4	1.4	0.5	0.0	0.0	−0.2	−0.7	−1.5	−1.1	−0.5	−0.3	0.9
					−1.9	−2.5	−1.6	−0.3	0.3	−0.3	−0.5	−0.1	0.6	1.5	2.3	2.1
15. ATLANTIC: Sierra Leone														
Freetown (SL)[4]	8°30N	13°14W	Feb. 1926–Jan. 1927(2)	1	−7.7	−3.0	−7.9	−5.3	−0.3	3.9	2.5	3.6	1.9	6.1	7.0	−0.7
				k = 1.00												
				P_g	14.0	11.0	11.0	11.0	11.0	12.5	13.0	12.5	12.5	12.5	11.0	11.0
				c	2.6	−0.4	−0.8	−0.8	−0.8	0.0	0.0	0.2	0.1	0.7	−0.6	0.1
					−5.1	−3.4	−8.7	−6.1	−1.1	3.9	2.5	3.8	2.0	6.8	6.4	−0.6
16. ATLANTIC: Gulf of Guinea, Africa														
Takoradi (GC)	4°53N	1°45W	1929–46(1)	18	0.4	3.4	4.5	4.3	−0.4	−5.8	−9.8	−10.0	−4.8	5.5	9.8	2.6
Accra (GC)	5°32N	0°12W	Apr. 1922–Apr. 1923, 1938(2)	2	0.6	6.4	6.4	5.1	−1.6	−7.4	−14.7	−11.3	−0.4	6.7	10.3	0.0
Lagos (Ni)	6°24N	3°24E	Apr. 1940–Mar. 1941(2)	1	−0.1	−0.4	−1.6	−0.4	−0.4	−1.0	−8.9	−5.9	2.1	12.4	7.4	−3.4
Forcados (Ni)	5°22N	5°26E	Sept. 1934–Aug. 1935(2)	1	−7.8	1.0	2.3	5.3	−2.0	−2.9	−1.1	−2.0	1.7	5.0	5.6	−5.1
Port Harcourt (Ni)	4°46N	7°00E	Mar. 1935–Feb. 1936(2)	1	−3.8	−9.3	6.6	5.7	−2.6	−4.7	−4.1	−2.0	0.2	11.2	6.0	−3.2
Calabar (Ni)	4°58N	8°19E	1937	1	−5.1	−8.5	−1.4	−3.3	−13.6	−7.2	3.7	5.3	15.0	19.9	3.1	−7.8
				k = .25	−1.6	0.3	3.4	3.3	−2.4	−5.2	−7.1	−6.2	−0.1	8.6	8.0	−1.0
				P_g	12.4	12.4	10.7	12.4	10.4	10.4	14.0	12.4	12.4	10.7	12.4	12.4
				c	1.0	1.0	−1.1	0.6	−1.4	−2.1	1.0	0.1	0.0	−1.1	0.8	1.5
				±1.69	−0.6	1.3	2.3	3.9	−3.8	−7.3	−6.1	−6.1	−0.1	7.5	8.8	0.5
17. ATLANTIC: Cape of Good Hope														
Capetown (SA)[5]	33°54S	18°25E	1888	1	−2.9	−2.0	3.2	1.3	−0.8	−2.0	−8.1	0.1	−1.4	5.6	6.2	0.4
				k = 1.00												
				P_g	13.9	14.9	15.9	17.6	17.6	19.3	20.0	20.0	18.3	17.6	17.6	15.2
				c	−2.9	−1.9	−1.3	0.4	0.4	1.4	1.6	2.3	0.5	0.4	0.6	−1.1
					−5.8	−3.9	1.9	1.7	−0.4	−0.6	−6.5	2.4	−0.9	6.0	6.8	−0.7

Station	Latitude	Longitude	Years
Punta Arenas (Ch)[5]	53°09S	70°54W	1942–46(4)
Deseado (Ar)[6]	47°45S	65°55W	1912–37(14)
Comodoro Rivadavia	45°52S	67°29W	1911–19(3), 1926–41(6)
Puerto Madryn (Ar)	42°46S	65°02W	1944–46(1)
San Antonio (Ar)	40°48S	64°52W	1910–24(8)
Belgrano (Ar)	38°53S	62°06W	1914–36(4), 1938
Quequén (Ar)	38°35S	58°42W	1910–46(7)
Mar Del Plata (Ar)	38°03S	57°33W	1910–13(2), 1915–46(2)

18. ATLANTIC: Magellan Strait

	Total Years	J	F	M	A	M	J	J	A	S	O	N	D
	5	−2.9	4.7	3.5	−1.5	6.6	0.7	−0.8	−8.1	−5.2	2.4	−1.1	1.6
k = .45													
	P_g	99.9	99.0	99.0	1.7	2.0	1.4	1.0	0.7	3.0	99.0	98.3	98.0
	c	0.1	−0.8	−1.2	1.5	1.8	0.5	−0.4	0.0	2.2	−1.2	−1.7	−1.3
		−2.8	3.9	2.3	0.0	8.4	1.2	−1.2	−8.1	−3.0	1.2	−2.8	0.3

19. ATLANTIC: Argentina, South

	26	6.2	1.6	−2.2	1.8	2.4	0.2	−0.9	−4.3	−4.8	−10.1	5.5	4.5
	25	0.6	4.4	5.4	−0.3	−3.6	−1.5	0.1	−3.8	−4.6	−3.3	2.7	3.9
	3	3.9	10.9	5.4	−4.1	1.9	7.4	−8.6	−5.9	−7.9	−2.3	−3.6	2.7
	15	7.4	5.7	2.5	−1.1	3.3	6.6	−4.4	−8.1	−7.0	−9.1	3.4	0.8
k = .13		4.5	4.7	2.3	−0.3	0.7	2.2	−2.4	−5.3	−5.7	−6.8	3.0	3.2
	P_g	7.1	10.1	9.1	8.5	8.1	9.8	10.8	9.8	10.8	9.8	9.8	4.7
	c	−1.4	1.6	0.2	−0.4	−0.8	0.2	0.7	0.4	1.3	0.9	1.1	−3.3
	±1.34	3.1	6.3	2.5	−0.7	−0.1	2.4	−1.7	−4.9	−4.4	−5.9	4.1	−0.1

20. ATLANTIC: Argentina, Transition

	24	7.6	7.5	6.4	2.8	2.4	−1.3	−4.7	−7.7	−9.4	−5.9	−0.5	3.3
	37	5.2	4.8	5.3	1.2	6.0	3.2	−2.1	−7.1	−10.5	−7.6	−1.0	2.1
	36	4.3	4.9	4.5	5.3	4.9	−0.3	−2.8	−6.4	−9.4	−6.0	−0.1	1.5
k = .10		5.6	5.6	5.3	3.1	4.6	0.6	−3.1	−7.0	−9.8	−6.5	−0.5	2.2
	P_g	9.8	12.8	13.2	14.2	12.8	15.2	15.9	15.9	16.6	13.9	12.8	9.5
	c	−3.3	−0.3	−0.3	0.7	−0.7	1.0	1.2	1.9	2.5	0.4	−0.5	−3.1
	±.66	2.3	5.3	5.0	2.4	3.9	1.6	−1.9	−5.1	−7.3	−5.1	−1.0	−0.9

21. ATLANTIC: North Brazil Current														
La Plata (Ar)	34°55S	57°56W	1916–34	19	6.9	6.9	5.9	4.9	−0.1	−5.1	−7.1	−6.1	−5.1	−4.1	−0.1	2.9
Buenos Aires (Ar)	34°36S	58°22W	1905–43, 1945–46	41	7.5	7.2	7.3	4.8	−2.0	−7.6	−10.1	−4.9	−3.0	−1.9	−0.1	2.5
Puerto de Colonia (Ur)	34°29S	57°51W	1938–46	9	7.8	4.1	7.0	6.4	−1.6	−4.6	−9.2	−3.4	−6.2	0.2	−1.2	0.9
Montevideo (Ur)	34°53S	56°16W	1938–46	9	2.8	2.1	6.2	9.4	2.4	1.9	−6.2	−1.5	−8.0	−5.7	−2.6	−0.7
Puerto de Punta del Este (Ur)	34°58S	54°57W	1938–45	8	0.3	1.4	5.3	10.9	5.2	4.3	−6.0	−1.8	−11.7	−6.5	0.0	−1.6
				k = .11	5.5	4.9	6.5	6.8	0.3	−3.2	−8.1	−3.9	−6.1	−3.4	−0.7	1.2
				P_g	11.8	12.8	14.2	15.6	15.9	17.6	17.6	17.6	16.6	14.9	13.2	11.5
				c	−2.6	−1.6	−0.6	0.8	1.1	2.1	1.6	2.3	1.0	0.1	−1.4	−2.5
				±1.09	2.9	3.3	5.9	7.6	1.4	−1.1	−6.5	−1.6	−5.1	−3.3	−2.1	−1.3
22. ATLANTIC: British Guiana														
Georgetown (Gu)	6°48N	58°10W	May 1927–Apr. 1928(2)	1	4.0	3.4	−2.4	−1.2	−4.3	−3.4	−4.0	−0.3	0.9	0.3	2.1	4.9
				k = 1.00												
				P_g	10.7	12.4	10.7	10.7	10.7	10.7	10.7	10.7	10.7	10.7	8.9	10.7
				c	0.5	2.2	0.1	0.1	0.1	−0.6	−1.1	−0.4	0.0	0.1	−1.5	1.0
					4.5	5.6	−2.3	−1.1	−4.2	−4.0	−5.1	−0.7	0.9	0.4	0.6	5.9
23. ATLANTIC: Venezuela														
Port of Spain (Tr)	10°39N	61°31W	Nov. 1937–Oct. 1938(2)	1	−12.8	−16.3	−9.6	−7.6	−1.7	3.0	5.1	9.0	8.4	11.3	11.1	0.1
Zaparita (Ve)	11°01N	71°39W	1939–46(3)	8	−4.5	−4.1	−5.2	−3.4	−0.4	0.6	0.4	0.3	1.0	5.6	7.7	1.9
Tablazo (Ve)	10°53N	71°37W	1944–46	3	−10.5	−13.5	−13.8	−5.3	4.8	8.1	5.1	1.4	1.4	5.7	11.5	5.4
Zapara Island (Ve)	10°58N	71°34W	1929–36(4), 1938–39, 1941	11	−6.4	−9.3	−9.0	−5.4	0.2	2.1	−0.1	2.1	4.5	7.5	11.1	2.3
				k = .22	−7.4	−9.3	−8.9	−5.0	0.8	3.0	1.8	2.1	3.1	6.9	10.1	2.6
				P_g	13.5	14.0	13.5	13.0	13.0	13.0	13.5	13.0	12.0	11.5	12.5	13.0
				c	1.0	1.5	0.6	0.1	0.1	−0.6	−0.6	−0.4	−1.5	−1.4	−0.2	1.0
				±1.27	−6.4	−7.8	−8.3	−4.9	0.9	2.4	1.2	1.7	1.6	5.5	9.9	3.6
24. ATLANTIC: Panama Canal Zone														
Cristobal (CZ)	9°21N	79°55W	1909–46	38	−0.4	−2.2	−2.7	−2.6	−1.9	−1.7	−0.4	0.5	1.6	3.4	5.1	1.5
				k = .16												
				P_g	11.0	14.0	11.0	11.0	11.0	11.0	11.0	11.0	11.0	11.0	11.0	11.0
				c	0.2	3.2	−0.2	−0.2	−0.2	−0.9	−1.4	−0.7	−0.8	−0.2	0.0	0.7
					−0.2	1.0	−2.9	−2.8	−2.1	−2.6	−1.8	−0.2	0.8	3.2	5.1	2.2

Station	Latitude	Longitude	Years	Total Years	J	F	M	A	M	J	J	A	S	O	N	D
25. ATLANTIC: Gulf of Mexico, West																
Galveston (US)	29°19N	94°47W	1908–46(1)	39	−11.2	−9.3	−5.7	1.1	5.9	4.1	−4.5	−1.7	13.2	12.9	1.8	−6.1
				k = .16												
				P_g	21.0	18.5	17.0	15.5	15.5	15.5	17.0	15.5	15.5	17.0	20.0	20.0
				c	4.1	1.6	−0.3	−1.8	−1.8	−2.5	−1.5	−2.3	−2.4	−0.3	2.9	3.6
					−7.1	−7.7	−6.0	−0.7	4.1	1.6	−6.0	−4.0	10.8	12.6	4.7	−2.5
26. ATLANTIC: Gulf of Mexico, East																
Pensacola (US)	30°24N	87°13W	1923–46(1)	24	−10.5	−10.1	−6.7	−2.0	1.2	3.0	2.5	7.0	12.3	9.6	0.6	−6.7
Cedar Keys (US)	29°08N	83°02W	1914–25(1)	12	−9.8	−10.0	−6.6	−3.2	1.8	5.1	8.6	8.5	8.9	4.1	−0.2	−7.1
Key West, C. Wharf (US)	24°34N	81°48W	1913–25	13	−7.0	−6.7	−6.3	−4.5	−1.2	−0.6	−0.9	2.8	9.8	10.7	6.5	−2.1
Key West, Naval Base	24°33N	81°48W	1926–46(2)	21	−6.2	−8.2	−8.0	−4.2	−2.5	−1.8	−1.5	3.6	8.9	13.0	7.6	−0.3
				k = .12	−8.3	−8.7	−7.0	−3.4	−0.3	1.1	1.6	5.3	10.1	9.9	3.9	−3.8
				P_g	21.0	18.5	17.0	15.5	15.5	15.5	17.0	15.5	15.5	17.0	20.0	20.0
				c	4.2	1.7	−0.2	−1.7	−1.7	−2.4	−1.4	−2.2	−2.3	−0.2	3.0	3.7
				±1.18	−4.1	−7.0	−7.2	−5.1	−2.0	−1.3	0.2	3.1	7.8	9.7	6.9	−0.1
27. ATLANTIC: Cuba and Cat Cay																
Havana (Cu)[2]	23°09N	82°20W	1947–51(1)	5	−8.1	−8.6	−3.8	−2.9	−1.4	1.3	0.5	6.3	9.8	6.9	0.5	−3.2
Pinar del Rio (Cu)[2,7]			1949–51(3)	3	−4.8	−12.2	−8.1	1.3	5.6	3.1	6.2		5.2	1.5	−2.6	0.4
Casilda (Cu)[2]	21°45N	79°59W	1949–51	3	−7.1	−8.5	−6.4	−2.8	2.2	2.4	0.9	5.8	10.5	7.1	−0.3	−3.9
Guantanamo Bay (Cu)[2]	19°54N	75°09W	1937–51(4)	14	−4.8	−5.6	−4.4	−3.5	−0.6	−0.7	0.4	2.9	6.8	7.3	4.0	−1.8
Baracoa (Cu)[2]	20°21N	74°30W	1949–51(3)	3	−11.9	−8.9	−5.4	0.1	9.6	6.3	−5.1	5.7	4.3	6.0	5.7	−6.4
Gibara (Cu)[2]	21°07N	76°08W	1949–51	3	−8.0	−9.0	−5.5	−2.0	3.0	0.8	0.4	6.0	7.3	7.0	2.7	−2.7
Cat Cay (Ba)[5]	24°19N	75°26W	1938–41(3), 1950–51(2)	5	−6.2	−6.5	−5.2	−2.7	−1.6	−0.2	2.7	7.5	10.0	6.6	−1.7	−2.6
				k = .17	−7.0	−8.1	−5.4	−2.0	2.0	1.5	0.8	5.3	7.6	6.2	1.5	−2.8
				P_g	18.5	18.0	17.3	16.5	15.5	15.5	16.7	16.0	14.5	13.7	15.5	18.0
				c	2.7	2.2	1.1	0.3	−0.7	−1.4	−0.7	−0.7	−2.3	−2.5	−0.5	2.7
				±.87	−4.3	−5.9	−4.3	−1.7	1.3	0.1	0.1	4.6	5.3	3.7	1.0	0.1

28. ATLANTIC: Florida Current														
Miami Beach (US)	25°46N	80°08W	1931–46(1)	16	−5.4	−6.3	−8.5	−4.1	−1.3	−3.4	−5.4	−0.9	8.6	16.5	10.5	−0.3
Mayport (US)	30°24N	81°26W	1928–46(1)	19	−6.5	−7.5	−9.6	−5.7	−3.2	−3.4	−7.4	−1.1	13.6	21.3	10.6	−0.9
Fernandina (US)	30°41N	81°28W	1897–1924(2)	28	−9.9	−8.7	−8.4	−3.8	0.5	0.8	−6.8	−4.1	14.5	21.2	8.7	−4.4
Charleston (US)	32°47N	79°55W	1921–46(1)	26	−8.7	−8.1	−8.6	−3.3	−1.7	−1.7	−4.7	0.7	13.2	17.3	7.8	−2.5
				k = .11	−7.8	−7.7	−8.7	−4.2	−1.3	−1.8	−6.0	−1.4	12.6	19.1	9.3	−2.2
				P_g	20.0	20.0	17.0	17.0	17.0	15.0	17.0	17.0	17.0	17.0	20.0	20.0
				c	2.6	2.6	0.2	−0.8	−0.8	−3.5	−2.0	−1.3	−1.4	−0.8	2.4	3.1
				±.76	−5.2	−5.1	−8.5	−5.0	−2.1	−5.3	−8.0	−2.7	11.2	18.3	11.7	0.9
29. ATLANTIC: Bermuda														
Ireland Island (Be)	32°19N	64°50W	1833–43(1)	11	1.0	1.0	−3.8	−5.7	−4.7	−3.8	−4.7	−1.1	2.3	10.5	5.6	3.5
St. Georges (Be)	32°22N	63°42W	1932–37(4)	6	0.7	−2.0	−4.1	−5.7	−2.3	−1.6	1.3	4.0	0.7	5.2	3.4	0.3
				k = .24	0.9	−0.2	−3.9	−5.7	−3.7	−2.9	−2.3	0.9	1.7	8.4	4.7	2.2
				P_g	20.0	20.0	20.0	18.5	19.0	20.0	21.5	20.0	18.0	18.0	18.0	18.5
				c	1.2	1.2	0.8	−0.7	−0.2	0.1	1.1	0.3	−1.8	−1.2	−1.0	0.2
				±1.13	2.1	1.0	−3.1	−6.4	−3.9	−2.8	−1.2	1.2	−0.1	7.2	3.7	2.4
30. ATLANTIC: Gulf Stream														
Hampton Roads (US)	36°57N	76°20W	1927–46(3)	20	−7.0	−6.8	−5.2	−0.6	−0.5	2.0	0.2	4.1	10.9	8.4	1.0	−6.4
Baltimore (US)	39°16N	76°35W	1902–46(1)	45	−12.8	−13.2	−8.2	−0.9	4.5	8.6	8.5	10.1	10.6	6.1	−3.2	−10.4
Atlantic City (US)	39°21N	74°25W	1911–20(1), 1922–46	35	−8.5	−7.2	−5.6	−1.4	0.2	3.6	2.9	6.5	8.0	6.6	0.1	−5.7
Fort Hamilton (US)	40°37N	74°02W	1893–1920	28	−9.0	−12.4	−8.1	0.7	3.2	5.9	4.4	7.4	6.8	6.5	−0.5	−5.4
New York, W. St. (US)	40°42N	74°01W	1928–46	19	−9.2	−9.5	−4.9	0.2	1.4	5.5	5.4	6.7	8.1	5.1	−0.5	−7.8
New York, Pier (US)	40°42N	74°01W	1920–27	8	−11.2	−4.2	−5.4	−1.2	4.3	4.0	3.1	5.3	6.2	3.4	0.4	−5.4
Newport (US)	41°30N	71°20W	1930–46(2)	17	−5.5	−6.1	−4.6	−2.5	−0.9	4.0	4.3	4.7	5.4	4.6	0.9	−4.4
				k = .08	−9.3	−9.1	−6.3	−0.8	1.9	5.1	4.5	6.9	8.3	6.0	−0.5	−6.8
				P_g	20.0	18.0	18.0	18.0	18.0	17.0	18.0	17.0	17.0	20.0	20.0	20.0
				c	2.1	0.1	−0.3	−0.3	−0.3	−2.0	−1.5	−1.8	−1.9	1.7	1.9	2.6
				±.77	−7.2	−9.0	−6.6	−1.1	1.6	3.1	3.0	5.1	6 4	7.7	1.4	−4.2

31. ATLANTIC: Gulf of Maine

Station	Latitude	Longitude	Years	Total Years	J	F	M	A	M	J	J	A	S	O	N	D
Boston (US)	42°21N	71°03W	1921–46(1)	26	−4.6	−3.5	−2.5	−0.3	0.7	3.4	1.8	1.8	2.0	2.6	1.3	−2.2
Portland (US)	43°40N	70°15W	1912–46(1)	35	−4.6	−3.8	−3.9	−0.4	1.5	3.7	2.8	1.8	1.4	2.0	0.8	−2.3
Eastport (US)	44°54N	66°59W	1929–46(1)	18	−1.6	−0.8	−1.1	0.1	0.1	1.6	1.6	−1.2	−0.7	0.9	0.9	−0.4
St. John (Ca)	45°15N	66°04W	1930–34, 1938, 1942, 1946	8	−1.5	−3.5	−1.8	3.5	6.4	3.6	0.9	−1.2	−2.5	0.1	−1.4	−2.7
				k = .11	−3.4	−3.0	−2.5	0.4	1.8	3.1	1.9	0.6	0.5	1.6	0.6	−1.9
				P_g	18.5	15.5	15.5	15.5	15.5	15.5	15.5	15.5	17.0	17.0	17.0	17.0
				c	2.7	0.7	−0.7	−0.7	−0.7	−1.4	−1.9	−1.2	0.2	0.8	1.0	1.7
				±.64	−0.7	−2.3	−3.2	−0.3	1.1	1.7	0.0	−0.6	0.7	2.4	1.6	−0.2

32. ATLANTIC: Gulf of St. Lawrence

Father Point (Ca)	48°31N	68°28W	1938–39, 1942(1), 1945–46	5	−2.7	−4.5	−3.0	1.9	4.3	5.0	1.6	−1.1	−3.9	0.7	−1.4	3.1
Portage Island (Ca)	47°08N	65°03W	1917–19(3) (July–Oct. only)	3							3.6	2.1	−1.2	0.3		
Point Peter (Ca)	48°38N	64°10W	1924–25(1)	2	−5.4	−12.1	−16.1	−5.1	1.0	5.0	4.4	5.9	3.2	6.5	5.3	7.4
				k = .32	−3.6	−7.0	−7.4	−0.4	3.2	5.0	3.0	1.6	−1.4	1.7	0.8	4.5
				P_g	14.0	12.5	12.0	14.0	13.5	12.5	12.0	13.5	15.5	15.0	14.0	14.0
				c	1.0	−0.5	−1.4	0.6	0.1	−1.6	−2.6	−0.4	1.5	1.6	0.8	1.5
				±1.61	−2.6	−7.5	−8.8	0.2	3.3	3.4	0.4	1.2	0.1	3.3	1.6	6.0

33. ATLANTIC: Nova Scotia and Prince Edward Island

Halifax (NS)	44°40N	63°34W	1922–25(1), 1927–28 (2), 1933, 1935–38, 1941–46	16	2.9	1.7	−0.3	−1.7	−3.5	−1.7	−4.7	−2.9	−2.2	3.0	4.5	5.4
Charlottetown (PEI)	46°13N	63°08W	1934, 1940, 1942, 1946	4	2.3	4.9	−2.9	−2.3	−4.3	−0.6	−1.8	−3.2	−3.7	2.1	3.2	6.3
St. Paul Island	47°12N	60°09W	1921–26(2)	6	0.0	−0.3	0.1	−2.4	−3.6	−1.4	−3.3	−1.4	−1.4	5.6	3.4	4.7
				k = .20	2.0	2.0	−0.8	−2.0	−3.7	−1.4	−3.6	−2.6	−2.4	3.4	3.9	5.4
				P_g	14.5	12.5	12.5	13.5	14.0	14.0	14.0	15.0	17.0	16.0	14.5	12.5
				c	0.8	−1.2	−1.6	−0.6	−0.1	−0.8	−1.3	0.4	2.3	1.9	0.6	−0.7
				±.57	2.8	0.8	−2.4	−2.6	−3.8	−2.2	−4.9	−2.2	−0.1	5.3	4.5	4.7

34. ATLANTIC: Newfoundland														
Harrington (Ca)	50°31N	59°27W	1940–42, 1945–46	5	2.4	2.1	−4.6	−6.5	−3.4	0.2	−3.1	−1.9	−1.3	5.1	5.1	6.0
Port Aux Basques (Ne)	47°34N	59°07W	1935–37(2)	3	0.0	5.8	−2.8	−1.6	−3.4	−0.3	3.3	−2.5	−0.3	−2.5	1.5	2.7
St. John's (Ne)	47°34N	52°42W	1935–37(2)	3	12.4	10.2	1.7	−4.4	−8.1	−11.7	−6.2	−5.6	0.8	1.1	1.4	8.4
				k = .30	4.9	6.0	−1.9	−4.1	−5.0	−3.9	−2.0	−3.3	−0.3	1.2	2.7	5.7
				P_g	10.5	9.5	10.0	12.5	13.0	13.5	13.5	14.0	15.5	14.5	12.5	9.5
				c	−1.4	−2.4	−2.3	0.2	0.7	0.5	0.0	1.2	2.6	2.2	0.4	−1.9
				±1.85	3.5	3.6	−4.2	−3.9	−4.3	−3.4	−2.0	−2.1	2.3	3.4	3.1	3.8
35. ATLANTIC: Hudson Bay														
Churchill (Ca)	58°47N	94°12W	1940–43	4	0.6	−8.3	−9.8	−11.3	−1.6	0.0	3.9	0.9	5.8	8.5	8.5	2.7
				k = .50												
				P_g	17.5	18.5	18.5	18.5	17.5	13.5	10.5	11.0	12.5	13.0	14.0	15.5
				c	2.9	3.9	3.5	3.5	2.5	−2.2	−5.7	−4.5	−3.1	−2.0	−0.8	1.4
					3.5	−4.4	−6.3	−7.8	0.9	−2.2	−1.8	−3.6	2.7	6.5	7.7	4.1
36. ATLANTIC: Greenland, South														
Ivigtut (Gr)[5]	61°12N	48°11W	1944–49(2)	6	6.6	−1.2	−0.6	−11.6	−12.8	−4.7	−2.2	−2.1	0.1	6.3	7.1	15.1
				k = .41												
				P_g	97.0	2.0	5.0	9.8	11.4	11.0	9.3	9.5	8.0	5.0	3.0	99.0
				c	−8.3	−3.3	−0.7	4.1	5.7	4.6	2.4	3.3	1.7	−0.7	−2.5	−5.8
					−1.7	−4.5	−1.3	−7.5	−7.1	−0.1	0.2	1.2	1.8	5.6	4.6	9.3
37. ATLANTIC: Iceland														
Reykjavik (Ic)[2]	64°09N	21°56W	1951	1	12.6	−1.0	−16.5	−15.8	−14.0	−8.5	−4.0	0.5	0.6	10.8	12.4	22.6
				k = 1.00												
				P_g	97.5	2.0	6.0	9.5	14.0	12.5	10.5	9.5	8.0	5.0	4.0	99.0
				c	−8.5	−4.0	−0.4	3.1	7.6	5.4	2.9	2.6	1.0	−1.4	−2.2	−6.5
					4.1	−5.0	−16.9	−12.7	−6.4	−3.1	−1.1	3.1	1.6	9.4	10.2	16.1
38. ARCTIC OCEAN: Greenland, North														
Cape Sheridan	82°27N	61°21W	Dec. 1908–June 1909(2)	1	1.0	5.2	−14.0	−3.9	−6.7	10.4						8.0
				P_g	15.0	17.0	21.0	23.5	22.5	18.5						15.5
				c	−3.7	−1.7	1.9	4.4	3.4	−1.3						−2.7
					−2.7	3.5	−12.1	0.5	−3.3	9.1						5.3

Station	Latitude	Longitude	Years	Total Years	J	F	M	A	M	J	J	A	S	O	N	D
39. ARCTIC OCEAN: Point Barrow																
Uglaamie (Al)[8]	71°15N	156°37W	Mar.–June, 1883				9.1	−3.0	−2.4	−3.6						
				P_g			22.0	19.0	17.5	16.0						
				c			3.6	0.6	−0.9	−3.1						
							12.7	−2.6	−3.3	−6.7						
40. PACIFIC: Aleutian Islands																
Massacre Bay (Al)[5]	52°50N	186°48W	1943–52(6)	10	6.5	1.1	−2.4	−8.7	−4.3	−3.8	−0.6	0.1	−1.2	1.7	5.1	6.6
Constantine Harbor (Al)[5]	51°25N	180°43W	1944–47(4)	4	−2.9					−4.7	−2.1	0.3	−2.0	3.3	6.2	9.1
Sweeper Cove (Al)[5]	51°51N	176°39W	1943–52(1)	10	5.4	5.8	−0.5	−6.4	−2.8	−3.4	−5.3	−3.3	−2.1	1.2	5.0	6.4
Dutch Harbor (Al)[5]	53°54N	166°32W	1934–39 ,1946–52(1)	13	1.9	4.4	−2.6	−5.4	0.1	−3.3	−5.8	−7.3	−1.0	5.1	5.2	8.7
				k = .17	3.1	3.8	−1.9	−6.7	−2.1	−3.8	−3.9	−3.2	−1.5	3.0	5.3	7.7
				P_g	2.7	2.0	8.0	9.5	9.5	11.2	13.7	12.5	9.5	7.0	3.8	2.0
				c	−4.4	−5.1	0.5	2.0	2.0	3.0	5.0	4.5	1.4	−0.5	−3.5	−4.6
				±.93	−1.3	−1.3	−1.4	−4.7	−0.1	−0.8	1.1	1.3	−0.1	2.5	1.8	3.1
41. PACIFIC: Alaska																
Seward (Al)	60°06N	149°27W	1925–38(2), 1944–46(2)	17	4.5	5.2	−1.6	−8.7	−9.7	−10.5	−7.5	−5.8	−1.9	11.2	12.6	11.9
Yakutat (Al)[5]	59°33N	139°44W	1940–52	13	10.4	2.5	−0.9	−6.6	−12.1	−11.4	−9.2	−7.5	−1.3	11.2	11.7	13.1
				k = .18	7.4	3.8	−1.2	−7.6	−10.9	−11.0	−8.4	−6.6	−1.6	11.2	12.2	12.5
				P_g	9.5	10.0	11.0	10.0	11.3	13.5	15.0	13.0	10.0	5.0	5.0	6.5
				c	0.0	0.5	1.1	0.1	1.4	2.9	3.9	2.6	−0.5	−4.9	−4.7	−2.5
				±.81	7.4	4.3	−0.1	−7.5	−9.5	−8.1	−4.5	−4.0	−2.1	6.3	7.5	10.0
42. PACIFIC: Alaska and British Columbia																
Sitka (Al)[5]	57°03N	135°20W	1938–52	15	9.5	4.0	0.1	−4.5	−9.7	−10.7	−9.5	−9.6	−3.2	8.2	11.2	14.5
Ketchikan (Al)	55°20N	131°38W	1919–46	28	9.6	4.7	−1.2	−5.4	−7.3	−6.6	−7.6	−9.2	−5.5	4.7	10.5	13.5
Prince Rupert (BC)	54°19N	130°20W	1933, 1939, 1945–46	4	11.5	0.8	2.0	−9.3	−5.0	−5.3	−5.3	−12.0	−2.2	−0.1	8.1	16.7
				k = .16	9.9	3.7	0.2	−5.8	−7.8	−7.9	−7.9	−9.9	−4.1	5.1	10.3	14.4
				P_g	10.0	12.0	12.0	12.5	14.0	15.3	17.0	16.5	14.0	10.5	9.0	9.0
				c	−2.2	−0.2	−0.6	−0.1	1.4	2.0	3.2	3.4	0.8	−2.1	−3.4	−2.7
				±.92	7.7	3.5	−0.4	−5.9	−6.4	−5.9	−4.7	−6.5	−3.3	3.0	6.9	11.7

43. PACIFIC: British Columbia and Washington														
Canoe Pass (BC)	50°15N	125°25W	June 1945–May 1946(2)	1	5.7	11.8	3.8	−2.3	−5.3	−17.2	−2.3	−5.0	−5.9	−4.7	5.1	16.3
Pt. Atkinson (BC)	49°19N	123°15W	1927–33, 1939, 1946	9	6.1	−1.6	−1.8	−9.2	−1.6	0.0	−0.9	−0.6	2.7	−4.3	−1.2	12.5
Vancouver (BC)	49°18N	123°07W	1920–23(2), 1931, 1935, 1941, 1945–46	9	8.3	3.6	0.1	−8.9	−6.4	−2.0	−2.3	−3.2	−2.1	−0.7	1.7	12.0
Victoria (BC)	48°26N	123°23W	Apr. 1923–Mar. 1924 (2), 1932, 1936, Apr. 1940–Mar. 1941(2), 1945–46	6	8.0	8.4	0.1	−6.0	−3.6	−5.3	−3.8	−5.0	−3.0	−2.6	0.8	11.7
Clayoquot (BC)	49°09N	125°55W	1935, 1941, 1946	3	18.6	15.6	7.4	−3.9	−9.1	−10.0	−10.3	−11.8	−5.8	−5.4	0.4	14.4
Neah Bay (US)[5]	48°22N	124°37W	1934–52(2)	19	11.8	11.2	4.1	−3.9	−8.5	−9.7	−10.6	−10.3	−7.4	0.3	8.3	14.6
Seattle (US)	47°36N	122°20W	1899–1946	48	9.3	7.0	1.5	−3.5	−4.5	−4.5	−4.8	−4.9	−4.8	−3.1	3.9	8.6
Crescent City (US)[5]	41°45N	124°12W	1933–47, 1950–52(1)	18	5.6	7.6	−0.4	−7.9	−7.0	−6.9	−3.7	−2.2	0.9	0.0	3.9	10.1
				k = .11	9.1	7.3	1.5	−5.7	−5.7	−5.8	−5.0	−5.2	−3.1	−2.2	3.3	11.6
				P_g	17.0	17.0	16.5	17.0	17.0	16.5	17.5	17.0	16.3	17.5	17.0	17.0
				c	0.6	0.6	−0.3	0.2	0.2	−1.0	−0.5	−0.3	−1.1	0.7	0.4	1.1
				±1.09	9.7	7.9	1.2	−5.5	−5.5	−6.8	−5.5	−5.5	−4.2	−1.5	3.7	12.7
44. PACIFIC: California Current														
San Francisco (US)	37°48N	122°28W	1897–1946(1)	50	1.8	1.4	−1.4	−5.4	−5.0	−2.3	1.5	2.4	4.1	2.1	−0.1	1.2
Los Angeles (US)	33°43N	118°16W	1923–46(1)	24	−1.7	−3.0	−6.1	−7.4	−5.4	−1.8	3.6	5.7	7.3	4.9	2.1	1.6
La Jolla (US)	32°52N	117°15W	1924–46(1)	23	−1.8	−3.2	−6.1	−7.3	−5.8	−1.9	3.2	5.9	7.7	4.8	2.4	1.8
San Diego (US)	32°42N	117°14W	1916–25	10	−0.8	−4.2	−5.7	−7.2	−5.7	−1.1	4.0	5.0	6.5	5.9	2.2	1.5
				k = .10	−0.4	−1.7	−4.4	−6.6	−5.4	−1.9	2.8	4.5	6.2	4.0	1.4	1.5
				P_g	19.5	18.5	17.5	15.5	14.5	12.5	12.5	13.3	12.8	15.5	18.0	19.5
				c	4.2	3.2	1.8	−0.2	−1.2	−3.9	−4.4	−2.9	−3.5	−0.2	2.5	4.7
				±.69	3.8	1.5	−2.6	−6.8	−6.6	−5.8	−1.6	1.6	2.7	3.8	3.9	6.2
45. PACIFIC: Mexico														
Guaymas (Me)[5]	27°51N	110°54W	1942–44(2)	3	−17.1	−15.6	−13.1	−9.5	−0.9	13.2	18.7	17.8	20.2	8.8	−9.6	−12.8
La Paz (Me)[5]	24°10N	110°19W	1950(1)	1								5.9	11.1	7.1	1.0	−4.7
Acapulco (Me)[5]	16°51N	99°55W	1949–50(2)	2	−1.8	−10.4	−13.7	−10.2	1.2	11.4	12.2	7.9	6.4	0.0	0.1	−3.1
Salina Cruz (Me)[5]	16°10N	95°12W	1941–44(2)	4	−20.1	−20.4	−9.1	−1.2	6.5	12.9	10.4	16.2	15.0	1.9	−6.1	−5.7
				k = .33	−15.2	−16.5	−11.6	−6.3	2.5	12.7	14.1	13.6	14.8	4.8	−5.0	−7.5
				P_g	15.2	15.9	14.2	13.5	12.8	11.8	11.8	10.8	12.2	13.5	15.2	17.6
				c	2.0	2.7	0.6	−0.1	−0.8	−2.5	−3.0	−3.3	−2.0	−0.1	1.8	4.9
				±2.06	−13.2	−13.8	−11.0	−6.4	1.7	10.2	11.1	10.3	12.8	4.7	−3.2	−2.6

46. PACIFIC: Central America

Station	Latitude	Longitude	Years	Total Years	J	F	M	A	M	J	J	A	S	O	N	D
San Jose (Gu)[5]	13°55N	90°50W	1949–50(1)	2	3.9	−3.2	−16.0	−9.2	−4.1	5.4	4.2	10.3	−1.6	3.2	3.4	3.7
La Union (ES)[5]	13°20N	87°49W	1948–50(1)	3	0.7	−4.5	−5.1	−6.8	0.8	3.4	4.7	2.7	2.8	3.1	−0.7	−1.0
San Juan del Sur (Ni)[5]	11°15N	85°53W	1949–50(2)	2	−8.8	−14.2	−8.1	−7.5	5.3	9.2	7.1	7.7	5.7	4.4	0.7	−1.4
Puntarenas (CR)[5]	9°58N	84°50W	1941–50(1)	10	1.4	−4.9	−7.5	−6.2	−0.1	2.0	4.0	4.5	1.8	0.9	0.4	3.7
Balboa (CZ)	8°58N	79°34W	1909–46	38	−8.1	−17.7	−17.5	−11.3	2.5	7.0	6.4	5.1	8.0	10.9	9.2	6.1
Naos Island (CZ)[5]	8°55N	79°32W	1949–50(1)	2	−9.9	−19.7	−17.5	−15.1	3.2	9.3	7.0	7.3	9.9	12.7	11.3	1.4
Buenaventura (Co)[5]	3°54N	77°6W	1941–46, 1948–50(1)	9	−1.8	−12.7	−13.4	−6.4	3.6	6.0	4.0	2.9	3.8	5.0	5.7	4.2
				k = .14	−3.7	−12.0	−12.9	−8.9	1.8	5.7	5.3	4.9	5.0	6.4	5.1	3.6
				P_g	13.9	13.2	12.5	12.5	12.5	12.5	12.5	12.5	12.5	12.5	12.8	13.9
				c	1.6	0.9	−0.2	−0.2	−0.2	−0.9	−1.4	−0.7	−0.8	−0.2	0.3	2.1
				±1.35	−2.1	−11.1	−13.1	−9.1	1.6	4.8	3.9	4.2	4.2	6.2	5.4	5.7

47. PACIFIC: Central South America

La Libertad (Ec)[5]	2°12S	80°55W	1948–50(3)	3	−1.9	−0.6	0.9	−2.8	2.4	5.3	2.1	−3.4	−3.7	−1.7	0.8	2.6
Talara (Pe)[5]	4°35S	81°17W	1942–50	9	3.8	6.2	4.2	2.7	2.3	2.5	−0.2	−3.4	−4.9	−4.9	−4.6	−3.7
Callao (Pe)[5]	12°03S	77°09W	1942–50	9	2.2	5.1	4.7	3.2	3.4	2.0	−0.6	−3.6	−5.1	−5.5	−3.2	−2.5
Matarani (Pe)[5]	17°00S	72°07W	1941–50(2)	10	3.6	3.2	3.9	2.4	3.6	0.1	−2.1	−4.1	−4.9	−4.0	−1.9	0.2
Valparaiso (Ch)[5]	33°01S	71°38W	1941–47(2)	7	3.4	2.5	3.0	2.4	−0.4	2.5	−1.0	−1.0	−4.5′	−5.0	−3.1	1.2
				k = .17	2.5	3.6	3.5	1.9	2.2	2.3	−0.5	−3.1	−4.7	−4.4	−2.6	−0.6
				P_g	12.5	13.2	13.9	14.5	15.9	16.2	16.2	16.9	16.6	16.6	15.2	13.9
				c	−2.1	−1.4	−1.1	−0.5	0.9	0.5	0.0	1.4	1.0	1.6	0.4	−0.2
				±.71	0.4	2.2	2.4	1.4	3.1	2.8	−0.5	−1.7	−3.7	−2.8	−2.2	−0.8

48. PACIFIC: Gulf de Ancud

Puerto Montt (Ch)[5]	41°29S	72°58W	1942–46(4)	5	−1.2	−4.4	−1.8	−1.5	2.0	2.2	2.3	2.0	2.4	−4.2	0.6	1.5
				k = .45												
				P_g	12.2	12.8	12.5	13.9	11.5	13.9	14.9	13.5	14.5	15.2	14.2	11.5
				c	−0.7	−0.1	−0.8	0.6	−1.8	−0.1	0.4	−0.3	0.6	1.9	1.1	−0.9
					−1.9	−4.5	−2.6	−0.9	0.2	2.1	2.7	1.7	3.0	−2.3	1.7	0.6

49. PACIFIC: Hawaii														
Honolulu (TH)	21°18N	157°52W	1905–46	42	−1.3	−1.9	−2.1	−3.2	−2.9	−2.2	−0.1	2.4	4.7	4.1	2.0	0.6
				k = .15												
				P_g	17.0	17.2	17.6	18.5	18.5	18.1	17.5	16.5	16.5	16.5	16.6	17.0
				c	0.2	0.4	0.4	1.3	1.3	0.2	−0.9	−1.2	−1.3	−0.7	−0.4	0.7
					−1.1	−1.5	−1.7	−1.9	−1.6	−2.0	−1.0	1.2	3.4	3.4	1.6	1.3
50. PACIFIC: Johnston Island														
Johnston Island[5,9]	16°45N	169°31W	1947–51(3)	5	−4.6	−4.1	−7.1	1.0	−4.3	−5.0	−2.4	5.6	11.0	4.8	0.5	4.6
				k = .58												
				P_g	14.5	14.5	15.5	15.5	15.0	15.0	14.5	13.5	13.5	13.5	14.2	14.0
				c	0.6	0.6	1.2	1.2	0.7	0.0	−1.0	−1.3	−1.4	−0.8	0.1	0.6
					−4.0	−3.5	−5.9	2.2	−3.6	−5.0	−3.4	4.3	9.6	4.0	0.6	5.2
51. PACIFIC: Palmyra Island														
Palmyra Island[5,10]	5°53N	162°05W	1947–49(3)	3												
				k = .58	−2.1	−2.1	−7.1	−9.4	−8.5	−11.8	−8.1	8.6	8.3	12.4	12.4	7.7
				P_g	11.8	10.8	11.8	14.2	14.2	13.2	13.5	13.5	13.5	12.5	12.2	11.8
				c	−0.5	−1.5	−0.9	1.5	1.5	−0.2	−0.4	0.3	0.2	−0.2	−0.3	0.0
					−2.6	−3.6	−8.0	−7.9	−7.0	−12.0	−8.5	8.9	8.5	12.2	12.1	7.7
52. PACIFIC: Samoa														
Pago Pago (Sa)[5]	14°17S	170°41W	1949–51	3	−2.2	2.3	4.0	3.4	3.4	−1.6	−2.8	−3.5	−2.0	−0.9	−0.9	0.7
				k = .58												
				P_g	11.8	9.8	11.8	13.5	13.5	14.2	14.5	14.9	13.5	12.2	12.2	11.8
				c	−0.5	−2.5	−0.9	0.8	0.8	0.8	0.6	1.7	0.2	−0.5	−0.3	0.0
					−2.7	−0.2	3.1	4.2	4.2	−0.8	−2.2	−1.8	−1.8	−1.4	−1.2	0.7
53. PACIFIC: Guam														
Apra Harbor (Gu)[5]	13°26N	144°39E	1949–51	3	−6.5	−4.4	0.1	2.9	4.6	5.7	5.9	4.3	2.8	−2.2	−7.3	−5.9
				k = .58												
				P_g	12.2	11.5	12.5	11.8	11.8	11.2	10.8	8.8	9.1	9.1	11.5	12.2
				c	1.6	0.9	1.5	0.8	0.8	−0.5	−1.4	−2.7	−2.5	−1.9	0.7	2.1
					−4.9	−3.5	1.6	3.7	5.4	5.2	4.5	1.6	0.3	−4.1	−6.6	−3.8

54. PACIFIC: Marshall Islands

Station	Latitude	Longitude	Years		Total Years	J	F	M	A	M	J	J	A	S	O	N	D
Kwajalein (MI)[5]	8°44N	167°44E	1946–51(3)		6	−6.0	−1.0	1.5	2.7	1.4	−0.4	0.2	0.8	2.4	1.3	−0.9	−2.1
				k = .41													
					P_g	11.8	9.8	11.8	12.5	12.5	12.5	12.5	12.5	12.5	9.1	11.8	11.2
					c	0.6	−1.4	0.2	0.9	0.9	0.2	−0.3	0.4	0.3	−2.5	0.4	0.5
						−5.4	−2.4	1.7	3.6	2.3	−0.2	−0.1	1.2	2.7	−1.2	−0.5	−1.6

55. PACIFIC: Solomon Islands, New Britain, New Guinea

Guadalcanal (SI)[5]	9°25S	159°59E	1947–49(3)		3	−3.5	−2.1	2.6	8.5	9.5	0.5	−5.0	−3.8	−2.3	−1.4	−0.3	−2.9
Rabaul (NB)[5,11]	4°13S	152°12E	1948–50(3)		2		3.0	7.8	7.6	3.9	0.0	−5.8	−4.9	−0.3			
Dregor Harbor (NG)[5]	6°39S	147°52E	July 1948–Oct. 1949(2)		2	−3.6	−2.4	−2.1	4.9	4.9	−0.9	−0.6	0.2	1.4	0.3	0.3	−2.7
Port Moresby (NG)	9°26S	147°06E	July 1939–June 1940(2)		1	−0.1	3.4	9.7	10.3	9.8	11.3	−4.7	−12.2	−5.2	−9.7	−6.4	−5.7
				k = .37		−2.7	0.0	4.1	8.0	7.5	2.3	−4.2	−4.9	−1.7	−3.1	−1.7	−3.6
					P_g	9.5	9.1	10.8	11.5	12.2	12.5	12.8	12.5	12.5	11.8	11.5	9.1
					c	−1.3	−1.7	−0.4	0.3	1.0	0.6	0.4	0.8	0.7	0.6	0.5	−1.2
					±1.37	−4.0	−1.7	3.7	8.3	8.5	2.9	−3.8	−4.1	−1.0	−2.5	−1.2	−4.8

56a. PACIFIC OCEAN: Banda Sea

Amboina (NEI)	3°42S	128°12E	1929–31(1)		3	1.0	4.6	6.9	5.2	−0.5	−2.7	−6.7	−8.6	−7.0	−1.1	4.0	5.1
				k = .58													
					P_g	8.5	9.1	9.1	9.1	10.1	10.8	11.8	10.8	11.5	11.2	9.1	9.1
					c	−1.0	−0.4	−0.8	−0.8	0.2	0.2	0.7	0.4	1.0	1.3	−0.6	0.1
						0.0	4.2	6.1	4.4	−0.3	−2.5	−6.0	−8.2	−6.0	0.2	3.4	5.2

56b. PACIFIC OCEAN: Celebes Island, South

Makassar (NEI)[12]	5°06S	119°24E	1925–31(1)		7	8.7	9.6	9.9	6.4	−1.8	−6.1	−8.9	−10.7	−6.9	−5.0	1.0	4.0
				k = .38													
					P_g	8.5	9.1	9.1	9.1	10.1	10.8	11.8	10.8	11.5	11.2	9.1	9.1
					c	−1.0	−0.4	−0.8	−0.8	0.2	0.2	0.7	0.4	1.0	1.3	−0.6	0.1
						7.7	9.2	9.1	5.6	−1.6	−5.9	−8.2	−10.3	−5.9	−3.7	0.4	4.1

56c. PACIFIC OCEAN: Java, East														
Djamoeanrif (NEI)	6°58S	112°45E	1925–31(1)	7	2.1	0.8	0.5	−4.0	−9.3	−5.2	1.3	3.4	4.6	3.0	−0.3	2.8
Sembilangan (NEI)	7°06S	112°42E	1925–31	7	2.4	3.1	1.0	−4.4	−10.2	−6.2	0.4	2.8	4.6	3.3	0.2	3.0
Soerabaja (NEI)	7°12S	112°36E	1925–31(1)	7	1.2	3.4	1.5	−4.3	−9.8	−6.1	0.1	2.2	4.5	4.2	0.5	2.7
				k = .21	1.9	2.4	1.0	−4.2	−9.8	−5.8	0.6	2.8	4.6	3.5	0.1	2.8
				P_g	8.5	9.1	9.1	9.1	10.1	10.8	11.8	10.8	11.5	11.2	9.1	9.1
				c	−1.0	−0.4	−0.8	−0.8	0.2	0.2	0.7	0.4	1.0	1.3	−0.6	0.1
				±.28	0.9	2.0	0.2	−5.0	−9.6	−5.6	1.3	3.2	5.6	4.7	−0.4	2.9
56d. PACIFIC OCEAN: Java Sea, South														
Toeban (NEI)	6°53S	112°03E	1929–31(1)	3	−7.4	−3.9	−2.0	3.2	12.3	8.5	1.1	−1.8	−4.9	−1.8	0.1	−4.0
Semarang (NEI)	7°00S	110°24E	1925–31	7	−2.6	−3.8	−3.8	2.3	8.3	6.6	−0.1	−1.3	−2.2	−1.8	−0.3	−2.4
Pekalongan (NEI)	6°52S	109°40E	1926–31	6	−4.0	−4.5	−2.2	2.8	9.8	7.9	0.9	−1.9	−3.0	−2.2	−1.1	−2.6
Tegal (NEI)	6°51S	109°07E	1926–31	6	−9.7	−7.0	−3.3	2.8	10.8	11.5	4.4	2.1	0.1	−1.3	−3.1	−7.9
Cheribon (NEI)	6°43S	108°34E	1925–31(2)	7	−6.1	−6.3	−4.4	3.1	9.8	8.5	0.9	0.2	−2.1	−0.6	0.6	−3.9
Tandjong-Priok (NEI)	6°06S	106°54E	1925–31(1)	7	−6.8	−5.9	−5.7	0.7	9.3	5.5	1.0	0.7	2.3	1.2	1.5	−3.7
Batavia (NEI)	6°10S	106°40E	1927–31(2)	5	−8.1	−8.5	−8.3	2.5	9.7	8.1	1.0	3.4	2.1	1.6	1.2	−4.9
				k = .16	−6.2	−5.6	−4.3	2.4	9.8	7.9	1.2	0.1	−1.0	−0.6	0.0	−4.0
				P_g	8.5	9.1	9.1	9.1	10.1	10.8	11.8	10.8	11.5	11.2	9.1	9.1
				c	−1.0	−0.4	−0.8	−0.8	0.2	0.2	0.7	0.4	1.0	1.3	−0.6	0.1
				±.62	−7.2	−6.0	−5.1	1.6	10.0	8.1	2.6	0.5	0.0	0.7	−0.6	−3.9
56. PACIFIC OCEAN: Sunda Islands Summary														
				k = .12	−1.9	−1.2	−0.7	1.0	2.4	1.9	−0.5	−0.7	−0.4	0.1	0.4	−0.6
				c	−1.0	−0.4	−0.8	−0.8	0.2	0.2	0.7	0.4	1.0	1.3	−0.6	0.1
				±1.42	−2.9	−1.6	−1.5	0.2	2.6	2.1	0.2	−0.3	0.6	1.4	−0.2	−0.5
57a. PACIFIC OCEAN: Borneo, South														
Bandjermasin (NEI)	3°18S	114°36E	1927–31	5	14.0	10.8	8.7	4.8	1.7	−7.3	−13.1	−18.7	−18.7	−8.5	4.6	22.2
S. Moesangketjil (NEI)	3°30S	114°30E	1930–31(1)	2	5.6	5.5	4.5	−0.3	2.6	−1.7	−5.6	−11.9	−11.8	−3.9	4.5	12.4
				k = .39	11.2	9.0	7.3	3.1	2.0	−5.4	−10.6	−16.4	−16.4	−7.0	4.6	18.9
				P_g	10.8	10.8	10.8	9.1	9.1	9.8	10.1	9.1	10.8	10.5	9.8	10.8
				c	1.2	1.2	0.8	−0.9	−0.9	−0.9	−1.1	−1.4	0.2	0.5	0.0	1.7
				±2.02	12.4	10.2	8.1	2.2	1.1	−6.3	−11.7	−17.8	−16.2	−6.5	4.6	20.6

57b. PACIFIC OCEAN: Karimata Strait

Station	Latitude	Longitude	Years	Total Years	J	F	M	A	M	J	J	A	S	O	N	D
Oepang (NEI)[21]	2°45S	104°58E	1928–31(3)	4	29.7	25.9	29.0	16.8	3.0	−20.7	−35.7	−33.8	−26.1	−14.6	5.9	20.8
Soengsang (NEI)	2°20S	104°45E	1928–31	4	12.7	9.3	4.8	0.8	−1.1	−4.6	−13.0	−15.2	−13.5	0.5	6.5	13.0
				k = .35	21.2	17.6	16.9	8.8	1.0	−12.6	−24.3	−24.5	−19.8	−7.0	6.2	16.9
				P_g	10.8	10.8	10.8	9.1	9.8	10.1	9.1	10.8	10.5	9.8	10.8	
				c	1.2	1.2	0.8	−0.9	−0.9	−0.9	−1.1	−1.4	0.2	0.5	0.0	1.7
				±5.58	22.4	18.8	17.7	7.9	0.1	−13.5	−25.4	−25.9	−19.6	−6.5	6.2	18.6

57c. PACIFIC OCEAN: Sumatra, East

Tambilahan (NEI)[21]	0°20S	103°09E	1928–30	3	11.9	4.6	12.4	−3.2	−4.5	−9.9	−12.3	−13.8	−8.6	1.6	11.0	11.0
Prigi-Radja (NEI)	0°15S	103°15E	1929–31(1	3	5.1	4.3	4.5	−6.2	−7.6	−3.6	−7.4	−7.5	−2.9	3.5	9.7	7.7
				k = .41	8.5	4.4	8.4	−4.7	−6.0	−6.8	−9.8	−10.6	−5.8	2.6	10.4	9.4
				P_g	10.8	10.8	10.8	9.1	9.1	9.8	10.1	9.1	10.8	10.5	9.8	10.8
				c	1.2	1.2	0.8	−0.9	−0.9	−0.9	−1.1	−1.4	0.2	0.5	0.0	1.7
				±1.71	9.7	6.0	7.6	−3.6	−13.3	−14.8	−16.3	−12.2	−5.1	3.8	26.9	11.5

57d. PACIFIC OCEAN: Singapore

Johore Bahru (Ma)	1°27N	103°46E	Dec. 1923–Nov. 1924 (2), Feb. 1929–Jan. 1930(2)	2	8.5	4.8	6.8	−2.7	−12.4	−13.9	−15.2	−10.8	−5.3	3.3	26.9	9.8
				k = .71												
				P_g	10.8	10.8	10.8	9.1	9.1	9.8	10.1	9.1	10.8	10.5	9.8	10.8
				c	1.2	1.2	0.8	−0.9	−0.9	−0.9	−1.1	−1.4	0.2	0.5	0.0	1.7
					9.7	6.0	7.6	−3.6	−13.3	−14.8	−16.3	−12.2	−5.1	3.8	26.9	11.5

57e. PACIFIC OCEAN: Gulf of Siam

Prachuap Kirikhan (Si)	11°48N	99°49E	1910–15(2), 1940–45	12	15.9	13.9	7.5	−0.5	−9.3	−20.1	−22.5	−18.7	−12.9	6.5	19.5	20.3
Bangkok Bar (Si)	13°29N	100°34E	1926–45	19	8.4	11.7	8.9	−0.6	−8.6	−15.0	−13.8	−11.5	−9.2	3.6	13.0	13.1
Fort Phrachula Chomklao (Si)	13°33N	100°35E	1940–45	6	5.8	9.9	6.4	−1.5	−3.0	−12.7	−12.3	−7.6	−7.8	3.4	9.6	9.7
Ko Sichang (Si)	13°09N	100°49E	1940–46	7	12.0	14.9	8.8	1.0	−7.7	−16.9	−14.0	−9.2	−7.5	−2.1	8.2	11.9
				k = .16	10.7	12.8	8.1	−0.3	−7.6	−16.4	−15.8	−12.1	−9.5	2.9	12.9	14.0
				P_g	10.8	10.8	10.8	9.1	9.1	9.8	10.1	9.1	10.8	10.5	9.8	10.8
				c	1.2	1.2	0.8	−0.9	−0.9	−0.9	−1.1	−1.4	0.2	0.5	0.0	1.7
				±1.50	11.9	14.0	8.9	−1.2	−8.5	−17.3	−16.9	−13.5	−9.3	3.4	12.9	15.7

57. PACIFIC OCEAN: Karimata Strait and Gulf of Siam, Summary

k = .13	12.1	11.4	9.5	0.8	−4.9	−12.7	−15.5	−14.4	−11.3	−0.1	10.9	14.2
c	1.2	1.2	0.8	−0.9	−0.9	−0.9	−1.1	−1.4	0.2	0.5	0.0	1.7
±1.79	13.3	12.6	10.3	−0.1	−5.8	−13.6	−16.6	−15.8	−11.1	0.4	10.9	15.9

58a. PACIFIC OCEAN: Celebes Sea, South

Menado (NEI) 1°32N 124°50E 1927–31

5	1.6	−0.8	3.1	4.1	1.4	−0.3	0.8	−3.4	−5.0	−2.2	−0.9	1.6
k = .45												
P_g	10.8	10.1	10.8	10.5	10.1	10.8	10.5	9.8	9.8	11.2	9.5	10.8
c	0.8	0.8	0.8	0.1	0.1	−0.6	−1.1	−1.8	−1.2	0.8	−0.4	1.7
	2.4	0.0	3.9	4.2	1.5	−0.9	−0.3	−5.2	−6.2	−1.4	−1.3	3.3

58b. PACIFIC OCEAN: Celebes Sea, North

Zamboanga (PI) 6°54N 122°04E 1922–23(1), 1927(1)

3	6.1	1.2	4.3	0.9	0.6	0.6	−4.0	−2.7	−2.1	0.0	−1.8	−2.7
k = .58												
P_g	10.8	10.1	10.8	10.5	10.1	10.8	10.5	9.8	9.8	11.2	9.5	10.8
c	0.8	0.8	0.8	0.1	0.1	−0.6	−1.1	−1.8	−1.2	0.8	−0.4	1.7
	6.9	2.0	5.1	1.0	0.7	0.0	−5.1	−4.5	−3.3	0.8	−2.2	−1.0

58c. PACIFIC OCEAN: Sulu Archipelago

Jolo (PI) 6°04N 121°00E 1924–27(3), 1930(1)

5	−4.6	−3.4	4.6	1.5	1.2	0.6	0.9	−0.6	−0.3	0.9	1.2	−3.4
k = .45												
P_g	10.8	10.1	10.8	10.5	10.1	10.8	10.5	9.8	9.8	11.2	9.5	10.8
c	0.8	0.8	0.8	0.1	0.1	−0.6	−1.1	−1.8	−1.2	0.8	−0.4	1.7
	−3.8	−2.6	5.4	1.6	1.3	0.0	−0.2	−2.4	−1.5	1.7	0.8	−1.7

58. PACIFIC OCEAN: Celebes Sea Summary

k = .28	1.0	−1.0	4.0	2.2	1.1	0.3	−0.8	−2.2	−2.5	−0.4	−0.5	−1.5
c	0.8	0.8	0.8	0.1	0.1	−0.6	−1.1	−1.8	−1.2	0.8	−0.4	1.7
±1.10	1.8	−0.2	4.8	2.3	1.2	−0.3	−1.9	−4.0	−3.7	0.4	−0.9	0.2

59a. PACIFIC OCEAN: Luzon

Manila (PI) 14°35N 120°58E 1901–20(1), 1926–34 (2), 1935–38

30	−12.0	−12.5	−9.5	−5.0	−0.9	3.4	10.0	13.9	12.5	7.2	−0.6	−6.5
k = .18												
P_g	13.2	12.8	12.5	10.5	10.5	9.8	9.5	7.8	9.1	11.5	11.8	12.2
c	2.8	2.4	1.7	−0.3	−0.3	−1.7	−2.5	−3.5	−2.3	0.7	1.2	2.3
	−9.2	−10.1	−7.8	−5.3	−1.2	1.7	7.5	10.4	10.2	7.9	0.6	−4.2

59b. PACIFIC OCEAN: San Bernardino Strait

Station	Latitude	Longitude	Years	Total Years	J	F	M	A	M	J	J	A	S	O	N	D
Port San Miguel (PI)	12°40N	123°35E	1914–15(2)	2	−10.1	−9.8	−8.2	−5.2	1.2	3.4	7.9	11.6	11.9	6.1	−2.7	−6.4
Biri Island (PI)	12°39N	124°22E	1926–27(2)	2	−7.9	−6.1	1.2	3.4	3.1	1.2	6.1	4.6	3.4	5.5	−6.7	−7.9
Batuan Bay (PI)	12°25N	123°47E	1926–27(2)	2	−11.6	−9.2	−2.1	3.1	5.2	3.7	2.7	5.8	6.7	7.6	−3.1	−8.8
				k = .41	−9.9	−8.4	−3.0	0.4	3.2	2.8	5.6	7.3	7.3	6.4	−4.2	−7.7
				P_g	13.2	12.8	12.5	10.5	10.5	9.8	9.5	7.8	9.1	11.5	11.8	12.2
				c	2.8	2.4	1.7	−0.3	−0.3	−1.7	−2.5	−3.5	−2.3	0.7	1.2	2.3
				±1.41	−7.1	−6.0	−1.3	0.1	2.9	1.1	3.1	3.8	5.0	7.1	−3.0	−5.4

59c. PACIFIC OCEAN: Sebu

Oloilo (PI)	10°42N	122°34E	1903–09(4)	7	−9.8	−9.2	−6.1	−1.2	1.8	4.0	7.3	7.0	5.8	4.0	0.9	−4.6
Sebu (PI)	10°18N	123°54E	1935–40(1)	6	−9.4	−10.3	−6.4	−2.7	1.6	4.9	7.1	8.0	7.7	4.3	0.3	−5.2
				k = .28	−9.6	−9.6	−6.2	−1.8	1.7	4.4	7.2	7.4	6.6	4.1	0.7	−4.8
				P_g	13.2	12.8	12.5	10.5	10.5	9.8	9.5	7.8	9.1	11.5	11.8	12.2
				c	2.8	2.4	1.7	−0.3	−0.3	−1.7	−2.5	−3.5	−2.3	0.7	1.2	2.3
				±.32	−6.8	−7.2	−4.5	−2.1	1.4	2.7	4.7	3.9	4.3	4.8	1.9	−2.5

59. PACIFIC OCEAN: Philippine Islands, East, Summary

				k = .17	−10.6	−10.4	−6.7	−2.5	1.0	3.6	7.9	9.8	9.0	5.8	−0.9	−6.1
				c	2.8	2.4	1.7	−0.3	−0.3	−1.7	−2.5	−3.5	−2.3	0.7	1.2	2.3
				±.92	−7.8	−8.0	−5.0	−2.8	0.7	1.9	5.4	6.3	6.7	6.5	0.3	−3.8

60. PACIFIC: Philippine Islands, West

Puerto Princesa (PI)	9°44N	118°43E	1916–18(1)	3	6.5	−4.4	−4.8	−5.4	−6.6	−6.9	−4.2	−2.3	11.4	6.2	6.8	3.8
Araceli (PI)	10°35N	119°59E	1913–15(3)	3	−4.2	−6.6	−5.7	−4.5	−4.2	−3.0	−1.4	5.6	11.4	10.5	1.3	1.0
Port Uson (PI)	12°01N	120°12E	1912–16(2)	5	−3.9	−6.9	−7.2	−6.6	−4.5	−2.3	3.5	5.9	7.4	6.8	4.1	3.2
				k = .30	−0.5	−6.0	−5.9	−5.5	−5.1	−4.1	−0.7	3.1	10.1	7.8	4.1	2.7
				P_g	12.5	11.8	11.8	10.8	10.1	9.8	9.8	8.5	9.1	11.5	10.8	11.8
				c	2.3	1.6	1.2	0.2	−0.5	−1.5	−2.0	−2.6	−2.1	0.9	0.4	2.1
				±1.41	1.8	−4.4	−4.7	−5.3	−5.6	−5.6	−2.7	0.5	8.0	8.7	4.5	4.8

61. PACIFIC: South China Sea

Macao (Ch)	22°12N	113°33E	1937–46	10	−2.8	−4.3	−4.6	−8.1	−5.3	−5.2	−2.8	1.1	7.9	14.0	7.8	2.0
Hong Kong (Ch)	22°18N	114°10E	May 1929–Apr. 1936(2)	1	−1.0	−8.5	−5.9	−8.4	−5.3	−14.2	−1.7	−0.5	12.7	23.3	12.7	−3.1
				k = .34	−2.4	−5.4	−4.9	−8.2	−5.3	−7.5	−2.5	0.7	9.1	16.3	9.0	0.7
				P_g	22.0	21.0	18.3	13.5	9.1	7.1	5.4	6.8	9.8	15.2	19.3	21.0
				c	8.5	7.5	4.4	−0.4	−4.8	−7.5	−9.7	−7.6	−4.7	1.3	5.6	8.0
				±1.45	6.1	2.1	−0.5	−8.6	−10.1	−15.0	−12.2	−6.9	4.4	17.6	14.6	8.7

62. PACIFIC: Formosa

Takao (Fo)	22°37N	120°16E	1904–43(1)	40	−12.6	−11.4	−6.7	−4.3	−0.4	4.7	10.4	12.9	10.7	7.1	−0.2	−9.9
Kirun (Fo)	25°09N	121°45E	1904–24(3)	21	−13.2	−12.3	−10.0	−6.0	1.9	8.9	14.7	17.8	14.4	3.3	−5.6	−13.5
				k = .14	−12.9	−11.8	−8.2	−5.1	0.6	6.6	12.4	15.1	12.4	5.4	−2.7	−11.4
				P_g	20.6	20.0	17.6	13.9	9.8	7.8	6.1	6.8	9.1	13.5	19.3	20.3
				c	7.3	6.7	3.9	0.2	−3.9	−6.6	−8.8	−7.4	−5.2	−0.2	5.8	7.5
				±1.25	−5.6	−5.1	−4.3	−4.9	−3.3	0.0	3.6	7.7	7.2	5.2	3.1	−3.9

63. PACIFIC: China

Yang-tsi-Kiang (Ch)	30°49N	122°38E	1923	1	−14.5	−13.6	−17.1	−9.0	0.9	6.3	10.0	10.3	25.7	11.9	0.5	−11.4
Shanghai (Ch)	31°24N	121°30E	1930	1	−36.9	−18.4	−14.9	−4.8	2.7	17.8	23.9	13.5	21.9	12.5	−5.8	−11.5
				k = .70	−25.7	−16.0	−16.0	−6.9	1.8	12.1	16.9	11.9	23.8	12.2	−2.7	−11.5
				P_g	26.5	24.5	21.0	15.0	11.7	7.0	5.8	6.3	12.5	19.5	23.7	26.0
				c	10.4	8.4	4.5	−1.5	−4.8	−10.2	−11.9	−10.7	−4.6	3.0	7.4	10.4
				±3.13	−15.3	−7.6	−11.5	−8.4	−3.0	1.9	5.0	1.2	19.2	15.2	4.7	−1.1

64. PACIFIC: China, Yellow Sea

Newchwang (Ch)	40°38N	122°10E	Feb. 1924–Jan. 1925(2)	1	−11.7	−28.5	−17.3	−7.4	4.2	16.4	31.3	27.1	14.7	3.9	−13.0	−19.7
				k = 1.00												
				P_g	29.4	26.5	21.5	15.0	10.0	5.4	5.0	7.0	15.0	20.5	24.7	27.6
				c	12.6	9.7	4.3	−2.2	−7.2	−12.5	−13.4	−10.7	−2.8	3.3	7.7	11.3
					0.9	−18.8	−13.0	−9.6	−3.0	3.9	17.9	16.4	11.9	7.2	−5.3	−8.4

65. PACIFIC: Korea

Genzan (Ko)[12, 13]	39°10N	127°27E	1932–44	13	−12.9	−13.2	−10.7	−7.1	0.8	9.1	13.5	17.5	14.3	2.2	−5.3	−8.3
				k = .28												
				P_g	25.8	23.4	19.8	14.5	10.8	6.5	6.5	8.0	14 0	19.5	22.8	24.5
				c	10.0	7.6	3.6	−1.7	−5.4	−10.4	−10.9	−8.7	−2.8	3.3	6.8	9.2
					−2.9	−5.6	−7.1	−8.8	−4.6	−1.3	2.6	8.8	11.5	5.5	1.5	0.9

66. PACIFIC: Japan, Oyashio

Station	Latitude	Longitude	Years	Total Years	J	F	M	A	M	J	J	A	S	O	N	D
Hanasaki (Ja)	43°17N	145°35E	1900-24(1)	25	4.7	−0.5	−3.0	−6.5	−3.5	−1.9	0.0	2.9	2.5	−0.6	−0.2	6.4
Honto (Ja)[13]	46°41N	141°51E	1922-44(1)	23	2.2	−3.0	−4.7	−5.0	−2.2	−0.3	3.0	3.4	0.1	−1.3	1.9	5.4
				k = .14	3.4	−1.8	−3.8	−5.8	−2.8	−1.1	1.5	3.2	1.3	−1.0	0.8	5.9
				P_g	13.0	13.5	13.5	13.0	11.0	9.5	9.5	11.0	13.5	15.0	13.5	12.5
				c	1.1	1.6	1.2	0.7	−1.3	−3.5	−4.0	−1.8	0.6	2.7	1.4	1.1
				±.67	4.5	−0.2	−2.6	−5.1	−4.1	−4.6	−2.5	1.4	1.9	1.7	2.2	7.0

67. PACIFIC: Japan, North Kuroshio

Wazima (Ja)[13]	37°24N	136°54E	1900-49	50	−5.3	−11.5	−14.5	−15.4	−5.9	2.7	10.3	15.1	12.8	6.7	4.5	1.0
Iwasaki (Ja)	40°35N	139°55E	1900-24	25	−6.2	−11.3	−14.5	−11.9	−4.8	2.2	9.0	14.8	10.5	5.4	4.9	1.5
Osyoro (Ja)[13]	43°13N	140°52E	1930-49(2)	20	−4.9	−8.5	−10.5	−7.7	−1.8	2.4	8.1	10.7	8.3	3.4	1.8	−1.2
Otaru (Ja)	43°13N	141°03E	1906-33	28	−5.8	−9.7	−10.0	−8.6	−2.4	3.2	8.2	12.2	8.4	3.6	2.1	−0.8
				k = .09	−5.6	−10.5	−12.7	−11.5	−4.0	2.6	9.1	13.5	10.3	5.0	3.5	0.3
				P_g	17.5	17.0	16.0	14.3	12.0	9.5	9.5	10.0	13.0	17.0	18.0	17.0
				c	3.7	3.2	2.8	0.1	−2.2	−5.4	−5.9	−4.7	−1.8	2.8	4.0	3.7
				±.81	−1.9	−7.3	−9.9	−11.4	−6.2	−2.8	3.2	8.8	8.5	7.8	7.5	4.0

68. PACIFIC: Japan, China Sea

Hukabori (Ja)	32°41N	129°49E	1900-24	25	−15.3	−16.9	−13.3	−9.0	−2.2	5.8	12.5	21.6	18.5	10.2	0.0	−11.6
Hamada (Ja)	34°55N	132°04E	1900-24	25	−13.1	−16.6	−16.7	−13.7	−3.8	6.6	15.0	21.4	15.6	9.4	2.4	−6.2
				k = .14	−14.2	−16.8	−15.0	−11.4	−3.0	6.2	13.8	21.5	17.1	9.8	1.2	−8.9
				P_g	23.0	21.0	19.4	15.5	12.0	8.5	8.5	8.2	12.5	18.2	21.5	22.5
				c	7.6	5.6	3.6	−0.3	−3.8	−8.0	−8.5	−8.1	−3.9	2.8	5.9	7.6
				±.98	−6.6	−11.2	−11.4	−11.7	−6.8	−1.8	5.3	13.4	13.2	12.6	7.1	−1.3

69. PACIFIC: Japan, Kuroshio														
Hososima (Ja)[13]	32°25N	131°40E	1900–49	50	−12.7	−12.7	−11.4	−8.6	−4.0	5.3	8.3	14.5	13.4	10.7	5.1	−7.5
Osaki Wan (Ja)[14]	34°08N	135°08E	1926–33(2)	8	−14.2	−15.8	−15.1	−9.0	−2.9	6.9	10.4	16.9	9.7	12.6	3.5	−3.6
Kusimoto (Ja)	33°28N	136°47E	1900–24	25	−10.9	−11.7	−12.2	−9.1	−2.4	4.9	8.4	14.3	13.7	11.1	1.1	−6.6
Aburatubo (Ja)[13]	35°09N	139°37E	1900–45(1), 1947–49(2)	49	−4.2	−6.3	−9.2	−8.5	−3.4	1.4	3.6	6.6	9.0	7.6	3.5	0.2
Aikawa (Ja)	38°18N	141°30E	1900–24(2)	25	−3.1	−7.3	−11.5	−11.8	−5.4	0.3	5.4	9.9	10.5	7.5	4.2	1.7
				k = .08	−8.6	−10.2	−11.4	−9.3	−3.7	3.5	6.8	11.8	11.4	9.6	3.6	−3.2
				P_g	19.0	18.0	17.5	15.0	12.0	9.5	9.5	9.0	12.0	17.0	20.0	20.0
				c	4.6	3.6	2.7	0.2	−2.8	−6.0	−6.5	−6.3	−3.4	2.2	5.4	6.1
				±1.18	−4.0	−6.6	−8.7	−9.1	−6.5	−2.5	0.3	5.5	8.0	11.8	9.0	2.9
70. PACIFIC: New Zealand, North														
Auckland (NZ)	36°51S	174°49E	Sept. 1917–Aug. 1919 (2), 1921–23, 1937, 1941	7	1.5	0.3	3.1	1.5	3.6	5.2	0.0	−2.4	−4.6	−2.7	−4.6	−0.6
Wellington (NZ)	41°17S	174°48E	Sept. 1918–Aug. 1919 (2), 1921–24, 1927, 1930, 1937, 1939, 1942	10	1.8	−0.3	1.2	0.2	1.5	3.6	0.2	−1.6	−3.4	−1.9	−1.6	0.2
				k = .24	1.6	0.0	2.2	0.8	2.6	4.4	0.1	−2.0	−4.0	−2.3	−3.1	−0.2
				P_g	11.8	14.2	15.9	15.9	13.9	10.8	11.5	11.2	13.9	12.8	12.5	10.8
				c	−0.6	1.8	3.1	3.1	1.1	−2.7	−2.5	−2.1	0.5	0.0	−0.1	−1.1
				±.51	1.0	1.8	5.3	3.9	3.7	1.7	−2.4	−4.1	−3.5	−2.3	−3.2	−1.3
71. PACIFIC: New Zealand, South														
Port Lyttelton (NZ)	43°36S	172°51E	1923–27	5	2.1	7.6	4.2	3.9	4.2	2.1	−2.2	−2.5	−4.0	−3.7	−3.4	−7.7
Dunedin (NZ)	45°53S	170°33E	1923–27, 1937	6	3.4	3.7	1.2	1.9	2.7	−1.8	0.0	−2.1	−3.3	−3.0	−1.8	−1.5
Bluff (NZ)	46°35S	168°22E	1917–22(3)	5	−5.0	1.1	5.9	3.2	1.3	−2.3	−2.0	−2.3	−3.8	2.3	−0.5	2.3
				k = .25	0.2	4.1	3.8	3.0	2.7	−0.7	−1.4	−2.3	−3.7	−1.5	−1.9	−2.3
				P_g	6.8	10.1	12.5	15.9	8.8	7.1	7.8	5.4	9.8	10.1	5.7	4.4
				c	−1.4	1.9	3.9	7.3	0.2	−2.2	−2.0	−3.7	0.6	1.5	−2.7	−3.3
				±1.26	−1.2	6.0	7.7	10.3	2.9	−2.9	−3.4	−6.0	−3.1	0.0	−4.6	−5.6

72. PACIFIC: Australia, East Coast

Station	Latitude	Longitude	Years	Total Years	J	F	M	A	M	J	J	A	S	O	N	D
Ballina (Au)	28°52S	153°37E	1928–38(5)	11	1.3	0.4	−1.1	8.4	9.3	4.4	−0.8	−2.9	−5.7	−5.1	−2.9	−5.1
Yamba (Au	29°36S	153°21E	1928–36(9)	9	−2.0	3.2	1.9	5.3	8.9	10.5	5.9	1.6	−6.9	−11.2	−7.5	−10.0
				k = .24	−0.4	1.8	0.4	6.8	9.1	7.4	2.6	−0.6	−6.3	−8.2	−5.2	−7.6
				P_g	11.2	12.5	14.9	16.2	16.6	16.9	18.3	17.9	16.9	15.9	12.8	10.5
				c	−3.4	−2.1	−0.1	1.2	1.6	1.2	2.1	2.4	1.3	0.9	−2.0	−3.6
				±1.53	−3.8	−0.3	0.3	8.0	10.7	8.6	4.7	1.8	−5.0	−7.3	−7.2	−11.2

73. PACIFIC: Australia, Southeast Coast

Newcastle (Au)	32°55S	151°48E	1928–38	11	−1.1	−0.2	0.6	4.3	2.6	5.9	1.3	−3.1	−1.9	−4.0	−4.5	−0.3
Sydney (Au)	33°51S	151°14E	1897–1927, 1934, 1937–38	33	0.7	−1.6	1.3	4.4	5.1	2.7	−0.4	−3.8	−3.6	−2.4	−2.5	−0.3
Williamstown (Au)	37°52S	144°55E	1928–39(1), 1943–44(2)	13	−0.3	−2.3	−2.8	3.9	3.0	3.6	1.3	1.1	−1.4	−1.9	−3.9	−0.6
				k = .14	0.0	−1.5	−0.1	4.2	3.9	3.7	0.5	−2.1	−2.5	−2.6	−3.4	−0.4
				P_g	12.5	14.2	15.9	18.6	15.6	15.2	19.3	14.5	14.5	13.9	12.5	10.8
				c	−1.8	−0.1	1.2	3.9	0.9	−0.2	3.4	−0.7	−0.8	−0.8	−2.0	−3.0
				±.65	−1.8	−1.6	1.1	8.1	4.8	3.5	3.9	−2.8	−3.3	−3.4	−5.4	−3.4

74. INDIAN OCEAN: Australia, South, I

Port Phillip Heads (Au)	38°18S	144°37E	1927–29(2), 1931	3	−2.7	−10.4	−9.1	0.9	4.6	6.9	11.3	3.7	7.0	1.7	−5.5	−8.1
Beachport (Au)	37°30S	140°00E	1927–31	5	−4.3	−9.6	−6.0	3.2	4.9	6.3	8.1	5.2	5.6	−1.8	−6.2	−5.3
Robe (Au)	37°09S	139°45E	July 1945–June 1946(2)	1	4.1	−7.7	−2.7	−7.0	9.9	0.5	−6.3	13.1	5.6	−4.8	1.8	−6.6
Port Adelaide (Au)	34°51S	138°30E	1882–91, 1933–37, 1941–45	21	−1.9	−8.0	−4.3	−0.9	5.5	9.4	6.0	3.9	1.2	−2.2	−6.4	−2.2
Second Valley (Au)	35°31S	138°10E	1938–42(1)	5	−7.1	−7.2	−4.3	−2.0	8.5	14.2	6.1	11.1	4.5	−9.6	−6.6	−7.0
				k = .19	−2.8	−8.5	−5.2	−0.6	6.1	8.5	6.3	6.0	3.8	−2.9	−5.6	−4.9
				P_g	12.5	14.2	16.6	19.3	15.9	16.2	19.3	16.6	15.9	15.2	12.8	11.5
				c	−2.5	−0.8	1.2	3.9	0.5	0.1	2.7	0.7	−0.1	−0.2	−2.4	−3.0
				±1.24	−5.3	−9.3	−3.0	3.3	6.6	8.6	9.0	6.7	3.7	−3.1	−8.0	−7.9

75. INDIAN OCEAN: Australia, South, II

Stenhouse Bay (Au)	35°15S	136°58E	1942–46(1)	5	−5.5	−5.8	−3.6	−0.6	8.5	9.1	7.9	4.3	3.4	−5.5	−5.8	−5.8
Port Wallaroo (Au)	33°56S	137°38E	1933–37	5	0.5	−4.5	−3.2	2.6	6.9	4.8	4.1	2.5	0.1	−2.8	−7.3	−3.9
Port Pirie (Au)	33°09S	138°01E	1933–37(1), 1941–45	10	0.8	−4.0	−1.0	0.0	4.8	3.6	5.0	−0.6	−0.6	−4.4	−3.4	−0.4
Whyalla (Au)	33°01S	137°34E	1943–46(1)	4	9.1	0.9	−0.6	0.0	3.6	1.5	−0.6	−6.7	−3.3	−6.1	1.2	1.8
				k = .21	1.2	−3.4	−2.0	0.4	5.8	4.7	4.2	−0.2	−0.2	−4.7	−3.8	−1.9
				P_g	11.5	13.5	16.2	19.3	16.2	16.6	19.6	17.2	16.6	15.9	12.8	12.2
				c	−3.6	−1.6	0.7	3.8	0.7	0.4	2.9	1.2	0.5	0.4	−2.5	−2.4
				±1.37	−2.4	−5.0	−1.3	4.2	6.5	5.1	7.1	1.0	0.3	−4.3	−6.3	−4.3

76. INDIAN OCEAN: Australia, Southwest

Franklyn Harbour (Au)	33°41S	136°56E	1935–39	5	−2.5	−1.7	−3.3	1.8	7.8	6.1	0.0	5.7	−5.2	−3.1	−4.5	−1.7
Port Lincoln (Au)	34°49S	135°52E	1920–24	5	−9.2	−7.3	−8.2	−5.5	2.4	11.3	11.6	4.9	−0.6	0.9	−1.5	0.0
Thevenard (Au)	32°09S	133°39E	1934–36, 1940–42	6	−6.7	−5.2	−0.9	0.9	7.6	6.4	8.8	5.5	4.3	−9.2	−6.1	−5.2
Albany (Au)	35°02S	117°54E	Oct. 1923–Sept. 1924(2)	1	−7.6	−7.2	−3.6	7.5	20.5	15.0	9.8	5.8	−3.3	−8.8	−14.1	−14.2
Fremantle (Au)	32°03S	115°44E	1937–38	2	−11.5	−5.7	−1.4	5.0	14.3	12.2	6.4	3.0	−1.7	−6.9	−9.0	−4.8
				k = .24	−7.0	−5.2	−3.7	0.9	8.8	9.4	7.1	5.1	−1.0	−4.8	−5.9	−4.1
				P_g	12.5	13.5	15.9	17.6	16.2	16.6	19.3	16.6	16.9	15.9	13.5	12.5
				c	−2.6	−1.6	0.4	2.1	0.7	0.4	2.6	0.6	0.8	0.4	−1.8	−2.1
				±1.65	−9.6	−6.8	−3.3	3.0	9.5	9.8	9.7	5.7	−0.2	−4.4	−7.7	−6.2

77. INDIAN OCEAN: Australia, West

Port Hedland (Au)	20°18S	118°35E	1913, 1927, 1932–33, 1938(1)	5	−0.7	5.4	17.6	14.5	8.4	−0.7	−6.8	−14.5	−9.9	−7.5	−4.4	−1.1
				k = .45												
				P_g	7.4	8.8	9.8	12.8	13.9	15.9	16.6	16.6	14.5	13.2	10.1	9.1
				c	−4.5	−3.1	−2.5	0.5	1.6	2.9	3.1	3.8	1.6	0.9	−2.0	−2.3
					−5.2	2.3	15.1	15.0	10.0	2.2	−3.7	−10.7	−8.3	−6.6	−6.4	−3.4

78. INDIAN OCEAN: Java, South

Patjitan (NEI)	8°12S	111°05E	1928–31	4	2.8	4.7	6.8	3.8	7.2	−1.8	−10.2	−8.8	−14.4	−0.4	3.3	6.9
Tjilatjap (NEI)	7°44S	109°00E	1925–31	7	6.6	4.1	7.8	6.3	9.9	−4.6	−10.8	−13.2	−16.5	−5.1	6.0	9.1
				k = .30	5.1	4.3	7.4	5.3	8.8	−3.5	−10.6	−11.4	−15.7	−3.2	4.9	8.2
				P_g	8.8	9.1	9.1	9.1	10.1	11.5	12.5	11.2	11.8	11.5	9.1	9.1
				c	−0.9	−0.6	−1.0	−1.0	0.0	0.7	1.2	0.6	1.1	1.4	−0.8	−0.1
				±.98	4.2	3.7	6.4	4.3	8.8	−2.8	−9.4	−10.8	−14.6	−1.8	4.1	8.1

Station	Latitude	Longitude	Years	Tota Years	J	F	M	A	M	J	J	A	S	O	N	D
79a. INDIAN OCEAN: Java, Southwest																
Plabocan-Ratoe (NEI)	7°00S	106°30E	1928–31(1)	4	−0.3	−0.3	1.6	1.5	13.9	0.2	−14.3	−7.8	−10.1	−1.1	7.7	8.7
				k = .50												
				P_E	9.1	9.1	9.1	9.1	9.1	10.8	11.8	10.5	11.5	11.5	9.1	9.1
				c	−0.4	−0.4	−0.8	−0.8	−0.8	0.2	0.7	0.1	1.0	1.6	−0.6	0.1
					−0.7	−0.7	0.8	0.7	13.1	0.4	−13.6	−7.7	−9.1	0.5	7.1	8.8
79b. INDIAN OCEAN: Sumatra, South																
Oosthaven (NEI)	5°27S	105°16E	1930–31(1)	2	−5.1	−10.2	−5.2	0.3	9.7	2.7	−0.6	−7.3	−7.7	1.0	13.6	9.8
Kroë (NEI)	5°11S	103°55E	1929–31(1)	3	−10.2	−8.1	−3.9	−3.5	13.8	5.1	−2.9	−6.8	−4.6	10.3	10.6	−0.1
				k = .45	−8.5	−8.8	−4.3	−2.2	12.4	4.3	−2.1	−7.0	−5.6	7.2	11.6	3.2
				P_E	9.1	9.1	9.1	9.1	9.1	10.8	11.8	10.5	11.5	11.5	9.1	9.1
				c	−0.4	−0.4	−0.8	−0.8	−0.8	0.2	0.7	0.1	1.0	1.6	−0.6	0.1
				±1.61	−8.9	−9.2	−5.1	−3.0	11.6	4.5	−1.4	−6.9	−4.6	8.8	11.0	3.3
79c. INDIAN OCEAN: Sumatra, West																
Benkoelen (NEI)	3°47S	102°15E	1925–31	7	−2.7	−9.5	−5.6	−0.3	9.7	0.0	0.5	−2.5	−2.3	4.3	6.9	1.6
Emmahaven (NEI)	0°58S	100°20E	1925–31	7	−6.0	−10.3	−6.0	−1.7	8.4	2.4	1.7	0.1	−0.7	4.8	6.7	1.1
Sibolga (NEI)	1°44N	98°46E	1930–31	2	−7.7	−7.9	−4.3	−2.5	12.0	5.4	−3.0	−3.5	−4.3	4.3	8.0	3.0
				k = .26	−4.8	−9.6	−5.6	−1.2	9.5	1.8	0.8	−1.5	−1.9	4.5	7.0	1.6
				P_E	9.1	9.1	9.1	9.1	9.1	10.8	11.8	10.5	11.5	11.5	9.1	9.1
				c	−0.4	−0.4	−0.8	−0.8	−0.8	0.2	0.7	0.1	1.0	1.6	−0.6	0.1
				±.66	−5.2	−10.0	−6.4	−2.0	8.7	2.0	1.5	−1.4	−0.9	6.1	6.4	1.7
79d. INDIAN OCEAN: Sumatra, North																
Belawan (NEI)	3°55N	98°43E	1925–31	7	−9.2	−14.9	−10.2	−1.9	9.3	7.8	5.9	5.3	1.6	5.8	3.4	−3.3
				k = .38												
				P_E	9.1	9.1	9.1	9.1	9.1	10.8	11.8	10.5	11.5	11.5	9.1	9.1
				c	−0.4	−0.4	−0.8	−0.8	−0.8	0.2	0.7	0.1	1.0	1.6	−0.6	0.1
					−9.6	−15.3	−11.0	−2.7	8.5	8.0	6.6	5.4	2.6	7.4	2.8	−3.2
79. INDIAN OCEAN: Java, Southwest, and Sumatra, West, Summary																
				k = .18	−5.8	−9.3	−5.2	−1.2	10.6	3.3	−0.9	−2.1	−3.0	4.6	7.3	1.9
				c	−0.4	−0.4	−0.8	−0.8	−0.8	0.2	0.7	0.1	1.0	1.6	−0.6	0.1
				±1.38	−6.2	−9.7	−6.0	−2.0	9.8	3.5	−0.2	−2.0	−2.0	6.2	6.7	2.0

				80a. INDIAN OCEAN: Malacca Strait										
Bengkalis (NEI)	1°28N	102°08E	1929–31(1)	3	−4.2	−7.8	−8.5	−6.2	4.0	0.4	−0.9	−0.3	−0.6	7.7	12.2	4.2
				k = .58												
				P_g	10.5	10.5	9.8	9.1	8.8	9.5	10.1	9.1	10.1	10.8	9.1	10.1
				c	1.2	1.2	0.1	−0.6	−0.9	−0.9	−0.8	−1.1	−0.2	1.1	−0.4	1.3
					−3.0	−6.6	−8.4	−6.8	3.1	−0.5	−1.7	−1.4	−0.8	8.8	11.8	5.5
				80b. INDIAN OCEAN: Malay Peninsula, West												
Bass Harbour (Ma)	6°18N	99°47E	1934	1	−4.5	−11.2	−9.1	0.8	2.9	−1.4	5.6	4.7	4.1	5.7	14.3	−12.1
Ko Ta-Phao Noi (Si)	7°50N	98°26E	1940–46(1)	7	−12.0	−14.7	−11.2	−2.4	6.7	8.1	9.0	2.5	3.6	3.9	5.6	1.4
				k = .39	−10.1	−13.8	−10.7	−1.6	5.8	5.7	8.2	3.0	3.7	4.4	7.8	−2.0
				P_g	10.5	10.5	9.8	9.1	8.8	9.5	10.1	9.1	10.1	10.8	9.1	10.1
				c	1.2	1.2	0.1	−0.6	−0.9	−0.9	−0.8	−1.1	−0.2	1.1	−0.4	1.3
				±1.91	−8.9	−12.4	−10.6	−2.2	4.9	4.8	7.4	1.9	3.5	5.5	7.4	−0.7
				80. INDIAN OCEAN: Malacca Strait Summary												
				k = .32	−8.2	−11.8	−9.9	−3.1	5.2	3.9	5.1	1.9	2.3	5.5	9.3	0.1
				c	1.2	1.2	0.1	−0.6	−0.9	−0.9	−0.8	−1.1	−0.2	1.1	−0.4	1.3
				±1.88	−7.0	−10.6	−9.8	−3.7	4.3	3.0	4.3	0.8	2.1	6.6	8.9	1.4
				81a. INDIAN OCEAN: Burma												
Rangoon (Bu)	16°46N	96°10E	1937–41	5	−40.9	−37.9	−34.8	−22.6	−4.4	20.0	32.2	47.5	38.3	26.1	−1.3	−22.6
Akyab (Bu)	20°08N	92°54E	1937–41	5	−33.0	−36.1	−30.0	−11.7	12.7	34.0	34.0	27.9	15.8	6.6	−5.6	−14.7
Chittagong (In)	22°20N	91°50E	1937–46(2)	10	−54.9	−54.9	−42.7	−24.4	9.1	45.7	60.9	64.0	42.6	9.1	−18.3	−36.6
				k = .23	−44.6	−44.7	−36.8	−20.3	6.3	35.0	45.0	49.0	33.7	13.2	−9.8	−26.3
				P_g	14.9	13.2	11.8	7.1	6.1	2.4	3.0	4.7	5.7	9.1	11.8	14.9
				c	6.7	5.0	3.2	−1.5	−2.5	−6.9	−6.8	−4.4	−3.5	0.5	3.4	7.2
				±5.64	−37.9	−39.7	−33.6	−21.8	3.8	28.1	38.2	44.6	30.2	13.7	−6.4	−19.1
				81b. INDIAN OCEAN: Kidderpore												
Kidderpore (In)[21]	22°32N	88°20E	1881–93(1), 1937–46	23	−60.6	−66.2	−54.8	−41.0	−21.3	−3.0	44.1	97.6	104.3	52.7	−10.5	−41.7
				k = .21												
				P_A	14.9	13.2	11.8	7.1	6.1	2.4	3.0	4.7	5.7	9.1	11.8	14.9
				c	6.7	5.0	3.2	−1.5	−2.5	−6.9	−6.8	−4.4	−3.5	0.5	3.4	7.2
					−53.9	−61.2	−51.6	−42.5	−23.8	−9.9	37.3	93.2	100.8	53.2	−7.1	−34.5

81. INDIAN OCEAN: Bay of Bengal, East, Summary

Station	Latitude	Longitude	Years		Total Years	J	F	M	A	M	J	J	A	S	O	N	D
				k = .16		−51.3	−53.6	−44.3	−28.9	−5.2	19.2	44.6	69.2	63.1	29.6	−10.1	−32.7
				c		6.7	5.0	3.2	−1.5	−2.5	−6.9	−6.8	−4.4	−3.5	0.5	3.4	7.2
				±2.81		−44.6	−48.6	−41.1	−30.4	−7.7	12.3	37.8	64.8	59.6	30.1	−6.7	−25.5

82. INDIAN OCEAN: Bay of Bengal, West

Dublat (In)	21°38N	88°08E	1937–43(1)		7	−19.0	−28.2	−28.2	−19.0	5.4	17.5	17.5	20.6	20.6	14.5	5.4	−6.8
Vizagapatam (In)	17°41N	83°17E	1937–46(1)		10	−8.1	−20.3	−23.3	−14.2	−2.0	4.1	1.0	1.0	7.1	22.4	22.4	10.2
				k = .24		−13.6	−24.3	−25.8	−16.6	1.7	10.8	9.3	10.8	13.9	18.5	13.9	1.7
				P_g		14.9	13.5	11.8	6.1	5.4	1.4	1.7	2.4	5.1	9.1	13.2	15.2
				c		7.1	5.7	3.6	−2.1	−2.8	−7.5	−7.7	−6.3	−3.7	0.9	5.2	7.9
				±4.50		−6.5	−18.6	−22.2	−18.7	−1.1	3.3	1.6	4.5	10.2	19.4	19.1	9.6

83. INDIAN OCEAN: Arabian Sea

Bombay (In)	18°55N	72°50E	1878–1946		69	3.4	−0.1	1.4	1.5	−3.0	4.0	−1.7	−1.0	−6.4	−4.7	1.2	5.4
Karāchi (In)	24°48N	66°58E	1937–46		10	−2.3	−3.5	−1.3	1.7	4.1	8.4	1.7	1.1	−4.4	−5.3	−0.4	−0.1
				k = .12		1.8	−1.0	0.7	1.6	−1.1	5.2	−0.8	−0.4	−5.9	−4.9	0.8	3.9
				P_g		15.9	14.5	11.5	8.5	5.7	1.4	0.0	2.4	5.1	11.5	13.9	15.6
				c		7.6	6.2	2.8	−0.2	−3.0	−8.0	−10.0	−6.8	−4.2	2.8	5.4	7.8
				±1.20		9.4	5.2	3.5	1.4	−4.1	−2.8	−10.8	−7.2	−10.1	−2.1	6.2	11.7

84. INDIAN OCEAN: Iran, Persian Gulf

Fao (Ir)	29°58N	48°30E	1945		1	−9.1	−17.4	−12.4	0.8	9.8	16.0	17.1	8.8	3.1	−6.0	−3.8	−6.9
Basrah (Ir)	30°31N	47°51E	1917–18		2	−31.4	−7.9	7.3	34.2	54.4	41.0	20.1	−5.4	−22.8	−30.0	−30.7	−28.5
				k = .58		−20.3	−12.7	−2.6	17.5	32.1	28.5	18.6	1.7	−9.9	−18.0	−17.3	−17.7
				P_g		20.0	18.3	15.2	11.5	8.8	4.0	1.4	2.4	7.4	13.2	17.6	18.3
				c		9.0	7.3	3.8	0.1	−2.6	−8.1	−11.2	−9.5	−4.6	1.8	6.4	7.8
				±8.75		−11.3	−5.4	1.2	17.6	29.5	20.4	7.4	−7.8	−14.5	−16.2	−10.9	−9.9

Généffé (Su)	30°10N	32°34E	1937–41	85. INDIAN OCEAN: Suez Canal										
Kabret (Su)	30°16N	32°30E	1923–27, 1932–41	5	5.7	4.6	−3.0	4.1	−1.1	−6.0	−2.3	−3.0	−7.0	−1.2	7.0	2.7
Déversoir (Su)	30°25N	32°21E	1937–41	15	4.3	2.0	−0.7	−0.5	−0.8	−5.5	−2.3	−2.8	−6.7	−2.2	7.8	7.0
				5	5.0	4.5	−3.5	3.0	−1.2	−6.3	−1.3	−1.9	−5.6	−1.3	5.8	3.3
				k = .21	4.8	3.3	−2.0	1.5	−1.0	−5.8	−2.0	−2.6	−6.5	−1.7	7.1	5.0
				P_g	17.6	15.9	12.5	11.5	10.8	8.5	7.4	6.8	10.8	11.8	14.9	15.9
				c	6.1	4.4	0.6	−0.4	−1.1	−4.1	−5.7	−5.6	−1.7	−0.1	3.2	4.9
				±.62	10.9	7.7	−1.4	1.1	−2.1	−9.9	−7.7	−8.2	−8.2	−1.8	10.3	9.9
				86. INDIAN OCEAN: Gulf of Suez												
Port Thewfik (Su)	29°57N	32°34E	1923–29, 1931–46	23	11.2	7.9	4.1	4.6	3.7	−7.3	−11.4	−13.3	−17.7	−5.9	11.1	12.4
				k = .21												
				P_g	17.6	15.9	12.5	11.5	10.8	8.5	7.4	6.8	10.8	11.8	14.9	15.9
				c	6.1	4.4	0.6	−0.4	−1.1	−4.1	−5.7	−5.6	−1.7	−0.1	3.2	4.9
					17.3	12.3	4.7	4.2	2.6	−11.4	−17.1	−18.9	−19.4	−6.0	14.3	17.3
				87. INDIAN OCEAN: Arabia, Red Sea												
Aden (Ar)	12°47N	44°59E	1879–93(1), 1937–46(4)	25	5.3	6.8	7.4	9.5	10.4	4.4	−5.9	−13.8	−12.5	−9.6	−3.3	1.4
				k = .20												
				P_g	14.9	12.8	11.2	9.8	8.1	4.7	4.0	4.7	7.1	9.8	12.5	14.5
				c	5.9	3.8	1.8	0.4	−1.3	−5.4	−6.6	−5.2	−2.9	0.4	3.3	6.0
					11.2	10.6	9.2	9.9	9.1	−1.0	−12.5	−19.0	−15.4	−9.2	0.0	7.4
				88. INDIAN OCEAN: Kenya, Tanganyika												
Kilindini (Ke)	4°04S	39°39E	Oct. 1932–Sept. 1933(2)	1	1.6	0.5	4.1	5.0	1.7	−1.8	−0.6	−2.5	−4.0	−2.1	1.1	−3.2
Dar-es-Salaam (Ta)	6°49S	39°19E	Apr. 1929–Mar. 1930(2)	1	0.8	2.7	0.9	4.8	−1.3	−0.9	−4.2	−6.5	−2.3	2.4	−0.9	4.7
				k = .70	1.2	1.6	2.5	4.9	0.2	−1.4	−2.4	−4.5	−3.2	0.2	0.1	0.8
				P_g	9.8	9.8	10.1	11.5	11.8	14.2	14.2	14.2	14.2	12.5	11.8	10.1
				c	−1.7	−1.7	−1.8	−0.4	−0.1	1.6	1.1	1.8	1.7	0.6	0.1	−0.9
				±1.22	−0.5	−0.1	0.7	4.5	0.1	0.2	−1.3	−2.7	−1.5	0.8	0.2	−0.1
				89. INDIAN OCEAN: Union of South Africa												
Durban (SA)	29°52S	31°03E	Oct. 1926–Sept. 1927 (2)	1	5.7	0.5	8.9	3.8	1.3	−7.0	−14.9	−0.8	−8.9	1.8	1.4	8.2
				k = 1.00												
				P_g	12.5	12.5	14.2	16.9	17.6	21.6	22.0	21.3	19.3	15.9	14.5	12.5
				c	−3.7	−3.7	−2.4	0.3	1.0	4.3	4.2	4.2	2.1	−0.7	−1.9	−3.2
					2.0	−3.2	6.5	3.5	2.3	−2.7	−10.7	3.4	−6.8	1.1	−0.5	5.0

90. ANTARCTIC OCEAN: Palmer Peninsula

Station	Latitude	Longitude	Years	Total Years	J	F	M	A	M	J	J	A	S	O	N	D
Marguerite Bay[15,17]	68°11S	67°00W	Apr. 1947–Feb. 1948	1	−3.5	3.2		11.1	2.1	−6.3	−0.8	−3.2	−0.2	−1.1	1.9	−2.9
Port Circoncision[16,17]	65°10S	64°14W	Feb.–Aug., Oct., Nov. 1909	1		−2.3	4.2	5.8	7.2	7.2	−1.0	3.4		−6.1	−8.5	
					−3.5	−0.7	4.2	6.8	5.7	−0.4	−0.9	−2.4	−0.2	−3.1	−2.0	−2.9

91. ANTARCTIC OCEAN: Adélie Land

Port Martin[18]	66°49S	141°24E	Aug., Sept. 1950, Feb., May–Oct., 1951			7.2			−0.8	−11.8	3.2	−5.8	4.2	3.7		
Cape Denison[19]	67°00S	142°40E	June–Aug., 1912							−8.1	−1.4	−4.8				
						7.2			−0.8	−10.0	0.9	−5.6	4.2	3.7		

92. ANTARCTIC OCEAN: Macquarie Island

Macquarie Island[19,20]	50°31S	158°58E	Aug. 1912–May 1913		−6.0	−12.1	−1.7	5.0	−4.5			−0.5	8.6	4.7	−2.3	9.2

FOOTNOTES

[1] Values taken as positive downward though given as positive upward. Confirmed by letter from J. A. Barahona Fernandes. The error seems to have arisen out of a confusion between "dessous" and "dessus"!

[2] Unpublished data furnished by Liverpool Observatory and Tidal Institute.

[3] (a) Thomson tide gauge, (b) Mier tide gauge.

[4] Changed October value from 7.778 to 6.778.

[5] Unpublished data from U. S. Coast and Geodetic Survey.

[6] Changed March value from 1.93 to 2.93.

[7] Combined La Coloma, 22°14N 83°34W, and Los Arroyos, 22°21N 84°23W.

[8] Report of the International Polar Expedition to Point Barrow, Alaska, by Lt. P. H. Ray, Washington, 1885.

[9] Omitted data for March, 1951.

[10] Three years data for August and September only; two years data for remaining months.

[11] July, August, September, 1948, February through August, 1949, February through April, 1950.

[12] Values taken as positive downward, though given as positive upward.

[13] Tidal Record 1930–49, Geophysical Survey Institute, Ministry of Construction, Japan, 1950.

[14] Values taken as positive upward, though given as positive downward.

[15] Tidal Work on Marguerite Bay, Antarctica, Ronne Antarctic Research Expedition, Office of Naval Research, 1948.
For following months data were available only for stated number of days: Feb., 17 days; Apr., 7 days; May, 13 days. Data complete for all other months.

[16] Deuxieme Expédition Antarctique Française (1908–1910, commandée par le Dr. Jean Charcot, Étude sur les Marées, by R.-E. Godfroy, Masson et C^{ie}, Paris.
For following months data were available only for stated number of days: Feb., 26 days; Aug., 6 days; Oct., 11 days. Data complete for all other months.

[17] In combining these two stations the values for the months where the data are incomplete have been multiplied by a factor proportional to the respective number of days for each station. Where the incomplete data represent a period of consecutive days at the beginning or end of a month, the months have been divided into two periods, which have been averaged separately and later combined.

[18] Nouveaux Enregistrements de Marée en Terre Adélie, by Bertrand Imbert, Extrait du Bulletin d'Information du Comité Central d'Océanographie et d'Étude des Côtes, V, 7, 1953.

[19] Australasian Antarctic Expedition, 1911–1914, Scientific Reports, Series A, Vol. II Oceanography, Part 2 Tidal Observations by A. T. Doodson, Dec. 1939.
Data available for stated number of days: June, 20 days; July, 22 days; Aug., 31 days.

[20] Analysed in separate months of 29 days each.

[21] Values may reflect other than oceanic conditions; station located upriver or at estuary head.

APPENDIX II

ATLANTIC OCEAN (ARCTIC SECTOR)

No.	Locality	Latitude	Longitude	BTs/Mo.	NB	Reference		J	F	M	A	M	J	J	A	S	O	N	D
1.	Barents Sea	70°–76°N	033°–040°E	0	62	Conseil (1904)	z_T		1.1			−1.3			−1.6			1.7	
							z_S		0.4			0.5			0.0			−0.7	
							z_α		1.2			−0.5			−1.5			0.8	

ATLANTIC OCEAN

2.	Norwegian Sea	65°–71°N	006°W–006°E	0	163	HYDRO	z_T		−6.8			−0.6	−0.4	1.8	3.2	2.7			
							z_S		2.0			0.3	−0.5	−0.3	−0.2	−1.4			
							z_α		−4.3			−0.4	−1.1	1.4	3.2	1.4			
3.	North Sea	55°–60°N	005°–010°E	57[1]	unk.	Dietrich (1950)	z_T	−1.0	−4.0	−4.5	−3.9	−2.7	−0.9	1.4	2.8	3.9	4.7	3.0	1.2
							z_S	0.0	−1.0	−1.3	−0.9	−0.7	−0.4	0.0	0.7	0.9	1.1	1.0	0.5
							z_α	−0.6	−2.7	−3.7	−3.7	−2.9	−1.3	0.6	2.7	4.3	3.4	2.5	1.2
4.	Bay of Biscay	40°–51°N	005°–022°W	0	unk.	Helland-Hansen (1930)	z_T	−4.7	−4.7	−4.6	−4.5	−2.0	1.1	4.3	6.1	5.6	4.5	2.6	−3.5
5.	Station "K"	45°N	016°W	0	19	COEC (1951)	z_T	−2.5	−3.0	−3.0	2.0	2.0	1.2	1.3	1.6	1.6	2.0	−0.6	−2.0
							z_S	0.8	0.3	−0.2	−2.2	−1.5	−0.5	0.2	0.5	0.6	0.8	0.5	0.5
							z_α	−1.7	−2.4	−3.2	−0.2	0.5	0.6	1.5	2.1	2.2	2.8	−0.2	−1.6
6.	Off Gibraltar	32°–37°N	010°–015°W	104[1]	—[2]	WHOI	z_T	0.3	−2.4	−3.5	−3.7	−2.6	−0.9	0.7	2.1	2.6	2.3	3.3	1.8
7.	Mediterranean	35°–40°N	015°–020°E	163[1]	—[2]	WHOI	z_T	−3.0	−4.6	−5.3	−5.4	−2.0	−0.2	3.2	3 4	2.3	5.2	5.8	0.4
8.	South of the Azores	32°–37°N	026°–031°W	87[1]	1	WHOI	z_T	1.9	−0.2	−3.2	−4.1	−4.7	−4.8	−2.8	−0.3	3.1	5.2	5.3	4.6
9.	Capetown	33°–36°S	012°–018°E	0	30	DISCOVERY (1944)	z_T	−3.1	−3.8	4.0	10.0	8.3	2.6	−15.1	−21.5	−10.6	6.8	13.0	9.3
							z_S	−1.7	3.6	0.6	−1.9	−2.5	−1.1	6.6	9.5	3.4	−4.8	−7.1	−5.9
							z_α	−5.0	−0.8	4.9	8.3	6.0	0.8	−8.3	−11.3	−7.1	2.3	6.6	3.6
10.	40,000 South	38°–42°S	001°W–003°E	0	15	DISCOVERY (1944)	z_T	1.5	2.2	2.9	2.2	0.3	−0.1	−0.1	−1.3	−2.6	−3.1	−1.9	0.0
							z_S	1.2	0.1	−1.4	−1.5	−0.1	0.5	0.2	−0.3	−0.8	−0.1	0.9	1.2
							z_α	2.7	2.4	1.6	0.8	0.2	0.3	0.1	−1.6	−3.3	−3.1	−1.1	1.1
11.	Falkland Is.	52°S	052°W	0	unk.	Deacon (1933)	z_T	1.8	3.2	4.5	4.6	3.9	1.1	−1.8	−4.2	−5.0	−4.6	−2.8	−0.4
							z_S	−0.7	0.2	0.7	1.2	1.5	1.1	0.5	0.0	−0.4	−1.1	−1.5	−1.3
							z_α	0.9	3.7	5.4	6.4	5.5	2.0	−1.3	−4.4	−5.9	−6.0	−4.6	−1.8
12.	Recife	04°–09°S	030°–035°W	12[1]	2	WHOI	z_T	1.1	2.2	3.3	2.8	0.1	−2.0	−2.4	−2.0	−1.6	−1.0	−0.6	0.0
13.	Puerto Rico	15°–20°N	063°–068°W	91[1]	3	WHOI	z_T	−2.5	−4.8	−4.5	−2.2	−0.1	0.7	1.1	2.0	3.4	4.1	2.6	0.2
14.	Gulf of Mexico	22°–27°N	082°–087°W	166[1]	4	WHOI	z_T	1.6	−2.7	−5.3	−4.7	−2.1	−0.2	1.0	1.9	2.2	2.3	3.2	2.9
15.	Florida C.	33°–35°N	070°–075°W	76[1]	1	WHOI	z_T	−5.3	−6.5	−8.8	−9.3	−5.0	0.4	4.5	8.4	10.0	8.5	3.5	0.6
16.	Bermuda	31°–34°N	062°–068°W	99[1]	132	Fuglister (1947)	z_T	−2.3	−4.9	−6.6	−6.9	−5.6	−3.8	0.3	4.5	7.6	8.9	6.7	2.2
							z_S	−0.1	−0.1	0.0	0.0	0.3	0.5	0.5	0.1	−0.3	−0.6	−0.4	0.0
							z_α	−2.6	−5.0	−6.4	−6.8	−5.3	−3.4	0.7	4.7	7.3	8.5	6.4	1.9

17. East Sargasso	30°–35°N	045°–050°W	101[1]	—[2]	WHOI											
18. North of Bermuda	34°–37°N	062°–068°W	70[1]	73	Fuglister (1947)	z_T	−0.8	−2.2	−3.9	−4.4	−2.7	−1.3	0.9	2.4	2.6	3.7	3.5	2.2
						z_T	−7.3	−10.6	−11.4	−10.2	−7.0	−2.0	5.0	10.9	14.0	12.0	6.4	0.3
						z_s	0.1	0.0	−0.2	−0.2	−0.1	−0.2	0.0	0.4	0.4	0.1	0.1	0.0
						z_x	−6.6	−10.1	−11.5	−10.6	−8.4	−2.3	5.2	11.6	14.8	12.2	6.5	−0.8
19. Gulf Stream	35°–37°N	070°–075°W	875[1]	—[2]	WHOI	z_T	−3.7	−5.4	−6.8	−5.5	−2.6	0.9	3.5	4.7	5.7	6.0	4.0	−0.7
20. Nova Scotia	40°–45°N	060°–065°W	506[1]	—[2]	WHOI	z_T	−0.9	−5.2	−9.7	−8.6	−5.5	−1.2	1.8	3.5	6.0	7.0	7.2	5.2
21. Newfoundland	47°–52°N	043°–048°W	146[1]	2	WHOI	z_T	−1.4	−2.7	−5.0	−4.1	−3.7	−1.8	1.0	2.8	3.8	3.7	3.1	3.2
22. Irminger Sea	60°–65°N	030°–035°W	267[1]	1	WHOI	z_T	−1.3	−2.5	−3.4	−3.3	−1.7	0.8	2.0	2.8	3.1	2.9	1.3	−0.7
						ARCTIC OCEAN												
23. Point Barrow	72°–73°N	156°–159°W	17	1	Worthington (1953)	z_T				−0.4					0.4			
						PACIFIC OCEAN												
24. Aleutian Is.	52°–53°N	179°E–180°	8	1	Pattullo (1950)	z_T	−0.4	−1.1	−1.4	−1.3	−0.8	−0.6	−0.6	0.5	1.7	1.4	1.6	0.8
25. Kodiak I.	56°30′N	152°30′W	unknown	1	Robinson (in press)	z_T	−0.8	−2.7	−3.2	−2.3	−1.7	−1.2	0.1	2.1	3.6	3.2	2.0	0.5
26. Gulf of Alaska	55°–60°N	145°–150°W	17	1	Robinson (in press)	z_T	0.8	−0.5	−1.5	−2.0	−1.9	−0.8	0.1	0.5	0.8	1.4	1.6	1.4
27. Vancouver I.	47°30′N	127°30′W	unknown	2	Robinson (in press)	z_T	−1.5	−2.5	−3.0	−2.9	−1.8	−0.2	1.6	3.1	3.8	2.4	1.1	−0.3
28. California C.[3]	36°–37°N	121°–122°W	0	1100	Skogsberg (1936)	z_T	1.2	−0.5	−1.3	−2.4	−3.6	−3.6	−1.8	−0.1	2.0	3.0	3.4	3.8
	32°–33°N	117°–118°W	12	5	SIO													
29. Ecuador	01°–06°S	080°–090°W	0	38	DISCOVERY (1949)	z_T		−0.2					0.6	1.8			−2.3	
						z_s		2.2					−1.8	−1.5			1.1	
						z_x		2.1					−1.1	0.2			−1.2	
30. Peru C.	09°–17°S	075°–085°W	0	38	DISCOVERY (1949)	z_T	−0.3	6.9				−3.7	−0.1	−2.7				
						z_s	1.4	−1.4				0.8	−0.6	−0.4				
						z_x	1.1	5.9				−2.9	−0.9	−3.1				
31. Station "Nan"	29°–31°N	139°–141°W	95	1	Robinson (1951)	z_T	−1.6	−2.4	−3.2	−3.3	−2.7	−1.5	0.8	2.8	3.6	3.0	3.8	0.4
32. Station "Papa"	48°–50°N	147°–149°W	56	2	LaFond	z_T	0.6	−0.4	−1.8	−2.5	−1.8	−1.0	0.9	1.8	2.1	1.8	0.8	0.8
33. Stn. 40150	40°30′N	150°30′W	unknown	1	Robinson (in press)	z_T	−3.0	−4.7	−5.4	−4.2	−2.6	−0.7	2.6	5.6	7.4	5.8	0.7	−1.7
34. Stn. 38158	37°–39°N	157°–159°W	21	3	Robinson (in press)	z_T	−0.8	−3.3	−3.8	−2.7	−1.2	1.3	2.6	2.5	1.9	1.9	1.3	0.9
35. Hawaii	20°–25°N	157°–160°W	56	6	Leipper (1950)	z_T	−1.6	−2.1	−2.3	−2.6	−2.0	−0.6	1.1	2.7	4.0	3.2	1.3	−0.7
36. Stn. "Quebec"	42°–44°N	166°–168°W	19	1	SIO	z_T	−4.1	−3.6	−0.8	1.8	0.9	−0.5	−0.6	1.5	3.5	2.3	0.3	−0.7
37. Stn. "Queen"	41°–43°N	172°–174°W	59	1	SIO	z_T	−2.5	−3.2	−3.2	−2.0	0.1	0.4	1.0	3.7	4.7	2.4	0.1	−1.3
38. Stn. "Victor I"	33°–35°N	172°–174°E	28	2	SIO	z_T	−2.0	−3.8	−3.5	−2.2	−0.7	1.7	2.6	2.2	2.9	2.7	1.4	−0.6
39. Stn. "Victor II"	30°–32°N	163°–165°E	48	2	SIO	z_T	−3.0	−4.7	−5.8	−6.9	−7.1	−3.6	2.3	4.4	5.7	7.9	7.4	2.9
40. Marshalls—15°N	14°–16°N	155°–175°E	unknown		Mao (1953)	z_T	Apr. through Sept.			8.4	Oct. through Mar.			−8.4				
						z_s	Apr. through Sept.			0.3	Oct. through Mar.			−0.3				
						z_x	Apr. through Sept.			8.8	Oct. through Mar.			−8.8				
41. Eniwetok	10°–12°N	161°–163°E	9	2	Robinson (1952)	z_T	0.0	−1.4	−3.4	−5.2	−4.0	−0.4	3.2	4.5	3.6	1.7	1.3	0.0

No.	Locality	Latitude	Longitude	BTs/Mo.	NB	Reference
42.	Marshalls—3°N	02°–04°N	155°–175°E	unknown		Mao (1953)
43.	Samoa	15°–19°S	170°–174°W	8	1	SIO
44.	New Caledonia	20°–25°S	160°–165°E	25	3	SIO
45.	Tasmania	42°–43°S	148°–149°E	0	13	CSIRO
46.	Sydney	34°–35°S	151°–152°E	0	64	CSIRO
47.	Truk	05°–10°N	150°–155°E	0	58	JAP-HYDRO
48.	Sulu Sea	07°–12°N	117°–123°E	13	7	Leipper (1947)
49.	Mindanao Deep	09°–10°N	126°–128°E	unknown	3	Leipper (1947)
50.	Manila	14°–16°N	118°–120°E	7	5	Leipper (1947)
51.	Marianas	18°–20°N	145°–150°E	0	36	JAP-HYDRO
52.	Formosa	23°–24°N	122°–123°E	0	198	JAP-HYDRO
53.	Okinawa	26°–27°N	126°–127°E	0	171	JAP-HYDRO
54.	Stn. "Tango"	29°–30°N	135°–136°E	0	80	JAP-HYDRO
55.	Kuroshio[3]	unknown		0	unk.	Koenuma (1939)
		34°–35°N	139°–140°E	0	118	Japanese
		37°–38°N	142°–143°E	0	216	JAP-HYDRO
56.	Korea	39°–40°N	129°–130°E	0	117	Japanese
57.	Central Sea of Japan	38°–39°N	135°–136°E	0	84	Japanese

	J	F	M	A	M	J	J	A	S	O	N	D
z_T	Apr. through Sept.			−3.0	Oct. through Mar.			3.0				
z_S	Apr. through Sept.			2.8	Oct. through Mar.			−2.8				
z_α	Apr. through Sept.			−0.4	Oct. through Mar.			0.4				
z_T	−1.4	0.4	1.3	1.4	1.2	1.5	0.7	−0.4	−0.8	−0.5	−1.0	−2.5
z_T	6.3	5.7	5.8	6.2	2.1	−5.7	−10.2	−5.1	−3.8	−2.5	−0.4	1.7
z_T	−4.4	1.8	5.8	8.0	8.8	7.9	4.9	−0.5	−7.4	−10.8	−7.4	−5.6
z_S	5.3	5.3	0.3	−3.4	−4.2	−5.7	−4.8	−3.4	−0.3	3.1	3.1	3.8
z_α	0.9	7.0	5.0	4.2	4.0	3.3	0.0	−3.9	−7.6	−7.6	−4.3	−2.0
z_T	−17.8	−13.4	−3.9	6.7	10.1	9.5	7.8	11.4	12.8	3.5	11.3	−17.3
z_S	8.9	9.7	8.4	4.1	−0.9	−5.5	−7.8	−8.8	−8.2	−5.6	0.0	5.6
z_α	−8.2	−3.0	3.9	10.4	9.1	4.1	0.3	3.1	5.1	−2.2	−11.3	−11.2
z_T	−4.3	6.3	8.1	3.2	8.1	5.1	2.6	1.2	−6.8	−9.2	−9.4	−6.4
z_S	−0.2	−0.2	0.3	0.3	0.1	−0.2	0.0	0.6	0.5	−0.2	−0.6	−0.3
z_α	−3.3	6.4	7.6	4.0	8.6	5.2	2.9	1.5	−6.4	−9.3	−10.0	−6.8
z_T	−2.1	−2.9	−3.0	−2.4	−1.9	0.5	0.5	0.9	3.6	5.0	2.6	0.0
z_T	−4.6	−2.8	−2.0	−2.3	1.7	3.1	1.1	0.6	1.0	0.9	2.7	−0.1
z_T	−1.8	−3.1	−3.9	−5.3	−4.1	0.9	4.3	3.4	2.6	3.5	3.0	0.5
z_T	−7.1	−3.4	−2.6	0.9	−0.3	3.0	4.9	4.2	5.1	1.4	−1.7	−6.0
z_S	−1.2	−1.9	−1.2	−1.2	−0.7	0.3	1.4	1.6	0.2	1.3	0.7	0.7
z_α	−7.3	−5.5	−4.1	−0.4	−1.3	3.1	6.1	6.8	5.2	3.9	−1.2	−5.9
z_T	−6.2	−4.7	0.9	3.3	2.8	1.2	1.1	4.0	4.7	1.3	−3.7	−6.1
z_S	1.3	0.3	−3.3	−3.8	−2.4	−0.8	1.6	2.7	2.2	1.3	−0.7	1.9
z_α	−4.3	−3.8	−2.1	−0.2	0.3	0.3	2.4	6.1	6.3	2.4	−3.8	−3.7
z_T	−1.8	−1.3	−4.3	−5.2	−2.1	3.5	8.9	3.6	2.4	−0.2	−0.8	0.0
z_S	−4.6	−5.8	−2.0	−1.3	−0.7	0.4	1.0	3.0	4.2	4.8	3.7	−1.9
z_α	−6.3	−7.1	−6.3	−6.4	−3.0	2.6	9.9	6.6	6.6	4.5	1.3	−1.9
z_T	−4.1	−7.0	−8.1	−8.4	−6.5	−1.6	3.2	6.7	9.1	10.9	5.8	−0.8
z_S	−0.7	−0.8	−0.6	−0.1	0.5	0.9	0.9	1.0	0.5	0.0	−0.5	−0.9
z_α	−5.1	−8.5	−9.6	−9.4	−6.9	−2.5	4.6	8.8	11.1	12.5	6.2	−1.7
z_T	−4.4	−5.5	−6.2	−6.4	−6.2	−3.2	−0.4	4.4	8.7	9.8	6.7	1.8
z_S	0.6	−0.7	−0.7	1.4	1.8	−1.5	−4.0	−2.9	1.2	2.4	1.9	1.4
z_α	−4.4	−6.6	−7.2	−5.2	−4.6	−4.8	−3.7	2.3	10.8	12.6	8.6	2.5
z_T	−3.7	−4.8	−5.1	−3.6	−1.0	0.1	1.9	3.4	3.6	4.4	3.8	1.0
z_S	0.3	−0.4	−0.5	−1.3	−1.7	−0.4	−0.3	0.5	1.4	0.7	1.1	0.6
z_α	−3.4	−5.0	−5.1	−5.0	−3.3	−0.9	1.4	4.2	5.2	5.5	5.0	1.3
z_T	−6.8	−12.5	−10.7	−6.6	−5.0	−4.6	−1.7	7.0	13.0	13.8	9.3	4.7
z_S	0.4	−0.3	−0.7	−0.8	−0.9	−1.0	−0.7	−0.1	0.4	0.9	1.2	1.3
z_α	−6.9	−11.2	−10.8	−7.4	−6.4	−6.2	−3.3	6.1	13.7	15.4	11.0	5.9

58. Oyashio C.	41°–43°N	144°–146°E	0	141	JAP-HYDRO	z_T	2.8	−6.6	−9.2	−9.4	−7.3	−3.7	0.3	6.3	8.4	6.4	7.6	4.4
						z_s	5.2	4.2	3.8	6.7	2.8	2.4	−4.0	−7.3	−11.8	−7.3	0.4	6.3
						z_α	7.2	−2.5	−5.1	−2.3	−4.9	−1.7	−4.2	−1.1	−2.8	−0.9	8.1	10.2
59. Stn. "Sugar"	43°–45°N	164°–166°E	24	2	SIO	z_T	−2.8	−3.5	−3.8	−3.5	−2.2	0.0	2.2	3.8	3.2	3.0	2.7	0.2
60. Station "Sierra"	47°–49°N	161°–163°E	38	1	SIO	z_T	−1.2	−2.2	−2.4	−2.9	−2.4	−0.5	0.5	2.3	3.8	3.6	1.6	−0.2
INDIAN OCEAN																		
91. Perth	32°–33°S	113°–114°E	0	14	CSIRO	z_T	−6.1	8.5	11.1	9.7	10.7	14.4	11.7	1.6	−7.2	−13.3	−19.5	−20.3
						z_s	6.8	7.7	−1.6	−1.9	−1.7	−1.6	−1.0	−0.4	−0.6	−3.7	−3.3	1.8
						z_α	0.0	14.6	9.4	7.7	8.9	12.4	10.7	0.8	−8.3	−16.7	−22.0	−17.9
62. Sumatra	04°–09°N	090°–095°E	10	1	SIO	z_T	−0.6	−2.2	0.8	4.0	5.1	2.9	3.5	1.6	−5.3	−7.5	−4.7	2.0
63. Bay of Bengal	17°–18°N	083°–084°E	unknown		LaFond (1954)	z_T				−6.8						6.8		
						z_s				−20.6						20.6		
						z_α				−27.4						27.4		
64. Central Arabian Sea	14°–19°N	064°–069°E	9	3	SIO	z_T	−7.8	−8.7	−6.1	−2.6	1.1	3.9	4.8	4.6	3.8	4.4	4.6	−2.0
65. Oman	18°–23°N	059°–064°E	24	2	SIO	z_T	0.9	2.6	1.8	−1.5	−1.6	7.7	2.1	−4.7	−8.6	−4.5	2.8	2.8
ANTARCTIC OCEAN																		
66. Davis Sea	65°–67°S	085°–089°E	0	19	von Drygalski (1926)	z_T	−0.2	−3.8	0.0			0.8			1.3		1.3	
						z_s	−1.3	2.1	1.9			−1.1			−0.1		−1.5	
						z_α	−1.2	1.9	1.8			−1.1			0.0		−1.4	
67. Bouvet I.	52°–57°S	003°W–004E	0	36	DISCOVERY (1944)	z_T	−0.5	0.2	−0.3	1.7	−0.4	−0.5	−0.4	0.1	0.1	0.6		−0.6
						z_s	−0.9	0.6	0.4	1.9	−1.0	0.0	1.8	−0.1	0.0	−2.0		−0.2
						z_α	−1.9	0.4	−0.2	3.5	1.8	−0.9	1.0	−0.4	−0.2	−1.9		−1.1
68. South Georgia I.	52°–53°S	037°–038°W	0	unk.	Deacon (1933)	z_T	0.8	1.2	1.0	0.6	−0.0	−0.5	−0.9	−1.0	−0.9	−0.6	−0.2	0.4
						z_s	0.1	0.7	0.7	0.2	−0.2	−0.3	−0.2	−0.1	−0.2	−0.2	−0.3	−0.3
						z_α	0.5	1.0	0.9	0.4	−0.8	−0.3	−0.7	−0.6	−0.4	−0.5	0.0	0.0
69. South Shetland I.	58°–63°S	055°–065°W	0	79	DISCOVERY (1941)	z_T		−3.3	1.6	3.1							0.0	−1.4
						z_s		2.9	−1.7	7.2							−6.6	−1.6
						z_α		−1.2	−0.5	8.8							−3.3	−3.9

FOOTNOTES

[2]Temperature data include both BT's and Nansen Bottle readings.

[3] Salinity found from scatter diagram of temperature and salinity observations and average TS relations given in *The Oceans*

[4]Data from the locations given were averaged together.

Chart 1. Seasonal departures in recorded (black curves) and steric (red) sea levels for all oceans. Each block is assigned a number. Black vertical numerals refer to group numbers in Appendix I. Connected black dots show locations of the individual tide gauge stations comprising the group. Monthly means for each station are given in Appendix I. Red numerals refer to Appendix II. Connected solid red circles indicate regions from which temperature and salinity observations were taken to compute z_α; open red circles refer to regions where temperature observations only were available, and z_T was computed (Section 3.2). Horizontal scale in each block represents time in months from the beginning of January to the end of December. Vertical scale shows monthly departures from the annual mean; each tick represents 5 cm. Recorded sea level curves (black) are drawn through monthly mean without smoothing; italic numbers following colon give estimates of the standard deviation in cm (see Section 2.42). Steric levels (red) have been subjected to some smoothing. The curves were dashed whenever monthly means were lacking. Group 38 in the high north is drawn on an insert with a special projection.